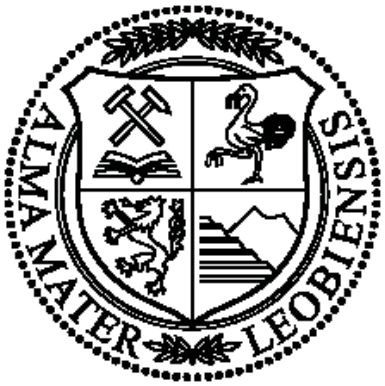

Compound-specific carbon isotope analysis of *n*-alkanes from source rocks and oils from the Paratethyan realm

Martin Sweda, BSc

Supervised by Univ.-Prof. Mag.rer.nat. Dr.mont. Reinhard F.Sachsenhofer

Chair of Petroleum Geology

Montanuniversitaet Leoben

A thesis submitted for the degree of

Master of Science

August 2018

EIDESSTATTLICHE ERKLÄRUNG

Ich erkläre an Eides statt, dass ich diese Arbeit selbstständig verfasst, andere als die angegebenen Quellen und Hilfsmittel nicht benutzt und mich auch sonst keiner unerlaubten Hilfsmittel bedient habe.

AFFIDAVIT

I declare in lieu of oath, that I wrote this thesis and performed the associated research myself, using only literature cited in this volume.

_____ _____

Datum Unterschrift

Danksagung

An dieser Stelle möchte ich mich bei allen bedanken, die mich während der Anfertigung dieser Arbeit unterstützt und motiviert haben.

Zuerst gebührt mein Dank Herrn Prof. Reinhard F. Sachsenhofer, der meine Masterarbeit betreut und begutachtet hat. Für die hilfreichen Anregungen, die konstruktive Kritik, sowie sein unendliches Maß an Geduld möchte ich mich herzlich bedanken.

Mein besonderer Dank geht auch an Herrn Dr. Reinhard Gratzer und Herrn Dr. Achim Bechtel für die Bewältigung der organischen Geochemie. Für die Einweisung im Labor und ihre unerschöpfliche Hilfsbereitschaft möchte ich mich herzlich bedanken.

Frau Dr. Magdalena Pupp, Frau Dr. Doris Groß, Herrn Dr. Bernhard Rupprecht, und Herrn Johannes Rauball MSc. möchte ich recht herzlich für die Proben und Probendaten danken.

Bei allen Mitarbeitern des Departments für Geowissenschaften möchte ich mich recht herzlich für die Hilfe und Unterstützung während meiner Diplomarbeit bedanken.

Meiner Familie danke ich besonders für den starken Rückhalt über die Dauer meines gesamten Studiums.

Abschließend möchte ich mich bei meinen Eltern bedanken, die mir mein Studium durch ihre Unterstützung ermöglicht haben.

Abstract

The Paratethyan realm extends from Switzerland to Kazachstan and hosts a significant number of petroleum provinces. Many of these provinces have been charged by Mesozoic and Cenozoic source rocks. For this study, 48 extracts of source rocks with Jurassic to Miocene ages and 29 oils from six petroleum provinces have been choosen for compound specific carbon isotope analysis of n-alkanes (CSIA-A) in order to (1) conduct oil-source correlations, (2) investigate the influence of stratigraphy on $\delta^{13}C$ composition of *n*-alkanes, and (3) observe the regional distribution of CSI patterns in Oligo-/Miocene and Mesozoic rocks. Samples were selected from the Molasse Basin (Germany, Austria), the Waschberg Zone (Austria), the Carpathian Fold-and-Thrust belt (Ukraine), the Carpathian Foredeep (Ukraine), the Western Black Sea shelf (Bulgaria), and the Rioni Basin (Georgia).

(1) Based on CSI-A patterns and biomarker ratios, the Voitsdorf and Haidenbach oils in the Upper Austrian part of the Molasse Basin could be correlated with the Oligocene Schöneck Formation. In contrast, deviant CSI-A patterns and the absence of oleanane suggest that oil stains in borehole Mank, located in the Lower Austrian part of the Molasse Basin, were produced by a Mesozoic source rock, which could have also generated oils recovered from Triassic rocks in borehole Urmannsau-1 (N. Calc. Alps). Oils from the eastern part of the Carpathian Fold-and-Thrust belt could be correlated with the Menilite Formation. The Jurassic Kokhanivka Formation is not a probable source rock for heavy oils in Jurassic reservoirs from the Mesozoic basement of the Carpathian Foredeep. The Tjulenovo oil (W. Black Sea) produced from Cretaceous reservoir rocks has been generated by either the Oligocene Ruslar Formation, the Oligo-/Miocene Kaliakra Canyon Fill, or both. The Shromisubani oil accumulated in Upper Miocene reservoirs in the Rioni Basin probably represents a mixture of oils generated in Oligocene Maikopian sediments and Eocene sediments of the Kuma Formation.
(2) Depth plots of $\delta^{13}C$ values of short-, mid-, and long chain n-alkanes of core samples from well Oberschauersberg-1 (Molasse Basin), cuttings samples from well Varna Zapad-1 (W. Black Sea), and outcrop samples from the Martvili section (Rioni Basin) were used to investigate stratigraphic controls on carbon isotopy of n-alkanes. The results show (i) a significant difference in $\delta^{13}C$ composition of individual *n*-alkanes in mid (*n*-C_{21}) and short chain range (*n*-C_{16}) between the Schöneck Formation and the overlying units. In contrast, isotope ratios of long chain n-alkanes (*n*-C_{26}) remain constant at the Schöneck/Dynow boundary and change only at the Dynow/Eggerding boundary. Mid chain *n*-alkanes of Eggerding Formation and Dynow marl show similar $\delta^{13}C$ values. The different behavior of mid & long chain *n*-alkanes may indicate that the isotopy of the CO_2 pool avaialable for land plants and aquatic organisms did not change simultaneously; (ii) in the Kaliakra Canyon Fill and the Ruslar Formation from the Varna Zapad-1 well offshore Bulgaria $\delta^{13}C$ values of mid and long chain *n*-alkanes get lighter with depth. Short chain *n*-alkanes do not follow this trend. The isotope-depth trend does not continue in the Eocene Avren Formation; (iii) in the Rioni Basin $\delta^{13}C$ values of mid and long chain *n*-alkanes do not show high variation with depth. Short chain *n*-alkanes on the other hand are significantly lighter in the Kuma Formation than in the Maikop Group.
(3) Regional distributions of CSI patterns in Oligo-Miocene and Mesozoic rocks have been illustrated using three paleogeographic maps. An unusual V-shape pattern is observed in samples from the Molasse Basin and the western Black Sea representing Pshekian horizons and the Solenovian Event, and in the Late Solenovian to Early Miocene fill of the Kaliakra Canyon (W. Black Sea).

Kurzfassung

Der Bereich der Paratethys erstreckt sich von der Schweiz bis nach Kasachstan und beheimatet eine Vielzahl an Erdölprovinzen. Viele dieser Provinzen beinhalten Kohlenwasserstoffe, die in meso- & känozoischen Muttergesteinen generiert wurden. Im Zuge dieser Arbeit wurden 48 Gesteinsextrakte von Proben mit triassischem bis miozänem Alter und 29 Öle aus sechs Sedimentbecken mittels komponentenspezifischer Isotopenanalyse (CSIA-A) untersucht, um (1) Öl-Herkunftsbestimmungen durchzuführen, (2) die stratigraphische Kontrolle der Kohlenstoffisotopie auf *n*-Alkane zu untersuchen, und (3) die regionale Verteilung der CSI Muster in Gesteinen mit oligo-/miozänem und mesozoischem Alter zu beobachten. Die Proben stammen aus dem Molasse Becken (Deutschland, Österreich), der Waschbergzone (Österreich), dem karpatischen Falten- & Überschiebungsgürtel und dessen Vorland (Ukraine), dem Schelf des westl. schwarzen Meeres (Bulgarien) und dem Rioni Becken (Georgien).

(1) Basierend auf CSI-A Mustern und Biomarker-Daten konnten die Öle aus Voitsdorf und Haidenbach (oberösterr. Molasse B.) mit der oligoz. Schöneck-Fm. korreliert werden. Abweichende CSI-A Muster und das Fehlen von Oleanan in Ölspuren in der Bohrung Mank (niederösterr. Molasse B.) lassen dagegen auf ein mesoz. Muttergestein schließen, das auch die Ölspuren in triass. Gesteinen der Bohrung Urmannsau-1 (Nördl. Kalkalpen) generiert haben könnte. Öle des karpatischen Falten- & Überschiebungsgürtels konnten eindeutig mit der Menilit-Fm. korreliert werden. Die jurass. Kokhanivka-Formation (karp. Vorlandbecken) ist kein mögliches Muttergestein für die schweren Öle, welche in jurass. Reservoirgesteinenen im mesoz. Untergrund des karpatischen Vorlandbeckens auftreten. Das Tjulenovo Öl (W. Schwarzes Meer), das aus kretaz. Speichergesteinen produziert wird, wurde entweder von der oligoz. Ruslar-Fm., der oligo-/mioz. Füllung des Kaliakra Canyons, oder beiden generiert. Das Shromisubani Öl in obermioz. Reservoirgesteinen im Rioni Becken stammt vermutlich teilweise aus oligoz. Maikop Sedimenten und eoz. Sedimenten der Kuma Fm.
(2) $\delta^{13}C$ Werte von kurz-, mittel- und langkettigen n-Alkanen von Kernproben der Bohrung Oberschauersberg-1 (Molasse Becken), von Bohrkleinproben der Bohrung Varna West-1 (W. Schwarzes Meer) und Oberflächenproben des Martvili Profils (Rioni Becken) wurden gegen die Tiefe aufgetragen um den Einfluss der stratigraphischen Position auf die C-Isotopie zu untersuchen. Die Ergebnisse zeigen (i) signifikant unterschiedliche $\delta^{13}C$ Werte mittel- (*n*-C_{21}) & kurzkettiger n-Alkane (*n*-C_{16}) zwischen der Schöneck-Fm. und überlagernden Einheiten. $\delta^{13}C$ Werte langkettiger n-Alkane (*n*-C_{26}) ändern sich dagegen erst ab der Dynow/Eggerding Grenze. Mittelkettige n-Alkane der Eggerding- & Dynow-Fm. zeigen ähnliche $\delta^{13}C$ Werte. Das unterschiedliche Verhalten von mittel- & langkettigen n-Alkanen deutet daraufhin, dass sich die Isotopie des CO_2 Reservoirs, welches für Landpflanzen und Wasserorganismen verfügbar war, nicht simultan änderte; (ii) In der Füllung des Kaliakra Canyons und der Ruslar-Fm. in der Bohrung Varna West-1 werden $\delta^{13}C$ Werte von mittel- und langkettigen n-Alkanen mit zunehmender Tiefe leichter. Kurzkettige n-Alkane folgen diesem Trend nicht. Der Isotopie-Tiefentrend endet an der Oberkante der eoz. Avren-Fm.; (iii) im Rioni Becken zeigen $\delta^{13}C$ Werte von mittel- und langkettigen n-Alkanen keine hohe Varianz mit der Tiefe. Jedoch sind kurzkettige n-Alkane in der Kuma Fm. signifikant leichter als in den Maikop Sedimenten.
(3) Die regionale Verteilung von CSI Mustern in oligo-/miozänen und mesozoischen Gesteinen wurde in drei paleogeographischen Karten veranschaulicht. Ein ungewöhnliches V-Muster wird für Proben des älteren Rupeliums (Pshekian und „Solenovian Event“) aus dem Molasse Becken und dem westl. Schwarzen Meer, sowie für oligo-/mioz. Proben aus dem Kaliakra Canyon (Schwarzes Meer) beobachtet.

Index

1 Introduction 8
2 Geological Setting 10
2.1 Evolution of the Paratethys 10
2.2 Geological evolution and petroleum systems 11
2.2.1 Molasse Basin 11
2.2.2 Calcareous Alps 12
2.2.3 Waschberg Zone 13
2.2.4 Carpathian Fold-and-Thrust Belt 13
2.2.5 Carpathian Foredeep 14
2.2.6 Western Black Sea 14
2.2.7 Rioni Basin 15
3 State of the Art 17
3.1 Oil-source rock correlations 17
3.2 Oil-oil correlations 18
3.3 OM source investigations 19
3.4 OM maturity investigations 20
3.5 Charge / Migration investigations 20
4 Samples and Methods 21
4.1 Samples 21
4.2 Methods 24
4.2.1 Sample Preparation 24
4.2.2 GC-MS 24
4.2.3 IR-MS 26
5 Results 27
5.1 Molasse Basin 27
5.1.1 Source rocks 27
5.1.2 Oils 32
5.2 Calcareous Alps 36
5.2.1 Bächental Marls 36
5.2.2 Oils 38
5.3 Waschberg Zone 41
5.3.1 Biomarker Composition 41
5.3.2 Isotope Ratios 42

5.4 Carpathian Fold-and-Thrust belt 44
5.4.1 Source rocks 44
5.4.2 Oils 48
5.5 Carpathian Foredeep 50
5.5.1 Rocks 50
5.5.2 Oils 52
5.6 Western Black Sea 54
5.6.1 Source rocks 54
5.6.2 Tjulenovo oil 57
5.7 Rioni Basin 59
5.7.1 Source rocks 59
5.7.2 Shromisubani oil 62
6. Discussion 64
6.1 Oil-Source correlations 64
6.1.1 Molasse Basin 64
6.1.2 Carpathian Fold-and-Thrust belt 65
6.1.3 Carpathian Foredeep 66
6.1.4 Western Black Sea and Rioni Basin 66
6.2 Stratigraphic control on carbon isotopy of *n*-alkanes 69
6.2.1 Oberschauersberg Well 69
6.2.2 Varna Zapad-1 Well 70
6.2.3 Martvili Section 71
6.3 Regional distribution of CSI patterns of the Paratethys 73
7 Summary and Conclusion 79
List of References 81
List of Figures 90
List of Tables 95
Appendix: Biomarkers: GC-MS (Chromatograms for saturated and aromatic fractions) 98

1 Introduction

The Paratethys hosts a significant number of petroleum provinces [Boote et al., 2018]. Amongst these are the North Alpine Foredeep (also called Molasse Basin), stretching from Switzerland across Bavaria to Austria, the Carpathian Foredeep (Czech Rep., Poland, Ukraine, Romania), the western Black Sea shelf (Romania, Bulgaria), and the Rioni Basin located between the Greater and Lesser Caucasus in western Georgia.

The petroleum systems are based on a variety of Mesozoic and Cenozoic source rocks [Boote et al., 2018]. Amongst these Oligocene (and Lower Miocene) source rocks are especially important and share a similar geological history, for they have been deposited in the partially isolated Paratethyan realm [Sachsenhofer et al., 2018a,b]. Nevertheless, these source rocks vary locally in maturity, organic matter type and carbon isotopic composition.

Understanding petroleum systems in these basins is key for successful petroleum operations [e.g. Magoon & Beaumont, 1999]. It requires an understanding of the petroleum systems elements (source rock, reservoir rock, seal rock, overburden rock) and processes (trap formation, generation – expulsion – migration – accumulation). Within this context, oil-source (and oil-oil) correlations are of prime importance as they allow to determine the effective source rocks, and hence help to determine migration pathways.

Oil-oil and oil-source correlations are traditionally accomplished by comparing elemental (e.g. nickel/vanadium [Barwise, 1990]), molecular (biomarker), and isotopic parameters using techniques such as gas chromatography (GC), gas chromatography with mass spectrometry (GC-MS), or isotope ratios. For the determination of isotope ratios, bulk stable isotope measurements of oils have been used in the petroleum industry since the 1970's [e.g. Stahl 1977, Schoell 1984; Sofer 1984]. The use of compounds-specific isotopic composition (e.g. of light hydrocarbons, alkanes and biomarkers) is less common. Nonetheless, these types of data have already been proven to be an efficient tool for oil-source correlation [e.g. Odden et al., 2000].

While compound specific isotope analysis (CSIA) of *n*-alkanes (CSIA-A) has been used in several studies throughout the world, especially in Asia [e.g. Jia et al., 2013; Cai et al., 2015], where the benefits of this method have contributed to its popularity, it has not been applied much in the Paratethyan basins. Studies from Bechtel et al. [2013] and Mayer et al. [2018b], which used $\delta^{13}C$ values of individual *n*-alkanes for derivation of migration pathways and oil-source rock correlations in the Molasse Basin and the Black Sea, respectively, represent the only examples. Therein an odd, V shape pattern of the carbon isotopic signature of *n*-alkanes was shown, which could not be explained yet. In general, the factors controlling the isotopy of individual compounds are still poorly understood.

The aim of this thesis is to evaluate the method and advantages of CSIA-A in Paratethyan basins, and based on the derived data, deepen our knowledge about the factors controlling the carbon isotopic signature of individual *n*-alkanes. As successful applications in other regions have shown [e.g. Jia et al al., 2013], CSIA will improve our understanding of the underlying petroleum systems, and with the better understanding of the controlling factors of carbon isotopy of individual compounds, possibly provide new exploration targets for oil and gas even beyond the Paratethyan basins. Furthermore, this thesis will represent the first and

biggest study on compound-specific isotope analysis of oils and source rocks in the Paratethys, and as such will provide a large pool of data which may offer new insights and be crucial for making exploration decisions even beyond.

2 Geological Setting

2.1 Evolution of the Paratethys

Most (Oligocene to Lower Miocene) source rocks included in the present study were deposited in the Paratethys Sea. The evolution of the Paratethys, therefore, is briefly summarized in this section.

The Paratethys Sea was a large epicontinental sea, stretching from western Europe to Kopetdagh (Figure 1). Based on different environmental histories, the Paratethys can be subdivided into the Western (incl. the western part of the Molasse Basin), the Central (incl. Carpathian Foredeep) and the Eastern Paratethys (incl. Black Sea). At present the Black Sea, the Caspian Sea and the Aral Sea are remains of the once huge Paratethys.

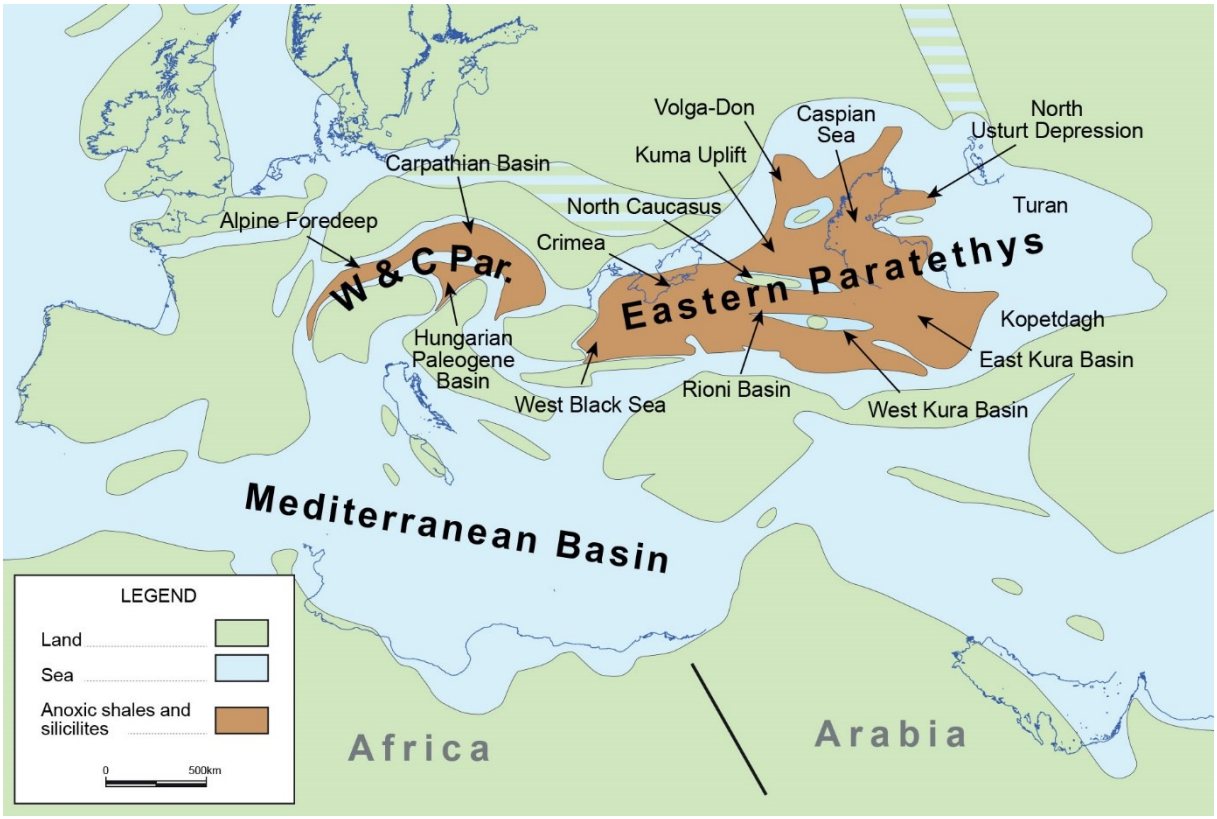

Figure 1. Paleogeography of the Paratethyan realm during early Oligocene time. (W & C Par.: Western and Central Paratethys) [Sachsenhofer et al., 2018].

Formation of the Paratethys is usually dated around the Eocene-Oligocene boundary, when tectonic activities along the Alpine front and a fall in sea level isolated the Tethys from the world ocean, leading to dysaerobic bottom conditions, which are well documented by the sedimentation of black shales (e.g. Menilite Formation, Maikop Group) [Rögl, 1999, Popov et al., 2004]. Basin isolation reached a maximum during the “Solenovian event”. Carbonate-rich rocks (e.g. Dynow Formation, Ostracoda Beds), which today form a Paratethys wide marker horizon were deposited during this event [Rögl, 1999, Popov et al., 2004]. Oxygenated bottom conditions were re-established however during the middle Oligocene, and the entire Paratethys returned to marine conditions in the Late Oligocene, as a result of the seaway broadening until the Early Miocene. Increased tectonic activities in the Late Oligocene led to a sea regression from the western Alpine Foredeep and subsequently limno-fluviatile sedimentation of Lower Freshwater Molasse started. In the Early Miocene (Burdigalian), the

counterclockwise rotation of Africa and Arabia resulted in a collision with Eurasia, and for the first time, the continents were connected with each other. In the east, the tectonic activities resulted in the isolation of the Eastern Paratethys; the Kotsakhurian Sea, with strongly reduced salinity and strong endemism came into existence. In the Central Paratethys, the Carpathian Foredeep became an isolated basin with thick evaporite sedimentation [Rögl, 1999]. Later, the Alpine Foredeep became dry land. The demise of the Paratethys commenced during the Badenian, when increasing continentalization and tectonic uplift caused the closure of open seaways, which led to a transformation of open marine environments into lacustrine deltaic systems. During this time, alternating phases of desiccation and flooding dominated the environment. Finally, the Carpathian Foredeep became dry land.

2.2 Geological evolution and petroleum systems

Source rocks and oil samples from various basins are included in the present study. The geological evolutions of these basins are briefly summarized in this section. In addition the investigated source rocks are briefly characterized together with the most important reservoir units. Epoch / Stage names are summarized in the stratigraphic chart at the end of the chapter (Figure 2). A summary of the source rocks and source rock parameters is given in Table 1.

Table 1. Summary of source rocks in key sections with bulk geochemical parameters (see text for references).

Province	Formation	Lithology	Age	TOC (%)	HI	Tmax (°C)	Rr,c (%)
Molasse Basin	Eggerding Fm.	marl, mudstone	Kiscellian	1.9 - 6.0	300 – 580	423	0.31
	Dynow Fm.	limestone, marl	Kiscellian	0.5 – 2.0	500-600	428 [A]	
	Schöneck Fm. (c)	black shale	E.Kiscellian	5.5	572 [A]	421 [A]	< 0.35
	Schöneck Fm. (b)	black marl	E.Kiscellian	2.5	484 [A]	410 [A]	< 0.35
	Schöneck Fm. (a)	black marl	E.Kiscellian	2.5	395 [A]	415 [A]	< 0.35
Calc. Alps	Allgäu Fm.	marl, bituminous	L.Toarcian	0.1 – 12.9	300 - 600	416 - 427	0.45
Waschberg Z.	Thomasl Fm.	shale	E. Oligocene	0.5 – 4.0	116 - 416	422	0.37
Carp. F&T Belt	Menilite Fm.	mainly shale	Kiscellian –Eggenburg.	0.7 - >10	381 [B]	422 [B]	
	Shypot Fm.	black shale	Barremian - Albian	2.0 – 4.0	< 200	454 - 458	
Carp. Foredeep	Kokhanivka Fm.	shale	M. Jurassic	0 - 12	33 - 143	438 - 445	
W.Black Sea	Kaliakra Can. Fill	(diatom.) shale	Solenovian – Kozakh.		116 – 480 [C]	< 430	
	Ruslar Fm.	sand-/limestone	Pshekian – Kalmykian	0.5 – 2.7	141 – 350 [C]	421 [C]	
	Avren Fm.	marl, sandy, calc.	Beloglinian	0.8 – 6.0	232 [C]	~430	
Rioni Basin	Maikop Group	shale, calc. shale	Pshekian – Kozakh.	2.7	278	418	0.30 – 0.45
	Kuma Fm.	marl	Lutetian – Bartonian	3.2	300 - 600	420	0.36 – 0.39

(TOC: total organic carbon; HI: hydrogen index in mg HC/g TOC; Rr: vitrinite reflectance, measured; Rc: vitrinite reflectance, calculated. – avg values if only one value given)
[A] Schulz, 2003; [B] Rauball & Sachsenhofer, 2017; [C] Rupprecht, 2014

2.2.1 Molasse Basin

The Alpine Foredeep, or Molasse Basin, is an east–west trending foreland basin, which resulted from the subduction of the southern margin of the European plate beneath the Adriatic plate [Ziegler, 1987]. The basement consists of crystalline rocks of the Bohemian Massif covered by autochthonous sediments of Jurassic and Cretaceous age. Molasse sedimentation commenced during late Eocene time and continued till Late Miocene time. The southern part of the Molasse Basin was overridden by the Alpine nappes (incl. Flysch and Helvetic units, Calcareous Alps) and incorporated within the overthrust belt [Wagner, 1996].

Whereas Mesozoic source rocks are present in the basement of the western part of the Molasse Basin [e.g. Wehner & Kuckelkorn, 1995], Lower Oligocene source rocks are most important in its central and eastern section [Schulz et al., 2002]. Accumulation of fine-grained rocks started around the Eocene–Oligocene boundary with the deposition of the Schöneck Formation.

The Schöneck Formation overlies Eocene sandstones or limestones. It was deposited in a stagnant basin with an oxygen-depleted (dysoxic to anoxic) bottom water [Schulz et al., 2002]. It is subdivided in marly members 'a' and 'b' containing globigerinoid planktonic foraminifera, and black shale member 'c' [Schulz et al., 2002]. Member 'c' is typically carbonate-free, but contains a few micritic limestone layers. Average TOC contents are about 2.5 wt% in members 'a' and 'b', and about 5.5 wt% in the shale member 'c' (max. 12%). The HI values reveal the presence of type II kerogen and display a general upwards increasing trend from 400 to 600 mg HC/g TOC [Sachsenhofer et al., 2017]. T_{max} (410 – 421°C) and vitrinite reflectance (R_r < 0.31%) show that the organic matter is immature [Schulz et al., 2002; Schulz, 2003].

The limestones and marls of the Dynow Formation follow above the Schöneck Formation. TOC contents are in the range of 0.5 wt% to 2.0 wt%. HI values are in the order of 500–600 mg HC/g TOC and reflect excellent preservation conditions due to prevailing anoxia. T_{max} (avg. 428°C) show that the organic matter is immature [Schulz, 2003; Schulz et al., 2004].

The marlstones and mudstones of the Eggerding Formation overlie the Dynow Formation. Oxygen-deficient conditions prevailed during the deposition. TOC contents (1.9 – 6.0 wt%) and HI values (300 – 580 mg HC/g TOC) are very high in the lower part. T_{max} (avg. 423°C) and vitrinite reflectance (0.31 $\%R_r$) show that the organic matter is immature. The upper part contains less organic matter [Sachsenhofer & Schulz, 2006; Sachsenhofer et al., 2010].

Main reservoir rocks for oil in the Austrian part of the basin include Upper Eocene non- and shallow-marine sandstone (Voitsdorf and Ampfing formations), tidal deposits (Cerithian Beds) and Upper Cretaceous (Cenomanian) shallow-marine sandstones. Microbial gas also occurs in Upper Oligocene and Lower Miocene reservoirs [e.g. Gross et al., 2018].

2.2.2 Calcareous Alps

The Calcareous Alps represent a fold-and-thrust belt at the northern front of the Eastern Alps. They extend from the Rhine Valley to the Vienna area, where they are deeply buried beneath the Miocene fill of the Vienna Basin. The Calcareous Alps are composed of mainly marine Permian to Paleogene units with a high percentage of Triassic and Jurassic carbonate rocks [e.g. Tollmann, 1976].

The stratigraphic succession of the Calcareous Alps includes organic matter rich intervals in several stratigraphic units (e.g. Reifling Limestone; [Gratzer et al., 2015]). The Bächental bituminous marls, which belong to the Sachrang Member of the Lower Jurassic Middle Allgäu Formation, even reach oil shale quality. They were deposited at the transition of distal slope to basin and represent an alternating, ~6 m thick succession of limestone and marl beds. TOC contents are in the range of 0.1 to 12.9 wt%. HI values are in the order of 300-600 mg HC/g TOC. T_{max} (416 - 427°C) and vitrinite reflectance (0.45 $\%R_c$) show that the organic matter is immature [Neumeister et al., 2015, 2016]. The paleogeography of the depositional area of the Bächental bituminous marls was controlled by extensional tectonics, related to late Hettangian rifting and Toarcian oceanic break-up in the Penninic realm [Ratschbacher et al., 2004, Neumeister et al., 2015].

The Calcareous Alps include important hydrocarbon deposits in the subsurface of the Vienna Basin [Wessely, 2006], but east of the Vienna Basin only uneconomic oil has been detected [Zimmer and Wessely, 1996]. Oil stains from the Urmannsau well [Wessely, 2006; Misch et al.,

2017] and from tunnel excavations (Falkenstein tunnel; [Gratzer et al., 2015]) are included in the present study.

2.2.3 Waschberg Zone

The Waschberg Zone, extending in Lower Austria from Stockerau northeasterly to Mikulov, is a tectonic nappe within the Alpine-Carpathian nappe system, which is thrust on autochthonous Molasse sediments. It includes strongly imbricated and tectonized Mesozoic rocks (klippen) and Eocene to Late Miocene Molasse sediments, and itself is overthrusted by flysch nappes [Rögl & Nagymarosy, 2004].

Organic matter rich Oligocene sediments occur in the Waschberg Zone. The Thomasl Formation, which is considered a time-equivalent to the Eggerding Formation in the Molasse Basin, is included in the present study. It is composed of calcareous shales with TOC contents ranging from 0.5 to 4.0 wt%. HI values (116 - 416 mg HC/g TOC) indicate the presence of type II and III kerogen. T_{max} (avg. 422°C) and vitrinite reflectance (0.37 $\%R_r$) show that the organic matter is immature [Pupp et al., 2018a]. Small hydrocarbon deposits have been detected in the Waschberg Zone [Wessely, 2006], but oil samples are not included in this study.

2.2.4 Carpathian Fold-and-Thrust Belt

The Carpathians are the eastern extension of the European Alps. They formed during the Alpine orogeny in the Mesozoic and Tertiary by moving the ALCAPA, Tisza and Dacia plates over subducting oceanic crust. The Outer Carpathians consist mainly of Upper Jurassic to Lower Miocene flysch deposits thrusted over molasse sediments of the Carpathian Foredeep [Mantovani et al., 2006; Oszczypko, 2006].

The Menilite Formation represents the youngest part of the flysch sequence and occurs in a wide depth range [Koltun, 1992]. It is the most important source rock in the Carpathian Fold-and-Thrust Belt, and can act also as a reservoir rock [Popadyuk et al., 2006]. The TOC content varies from 0.7 to >10 wt% and is dominated by type II kerogen and locally type II-III, typically with high hydrogen indices [Boote et al., 2018]. The studied samples are from the Chechva River section (see Figure 2), where T_{max} (avg. 422°C) show that the organic matter is immature [Rauball & Sachsenhofer, 2017].

Other source rocks in the Carpathian Fold-and-Thrust Belt are the Lower Cretaceous black shales of the Spas and Shypot formations. The Shypot Formation, which is included in the present study, has typically TOC contents of 2 to 4 wt% (maximum 8%) and hydrogen indices of <200 mgHC/gTOC [Boote et al., 2018]. T_{max} (454 - 458°C) show that the organic matter is in the oil window [Koltun et al., 1998].

The Ukrainian part of the Carpathian Fold-and Thrust Belt includes a major oil province. Beside the Menilite Formation, important reservoir rocks in the study area include the Middle Eocene Wyhoda Formation and the Stryi Formation. The Wyhoda Formation consists of thin- to middle-bedded siliciclastics, which form the flysch succession containing massive or coarse-bedded sandstones. The Stryi Formation consists mostly of sandstones, silts with interbeds of sandy limestones, gravelites and conglomerates, which are stacked up in a typical flysch pattern. The Stryi Formation is as much as 1.5 km thick [Popadyuk et al., 2006].

2.2.5 Carpathian Foredeep

The Carpathian Foredeep is the largest foredeep basin in Europe. It developed during the Early and Middle Miocene as a peripheral flexural foreland basin in front of the advancing Carpathian front. There were three periods of intense foreland subsidence: during the Early Miocene, Early Badenian, and Late Badenian to Sarmatian times. Evaporites (halite and potash) are important constituent of the sedimentary column [Peryt & Peryt, 2016]. Miocene Molasse sediments are underlain by the basement of the European Platform, covered mainly by Permo-Mesozoic terrestrial and shelf sediments and locally by Paleogene deposits.

The Carpathian foredeep contains mainly microbial gas in Miocene reservoirs [Kotarba & Koltun, 2006], but minor oil deposits, probably charged from Middle Jurassic black shales (Kokhanivka Formation), occur in the Mesozoic basement [e.g. Kotarba & Koltun, 2006; Sachsenhofer & Koltun, 2012]. The Kokhanivka Formation, which is present in the northwest part of the foredeep, is about 500 m thick; TOC contents exceed 12 percent locally, type II kerogen is present. T_{max} (438 - 445°C) show that the organic matter is at the beginning of the oil window [Koltun et al, 1998; pers.comm. J.Rauball,2018].

2.2.6 Western Black Sea

The Black Sea is a Late Cretaceous – Paleogene back-arc extensional basin. It developed north of a magmatic arc, which formed in the Albian by the northwards subduction of the Neo-Tethys Ocean [e.g. Banks & Robinson, 1997; Nikishin et al., 2001, 2003]. In the west, it is confined by the Moesian platform. Early Eocene loading of the Moesian Platform by Balkan thrust sheets formed the Kamchia Foredeep [Robinson et al., 1996], which became the deep western branch of the Western Black Sea [Georgiev, 2000]. Accumulation of sediments commenced shortly thereafter.

A middle Eocene deepening of the northern part of the Kamchia Foredeep resulted in the accumulation of the Avren Formation (Middle to Upper Eocene), which is up to 1.5 km thick. It is composed of sandy marls with limestone and sandstone intercalations. TOC contents are typically low, but may range up to ~6.0 wt%. HI values are in the order of 50-200 mg HC/g TOC [Sachsenhofer et al., 2009]. T_{max} (avg. ~430°C) show that the organic matter is immature [Stummer, 2006].

The overlying Oligocene Ruslar Formation is made up predominantly of finely laminated pelitic rocks with rare sandstones, siltstones and limestone beds representing outer shelf to shoreface facies. The thickness of the Ruslar Formation varies considerably from 60 to 70 m in the Varna area to 500 m in the shelf sector of the Kamchia Basin to over 1500 m in the deep offshore of the Western Black Sea Basin. Dysoxic to anoxic conditions prevailed during its deposition. TOC contents vary between 0.5 and 2.7 wt%, but are mostly in the range of 1 to 2 wt%. HI values are in the order of 77-270 mg HC/g TOC. The kerogen is mainly of type III, but some units contain a type II kerogen [Sachsenhofer et al., 2009]. T_{max} (avg. 421°C) show that the organic matter is immature [Rupprecht, 2014].

Offshore Bulgaria the Ruslar Formation is cut by the deep Kaliakra canyon, filled by Oligocene to Lower Miocene deposits. The Kaliakra Canyon Fill includes source rocks with up to 4.3 wt% TOC and type II kerogen (HI up to 530 mgHC/gTOC). T_{max} (< 430°C) show that the organic matter is immature [Mayer et al., 2018a].

2.2.7 Rioni Basin

The Rioni Basin at the eastern end of the Black Sea is an intermontane foredeep that has formed after the Transcaucasian Massif started subsiding in the Late Eocene [e.g. Adamia et al., 2010; Brunet et al., 2002]. It represents the western basin within the Transcaucasian Massif and is separated by an intervening basement culmination from the Kura Basin in the east. The Eocene to Pliocene basin fill includes mudstones, sandstones, terrigenous and carbonate turbidites as well as limestones [e.g. Adamia et al., 2010].

Two distinct source rock intervals are present in the Rioni Basin:

The Kuma Formation in the Rioni Basin is composed of fully-marine marls and is about 40 m thick. At the investigated section near Martvili, the formation is thermally immature and has an average TOC of 3.2 wt%. HI of 300-600 mg HC/g TOC indicates type II kerogen. T_{max} (avg. 420°C) and vitrinite reflectance (0.36 – 0.39 $\%R_r$) show that the organic matter is immature [Pupp et al., 2018b]. The formation is overlain by Upper Eocene marls (Belaya Glina Formation) deposited in an oxygenated, semi-open subtropical sea.
The Maikopian sediments follow above the Eocene marls. The Oligocene succession shows two distinct parts; the lower part, 60 m thick, contains high quantities (avg. 2.7 wt% TOC) of type II-III kerogen (avg HI: 278 mg HC/g TOC). The upper part, which is largely carbonate free, is 424 m thick, and less abundant in organic matter - (~2.0 % TOC), which is dominantly composed of type III kerogen (avg. HI: 140 mg HC/g TOC). T_{max} (avg. 418°C) and vitrinite reflectance (0.30 – 0.45 $\%R_r$) show that the organic matter is immature [Pupp et al., 2018b].

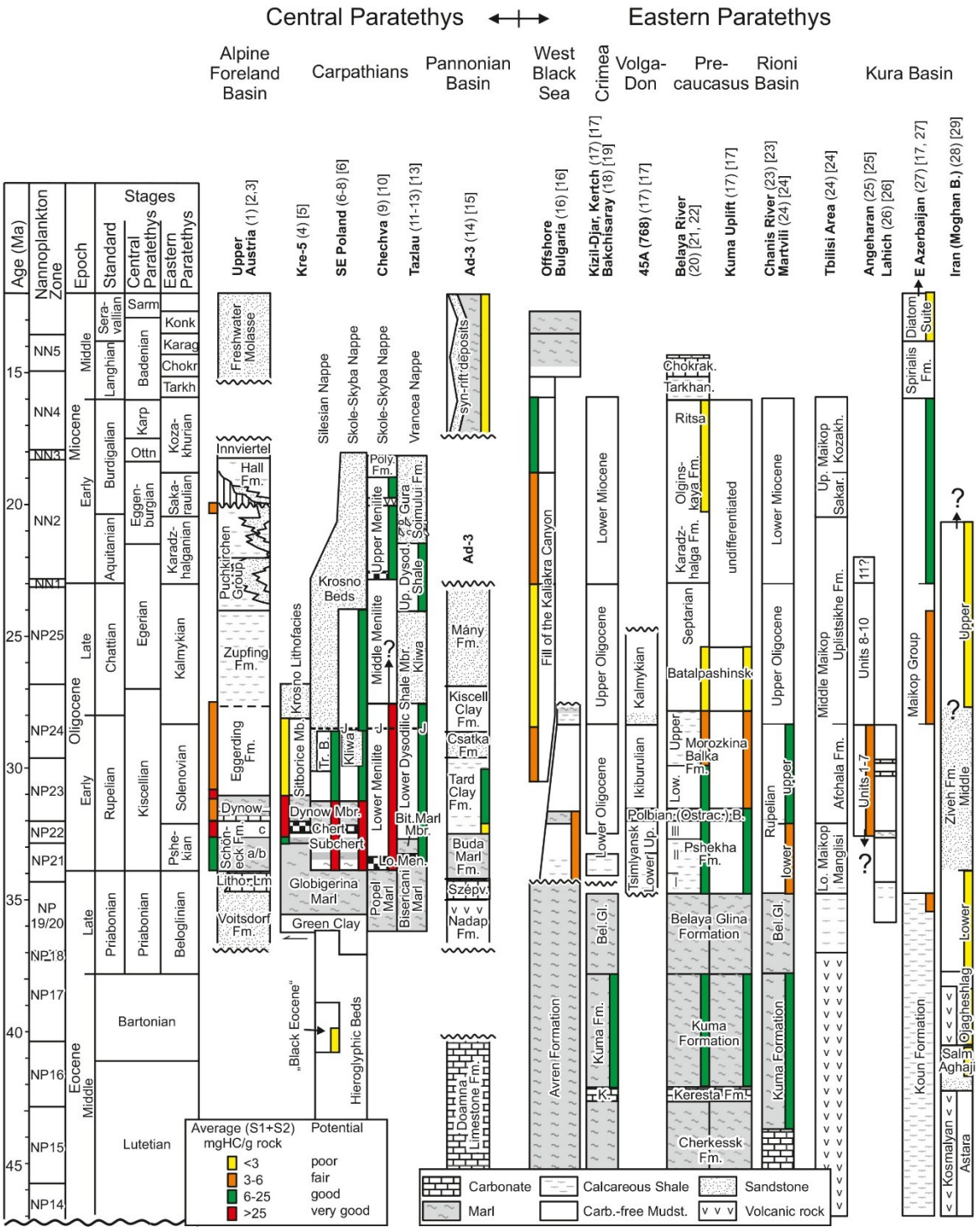

Figure 2. Stratigraphic chart of the investigated sections [Sachsenhofer et al., 2018].

3 State of the Art

Compound specific carbon isotope analysis of individual *n*-alkanes have found several distinctive applications in petroleum exploration and development activities. Amongst these are (3.1) oil-source rock correlations [Murray et al., 1994; Chung et al., 1994; Xiong & Geng, 2000; Odden et al., 2002; Li & Guo, 2010; He et al., 2012; Ohm et al., 2012; Jia et al., 2013; Cai et al., 2015; Cheng et al., 2015; Huang et al., 2016; Mayer et al., 2018b], (3.2) oil-oil correlations / identification of mixed sources in oils [Rooney et al., 1998; Whiticar & Snowden, 1999; Harris et al., 2003; Li & Xiong, 2009; Li & Guo, 2010; He et al., 2012; Liu et al., 2016; Cheng et al., 2015], (3.3) organic matter source investigations (e.g. for paleoenvironmental and paleoclimate reconstructions) [Rieley et al., 1991; Collister et al., 1994b; Murray et al., 1994; Lichtfouse et al., 1994; Pagani et al., 1999; Brincat et al., 1999; Odden et al., 2002; Chikaraishi & Naraoka, 2002; Maioli et al., 2012; Hockun et al., 2016], (3.4) organic matter maturity determinations [Bjorøy et al., 1991, 1992; Clayton & Bjorøy, 1994; Rooney et al., 1998; Harris et al., 2003; Tang et al., 2005; Liao et al., 2012], and (3.5) charge and migration investigations [Xiong et al., 2001; Liao et al., 2004, Bechtel et al., 2013; Mayer et al., 2018b].

Within the implementation of practical applications such as listed above, several case studies have revealed fundamental insights on the factors contributing to the carbon isotopic composition of *n*-alkanes. In this regard, they have shown: (a) that source rock depositional setting is the primary control on the shape of the *n*-alkane isotope signature, with negatively sloping curves being characteristic of fluvio-deltaic and freshwater transitional oils, and flat or positively sloping curves typical of marine oils [Murray et al., 1994]; (b) that the $\delta^{13}C$ values of *n*-alkanes sourced from terrestrial source organic matter are heavier than the *n*-alkanes sourced from aquatic source organic matter [e.g. de Leeuw et al., 1991]; (c) that expelled hydrocarbons are usually lighter (depleted in ^{13}C) than the hydrocarbons remaining in the source rock at the same maturity [Liao et al., 2004]; (d) that parameters such as the oleanane/hopane ratio may overestimate the higher plant contribution to marine oils [Murray et al., 1994], (e) that with increasing temperature the *n*-alkanes become more positive in $\delta^{13}C$ values [Rooney et al., 1998]; (f) that isotopic variations of *n*-alkanes can be dependent upon maturity [Bjorøy et al., 1992]; (g) that the mixing of oils with different thermal maturities from the same source rock has no significant influence on the carbon isotopic profile of *n*-alkanes in mixed oils [Cheng et al., 2015].

Despite the wider use in studies from around the world, especially in Asia, CSIA-A has not been applied within research of Paratethyan basins. Studies from Bechtel et al. [2013] and Mayer et al. [2018b], which used $\delta^{13}C$ values of *n*-alkanes for oil-source rock correlations and the reconstruction of migration pathways, represent the only examples.

3.1 Oil-source rock correlations

Odden et al. [2000] used CSIA-A on oils, thermal extracts and kerogen pyrolysates of 6 source rock samples from offshore Mid-Norway. Their study shows that trends of absolute isotope data and specific isotopic fingerprints are useful for petroleum-source rock correlations. Their study also showed that individual components generated by pyrolysis of kerogens are isotopically heavier than those from the thermal extracts, as is expected from models of kinetic isotope effects.

Xiong & Geng [2000] determined carbon isotopic compositions of *n*-alkanes from 8 crude oils and their asphaltene pyrolysates from the Liaohe Basin, China, and demonstrated that carbon isotopic signatures of *n*-alkanes from source rocks and related oils can be used for oil-source rock correlation. Their study also suggests that the comparision of the *n*-alkane isotope compositions of the oils with those of asphaltene pyrolysates is a viable method for the differentiation of organic facies variation and post-generation alterations.

Li & Guo [2010] used compound specific isotope analysis in oil-source identification for oils in Dongying Depression, Bohai Bay Basin.

Ohm et al. [2012] compared the carbon isotope profiles from *n*-alkanes from DST oils from both flanks and crest of the Embla field, North Sea. Their study showed that the oils from the flanking wells are isotopically heavier than the wells on the crest, thus indicating that biodegradation of a preexisting oil removed most of the *n*-alkanes, and therefore the isotope variation is suggested to mostly reflect the later arriving oil.

Cai et al. [2015] compared the carbon isotope profiles of *n*-alkanes of 17 oils and 8 source rocks from the Tarim Basin, China, in order to correlate the oils to the sources.

Cheng et. al [2015] studied the characteristics and origin of carbon isotopes of *n*-alkanes in crude oils from the western Pearl River Mouth Basin (South China sea). Their study showed, that carbon isotopes of *n*-alkanes in the crude oils and the extracts of two effective source rocks in the basin exhibit clear differences. The carbon isotopic profiles of their *n*-alkanes in the oils show a “V” feature with increasing carbon number.

Huang et al. [2016] compared the carbon isotope profiles of *n*-alkanes of 10 oils and rock extracts from the Tarim Basin, China, in order to correlate the oils to the sources.

3.2 Oil-oil correlations

Rooney et al. [1998] pioneered CSIA of hydrocarbons in the gasoline-range fraction (C_5-C_9) as a tool for characterizing mixed oils on 6 samples from the Clair field, west of Shetland Island, and 3 samples from the South Viking Graben, North Sea. Their study indicated, that with increasing temperature the *n*-alkanes become more positive in $\delta^{13}C$ values.

Whiticar & Snowdon [1999] compared the stable carbon isotopic ratio of *n*-, iso-, and cylco-alkanes of hydrocarbons in the gasoline-range fraction (C_5-C_8) of 42 oils/condensates from the Western Canada Sedimentary Basin. Their study showed that the resulting isotopic signatures for oil / condensates provide a diagnostic geochemical technique for oil-oil and oil-source condensates; oils from similar or the same sources produce isotopic signatures that are highly correlated.

Harris et al. [2003] divided 27 oils from the Western Canada Sedimentary Basin into six groups on the basis of stable carbon isotope composition of selected gasoline range compounds (short chain *n*-alkanes).

Li & Xiong [2009] compared the carbon isotope profiles of *n*-alkanes of two oils from the South China Sea and their mixed oils, and were able to estimate the contribution proportion of each source in mixed oils

He et al. [2012] compared the carbon isotope profiles of *n*-alkanes of 12 oil samples from the Barents Sea and northern Timan-Pechora Basin, Russia. They were able to distinguish 5 oil families and to deconvolute co-sourced oils.

Liu et al. [2016] used CSIA-A on 13 oil and condensate samples of the north-central West Siberian Basin to investigate the existence of deep sources and to identify and deconvolute the components of oil mixtures. They were able to recognize three oil families.

3.3 OM source investigations

Rieley et al. [1991] compared carbon isotope ratios of *n*-alkanes from the leaves of lakeside trees with those from lake sediments. They were able to discriminate between diverse sources of sedimentary carbon, and conclude, that the *n*-alkanes extracted from the lake sediments are derived from a mixed input of deciduous leaf waxes.

Murray et al. [1994] measured *n*-alkane isotope profiles for 29 Late Cretaceous/Tertiary oils from SE Asia, China, Papua New Guinea, New Zealand and USA. Their research indicated, that source rock depositional setting is the primary control on the shape of the *n*-alkane isotope profile. They explain the difference as probably related to the bacterial reworking of higher plant matter in fluvio-deltaic environments.

Lichtfouse et al. [1994] compared a Pliocene oil shale from Pula (Hungary), a C3 plant and a C4 plant using isotopic composition of bulk organic matter, along with distributions and carbon isotope ratios of *n*-alkanes from organic extracts.

Collister et al. [1994b] performed CSIA-A on extracts from the Green River Oil Shale (Piceance Creek Basin, Colorado) in an attempt to relate the carbon isotopic signature of individual *n*-alkanes to organic material precursors. In their study, systematic variations in the ^{13}C contents of individual *n*-alkanes were modelled quantitatively and interpreted as indicating contributions from at least five distinct sources.

Pagani et al. [1999] measured and compared carbon isotope compositions of *n*-alkanes, pristane and phytane. Their study indicates that *n*-alkane $\delta^{13}C$ compositions and abundance distributions can be used for depositional environment source correlation.

Chikaraishi & Naraoka [2002] used CSIA-A on 26 species of terrestrial plants and 6 species of aquatic plants from natural environments from Japan and Thailand. Their study showed that in C3 plants, angiosperms have *n*-alkanes depleted in ^{13}C relative to gymnosperms. C4 plants are significantly enriched in ^{13}C compared to C3 plants. CAM plants vary widely in $\delta^{13}C$ relatively to those of C3 and C4 plants. Their study also indicated that all *n*-alkanes from various plant classes are more depleted in ^{13}C than relative to environmental water and bulk tissue.

Maioli et al. [2012] determined the carbon isotopic compositions of *n*-alkanes of surface sediments of five Brazilian estuarine system in order to evaluate organic matter sources. Through Principal Component Analysis they were able to verify the petrogenic influence in the n-alkane sources.

Hockun et al. [2016] determined the carbon isotopic compositions of *n*-alkanes of different OM sources from Laguna Potrok Aike (Argentina) to distinguish their relative contributions to lake sediments with the purpose of evaluating their use for paleo-environmental reconstructions. In

addition to other insights, their study showed that sedimentary mid chain *n*-alkane (*n*-C_{23}) is predominantly composed of submerged aquatic plants, whereas long-chain *n*-alkanes (*n*-C_{29} to *n*-C_{31}) are mostly derived from terrestrial sources from southern Patagonia.

3.4 OM maturity investigations

Bjorøy et al. [1991] showed that there are clear differences in the carbon isotope composition of *n*-alkanes and acyclic isoprenoids in oils.

Bjorøy et al. [1992] correlated isotopic variations in *n*-alkanes with maturity by analysis of hydrous pyrolysis products and oil.

Clayton & Bjorøy [1994] studied the effect of maturity on $^{13}C/^{12}C$ ratios of individual compounds in North Sea oils. They found that 50 to 90% of the carbon isotope variation in individual compounds from four North Sea oils was due to differences in thermal maturity.

Tang et al. [2004] proposed a kinetic model for thermally induced carbone isotope fractionation of individual *n*-alkanes in crude oil to simulate the ^{13}C isotope enrichments during artificial thermal maturation of a North Sea crude oil. Their study showed, that average $\delta^{13}C$ values increase by 4%, and that ^{13}C enrichment shows no significant dependence on hydrocarbon chain length.

Liao et al. [2012] have studied the characteristics of $\delta^{13}C$ of *n*-alkanes released from thermally altered solid bitumens at various maturities by catalytic hydropyrolysis. Their result showed that the distributions of $\delta^{13}C$ of *n*-alkanes in hydropyrolysates are insensitive to the temperature used for bitumen artificial maturation, and therefore the $\delta^{13}C$ values of *n*-alkanes in hydropyrolysates may provide useful information in bitumen-bitumen correlation for paleo-reservoir solid bitumens.

3.5 Charge / Migration investigations

Liao et al [2004] studied the influence of hydrocarbon expulsion on carbon isotopic compositions of individual *n*-alkanes in pyrolysates of terrestrial kerogens on samples from the Tuha, Fushun and Liaohe Basin, China. In their study, the expelled hydrocarbons are usually lighter (depleted in ^{13}C) than the hydrocarbons remaining in the source rock at the same maturity.

Xiong et al. [2001] determined compound specific $\delta^{13}C$ values of *n*-alkanes in pyrolysates. Their results indicated that liquid *n*-alkanes are mainly derived from the primary cracking of kerogen during early hydrocarbon generation and that HC expulsion has no considerable effect on the carbon isotopic composition of liquid *n*-alkanes.

Bechtel et al. [2013] investigated the influence of migration distance, maturity and facies on the stable isotopic composition of *n*-alkanes and on carbazole distributions in oils and source rocks of the Alpine Foreland Basin of Austria. Their results reflected a W–E trend towards lower $\delta^{13}C$ of *n*-alkanes.

4 Samples and Methods

4.1 Samples

48 rock samples and 29 oil samples have been selected for the present thesis and were provided by staff members from the Chair of Petroleum Geology at Montanuniversitaet Leoben (Prof. Sachsenhofer, Dr. Gratzer, Dr. Bechtel, Dr. Groß, Dr. Pupp, Dr. Rupprecht, J. Rauball) and by Juriy Koltun (Ukrainian Academy of Sciences).

The Molasse Basin is represented by seven core samples from boreholes in Bavaria (Schöneck Fm. units b and c; Dynow marl; [Pupp, 2018]), eight core samples from borehole Oberschauersberg in Upper Austria (Schöneck Fm. units a, b and c; Dynow marl; Eggerding Fm.; [Schulz et al., 2002]) and 14 oil samples. 12 of the latter are from different boreholes in the Voitsdorf Field (Upper Austria) in order to investigate in-field variability. Oil stains from cores in a borehole located in Lower Austria (Mank; [Misch et al., 2017]) are also included. Original names of Oberschauersberg samples (as labelled by RAG and used in Schulz et al. [2002]) read as follows: Osch-1 = Osch-1-3-15-74-78; Osch-2 = Osch-1-2-5-20-23; Osch-3 = Osch-1-2-1-53-57, Osch-4 = Osch-1-3-12-10-15; Osch-5 = Osch-1-2-17-1369; Osch-6 = Osch-1-2-15-1371, Osch-7d = D-17b; Osch-8d = D-25b.

The Calcareous Alps are represented by three Jurassic rock samples (Allgäu Fm.; Bächental open pit mine in Tyrol; [Neumeister et al., 2015, 2016]), three Triassic oil stained samples (Reifling Fm.; Falkenstein Tunnel; [Gratzer et al., 2015]), as well as oil stains recovered from borehole Urmannsau-1 (Lower Austria; [Misch et al., 2017]).

Three cuttings samples from the Waschberg Zone (Oligocene Thomasl Fm., Lower Austria; [Pupp et al., 2018a,c]) are included in the sample set to observe lateral variations within the Lower Oligocene source rocks.

All samples from the Carpathian Fold-and-Thrust Belt are from Ukraine (Eastern Carpathians). Rock samples include three Cretaceous (Shypot Fm.; Bystritz section; Chornogora Nappe) and four Oligocene to Lower Miocene outcrop samples (Menilite Fm.; Chechva River section; Skyba Nappe [Sachsenhofer et al., 2018b]). Five oil samples are from the Boryslav and Dolyna petroleum districts [Popadyuk et al., 2006; Kotarba et al., 2007; Wieclaw et al., 2012].

The Carpathian Foreland is represented by four core sample with a Middle Jurassic age (Kokhanivka Fm.) and three oil samples (Kokhanivka Zone in Ukraine [Kosakowski et al., 2012]).

Eleven cuttings samples and one oil sample are from the Western Black Sea, near Varna (wells Varna Zapad-1 & Galata-1: Ruslar Fm., Avren Fm., Tjulenovo oil; [Rupprecht, 2014; Mayer et al., 2018a,b]).

Five rock samples and one oil sample are from the Rioni Basin in Georgia (Martvili section: Kuma Fm. and Maikop Group, Shromisubani oil; [Pupp, 2018; Pupp et al., 2018b; Mayer et al., 2018a,b]).

All samples, sample locations and formation ages are listed in Table 2. Sample locations are shown in Figure 3.

Figure 3. Approximate sample locations. (W.Bav*: Western Bavaria; E.Bav*: Eastern Bavaria; Osch*: Oberschauersberg; V*: Vo
oil producing region; DOPR*: Dolyna oil producing region).

Table 2. List of rock and oil samples together with province, location, stratigraphy, formation and sample type.

Province	Location / Country	Sample	Stratigraphy	Formation	Type
Rock samples					
Molasse Basin	W. Bavaria / GER	B-21	Lower Oligocene	Dynow Fm.	core
		B-32	Lower Oligocene	Schöneck c	core
		B-40	Lower Oligocene	Schöneck c	core
		B-47	Lower Oligocene	Schöneck c	core
	E.Bavaria / GER	A-01	Lower Oligocene	Schöneck b	core
		A-09	Lower Oligocene	Schöneck b	core
		A-14	Lower Oligocene	Schöneck b	core
	Oberschauersberg / AUT	Osch-5	Middle Oligocene	Eggerding Fm.	core
		Osch-6	Middle Oligocene	Eggerding Fm.	core
		Osch-8d	Lower Oligocene	Dynow	core
		Osch-7d	Lower Oligocene	Dynow	core
		Osch-2	Lower Oligocene	Schöneck c	core
		Osch-3	Lower Oligocene	Schöneck c	core
		Osch-1	Lower Oligocene	Schöneck b	core
		Osch-4	Lower Oligocene	Schöneck a	core
Calcareous Alps	Bächental / AUT	BT-35	Lower Jurassic	Allgäu Fm.	outcrop
		BT-26	Lower Jurassic	Allgäu Fm.	outcrop
		BT-25	Lower Jurassic	Allgäu Fm.	outcrop
Waschberg Zone	Thomasl / AUT	THO-1650	Oligocene	Thomasl Fm.	cuttings
		THO-1720	Oligocene	Thomasl Fm.	cuttings
		THO-1760	Oligocene	Thomasl Fm.	cuttings
Carp. F&T Belt	Chechva R. / Spas	U-C-63	Lower Miocene	Menilite Fm.	outcrop
		U-C-4	Lower Miocene	Menilite Fm.	outcrop
		U-B-22	Lower Oligocene	Menilite Fm.	outcrop
		U-66	Lower Oligocene	Menilite Fm. (Chert hor.)	outcrop
	Bystrets / U	J-05	Cretaceous	Shypot Fm.	core
		J-39	Cretaceous	Shypot Fm.	core
		J-77	Cretaceous	Shypot Fm.	core
Carp. Foredeep	Kokhanivka / U	J-MS-2523	Middle Jurassic	Kokhanivka Fm.	core
		J-K6-3428	Middle Jurassic	Kokhanivka Fm.	core
		J-K6-3493	Middle Jurassic	Kokhanivka Fm.	core
		J-K6-3521	Middle Jurassic	Kokhanivka Fm.	core
W. Black Sea	Varna (Galata-1 Well) / BGR	Gal-880	Miocene	Kaliakra Cany. Fill	cuttings
		Gal-910	Miocene	Kaliakra Cany. Fill	cuttings
	Varna (Zapad-1 Well) / BGR	VarZ1-480	Miocene	Kaliakra Cany. Fill	cuttings
		VarZ1-570	Miocene	Kaliakra Cany. Fill	cuttings
		VarZ1-600	Miocene	Kaliakra Cany. Fill	cuttings
		VarZ1-660	Miocene	Kaliakra Cany. Fill	cuttings
		VarZ1-753	Miocene	Kaliakra Cany. Fill	cuttings
		VarZ1-817	Lower Oligocene	Ruslar Fm.	cuttings
		VarZ1-883	Lower Oligocene	Ruslar Fm. (NP23)	cuttings
		VarZ1-892	Lower Oligocene	Ruslar Fm.	cuttings
		VarZ1-928	Eocene	Avren Fm.	cuttings
Rioni Basin	Martvili / GE	R-102	Lower Oligocene	Maikopian sed.	outcrop
		R-94	Lower Oligocene	Maikopian sed.	outcrop
		R-08	Lower Oligocene	Maikopian sed.	outcrop
		R-59	Eocene	Kuma Fm.	outcrop
		R-31	Eocene	Kuma Fm.	outcrop
Oils			***Reservoir Strat.***	***Res. Fm.***	
Molasse Basin	Voitsdorf / AUT	V-01	Upper Eocene	Voitsdorf Fm.	oil
		V-02	Upper Eocene	Voitsdorf Fm.	oil
		V-08	Upper Eocene	Voitsdorf Fm.	oil
		V-11	Upper Eocene	Voitsdorf Fm.	oil
		V-13	Upper Eocene	Voitsdorf Fm.	oil
		V-15	Upper Eocene	Voitsdorf Fm.	oil
		V-19	Upper Eocene	Voitsdorf Fm.	oil
		V-21	Upper Eocene	Voitsdorf Fm.	oil
		V-23	Upper Eocene	Voitsdorf Fm.	oil
		V-33	Upper Eocene	Voitsdorf Fm.	oil
		V-39	Upper Eocene	Voitsdorf Fm.	oil
		V-41	Upper Eocene	Voitsdorf Fm.	oil
	Haidenbach / AUT	HNB-1	Upper Cretaceous		oil
	Mank / AUT	Mank-157			oil
Calcareous Alps	Falkenstein Tunnel / AUT	KB-04	Triassic	Reifling Fm.	oil stain
		KB-05	Triassic	Reifling Fm.	oil stain
		KB-07	Triassic	Reifling Fm.	oil stain
	Urmannsau / AUT	Urman-152	Mesozoic	Allgäu Fm.	oil stain
		Urman-758	Mesozoic	Wetterstein Fm.	oil stain
Carp. F&T Belt	[1]Pivnichna Dolyna 168 / U	PIV168	Middle Eocene	Wyhoda Fm.	oil
	[2]Voliya Blazhivska / U	VOL31	Oligocene	Menilite Fm.	oil
	[2]Nova Skhidnytsya 25 / U	NS25	Upper Cretaceous	Stryi Fm.	oil
	[2]Maslovetska / U	VM2	Upper Cretaceous	Stryi Fm.	oil
	Mala Volosyanka / U	MVOS	Oligocene	Menilite Fm.	oil seep
Carp. Foredeep	Orkhovychi / U	ORK2	Upper Jurassic	Limestone	oil
	Orkhovychi / U	ORK5	Upper Jurassic	Limestone	oil
	Kokhanivka / U	KOK26	Upper Jurassic	Limestone	oil
W. Black Sea	Tjulenovo / BGR	TJU	Oligocene		oil
Rioni Basin	Shromisubani / GE	PG	Upper Miocene (Meotian)		oil

[1] Dolyna oil producing region, [2] Boryslav oil producing region

(GER: Germany; AUT: Austria; U: Ukraine; BGR: Bulgaria; GE: Georgia; NP23: nannoplankton-zone 23)

4.2 Methods

The samples were prepared (4.2.1) and analyzed with GC-MS (4.2.2.2) for biomarker composition and IR-MS (4.2.3.2) for compound-specific carbon isotope data. The laboratory methods and geochemical analysis followed procedures that are well established at the Chair of Petroleum Geology [e.g. Bechtel et al., 2012].

4.2.1 Sample Preparation

Representative samples from the powdered source rock samples were extracted using dichloromethane in a Dionex ASE 200 Accelerated Solvent Extractor at 75°C and 50 bar. Oil samples were directly diluted with a hexane mixture. Subsequently the fractions of the hexane soluble organic matter were separated into saturated hydrocarbons and aromatic hydrocarbons by medium pressure liquid chromatography using a Köhnen–Willsch MPLC instrument [Radke et al., 1980]. Low polar compounds (NSO) and asphaltenes were thereby removed.

4.2.2 GC-MS

A short description of GC-MS method by Stashenko & Martínez [2014] is given in 4.2.2.1. The workflow is described in 4.2.2.2.

4.2.2.1 GC-MS Overview

Gas Chromatography

In a gas chromatographic system (Figure 4), the sample to be analyzed may be a liquid solution or a collection of molecules adsorbed on a surface. During the transfer into the GC, the sample is volatilized by rapid exposure to a zone kept at relatively high temperature (200-300°C) and mixed with a stream of carrier gas (Ar, He, N2 , or H2). The resulting gaseous mixture enters the separation section, a chromatographic column, which in its current version is a fused-silica tubular capillary coated internally with a thin polymer film. Upon their displacement through the column, analyte molecules are partitioned between the gas carrier stream (mobile phase) and the polymer coating (stationary phase), to an extent which depends mainly on their chemical structure. At the end of the separation section, the molecules reach a detection system in which a specific physical property (thermal conductivity) or a physico-chemical process (ionization in a flame, electron capture) gives rise to an electric signal which is proportional to the amount of molecules of the same identity. A data system permits to process these data to produce a graph of the variation of this detector signal with time (chromatogram). Thus, four principal sections are distinguish- able in the chromatograph: introduction (injector), separation (chromatographic column), detection, and data handling units. Each section has its own function and its responsibility for the quality of the analysis and the results obtained. Substances with low vapor pressure will not enter the chromatographic column, will accumulate at the injection system, and may eventually clog its conduits. Very polar, thermolabile, ionic and high-molecular weight compounds are not compatible with regular GC analysis. Depending on the molecular structure of the analyte and the functional groups available, it is possible in some cases to obtain a chemical derivative which has a higher vapor pressure and is therefore more amenable to GC analysis [Stashenko & Martínez, 2014].

Mass Spectrometry

A mass spectrometer (Figure 4) attached to the gas chromatograph consists of an ionization chamber which in the large majority of situations uses electron ionization or electron impact

(EI) to provide the energy to the analytes which could fragment and generate the ions to be detected. Ions formed in the ionization chamber are removed therefrom by a series of electrodes that collimate (focus) and accelerate and direct them to a mass analyzer. The potential energy created by the accelerating field (E) is converted into kinetic energy. The analyzer separates ions according to their m/z ratio. Several types of mass analyzers may be used in the GC-MS equipment. Quadrupole (Q) and ion trap (IT) are the most common; in recent years, there has been an increase in the use of time-of-flight analyzers (TOF) [Stashenko & Martínez, 2014].

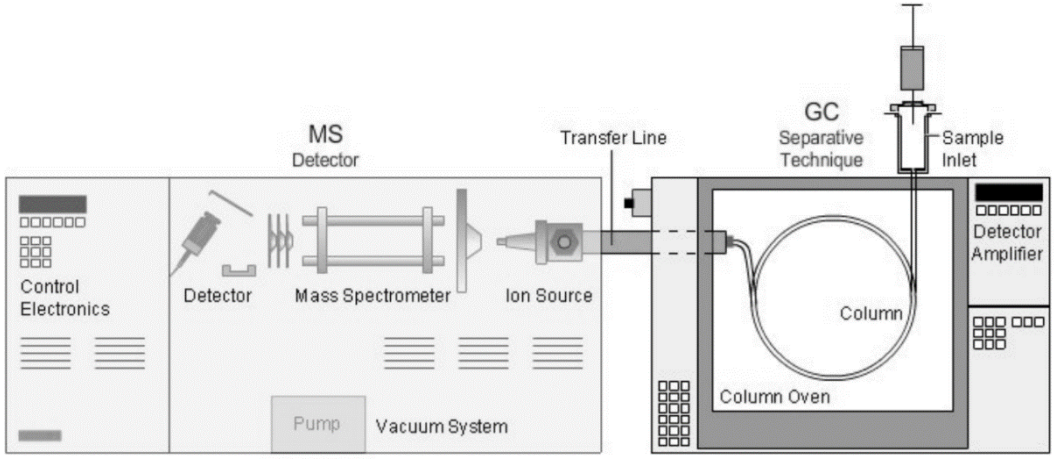

Figure 4. Schematic diagram of GC-MS system [Hussain & Maqbool, 2014].

Gas Chromatography – Mass Spectrometry

The need to unequivocally identify the components of complex mixtures was the motivation for the development of different instrumental coupling techniques (tandem), including the widely and successfully used (with volatilizable substances), gas chromatography coupled with mass spectrometry (MS). GC-MS is an extremely favorable, synergistic union, as the compounds susceptible to be analyzed by GC (low-molecular weight, medium or low polarity, in ppb-ppm concentration) are also compatible with the MS requirements. Besides both analyses proceed in the same aggregation state (vapor phase) [Stashenko & Martínez, 2014].

4.2.2.2 GC-MS Workflow

To obtain biomarker data the saturated and aromatic hydrocarbon fractions were analyzed by a gas chromatograph equipped with a 30 m DB-5MS fused silica column (i.d. 0.25 mm; 0.25 mm film thickness), coupled to a ThermoFisher ISQ dual-quadrupole mass spectrometer. Using He as a carrier gas, the oven temperature was programmed from 70°C to 300°C at 4°C/min increase, followed by an isothermal period of 15 min. The samples were injected splitlessly with an injector temperature of 275°C. The spectrometer was operated in the EI (electron ionization) mode over a scan range of *m/z* 50 to 650 at 0.7 s total scan time.
The GC-MS data were processed in an Xcalibur data system. Individual compounds were identified on the basis of retention time in the total ion current (TIC) chromatogram and comparison of the mass spectra with published data. Percentages and absolute concentrations of various compound groups in the saturated and aromatic hydrocarbon fractions were calculated using peak areas in the gas chromatograms and their relations to the internal standards (1,1-binaphthyl or deuterated *n*-tetracosane). The concentrations were normalized to TOC.

4.2.3 IR-MS

A short description of GC-MS method by Pedentchouk & Turich [2017] is given in 4.2.3.1. The workflow is described in 4.2.3.2.

4.2.3.1 IR-MS Overview

Figure 5 shows a simplified schematic of a GC-IRMS system equipped with a combustion reactor for $\delta^{13}C$ measurements. The *n*-alkane-containing fraction is injected into the GC, where compounds are separated on a capillary column and then converted to CO_2 in the reactor, using a source of O_2 and a catalyst. The CO_2 gas is then transferred into the mass spectrometer, where it is ionized. Faraday cups for *m/z* 44, 45 and 46 are then used to collect ions corresponding to $^{12}C^{16}O_2$, $^{13}C^{16}O_2$ and $^{12}C^{18}O^{16}O$ isotopomers, respectively (Other isotopomers potentially adding to *m/z* 45 and 46 are quantitatively insignificant). The $\delta^{13}C$ values of individual compounds are calculated relative to either a reference gas or a co-injected compound with a known isotopic $\delta^{13}C$ value [Pedentchouk & Turich, 2017].

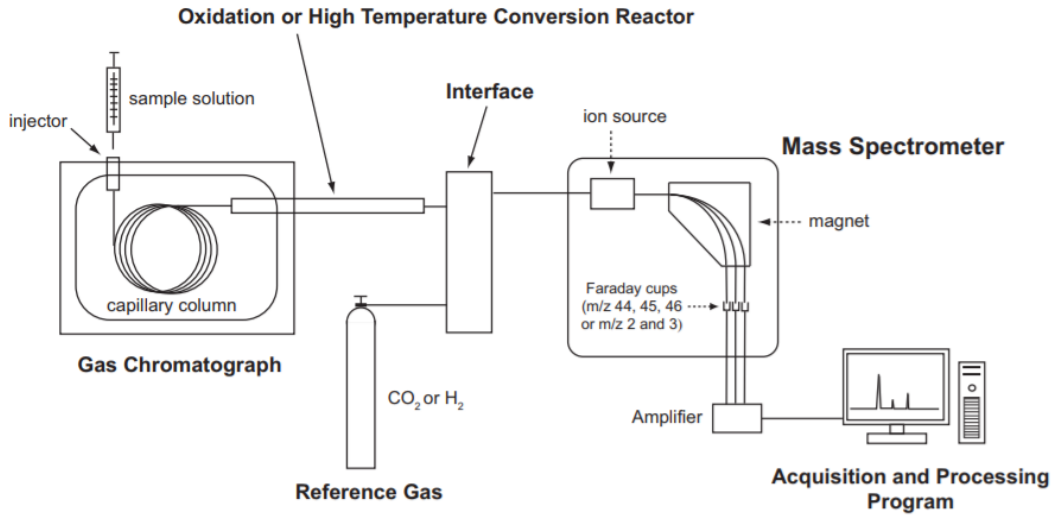

Figure 5. A simplied schmeatic of a GC-IRMS system for δ13C measurements [Pedentchouk & Turich, [2017].

4.2.3.2 IR-MS Workflow

The *n*-alkanes were separated from branched/cyclic hydrocarbons by an improved 5 Å molecular sieve method [Grice et al., 2008] for the analysis of stable carbon and hydrogen isotope ratios on individual *n*-alkanes and isoprenoids. Stable C and H isotope measurements were made using a Trace GC-ultra gas chromatograph attached to the ThermoFisher Delta-V isotope ratio mass spectrometer (irMS) via a combustion and high temperature reduction interface, respectively (GC Isolink, ThermoFisher). The GC coupled to the irMS was equipped with a 30 m DB-5MS fused silica capillary column (i.d. 0.25 mm; 0.25 lm film thickness). The oven temperature was programmed from 70–300°C at a rate of 4°C/min followed by an isothermal period of 15 min. Helium was used as carrier gas. The sample was not split and was injected at 275°C. For calibration, a CO_2 or H_2 standard gas was injected at the beginning and at the end of each analysis. Isotopic compositions are reported in the δ notation relative to the PDB for C ($\delta^{13}C=[(^{13}C/^{12}C)_{sample}/(^{13}C/^{12}C)_{std} - 1] *1000$). Analytical reproducibility (0.2‰ for $\delta^{13}C$) was controlled by repeated measurements of *n*-alkane standard mixes.

5 Results

5.1 Molasse Basin

5.1.1 Source rocks

5.1.1.1 Biomarker Composition

Core samples from the Molasse Basin included in the present study have been previously described by Schulz et al. [2002] (Oberschauersberg samples) and Pupp [2018] (samples from Bavaria).They are characterized by relative proportions of hydrocarbon fractions between 29 and 54% to fractions of nitrogen-, sulphur-, and oxygen-bearing (NSO) compounds and asphaltenes between 46 and 78%.

Gas Chromatograms (GC) of the saturated and aromatic hydrocarbons of four rocks, two from Bavaria and two from Oberschauersberg, respectively, are shown in Figure 6 and Figure 7 (additional chromatograms of all source rocks from the Molasse Basin are compiled in the Appendix). There are minor differences in the molecular composition of the hydrocarbons between the samples, as reflected by organic geochemical facies and maturation parameters (Table 3).

The saturated hydrocarbons are dominated by *n*-alkanes, steranes, and hopanes (Figure 6).

n-alkanes - The *n*-alkane distribution is diverse. It shows maximum intensities in all chain ranges in the Schöneck Formation, whereas maximum intensities lie in short chain (*n*-C_{15} to *n*-C_{19}) range in the Eggerding Formation, and mid (*n*-C_{21} to *n*-C_{25}) and long (*n*-C_{27} to *n*-C_{31}) chain range in the Dynow marl. A weak odd-over-even predominance of long-chain *n*-alkanes is indicated by carbon preference indices, CPI after Bray & Evans [1961], between 1.5 and 1.9 for Schöneck b (A-, Osch-1), Schöneck c (Osch-3), Schöneck a (Osch-4) and Eggerding Fm. (Osch-6). This reflects a contribution of higher land plants beside algae and microorganisms to the organic matter of the source rock as long-chain *n*-alkanes are thought to be primarily derived from waxes of higher land plants [Eglinton & Hamilton, 1967].

Acyclic isoprenoids - Pristane and phytane form from the phytyl side chain from chlorophyll-a molecule in phototrophic organisms under oxic (pristane) and anoxic (phytane) conditions [Didyk et al., 1978]. According to Didyk et al. [1978], pristane/phytane (Pr/Ph) ratios below 1.0 indicate anaerobic conditions during early diagenesis, whereas values above 1.0 were interpreted as reflecting oxic environments. However, Pr/Ph ratios can also be affected by maturation [Tissot & Welte, 1984] and by differences in the precursors of acyclic isoprenoids, i.e. bacterial origin [Volkman & Maxwell, 1986]. Pr/Ph ratios range from 1.3 to 2.2 in W. Bavaria (Schöneck c; Dynow Fm.) and from 0.7 to 1.1 in E. Bavaria (Schöneck b), and amount to 1.3 at Oberschauersberg (Schöneck a to Eggerding Fm.), reflecting stratigraphic (and spatial) trends in redox conditions. Pr/Ph ratio of unit a (Pr/Ph = 2.5) is very high. However, as the Schöneck Formation reportedly was deposited under highly anoxic conditions [Schulz et al., 2002], it is suggested, that differences in Pr/Ph precursors [Volkman & Maxwell, 1986] could have affected the Pr/Ph ratio. Unit c Pr/Ph ratios of 0.8 (Osch-3) and 2.9 (Osch-2) can be explained by the relative sample locations; the lower part of unit c, including sample Osch-3, was deposited in an anoxic environment, whereas the upper part of unit c, including sample Osch-2, was deposited under less anoxic conditions [Schulz et al., 2002; Sachsenhofer et al., 2010]. Dynow Formation Pr/Ph ratios of 2.5 and 3.6 in Oberschauersberg and 2.2 in W. Bavaria are consistent with literature, which has described the Dynow marl deposition to have occurred

under less oxygen-depleted conditions [Schulz et al., 2002; Sachsenhofer et al., 2010]. Pr/Ph ratios of the Eggerding Formation (Osch-5, Osch-6) range from 0.6 to 1.2.

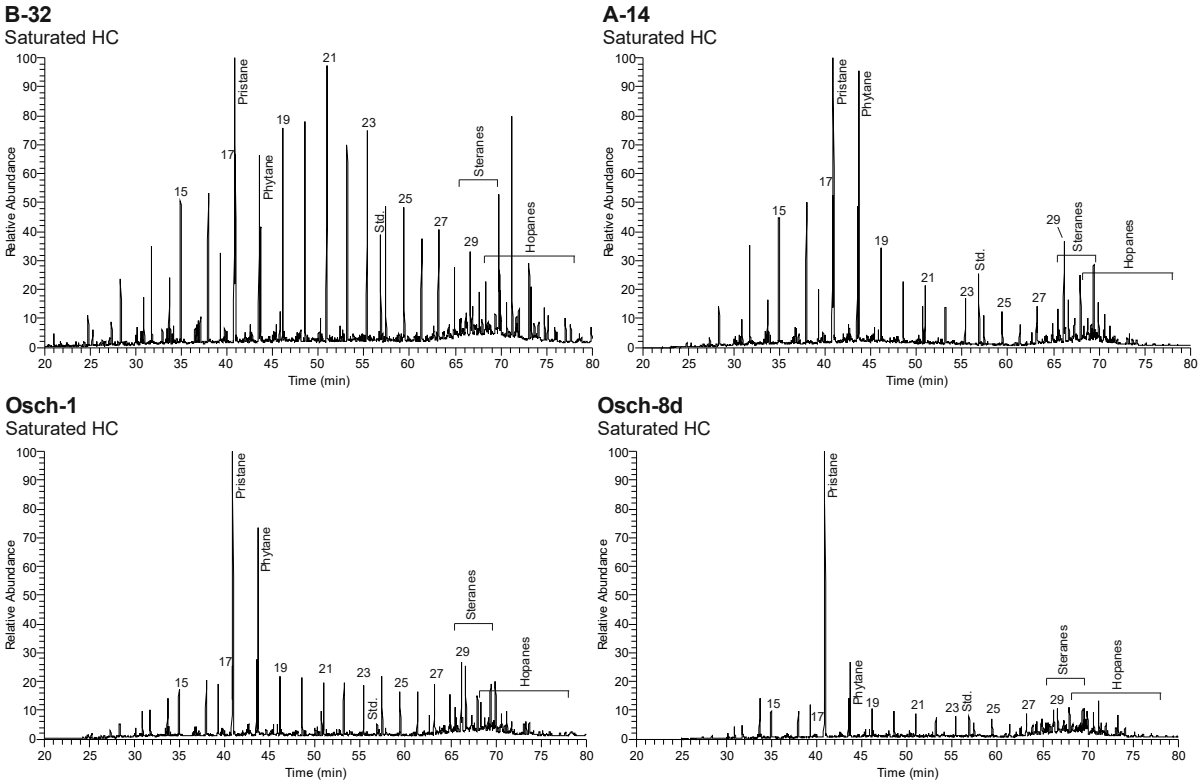

Figure 6. Chromatograms (Total Ion Current) of the saturated hydrocarbon fractions of core samples B-32 (Schöneck b), A-14 (Schöneck b), Osch-1 (Schöneck b) and Osch-8d (Dynow) from the Molasse Basin. *n*-Alkanes are labelled according to their carbon number. Std. = standard (1,1-binaphthyl).

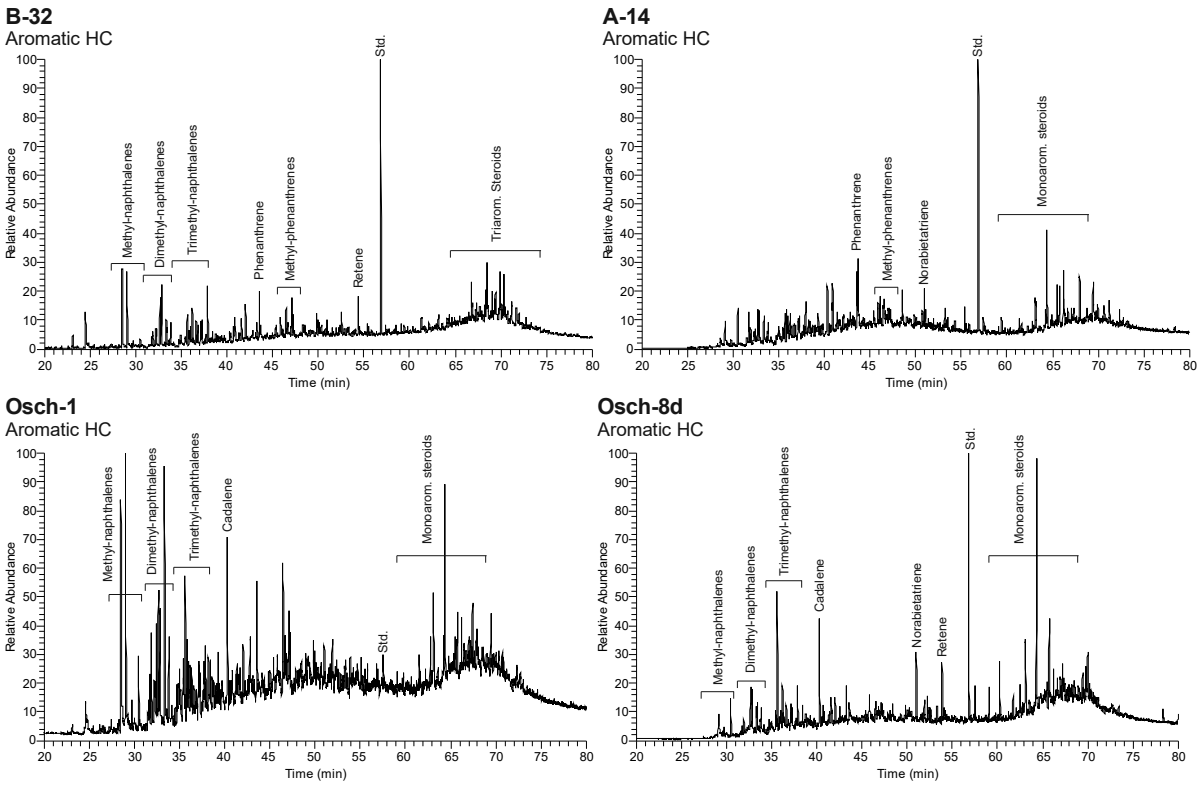

Figure 7. Chromatograms (Total Ion Current) of the aromatic hydrocarbon fractions of core samples B-32 (Schöneck b), A-14 (Schöneck b), Osch-1 (Schöneck b) and Osch-8d (Dynow) from the Molasse Basin. Std. = standard (1,1- binaphthyl).

Table 3. Bulk organic geochemical parameters, concentration and concentration ratios of specific biomarkers of source rocks from the Molasse Basin.

Sample	Formation	TOC (wt%)	HI	Tmax (°C)	Sat.HC (%)	Aro.HC (%)	N+A (%)	*n*-alk	*n*-C_{15-19}/ Σ*n*-alk.	*n*-C_{21-25}/ Σ*n*-alk.	*n*-C_{27-31}/ Σ*n*-alk.	CPI
W. Bavaria												
B-21	Dynow	2.37 [A]	644 [A]	432 [A]	27	19	54	5001	0.20	0.32	0.25	0.9
B-32	Schöneck c	8.58 [A]	637 [A]	436 [A]	35	17	49	5953	0.28	0.32	0.16	0.8
B-40	Schöneck c	4.30 [A]	514 [A]	430 [A]	41	13	46	9103	0.29	0.39	0.15	1.2
B-47	Schöneck c	2.15 [A]	473 [A]	428 [A]	37	17	46	5179	0.43	0.29	0.14	1.1
E. Bavaria												
A-01	Schöneck b	7.45 [A]	522 [A]	419 [A]	24	7	69	3560	0.26	0.34	0.23	1.6
A-09	Schöneck b	3.23 [A]	443 [A]	415 [A]	16	13	71	1180	0.46	0.19	0.23	1.6
A-14	Schöneck b	3.37 [A]	515 [A]	413 [A]	14	9	77	5905	0.48	0.21	0.21	1.6
Oberschauersberg												
Osch-5	Eggerding	n.a.	n.a.	n.a.	21	9	71	n.a.	0.37	0.26	0.24	1.0
Osch-6	Eggerding	n.a.	n.a.	n.a.	22	11	67	n.a.	0.35	0.27	0.29	1.5
Osch-8d	Dynow	2.13 [B]	632 [B]	426 [B]	17	14	69	1735	0.36	0.24	0.31	1.3
Osch-7d	Dynow	1.87 [B]	442 [B]	430 [B]	22	14	64	1625	0.32	0.24	0.34	1.3
Osch-2	Schöneck c	2.40 [B]	600 [B]	425 [B]	21	15	63	1870	0.38	0.29	0.23	1.1
Osch-3	Schöneck c	4.60 [B]	n.a. [B]	n.a.	17	9	74	4896	0.37	0.34	0.19	1.5
Osch-1	Schöneck b	3.00 [B]	501 [B]	411 [B]	12	10	78	596	0.30	0.27	0.32	1.9
Osch-4	Schöneck a	2.00 [B]	399 [B]	417 [B]	11	14	74	977	0.32	0.25	0.33	1.6

Sample	Pr/Ph [rel.prop]	Pri/*n*-C_{17} [rel.prop]	Ph/*n*-C_{18} [rel.prop]	Steranes (µg/gTOC)	Hopanes (µg/gTOC)	St/ Hop	OI (%)	ααα R+S Steranes C_{27}/ ΣC_{27-29}St.	ααα R+S Steranes C_{28}/ ΣC_{27-29}St.	ααα R+S Steranes C_{29}/ ΣC_{27-29}St.
W. Bavaria										
B-21	2.21	4.98	2.25	1469	587	2.50	12.6	0.30	0.37	0.33
B-32	1.40	2.58	1.85	1428	2567	0.55	7.0	0.29	0.34	0.37
B-40	2.08	1.91	0.84	554	893	0.62	18.3	0.37	0.30	0.32
B-47	1.33	2.68	1.95	492	250	1.96	33.0	0.43	0.30	0.27
E. Bavaria										
A-01	0.71	1.24	1.28	1333	1126	1.16	16.0	0.35	0.31	0.33
A-09	0.91	3.75	4.14	1038	328	3.16	32.2	0.40	0.33	0.27
A-14	1.09	2.18	2.49	321	149	2.14	26.6	0.37	0.33	0.30
Oberschauersberg										
Osch-5	0.67	4.35	5.41	n.a.	n.a.	7.92	24.4	0.24	0.43	0.34
Osch-6	1.19	2.62	2.39	n.a.	n.a.	7.10	23.2	0.26	0.44	0.31
Osch-8d	3.64	10.58	2.82	619	809	0.77	10.8	0.28	0.42	0.30
Osch-7d	2.48	11.01	3.33	797	865	0.92	13.2	0.25	0.41	0.34
Osch-2	2.86	9.09	1.39	870	1033	0.84	20.8	0.31	0.33	0.36
Osch-3	0.81	3.53	3.86	1966	865	2.27	17.0	0.46	0.32	0.22
Osch-1	1.31	7.06	4.40	634	380	1.66	34.9	0.40	0.30	0.30
Osch-4	2.45	6.73	2.09	71	206	0.34	50.4	0.39	0.28	0.33

(TOC: total organic carbon; HI: hydrogen index in mg HC/g TOC; Sat.HC: saturated hydrocarbon; Aro.HC: aromatic hydrocarbons; N+A: NSO compounds + asphaltenes; n-alk: n-alkane concentration in µg/g TOC; CPI: carbon preference index; Pr/Ph: pristane/phytane ratio; St/Hop: steranes / hopanes; OI: oleanane index)
[A] Pupp [2018]; [B] Schulz [2003]

The ratio between pristane and phytane and *n*-alkanes are controlled by the type and maturity of organic matter and by biodegradation. High Pr/*n*-C_{17} and Ph/*n*-C_{18} ratios indicate lower algal and bacterial sedimentary matter input to the source rocks, as these compounds contain smaller quantities of *n*-alkanes relative to acyclic isoprenoids compared to higher land plants [Tissot & Welte, 1984]. As *n*-alkanes are preferably removed during biodegradation, Pr/*n*-C_{17} and Ph/*n*-C_{18} ratios increase with biodegradation. Figure 8 shows a cross-plot of Pr/*n*-C_{17} versus Ph/*n*-C_{18} for all rock and oil samples. The samples from Oberschauersberg overall show higher Pr/*n*-C_{17} and Ph/*n*-C_{18} ratios than the samples from Bavaria. An immature to early mature stage for all samples is indicated after Connan & Cassou [1980] and is consistent with low T_{max} values (Table 3). Dynow marl of Oberschauersberg (Osch-7d, Osch-8d) with Pr/*n*-C_{17} ratio above 10 is not displayed on the diagram.

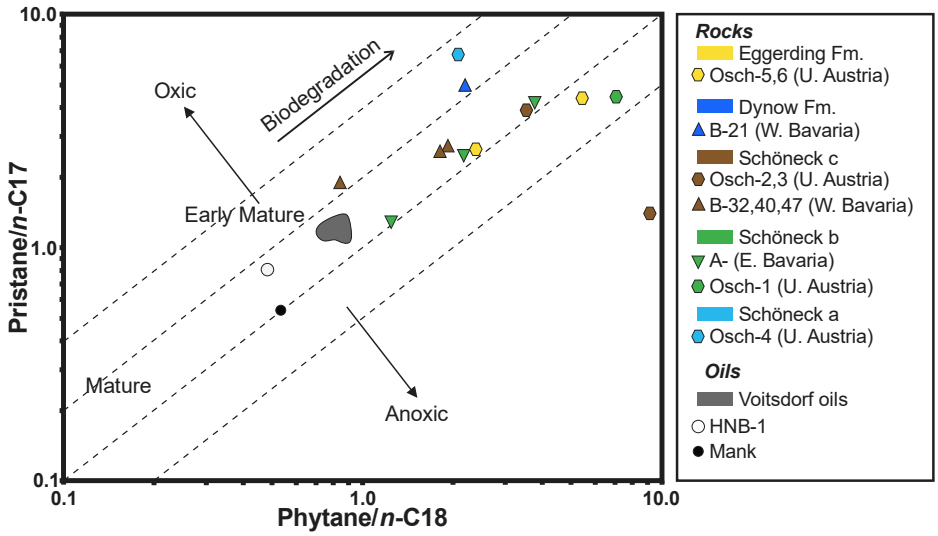

Figure 8. Correlation diagram of pristane/*n*-C17 ratios versus phytane/*n*-C18 ratios of rock and oil samples from the Molasse Basin for the assessment of oil sources, as well as the effects of maturation and biodegradation (modified after Connan & Cassou [1980]).

Steranes and hopanes – Algae are thought to be the biological source of C_{27} steranes, whereas C_{29} steranes are thought to be primarily sourced from higher land plants [Volkman & Maxwell, 1986]. The relative proportion of these compounds can therefore be used as an environmental indicator [Huang & Meinschein, 1979]. Figure 9 shows a triangalur plot of the relative distributions of C_{27}, C_{28} and C_{29} ααR+S steranes. Transitional depositional environments of open marine to estuarine/bay are suggested for Schöneck Fm. and Dynow Fm. / Eggerding Fm. respectively. Samples from the Dynow and Eggerding formations are slightly enriched in C_{28} steranes. These results are consistent with literature [Sachsenhofer et al., 2010].

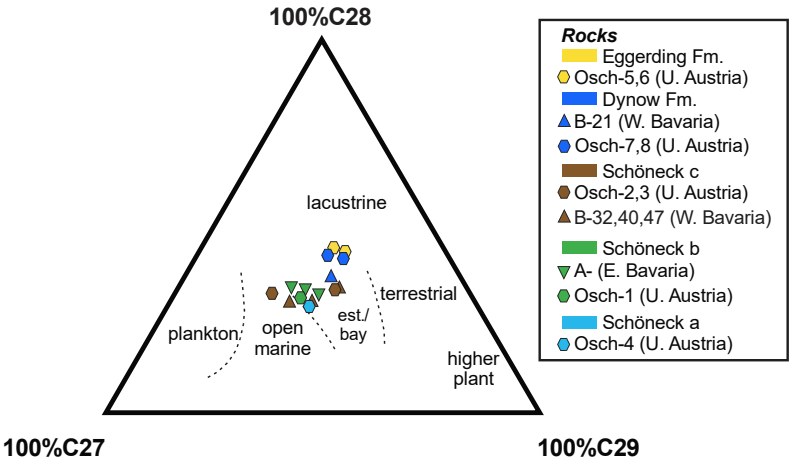

Figure 9. Ternary diagram of relative proportions of C27, C28 and C29 steranes in samples from Molasse Basin source rocks (modified after Huang & Meinschein [1979]).

Biological precursors of hopanes are mainly prokaryotes (i.e. bacteria) [Ourisson et al., 1979], whereas sterane precursors are mainly eukaryotes (i.e. algae, land plants). Hence sterane/ hopane ratios (St/Hop) can be used as a measure of organic matter production by eukaryotes versus bacterial activity. Low sterane/hopane ratios are considered to indicate lacustrine or special, bacterial influenced facies, whereas high ratios (> 1.0) are indicative of marine organic facies [Mackenzie, 1984]. In unit b St/Hop ratios > 1.0 are consistent with marine organic facies [Sachsenhofer et al., 2010]. Unit c shows varying St/Hop ratios between 0.6 and 2.0 in W. Bavaria and 0.8 and 2.3 in Oberschauersberg, which indicate varying environments; this is confirmed at least in Oberschauersberg by different redox conditions during deposition of the

lower and upper parts of unit c [Schulz et al., 2002; Sachsenhofer et al., 2010]; the lower part (sample Osch-3), which was deposited in an anoxic environment, has a high St/Hop ratio (2.3), whereas the upper part (Osch-2), with a low St/Hop ratio (0.8), was deposited under less anoxic conditions.

Oleanane in crude oils and rock extracts is a marker for both source input and geologic age. This compound originates from products (i.e. betulins) of angiosperms. Based on tentative fossil evidence, angiosperms probably originated in the Triassic Period or earlier [Peters & Moldowan, 1993]. Nevertheless, the occurrence of (significant amounts of) oleanane indicates an age of Late Cretaceous or younger. Oleanane is quantified by the oleanane index OI = (Oleanane / C_{30} Hopane) x 100. The source rocks of the Molasse Basin show strongly varying, but typically high oleane index values (Table 3).

Aromatic hydrocarbons - Aromatic hydrocarbon fractions show high intensities of methylated (C_1 to C_4) naphthalenes and monoaromatic steroids (Figure 7). Additional compounds present in considerable quantities are higher plant biomarkers. Cadalene is present in all samples, whereas norabietatriene, simonellite, and retene, all more specific markers for conifers [Peters & Moldowan, 1993], are found in the upper part of Eggerding Fm, Dynow, and the upper part of unit c. Terrestrial influence, already indicated previously, is suggested, however, a marine setting can not be excluded, as retene and cadalene have been proven to also occur in marine sedimentary rocks [van Aarssen et al., 2000].

5.1.1.2 Isotope Ratios

The data on $\delta^{13}C$ obtained from GC-IRMS are listed in Table 4. Figure 10 illustrates a graphical presentation of the GC-IRMS results.

The obtained $\delta^{13}C$ values show regional variations. For example, the mean $\delta^{13}C$ of *n*-C_{17} varies from -29.6‰ in the western Bavaria (B-) to -28.7‰ in eastern Bavaria (A-), and -30.5‰ in Upper Austria (Osch-). The isotopically lightest unit is Schöneck c (Osch-2, Osch-3) with -30.9‰ mean $\delta^{13}C$ (*n*-C_{17}), followed by Schöneck a (Osch-4). This result corresponds well with Schulz et al. [2002], who found that the black shales from Schöneck c show isotopically lighter $\delta^{13}C$ values of organic matter compared with the relatively heavy values in units a and b. Interestringly, the lower part of unit c (anoxic), shows smaller $\delta^{13}C$ values up to *n*-C_{18}, and higher $\delta^{13}C$ values from *n*-C_{20} upwards, than the upper part of unit c (less anoxic). Dynow marl represents the isotopically heaviest Oberschauersberg samples.

All samples except the Eggerding Formation show a characteristic V shape pattern, reflecting a decrease in $\delta^{13}C$ values from *n*-C_{17} to *n*-C_{21} and an increase thereafter, with lowest $\delta^{13}C$ values at *n*-C_{21} up to -32.7‰ in Schöneck c (Osch-2). This maybe explained as a result from the loss of light hydrocarbons [Bechtel et al., 2013]. However, decreasing $\delta^{13}C$ values of short chain *n*-alkanes have been reported from numerous oils and marine source rocks [Bjorøy, 1994], and the V shape pattern has been found outside the Molasse Basin in oils [Cheng et al., 2015].

Table 4. Carbon isotopic composition of individual *n*-alkanes of source rocks from the Molasse Basin.

	n-C16	*n*-C17	*n*-C18	*n*-C19	*n*-C20	*n*-C21	*n*-C22	*n*-C23	*n*-C24	*n*-C25	*n*-C26	*n*-C27	*n*-C28	*n*-C29
	δ13C (‰; PDB)													
W. Bavaria														
B-21	-28.5	-29.0	-29.4	-29.6	-30.0	-30.4	-31.0	-30.7	-30.5	-30.2	-29.9	-29.4	-29.1	-28.7	-28.8
B-32	-28.9	-29.1	-29.6	-29.9	-30.4	-31.0	-31.4	-31.3	-31.0	-30.8	-30.4	-29.9	-29.6	-29.2	-29.3
B-40	-28.4	-29.1	-29.5	-30.1	-30.4	-31.1	-31.6	-31.4	-30.9	-30.8	-30.3	-29.8	-29.5	-29.1	-29.4
B-47	-28.9	-29.2	-29.8	-29.7	-30.1	-30.8	-31.5	-31.1	-30.7	-30.6	-30.2	-29.7	-29.4	-29.1	-29.3
E. Bavaria														
A-01	-28.1	-28.3	-28.9	-29.4	-30.0	-30.4	-30.9	-30.7	-30.2	-29.7	-29.2	-28.8	-28.6	-28.3	-28.4
A-09	-27.5	-27.9	-28.4	-28.8	-29.4	-30.0	-30.7	-30.5	-30.0	-29.6	-29.2	-29.0	-28.6	-28.3	-28.1
A-14	-27.7	-27.8	-28.8	-29.2	-29.7	-30.3	-31.0	-30.8	-30.4	-29.8	-29.3	-28.8	-28.5	-28.3	-28.1
Oberschauersberg														
Osch-5	-29.7	-30.5	-30.7	-31.3	-31.4	-31.5	-31.5	-31.7	-31.5	-31.4	-31.7	-31.8	-31.4	-31.6	
Osch-6	-29.5	-29.9	-30.5	-31.1	-31.0	-31.2	-31.3	-31.7	-31.4	-31.2	-31.5	-31.7	-31.6	-31.4	
Osch-8d	-29.3	-29.4	-29.6	-30.2	-30.8	-31.1	-31.3	-30.9	-30.9	-30.3	-30.1	-29.8	-29.7		
Osch-7d	-28.8	-29.4	-29.8	-30.4	-30.7	-30.9	-31.2	-31.0	-30.8	-30.5	-30.3	-29.9	-29.6		
Osch-2	-29.5	-30.3	-30.7	-31.2	-31.8	-32.0	-32.7	-31.8	-31.5	-31.1	-30.6	-30.2	-29.8	-29.7	
Osch-3	-29.4	-30.4	-31.0	-31.6	-31.8	-31.8	-32.5	-31.7	-31.3	-30.9	-30.7	-30.1	-29.8	-29.6	
Osch-1	-29.8	-30.2	-30.5	-31.0	-31.6	-31.7	-32.4	-31.5	-31.2	-30.8	-30.5	-30.3	-29.9	-29.7	
Osch-4		-30.3	-30.9	-31.3	-31.7	-31.9	-32.6	-31.5	-31.4	-31.1	-30.7	-30.2	-30.0	-29.7	

PDB = Peedee Belemnite (int. Standard)

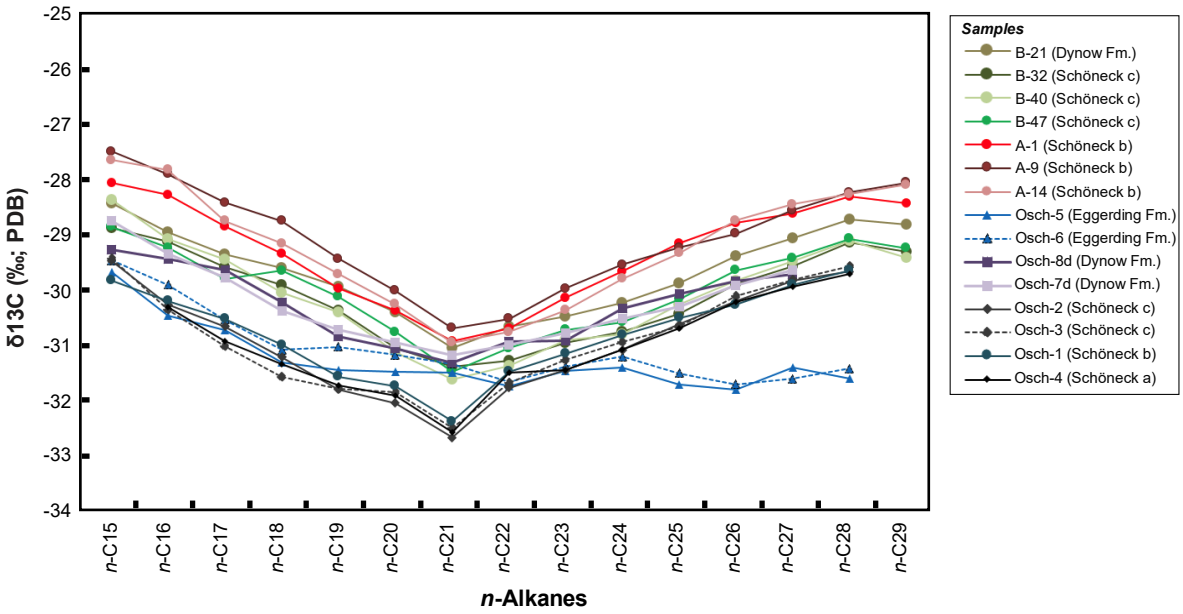

Figure 10. Carbon isotopic composition of individual *n*-alkanes of source rocks from the Molasse Basin.

5.1.2 Oils

5.1.2.1 Biomarker Composition

The oil samples from the Molasse Basin are characterized by relative proportions of hydrocarbon fractions between 12 and 52% and NSO compounds plus asphaltenes between 30 and 83%. The lowest proportions of saturated hydrocarbons (12%, 16%, 17%) occur in Voitsdorf oils V-21, V-11 and in the shallow (157 m) oil stain from borehole Mank-1 (sample Mank-157). In the remaining oil samples relative proportions of saturated hydrocarbons are similar (average 45%). API gravity data from Gratzer et al. [2011] show a value of 35° API for the Voitsdorf oil, classifying this oil as light crude oil [Tissot & Welte, 1984].

Gas Chromatograms (GC) of the saturated and aromatic hydrocarbons of four oils (Voitsdorf [V]-8; V-23; Haidenbach [HNB]-1, Mank-157) are shown in Figure 11 and Figure 12 (additional chromatograms of all oils from the Molasse Basin are compiled in the Appendix). Major differences in the molecular composition of the hydrocarbons exist between Voitsdorf and Haidenbach oils and Mank oil stains. Concentrations and concentration ratios in the hydrocarbon fractions are listed in Table 5. GC traces of Voitsdorf oils from Gratzer et al. [2011]

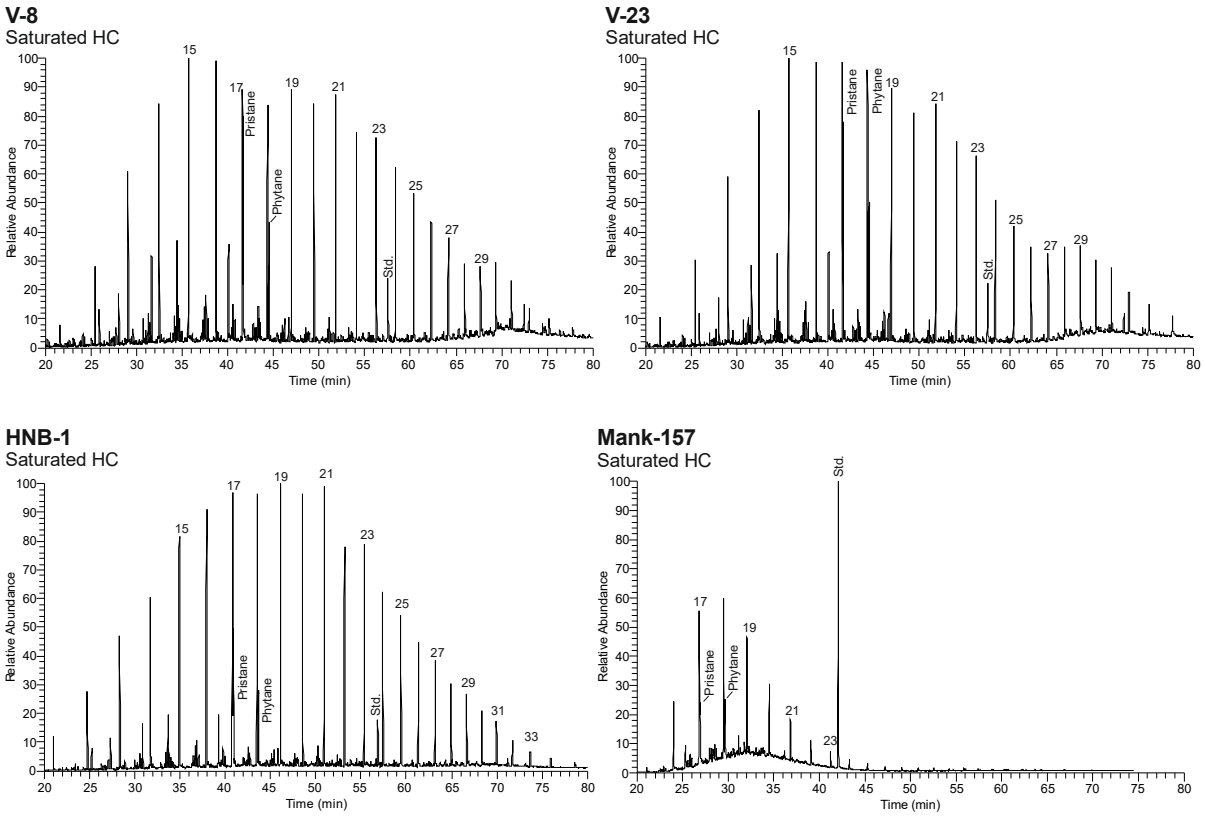

Figure 11. Chromatograms (Total Ion Current) of the saturated hydrocarbon fractions of Molasse oil samples V-8, V-23, HNB-1 & Mank-157. *n*-Alkanes are labelled according to their carbon number. Std. = standard (deuterated n-tetracosane: V- samples; 1,1-binaphthyl: HNB-1 and Mank-157 samples).

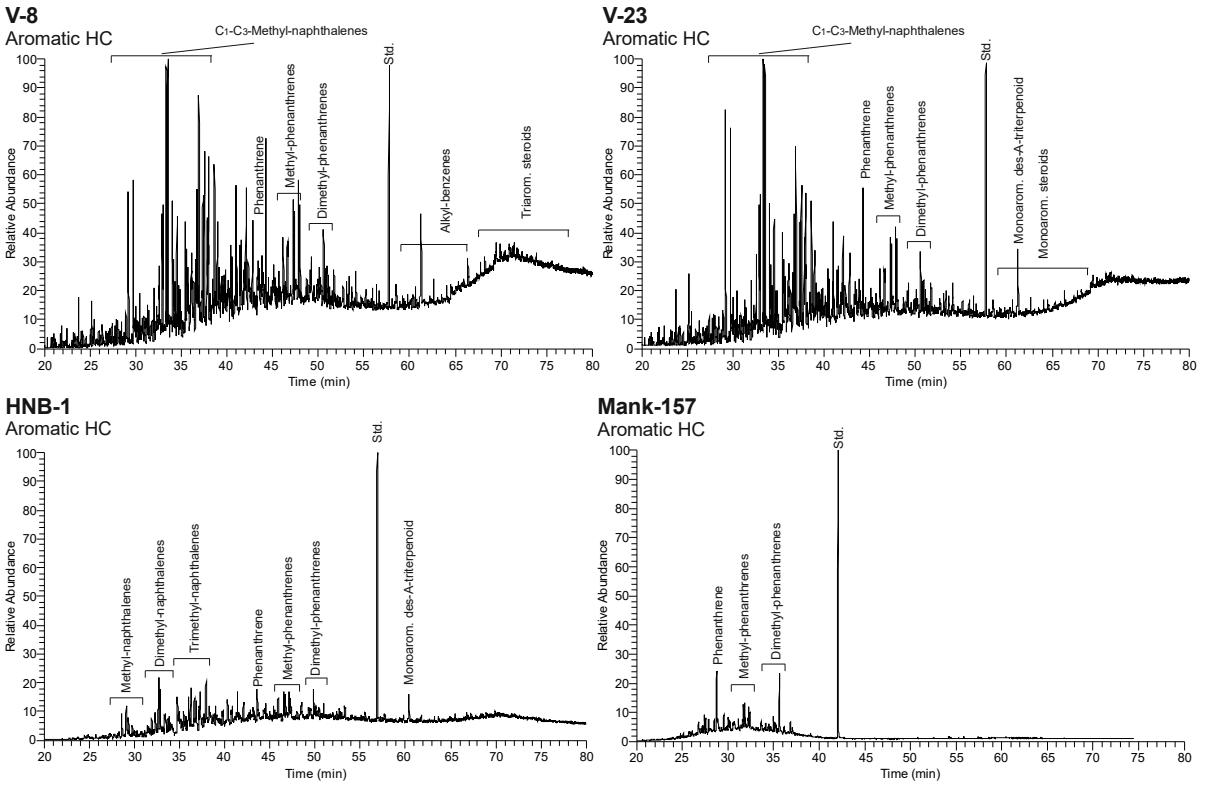

Figure 12. Chromatograms (Total Ion Current) of the aromatic hydrocarbon fractions of Molasse oil samples V-8, V-23, HNB-1 & Mank-157. Std. = standard (deuterated n-tetracosane: V- samples; 1,1-binaphthyl: HNB-1 and Mank-157 samples).

differ significantly from the GC traces presented here due to different measuring methods. Gratzer et al. [2011] used a GCQ ion trap MS that prefers fragments with higher masses; which led to higher intensity appearing of high-molecular compounds.

The saturated hydrocarbons consist of *n*-alkanes, steranes are present only in very low concentrations. The GC traces of Voitsdorf and Haidenbach oils differ strongly from Mank oil stains, as the oil stains are strongly depleted in saturated and aromatic hydrocarbons.

Table 5. Organic geochemical parameters, concentration and concentration ratios of specific biomarkers of oils from the Molasse Basin.

Sample	Gr.[A] (API°)	Sat.HC (%)	Aro HC (%)	N+A (%)	*n*-C_{15-19}/ Σ*n*-alk.	*n*-C_{21-25}/ Σ*n*-alk.	*n*-C_{27-31}/ Σ*n*-alk.	CPI	Pr/Ph [rel.prop]	Pr/*n*-C_{17} [rel.prop]	Ph/*n*-C_{18} [rel.prop]	MPI-1[A]	OI (%)
Voitsdorf													
V-01	35	52	18	30	0.33	0.35	0.16	1.1	1.43	1.11	0.84	0.77	9.4
V-02	35	41	15	44	0.33	0.32	0.16	1.1	1.48	1.09	0.89	0.76	10.7
V-08	35	44	15	41	0.33	0.34	0.15	1.1	1.84	1.17	0.74	0.80	9.1
V-11	35	16	6	79	0.33	0.11	0.10	0.3	1.35	1.37	0.87	0.77	10.3
V-13	35	50	16	35	0.33	0.34	0.15	1.0	1.88	1.23	0.74	0.78	11.8
V-15	35	48	16	36	0.33	0.24	0.15	1.0	1.47	1.15	0.81	0.77	10.0
V-19	35	37	13	50	0.33	0.33	0.16	1.1	1.51	1.08	0.89	0.77	8.7
V-21	35	12	4	83	0.33	0.05	0.13	0.5	1.44	1.10	0.74	n.a	9.4
V-23	35	38	13	49	0.33	0.37	0.10	1.4	1.56	1.14	0.79	0.78	8.9
V-33	35	n.a.	n.a.	n.a	0.33	0.16	0.16	n.a.	1.50	1.12	0.77	0.79	10.5
V-39	35	49	18	34	0.33	0.34	0.14	1.0	1.85	1.15	0.72	0.78	11.0
V-41	35	48	17	35	0.33	0.24	0.13	1.4	1.88	1.26	0.72	0.78	10.1
Haidenbach													
HNB-1	n.a.	45	10	45	0.33	0.37	0.14	1.4	1.70	0.87	0.48		6.5
Mank													
Mank-157	n.a.	17	7	76	0.73	0.15	0.00	3.4	0.95	0.54	0.54	n.a.	0

(Gr: gravity; API: american petroleum institute; Sat.HC: saturated hydrocarbon; Aro.HC: aromatic hydrocarbons; N+A: NSO compounds + asphaltenes; CPI: carbon preference index; Pr/Ph: pristane/phytane ratio, MPI-1: methylphenanthrene index; OI: oleanane index)

[A]Data from [Gratzer et al., 2011]

n-alkanes - *n*-alkane distribution shows maximum intensities in the short and mid chain range (Figure 11). The small concentrations of long-chain *n*-alkanes in all oils is consistent with little higher plant contribution to the organic matter composition of the source rock, although higher maturity, as indicated by methylphenanthrene indices between 0.77 and 0.80, could have played a role as well. The average CPI of Voitsdorf oils is 1.0.

acyclic isoprenoids - pristane/phytane ratios exceed 1.0 for Voitsdorf oils (average Pr/Ph ratio: 1.6) and the Haidenbach oil (Pr/Ph: 2.1), and below 1.0 for oil stains in borehole Mank (Pr/Ph: 0.95). Low Pr/*n*-C_{17} and Ph/*n*-C_{18} ratios reflect a higher degree of maturity compared to that of the studied (immature) source rocks (Figure 8).

steranes and hopanes – oleanane indices in the Voitsdorf oils are high and vary between 8.4 and 11.8. The Haidenbach oil shows a smaller value (OI: 6.5). Mank oil stains do not contain oleanane.

Aromatic hydrocarbons - Aromatic hydrocarbon fractions show high intensities of methylated (C_1 to C_3) phenanthrenes in all Molasse oils, as well as high abundancies of methylated (C_1 to C_4) naphthalenes, alkylated (C_{17} to C_{19}) benzenes, monoaromatic steroids and presence of angiosperm biomarker monoaromatic des-A-triterpenoid in Voitsdorf and Haidenbach oils (Figure 12).

5.1.2.2 Isotope Ratios

The data on $\delta^{13}C$ obtained from GC-IRMS are listed in Table 6. Figure 13 illustrates a graphical presentation of the GC-IRMS results.

Table 6. Carbon isotopic composition of individual *n*-alkanes of oils from the Molasse Basin.

	n-C15	*n*-C16	*n*-C17	*n*-C18	*n*-C19	*n*-C20	*n*-C21	*n*-C22	*n*-C23	*n*-C24	*n*-C25	*n*-C26	*n*-C27	*n*-C28	*n*-C29
	δ13C (‰; PDB)														
Voitsdorf															
V-01	-29.8	-30.0	-30.9	-31.2	-32.2	-32.2	-33.1	-31.7	-31.7	-31.0	-30.9	-30.6	-30.4	-30.2	-30.8
V-02	-30.1	-30.4	-31.1	-31.6	-32.5	-32.3	-33.3	-31.8	-31.7	-30.9	-30.8	-30.5	-30.3	-30.8	-31.1
V-08	-30.7	-30.7	-31.2	-31.5	-32.4	-32.3	-33.3	-31.8	-31.4	-31.0	-30.7	-31.0	-30.4	-30.7	-30.9
V-11	-30.0	-31.0	-31.3	-31.3	-32.3	-32.1	-32.9	-31.6	-31.6	-30.8	-31.0	-30.4	-30.9	-31.1	-31.2
V-13	-30.2	-30.5	-31.0	-31.6	-32.3	-32.3	-33.4	-31.9	-31.7	-31.1	-31.0	-30.7	-30.7	-30.4	-30.9
V-15	-30.0	-30.9	-31.4	-31.7	-32.4	-32.7	-33.3	-31.6	-31.8	-30.9	-30.7	-30.6	-30.9	-30.4	-30.7
V-19	-30.2	-30.3	-31.0	-31.4	-32.5	-32.2	-33.3	-31.7	-31.9	-31.1	-31.0	-30.5	-30.6	-30.7	-30.9
V-21	-29.7	-30.1	-30.8	-31.4	-32.5	-32.3	-33.6	-31.8	-31.9	-31.1	-31.1	-30.3	-30.6	-30.5	-30.7
V-23	-30.0	-30.1	-31.0	-31.6	-32.5	-32.5	-33.6	-32.1	-31.8	-31.0	-30.9	-30.9	-30.7	-30.3	-31.1
V-33	-29.9	-30.0	-30.9	-31.6	-32.7	-32.6	-33.6	-32.3	-31.9	-31.1	-31.2	-30.2	-30.9	-30.1	-31.0
V-39	-30.0	-30.1	-31.1	-31.7	-32.8	-32.6	-33.6	-32.1	-32.0	-30.9	-30.9	-30.6	-30.7	-30.3	-31.1
V-41	-30.2	-30.3	-31.2	-31.7	-32.9	-33.0	-33.7	-31.9	-31.9	-31.0	-31.1	-30.8	-31.2	-30.7	-31.1
Haidenbach															
HNB-1	-29.5	-29.6	-30.0	-30.6	-31.3	-31.5	-32.3	-31.4	-31.0	-30.6	-30.3	-30.3	-30.1	-29.7	-29.8
Mank															
Mank-157			-27.3	-27.5	-27.9	-28.0	-27.9	-28.1	-28.0	-28.2	-28.6	-28.8	-29.0	-28.9	-28.5

PDB = Peedee Belemnite (int. Standard)

The Voitsdorf and Haidenbach oils differ sharply from Mank oil stains, both in terms of isotopic weight and isotopic distribution.

Voitsdorf oils with a mean $\delta^{13}C$ (*n*-C_{17}) of -31.1‰ are on average 1.1‰ isotopically lighter than the Haidenbach oil with $\delta^{13}C$ (*n*-C_{17}) of -30.0‰. Mank oil with $\delta^{13}C$ (*n*-C_{17}) of -27.3‰ is isotopically very heavy. Biodegradation, in which ^{12}C is preferably removed and thus ^{13}C enriched due to energy [Clayton, 1991] might be an explanation.

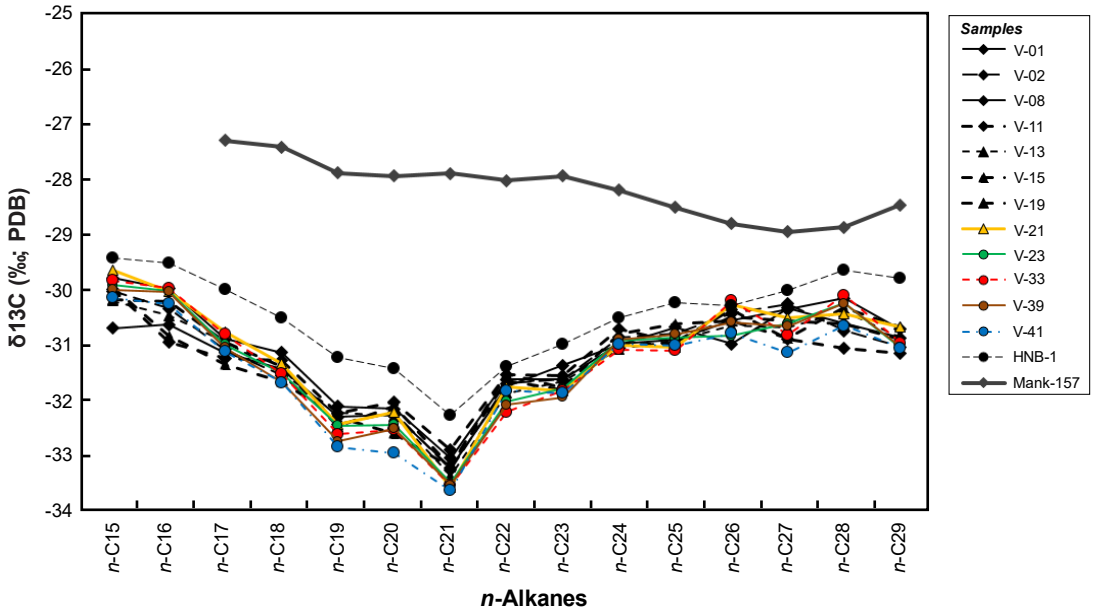

Figure 13. Carbon isotopic composition of individual n-alkanes of oils from the Molasse Basin.

5.2 Calcareous Alps

5.2.1 Bächental Marls

5.2.1.1 Biomarker Composition

Biomarker compositions of a high number of Bächental marls have been determined by Neumeister et al. [2015]. Three representing samples of Subunit 2 of the Middle Allgäu Formation (Sachrang Member) [Neumeister et al., 2015] were re-investigated in the frame of this thesis.

Gas Chromatograms (GC) of the saturated and aromatic hydrocarbons of sample BT-25, are shown in Figure 14 (additional chromatograms of all rock samples from the Calcareous Alps are compiled in the Appendix). There are only minor differences in the molecular composition of the hydrocarbons between the samples, as reflected by organic geochemical facies and maturation parameters (Table 7). GC traces of Bächental bituminous marls from Neumeister et al. [2015] differ from the GC traces presented here due to different measuring methods.

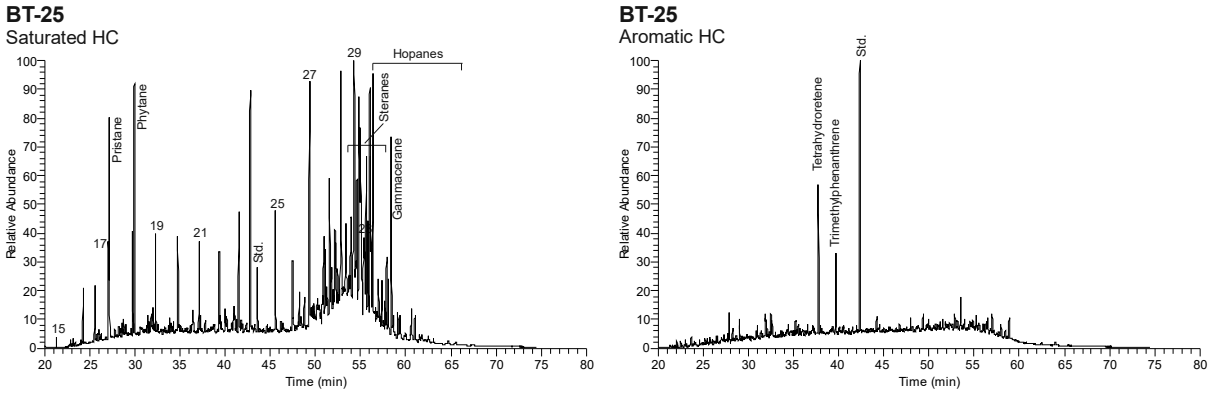

Figure 14. Chromatograms (Total Ion Current) of the saturated and aromatic hydrocarbon fractions of rock sample BT-25 from the Bächental bituminous marls (Calc. Alps). *n*-Alkanes are labelled according to their carbon number. Std. = standard (deuterated n-tetracosane).

Table 7. Bulk organic geochemical parameters, concentration and concentration ratios of samples of the Bächental bituminous marls from the Calcareous Alps.

Sample	TOC[A] (wt%)	HI[A]	*n*-C_{15-19}/ Σ*n*-alk.	*n*-C_{21-25}/ Σ*n*-alk.	*n*-C_{27-31}/ Σ*n*-alk.	CPI	Pr/Ph [rel.prop]	Pri/*n*-C_{17} [rel.prop]	Ph/*n*-C_{18} [rel.prop]	St/ Hop	GI[A] (%)
BT-35	9.40	666	0.26	0.30	0.32	1.24	0.91	3.58	4.20	1.0	0.80
BT-26	7.60	653	0.25	0.26	0.39	2.81	0.86	3.83	4.28	1.6	0.71
BT-25	12.90	622	0.20	0.28	0.39	2.09	0.86	3.53	3.97	1.1	0.77

	ααα R+S Steranes		
	C_{27}/ ΣC_{27-29}St.	C_{28}/ ΣC_{27-29}St.	C_{29}/ ΣC_{27-29}St.
BT-35	0.24	0.33	0.42
BT-26	0.26	0.31	0.43
BT-25	0.21	0.34	0.45

(TOC: total organic carbon; HI: hydrogen index in mg HC/g TOC; CPI: carbon preference index; Pr/Ph: pristane/phytane ratio; GI: gammacerane index; OI: oleanane index)
[A]data from Neumeister et al. [2015]

The Bächental bituminous marls are thermally immature (T_{max}: 416–427°C; 0.45 $\%R_c$) [Neumeister et al., 2015]. This is also reflected by (a) the *n*-alkane distribution with maximum intensities in the long chain range (b) high CPI values (c) high Pr/*n*-C_{17} and Ph/*n*-C_{18} ratios (d) the ratio of aromatic biomarkers tetrahydroretene and trimethylphenanthrene. Tetrahydroretene has been found to be a precursor of trimethylphenanthrene, and the concentration of trimethylphenanthrene supposedly increases over the concentration of tetrahydroretene with increasing maturity [Moldowan et al., 1985].

In the extensive work of Neumeister et al. [2015], a restricted, anoxic, highly saline marine environment was interpreted for the deposition of the Bächental bituminous marls. This is consistent with (a) low Pr/Ph ratios - which on the basis of limited thickness (~6 m) and similar isotopic composition have been reported as not have been influenced by maturation or different precursors for isoprenoids [Neumeister et al., 2015], (b) high abundance of gammacerane, and (c) sterane/hopane ratios > 1.0, which indicate marine organic facies [Mackenzie, 1984]. The predominance of C_{29} steranes in the sterane fraction can only be explained with other precursors than higher land plants.

Gammacerane is a biomarker for water column stratification - commonly associated with elevated salinity and restricted lakes [Sinninghe et al., 1995]. Although gammacerane can occur also outside such deposits [Sinninghe et al., 1995], the occurrence of bottom waters with elevated salinity in the Bächental Basin has been confirmed by increased hopane isomerization ratios, which result from diagenetic processes specific for hypersaline conditions [Neumeister et al., 2015]. The gammacerane indices (GI = gammacerane / (gammacerane + αβ C30 hopane)) presented in Table 7 have been calculated by [Neumeister et al., 2015] and range from 0.71 to 0.80.

Oleanane does not occur in the samples, as can be expected of rocks of this age.

5.2.1.2 Isotope Ratios

The data on $\delta^{13}C$ obtained from GC-IRMS are listed in Table 8. Figure 15 illustrates a graphical presentation of the GC-IRMS results.

Table 8. Carbon isotopic composition of individual *n*-alkanes of samples of the Bächental bituminous marls from the Calcareous Alps.

Sample	*n*-C16	*n*-C17	*n*-C18	*n*-C19	*n*-C20	*n*-C21	*n*-C22	*n*-C23	*n*-C24	*n*-C25	*n*-C26	*n*-C27
	δ13C (‰; PDB)											
BT-35	-31.5	-31.8	-32.1	-32.3	-32.5	-31.9	-31.8	-31.6	-31.0	-30.6	-30.3	-30.2
BT-26		-31.4	-31.7	-32.2	-32.3	-32.0	-31.7	-31.5	-31.2	-30.8	-30.6	-30.5
BT-25	-31.3	-31.5	-31.8	-32.1	-31.9	-31.6	-31.7	-31.3	-30.8	-30.7	-30.5	-30.3

PDB = Peedee Belemnite (int. Standard)

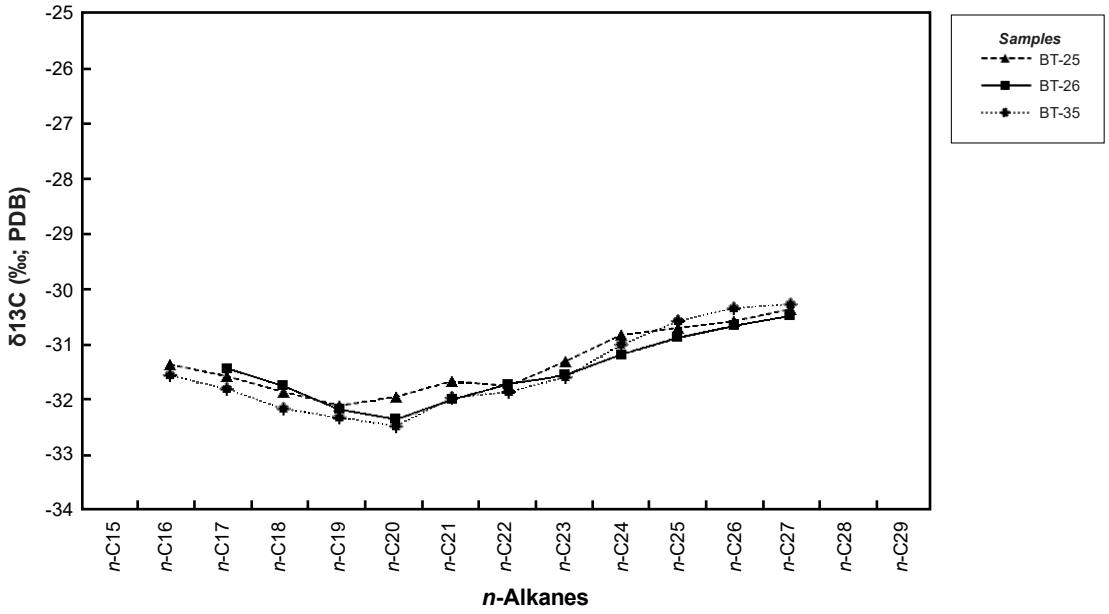

Figure 15. Carbon isotopic composition of individual *n*-alkanes of the Bächental bituminous marls from the Calcareous Alps.

There are only minor differences in the carbon isotopic composition of the Bächental bituminous marls between the samples. The rocks are isotopically light with a mean $\delta^{13}C$ (*n*-C_{17}) of -31.6‰. The $\delta^{13}C$ values are decreasing from *n*-C_{16} to *n*-C_{20} and increasing thereafter in samples BT-26 and BT-35, the BT-25 pattern deviates from the other samples at *n*-C_{20} to *n*-C_{21}.

5.2.2 Oils

5.2.2.1 Biomarker Composition

Oil stains recovered from the Falkenstein tunnel (A9 Pyhrn Autobahn; Northern Calcareous Alps) have been thoroughly studied by Gratzer et al. [2015]. They occur within the Triassic Reifling Formation and are thought to have been generated in marly zones within the Reifling limestone [Gratzer et al., 2015]. Oil stains recovered from borehole Urmannsau-1 (Lower Austria) occur in the Wetterstein Formation [Misch et al., 2017].

Gas chromatograms (GC) of the saturated and aromatic hydrocarbons of one Falkenstein tunnel oil stain and from oil stains in Urmannsau-1 (152 m depth) are shown in Figure 16 and Figure 17 (additional chromatograms of all oil samples from the Calcareous Alps are compiled in the Appendix). Concentrations and concentration ratios in the hydrocarbon fractions are listed in Table 9.

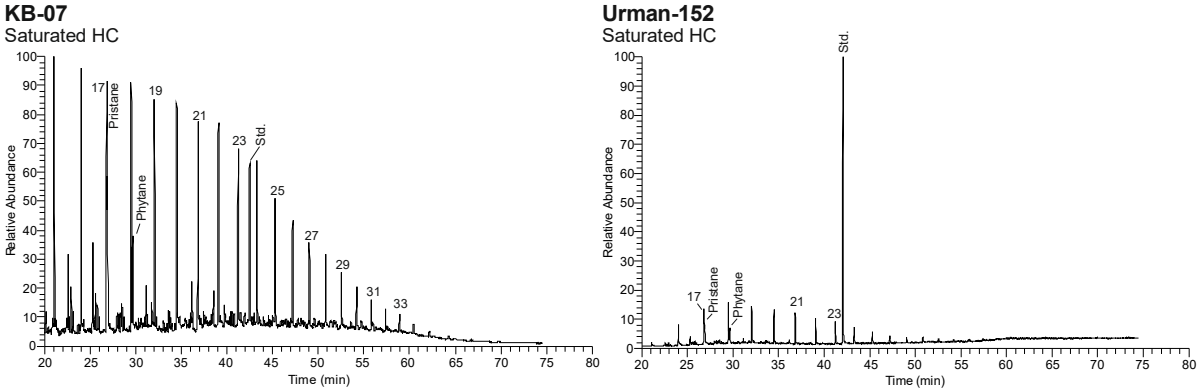

Figure 16. Chromatograms (Total Ion Current) of the saturated hydrocarbon fractions of oil stain samples from the Falkenstein tunnel (KB-07) and Urmannsau borehole (Urman-152) (both Calc. Alps). *n*-Alkanes are labelled according to their carbon number. Std. = standard (deuterated n-tetracosane: KB- samples; 1,1-binaphthyl: Urman- samples).

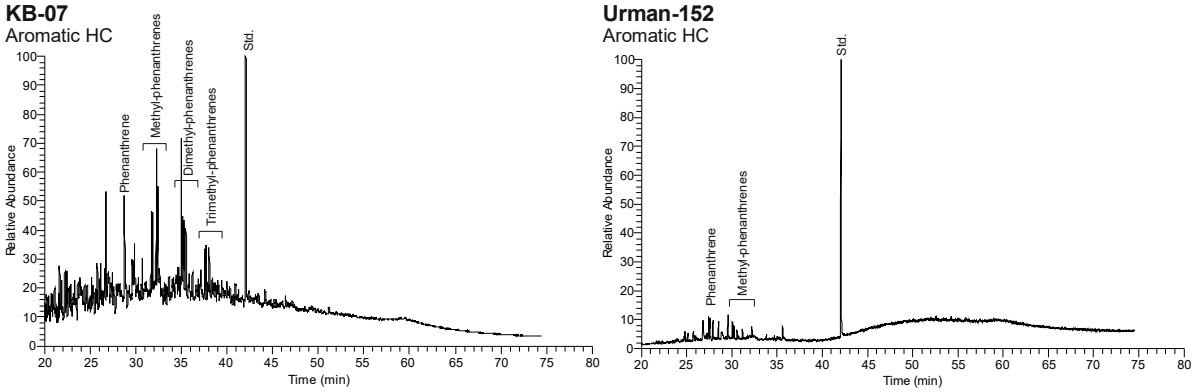

Figure 17. Chromatograms (Total Ion Current) of the aromatic hydrocarbon fractions of oil stain samples from the Falkenstein tunnel (KB-07) and Urmannsau borehole (Urman-152 (both Calc. Alps). Std. = standard (deuterated n-tetracosane: KB- samples; 1,1-binaphthyl: Urman- samples).

The *n*-alkane distribution shows maximum intensities in the short chain range and very low intensities in long chain range. In the Falkenstein tunnel oil stains carbon preference indices lie between 0.6 and 1.0; absence of terrestrial organic matter input is suggested. Extremely

high CPI values in Urmannsau-1 oil stains are to be considered with care, as concentrations of long chain *n*-alkanes in these samples are at minimum. Pristane/phytane ratios range from 1.4 to 1.6 in Falkenstein tunnel oil stains, and from 0.7 to 1.0 in Urmannsau-1 oil stains. Oleanane does not occur in any of the samples.

Table 9. Organic geochemical parameters, concentration ratios of specific biomarkers of oil stain samples from the Falkenstein tunnel and Urmannsau borehole (Calc. Alps).

Sample	*n*-C15-19/ Σ*n*-alk.	*n*-C21-25/ Σ*n*-alk.	*n*-C27-31/ Σ*n*-alk.	CPI	Pr/Ph [rel.prop]	Pri/*n*-C17 [rel.prop]	Ph/*n*-C18 [rel.prop]	OI (%)
Falkenstein tunnel								
KB-04	0.44	0.28	0.13	1.03	1.56	1.02	0.72	0
KB-05	0.43	0.28	0.14	0.89	1.61	1.01	0.69	0
KB-07	0.44	0.32	0.12	0.57	1.35	1.37	0.54	0
Urmannsau-1								
Urman-152	0.48	0.39	0.00	24.1	0.98	0.55	0.51	0
Urman-758	0.46	0.39	0.00	8.10	0.71	0.53	0.54	0

(CPI: carbon preference index, Pr/Ph: pristane/phytane ratio; OI: oleanane index)

5.2.2.2 Isotope ratios

The data on $\delta^{13}C$ obtained from GC-IRMS are listed in Table 10. Figure 18 illustrates a graphical presentation of the GC-IRMS results.

Table 10. Carbon isotopic composition of individual *n*-alkanes of oil stain samples from the Falkenstein tunnel and Urmannsau borehole (Calc. Alps).

Sample	*n*-C15	*n*-C16	*n*-C17	*n*-C18	*n*-C19	*n*-C20	*n*-C21	*n*-C22	*n*-C23	*n*-C24	*n*-C25	*n*-C26	*n*-C27	*n*-C28	*n*-C29
	δ13C (‰; PDB)														
Falkenstein tunnel															
KB-04			-32.8	-32.5	-32.8	-32.7	-32.6	-32.8	-32.7	-32.7	-32.9	-33.0	-32.6	-32.8	
KB-05		-32.1	-32.6	-32.6	-32.7	-32.5	-32.7	-32.8	-32.5	-32.7	-33.2	-32.6	-32.4	-32.5	-32.2
KB-07			-32.2	-31.8	-32.0	-31.8	-32.1	-32.2	-32.4	-33.0	-32.7	-32.8	-32.3	-32.4	
Urmannsau-1															
Urman-152		-26.3	-26.6	-27.1	-27.3	-27.8	-28.2	-28.5	-28.8	-28.4	-28.8	-28.7	-28.6	-28.7	-29.1
Urman-758			-26.8	-27.1	-27.2	-27.4	-27.6	-27.9	-28.2	-28.6	-28.7	-28.5	-28.6	-28.3	-28.5

PDB = Peedee Belemnite (int. Standard)

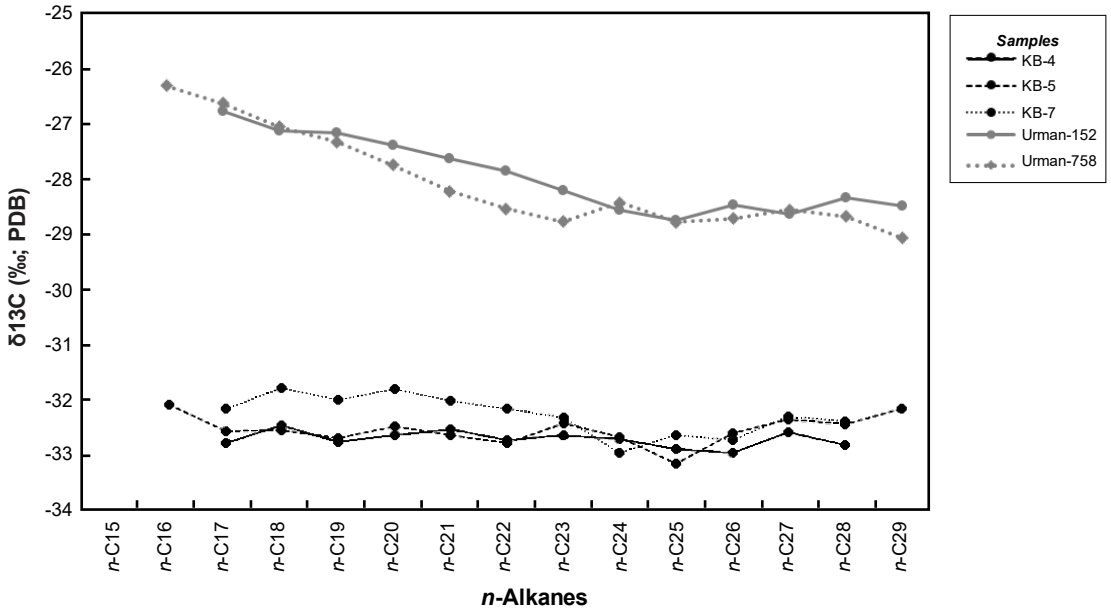

Figure 18. Carbon isotopic composition of individual *n*-alkanes of oil stain samples from the Falkenstein tunnel and Urmannsau borehole (Calc. Alps).

The Falkenstein tunnel oil stained samples, which show a straight distribution, are isotopically light with an average $\delta^{13}C$ (*n*-C_{17}) value of -32.5‰. This is remarkable, as oil stains, which are often biodegraded, are usually heavier. Urmannsau-1 oil stains, on the contrary, are

isotopically heavy, with an average $\delta^{13}C$ (*n*-C_{17}) value of -26.7‰. They show a negatively sloping curve up to *n*-C_{24}; $\delta^{13}C$ values decrease from *n*-C_{16} (-26.3‰) to *n*-C_{24} (avg. -28.5‰), after which there is an even curve.

The notable difference between the samples, observed in the deviating pattern of sample KB-7, is astounding, as the samples more or less constitute the same oil. Up to 0.9‰ difference is observed at *n*-C_{20}.

5.3 Waschberg Zone

5.3.1 Biomarker Composition

Oligocene rocks from Thomasl Formation in the Waschberg Zone have been investigated by Pupp et al. [2018a]. Three of these samples (all of them cuttings samples) were re-investigated in this study. They are characterized by relative proportions of hydrocarbon fractions between 22 and 36% to fractions of NSO compounds and asphaltenes between 63 and 78%.

Gas chromatograms (GC) of the saturated and aromatic hydrocarbon fractions are shown in Figure 19 (chromatograms of all samples from the Waschberg Zone are compiled in the Appendix). There are only minor differences in the molecular composition of the hydrocarbons between the samples, as reflected by organic geochemical facies and maturation parameters (Table 11).

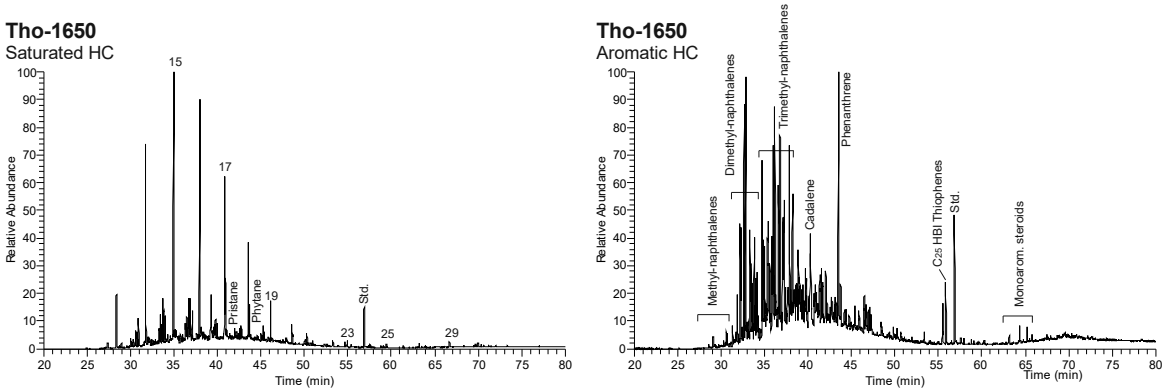

Figure 19. Chromatograms (Total Ion Current) of the saturated and aromatic hydrocarbon fractions of cuttings sample THO-1650 from the Thomasl Fm. (Waschberg Zone). *n*-Alkanes are labelled according to their carbon number. Std. = standard (1,1-binaphthyl).

Table 11. Bulk organic geochemical parameters, concentration and concentration ratios of specific biomarkers of cuttings samples the Thomasl Fm. from the Waschberg zone.

Sample	TOC [A] (wt%)	HI [A]	Tmax [A] (%)	EOM	Sat.HC (%)	Aro HC (%)	N+A (%)	*n*-alk	*n*-C15-19/ Σ*n*-alk.	*n*-C21-25/ Σ*n*-alk.	*n*-C27-31/ Σ*n*-alk.	CPI
THO-1650	1.88	165	424	30	27	5	69	1192	0.90	0.02	0.03	2.73
THO-1720	2.66	223	418	24	16	6	78	542	0.67	0.07	0.17	1.68
THO-1760	3.33	116	426	17	28	8	63	900	0.87	0.04	0.06	2.06

Sample	Pr/Ph [rel.prop]	Pri/*n*-C17 [rel.prop]	Ph/*n*-C18 [rel.prop]	Steranes (µg/g TOC)	Hopanes (µg/g TOC)	ααα R+S Steranes C27/ ΣC27-29St.	ααα R+S Steranes C28/ ΣC27-29St.	ααα R+S Steranes C29/ ΣC27-29St.
THO-1650	1.84	0.56	0.56	5	n.a.	0.39	0.22	0.40
THO-1720	1.63	0.81	0.87	60	n.a.	0.34	0.35	0.32
THO-1760	1.80	0.91	0.93	15	n.a.	0.34	0.30	0.36

(TOC: total organic carbon; HI: hydrogen index in mg HC/g TOC; EOM: extractable organic matter in mg/g TOC; Sat.HC: saturated hydrocarbons; Aro.HC: aromatic hydrocarbons; N+A: NSO compounds + asphaltenes; n-alk: n-alkane concentration in µg/g TOC; CPI: carbon preference index; Pr/Ph: pristane/phytane ratio; n.a.: no data)

[A] Data from Pupp et al. [2018]

The saturated hydrocarbons are dominated by *n*-alkanes. Steranes are present in minor concentrations, whereas hopanes are absent. The *n*-alkane fraction consists nearly exclusively of short chain length *n*-alkanes. Pr/Ph ratios are relatively high and indicate oxic conditions during deposition. This is consistent with Pupp et al. [2018a], who reported changing oxygen-availability and salinity on the basis of Pr/Ph and TOC/S ratios. Pr/*n*-C_{17} and Ph/*n*-C_{18} ratios are low (<1.0).

A transitional depositional environment with both marine and terrestrial influence is suggested. This is based on (a) equal sterane proportions, as shown in Figure 20, (b) the presence of higher plant biomarker cadalene in the aromatic hydrocarbon fraction, (c) the presence of C_{25}

HBI (highly branched isoprenoids), which are strong markers for diatoms [e.g. Volkman et al, 1994] in sample THO-1650 (diatoms are commonly associated with marine environments). This is consistent with Pupp et al. [2018a], who suggested a nearshore depositional environment on the basis of biomarker composition.

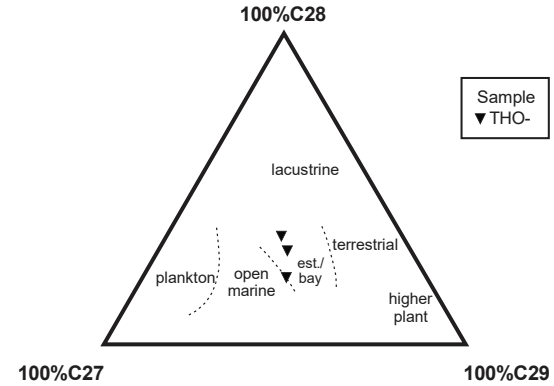

Figure 20. Ternary plot of relative proportions of C27, C28 and C29 steranes in cuttings samples from the Thomasl Fm. (Waschberg Zone; modified after Huang & Meinschein [1979]).

5.3.2 Isotope Ratios

The data on $\delta^{13}C$ obtained from GC-IRMS are listed in Table 12. Figure 21 illustrates a graphical presentation of the GC-IRMS results.

Table 12. Carbon isotopic composition of individual *n*-alkanes of cuttings samples from the Thomasl Fm. (Waschberg Zone).

Sample	*n*-C15	*n*-C16	*n*-C17	*n*-C18	*n*-C19	*n*-C20	*n*-C21	*n*-C22	*n*-C23	*n*-C24	*n*-C25	*n*-C26	*n*-C27	*n*-C28	*n*-C29
	δ13C (‰; PDB)														
THO-1650	-28.3	-28.5	-28.6	-28.7	-28.9	-28.8	-29.0	-28.5	-28.8	-29.3	-29.0	-29.4	-29.3	-29.7	
THO-1720	-28.3	-28.0	-28.3	-28.1	-28.3	-28.5	-29.0	-28.6	-28.9	-29.0	-29.2	-29.4	-29.5	-29.9	
THO-1760	-28.2	-28.3	-28.3	-28.3	-28.4	-28.7	-29.1	-28.9	-29.0	-29.1	-29.4	-29.6	-29.4	-30.1	-29.8

PDB = Peedee Belemnite (int. Standard)

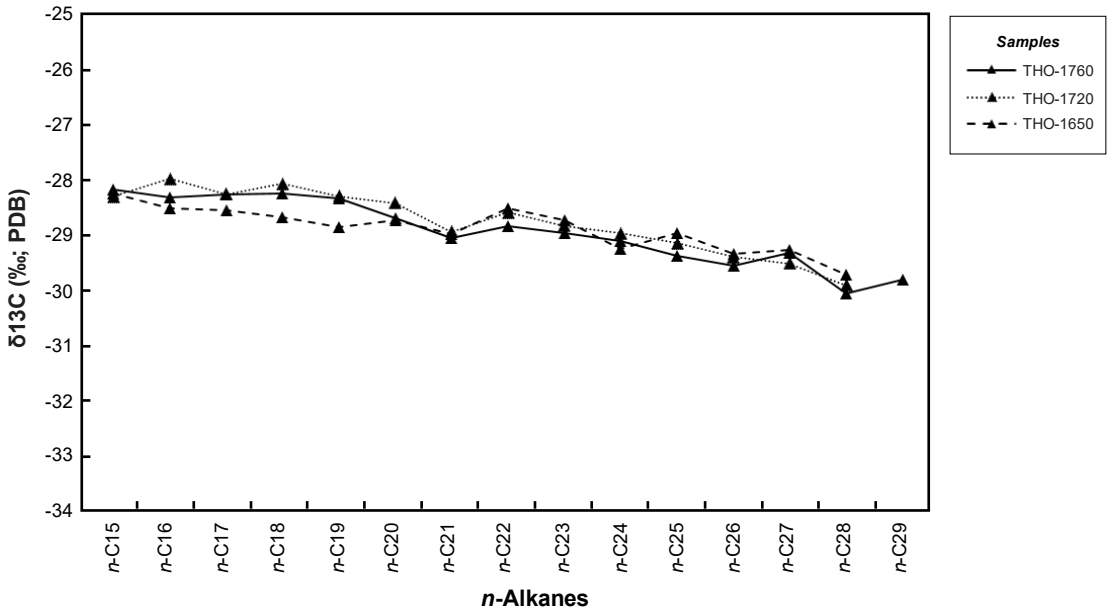

Figure 21. Carbon isotopic composition of individual *n*-alkanes of cuttings samples from the Thomasl Fm. (Waschberg Zone).

There is only minor variation in the isotopic composition of *n*-alkanes between the rock samples. The $\delta^{13}C$ value of *n*-C_{17} is -28.4‰ on average. The *n*-alkanes are becoming isotopically lighter with higher carbon numbers; $\delta^{13}C$ values decrease slowly, from mean $\delta^{13}C$

(*n*-C_{15}) of -28.3‰ to mean $\delta^{13}C$ (*n*-C_{28}) of -29.9‰, resulting in a flat, slightly negatively sloping curve. Reports of such curves being indicative of aquatic depositional environments [Murray et al., 1994] are consistent with an estuarine/bay depositional environment.

5.4 Carpathian Fold-and-Thrust belt

5.4.1 Source rocks

5.4.1.1 Biomarker Composition

The Menilite Formation exposed along the Chechva River in the Ukrainian part of the Carpathian Fold-and-Thrust belt is thermally immature (avg. T_{max}: 422°C [Rauball & Sachsenhofer, 2017]) and contains excellent source rocks [Sachsenhofer et al., 2018]. Biomarker composition of these rocks are currently studied by Rauball et al. [in prep.]. Two Oligocene (U-66, U-B-22) and two Lower Miocene (U-C-63, U-C-4) samples are included in the present study. Their rock extracts are characterized by relative proportions of (saturated + aromatic) hydrocarbon fractions between 22 and 38% and between 62 and 78% for NSO compounds plus asphaltenes. Aromatic hydrocarbons are predominant over saturated hydrocarbons in all samples, except for U-C-63.

Thermally mature Cretaceous rock samples of the Shypot Formation from the Carpathian Fold-and-Thrust belt (T_{max}: 454 - 458°C [Koltun et al., 1998]) are currently under investigation by Rauball et al. [in prep.]. Three of these samples are included in the present study. Their rock extracts are characterized by relative proportions of (saturated + aromatic) hydrocarbon fractions between 43 and 65% and between 35 and 57% for NSO compounds plus asphaltenes. Concentrations of saturated and aromatic hydrocarbons are similar (average: 26% and 25% of the EOM, respectively).

Gas chromatograms (GC) of the saturated and aromatic hydrocarbon fractions of samples from Menilite Formation (U-C-4) and from the Shypot Formation (J-39), are shown in Figure 22 and Figure 23 (chromatograms of all rock samples from the Carpathian Fold-and-Thrust belt are compiled in the Appendix). There are a few differences in the molecular composition of the hydrocarbons between the samples, as reflected by organic geochemical parameters (Table 13).

In the Menilite Formation the saturated hydrocarbons are dominated by *n*-alkanes, steranes, and hopanes. The saturated hydrocarbons of the Shypot Formation consist almost exclusively of *n*-alkanes.

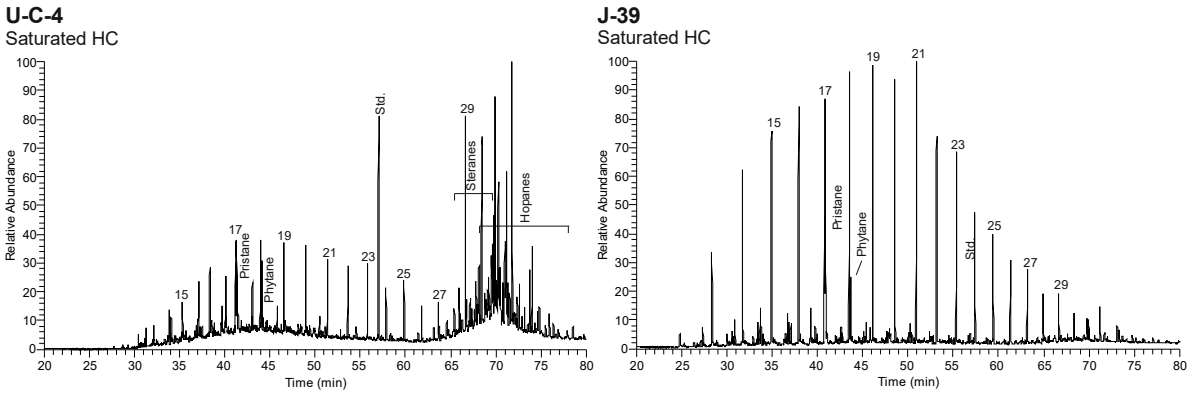

Figure 22. Chromatograms (Total Ion Current) of the saturated hydrocarbon fractions of samples of the Menilite Fm. (U-C-4) and Shypot Fm. (J-39) from the Carpathian Fold-and-Thrust belt. *n*-Alkanes are labelled according to their carbon number. Std. = standard (deuterated n-tetracosane).

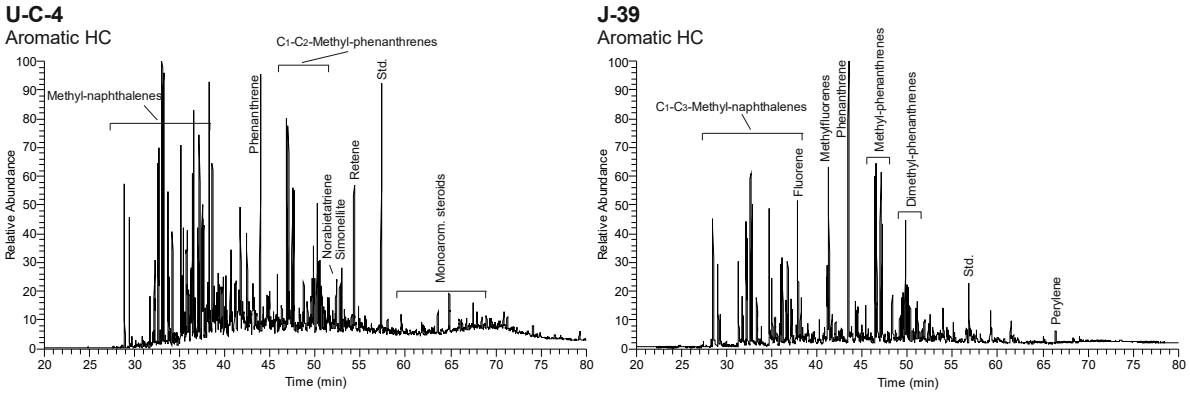

Figure 23. Chromatograms (Total Ion Current) of the aromatic hydrocarbon fractions of samples of the Menilite Fm. (U-C-4) and Shypot Fm. (J-39) from the Carpathian Fold-and-Thrust belt. Std. = standard (deuterated n-tetracosane).

Table 13. Bulk organic geochemical parameters, concentration and concentration ratios of specific biomarkers of samples of the Menilite Fm. and Shypot Fm. from the Carpathian Fold-and-Thrust belt.

Sample	Age	TOC[A] (wt%)	HI[A]	Tmax[A] (%)	Sat.HC (%)	Aro HC (%)	N+A (%)	*n*-alk (µg/g TOC)	*n*-C15-19/ Σ*n*-alk.	*n*-C21-25/ Σ*n*-alk.	*n*-C27-31/ Σ*n*-alk.	CPI
Menilite Fm.												
U-C-63	Mio.	5.94	429	423	14	10	76	367	0.21	0.42	0.23	1.21
U-C-4	Mio.	12.80	445	420	8	14	78	173	0.28	0.31	0.27	1.45
U-B-22	Oli.	16.22	412	416	15	23	62	774	0.21	0.44	0.19	1.13
U-66	Oli.	19.85	501	424	8	14	78	103	0.48	0.24	0.15	0.97
Shypot Fm.												
J-05	Cret.	4.23	88	462	28	38	35	n.a.	0.33	0.38	0.12	1.19
J-39	Cret.	8.15	178	458	25	21	54	n.a.	0.38	0.36	0.10	1.11
J-77	Cret.	3.99	171	451	26	16	57	n.a.	0.44	0.32	0.10	1.16

Sample	Pr/Ph [rel.prop]	Pri/*n*-C17 [rel.prop]	Ph/*n*-C18 [rel.prop]	St.*	Hop*	St/ Hop	MPI-1/ Rc	OI (%)	αααR+S Steranes C27/ ΣC27-29 St.	αααR+S Steranes C28/ ΣC27-29 St.	αααR+S Steranes C29/ ΣC27-29 St.
Menilite Fm.											
U-C-63	0.45	2.78	6.82	116	102	1.2	0.76/ n.a.	5.6	0.31	0.36	0.33
U-C-4	1.37	1.45	1.18	119	123	1.0	1.04/ n.a.	13.9	0.26	0.34	0.39
U-B-22	2.50	13.09	4.11	132	74	1.8	0.85/ n.a.	24.1	0.32	0.19	0.49
U-66	1.47	1.08	0.82	92	75	1.2	0.80/ n.a.	12.3	0.26	0.44	0.30
Shypot Fm.											
J-05	1.23	0.94	0.68	n.a.	n.a.	n.a.	0.83/ 0.9	10.6	n.a.	n.a.	n.a.
J-39	1.93	0.88	0.43	n.a.	n.a.	n.a.	0.96/ 1.0	5.9	n.a.	n.a.	n.a.
J-77	1.08	0.92	0.52	n.a.	n.a.	n.a.	0.72/ 0.8	20.5	n.a.	n.a.	n.a.

(TOC: total organic carbon; HI: hydrogen index in mg HC/g TOC; EOM: extractable organic matter in mg/g TOC; Sat.HC: saturated hydrocarbons; Aro.HC: aromatic hydrocarbons; N+A: NSO compounds + asphaltenes; CPI: carbon preference index; Pr/Ph: pristane / phytane; conc: absolute concentration in µg/g TOC; St.*: sterane concentrations in µg/g TOC; Hop.*: hopane concentrations in µg/g TOC; MPI-1: methylphenanthrene index; Rc: vitrinite reflectance, calculated; n.a.: no data)
[A]Data from J. Rauball [pers.comm. 2018]

n-alkanes - The *n*-alkane distribution is diverse in the Menilite Formation, but generally shows maximum intensities in the mid and long chain ranges. The same pattern prevails in the Shypot Formation, although, compared to the Menilite Formation, it is more depleted in long chain *n*-alkanes, which is likely due to a higher degree of maturity (T_{max}: 451 – 462°C). A weak odd-over-even predominance of long-chain *n*-alkanes in both formations, as indicated by carbon preference indices between 1.1 and 1.5 (excluding sample U-66), is consistent with land plant precursors.

Acyclic isoprenoids - Pr/Ph ratios range from 0.4 to 1.5 in the Menilite Formation, and from 1.0 to 2.0 (average Pr/Ph = 1.4) in the Shypot Formation. However, other factors have most likely affected the Pr/Ph ratio, as both the Menilite Formation and the Shypot Formation reportedly have been deposited under anoxic conditions [Koltun, 1992; Senkovsky et al., 2010], the latter of which has been deposited during the oceanic anoxic event (OAE-1) [Senkovsky et al., 2010]. Pr/*n*-C_{17} and Ph/*n*-C_{18} ratios are higher in the Menilite Formation than in the Shypot Formation

reflecting differences in maturity. Figure 24 shows a cross-plot of Pr/*n*-C_{17} versus Ph/*n*-C_{18} (sample U-B-22 with Pr/*n*-C_{17} >10 is not displayed).

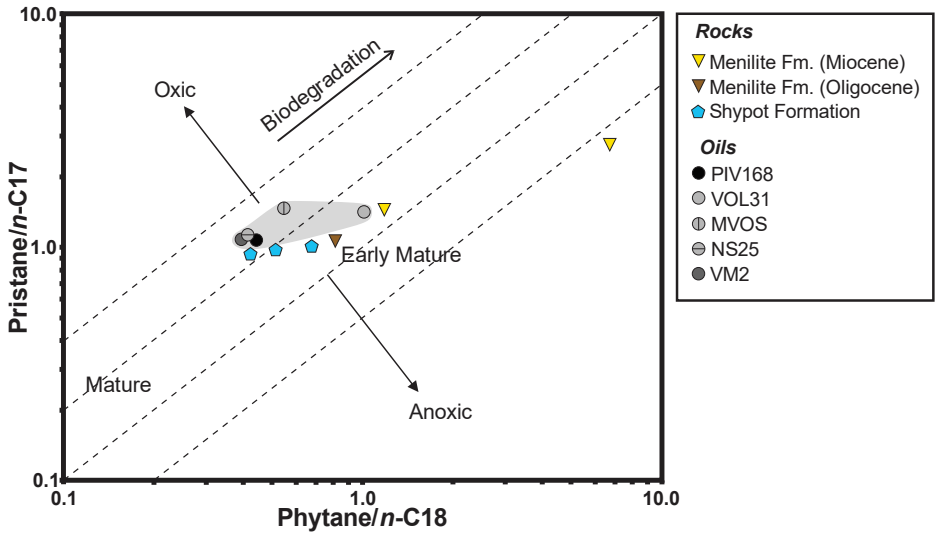

Figure 24. Correlation diagram of Pr/*n*-C17 ratios versus Ph/*n*-C18 ratios of rock and oil samples from the Carpathian Fold-and-Thrust belt for the assessment of oil sources, as well as the effects of maturation and biodegradation (modified after Connan & Cassou [1980]).

Steranes and hopanes – While steranes are depleted in the Shypot Formation, they are present in high concentrations in the Menilite Formation, ranging from 92 to 112 µg/g TOC, with varying dominance of C_{28} and C_{29} steranes. The relative sterane distribution is shown in Figure 25.

Hopanes are likewise depleted in the Shypot Formation. In the Menilite Formation, hopane concentrations are smaller than sterane concentrations. St/Hop ratios exceed 1.0 on average.

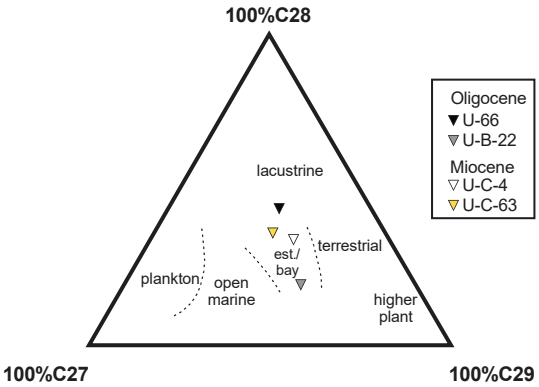

Figure 25. Ternary plot of relative proportions of C27, C28 and C29 steranes in samples of the Menilite Fm. from the Carpathian Fold-and-Thrust belt (modified after Huang & Meinschein [1979]).

Aromatic hydrocarbons – Aromatic hydrocarbon fractions show high intensities of naphthalene, methylated (C_1 to C_3) naphthalenes, phenanthrene, and methylated (C_1 to C_2) phenanthrenes across both Formations (Figure 23). Additionally, monoaromatic steroids occur in the Menilite Formation. Methylphenanthrene indices (MPI-1) based on phenanthrene and four isomers (3-, 2-, 9-, 1-) of methylphenanthrene [after Radke & Welte, 1983] were calculated and pretend similar maturities in all samples (average MPI-1=0.80 in Menilite Fm.; average MPI-1=0.84 in Shypot Fm.). According to the empirical relationship between MPI-1 and vitrinite reflectance [Radke et al., 1984] these values correspond to an equivalent average vitrinite reflectance (R_C) of 0.88 for Menilite Formation and 0.90 for Shypot Formation respectively. The calculation is based on the relationship R_C=0.6*MPI-1+0.4 and is valid for type-III organic matter. The results

are justified for the Shypot Formation, which is in the oil window (T_{max}: 454 - 458°C [Koltun et al., 1998]). However, the calculated R_C of the Menilite Formation is too high, as T_{max} values (avg. 422°C [Rauball & Sachsenhofer, 2017]) have shown that the Menilite Formation is immature. This may reflect that the Menilite Formation contains type-II organic matter.
Additional compounds present in considerable quantities in the Menilite Formation are cadalene, norabietatriene, simonellite, and retene, which suggest higher land plants (conifers) contribution to the sedimentary organic matter. Triaromatic triterpenoid, which is a biomarker for angiosperms [Peters & Moldowan, 1993], is present in sample U-C-63. In the Shypot Formation, perylene, which is a higher plant marker [Aizenshtat, 1973], occurs in all samples, and α-phyllocladane (a tetracyclic diterpane), which is a marker for conifers [Noble et al., 1985], is present in sample J-05. Oddly, polycyclic aromats fluorene and methylfluorene, both of which are commonly associated with coals, occur in the Shypot Formation. Their presence indicates extensive oxidation [Curry et al., 1994].

5.4.1.2 Isotope Ratios

The data on $\delta^{13}C$ obtained from GC-IRMS are listed in Table 14. Figure 26 illustrates a graphical presentation of the GC-IRMS results.

Table 14. Carbon isotopic composition of individual *n*-alkanes of samples from the Menilite Fm. and Shypot Fm. (Carpathian Fold-and-Thrust belt).

Sample	*n*-C15	*n*-C16	*n*-C17	*n*-C18	*n*-C19	*n*-C20	*n*-C21	*n*-C22	*n*-C23	*n*-C24	*n*-C25	*n*-C26	*n*-C27	*n*-C28	*n*-C29
	δ13C (‰; PDB)														
Menilite Fm.															
U-C-63	-26.5	-27.1	-26.9	-26.8	-26.9	-27.3	-27.5	-27.2	-27.0	-26.9	-27.0	-26.8	-27.5	-27.1	-27.5
U-C-4	-26.1	-25.8	-26.4	-26.6	-26.9	-27.4	-27.3	-27.2	-26.9	-26.8	-27.2	-26.9	-27.4	-27.0	-27.5
U-B-22	-25.8	-26.0	-26.5	-26.7	-26.8	-27.0	-27.5	-27.3	-27.4	-26.8	-27.3	-27.2	-27.5	-27.2	-27.6
U-66	-25.8	-26.2	-26.7	-26.8	-26.9	-27.1	-27.4	-27.2	-26.9	-26.7	-27.2	-26.9	-27.5	-26.9	-27.4
Shypot Fm.															
J-05	-28.6	-28.9	-29.3	-29.5	-30.3	-30.4	-30.5	-30.8	-30.5	-30.9	-31.0	-31.2	-31.5	-31.7	-31.8
J-39	-28.4	-29.0	-29.2	-29.4	-29.9	-30.4	-30.7	-30.5	-30.7	-31.1	-30.8	-31.0	-31.5	-31.6	-32.2
J-77	-28.9	-29.3	-29.4	-29.5	-30.1	-30.3	-30.5	-30.3	-30.4	-30.6	-31.3	-31.7	-31.5	-31.7	-31.9

PDB = Peedee Belemnite (int. Standard)

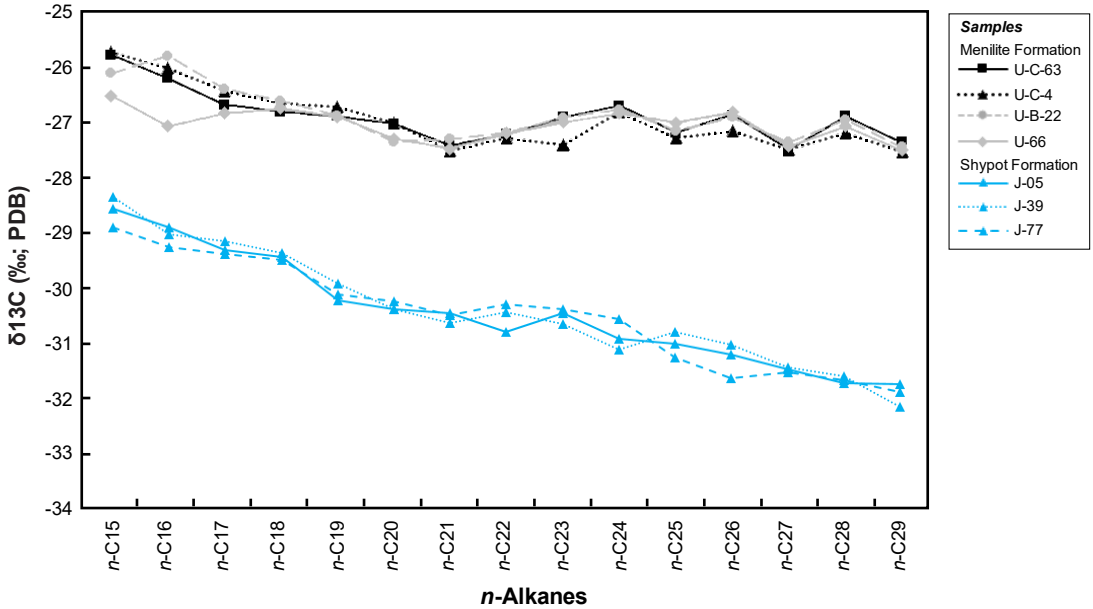

Figure 26. Carbon isotopic composition of individual *n*-alkanes of samples from the Menilite Fm. and Shypot Fm. (Carpathian Fold-and-Thrust belt).

There is a strong contrast between the isotopic composition of the Menilite Formation and Shypot Formation. The Menilite Formation is isotopically heavy (average $\delta^{13}C$ (*n*-C_{17}) =

-26.6‰) and has a flat curve, while the lighter Shypot Formation has a negatively dipping curve, with average $\delta^{13}C$ values decreasing from -29.3‰ at *n*-C_{17} to -32.0‰ at *n*-C_{29}. In the Menilite Formation the slightly lower $\delta^{13}C$ values of odd carbon numbered homologues in the *n*-C_{23} to *n*-C_{29} range is remarkable. It is interpreted to reflect the contribution of leaf lipids of plants [Collister et al., 1994a].

5.4.2 Oils

5.4.2.1 Biomarker Composition

Oils were recovered from well Pivnichna Dolyna-168 (sample PIV168) in the Dolyna oil producing region, well Voliya Blazhivska-31 (VOL31) in the Boryslav oil producing region, wells Verkhnio Maslovetska-2 (VM2) and Nova Skhidnytsya-25 (NS25) in the Skyba nappe and from the abandoned well Mala Volosyanka (sample MVOS). PIV168 produces from the Eocene Wyhoda Formation, VOL31 produces from the Oligocene Menilite Formation. Oils from VM2 and NS25 are produced from the Upper Cretaceous Stryi Formation, and MVOS - which constitutes an oil seep [pers.comm. Y.Koltun] - occurs within Oligocene strata.

The oils are characterized by relative proportions of hydrocarbon fractions between 9 and 59% and of fractions of NSO compounds and asphaltenes between 41 and 91%. API gravity data from Wieclaw et al. [2012] and Kotarba et al. [2007] show values of 23.3°API (VOL31) and 34.7°API (NS25) for oils from Boryslav oil producing region, classifying these oils as medium to light crude oils [Tissot & Welte, 1984].

Gas chromatograms (GC) of the saturated and aromatic hydrocarbon fractions of oil sample NS25 is shown in Figure 32 (chromatograms of all oil samples from the Carpathian Fold-and-Thrust belt are compiled in the Appendix). There are only minor differences in the molecular composition of the hydrocarbons between the samples, as reflected by organic geochemical facies and maturation parameters (Table 19).

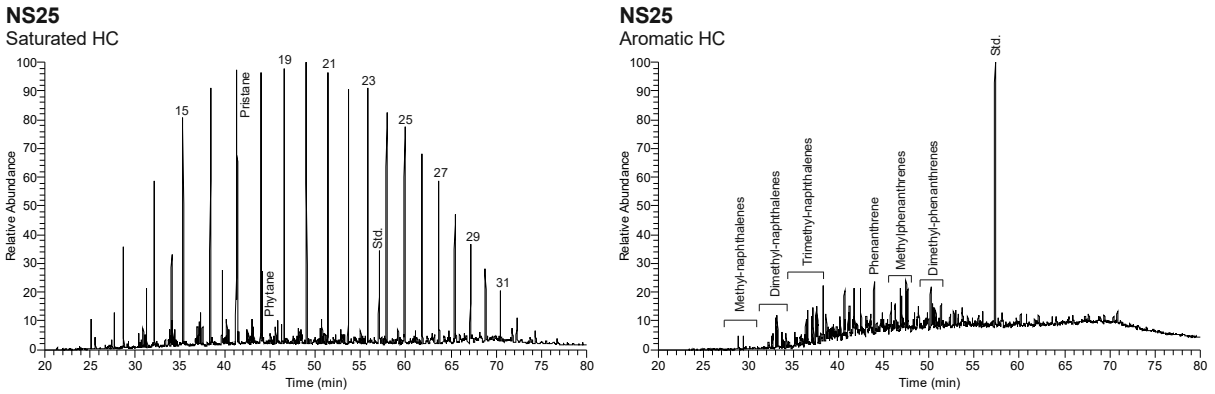

Figure 27. Chromatograms (Total Ion Current) of the saturated and aromatic hydrocarbon fractions of oil sample NS25 from the Carpathian Fold-and-Thrust belt. *n*-Alkanes are labelled according to their carbon number. Std. = standard (deuterated n-tetracosane).

Table 15. Organic geochemical parameters, concentration ratios of specific biomarkers of oils from Carpathian Fold-and-Thrust belt.

Sample	Grav. (API°)	Sat.HC (%)	Aro.HC (%)	N+A (%)	*n*-C15-19/ Σ*n*-alk.	*n*-C21-25/ Σ*n*-alk.	*n*-C27-31/ Σ*n*-alk.	CPI	Pr/ Ph	Pri/*n*-C17 [rel.prop]	Ph/*n*-C18 [rel.prop]	MPI-1	OI (%)
PIV168		4	5	91	0.38	0.34	0.14	1.09	2.4	1.07	0.44	0.67	16
VOL31	[A]23.3	26	15	58	0.34	0.33	0.18	1.04	1.3	1.41	1.01	n.a.	17
NS25	[A]34.7	41	18	41	0.35	0.35	0.16	1.10	2.6	1.12	0.41	0.90	16
VM2		1	52	47	0.37	0.34	0.15	1.09	2.6	1.09	0.40	0.78	22
MVOS		39	15	45	0.39	0.35	0.13	1.08	2.6	1.47	0.55	0.78	29

(API: american petroleum institute; Sat.HC: saturated hydrocarbons; Aro.HC: aromatic hydrocarbons; N+A: NSO compounds + asphaltenes; CPI: carbon preference index; Pr/Ph: pristane/phytane ratio; MPI-1: methylphenanthrene index; OI: oleanane index)
[A]Data from Wieclaw et al. [2012]

The saturated hydrocarbons are dominated by *n*-alkanes. Steranes and hopanes are depleted.

The *n*-alkane distribution shows maximum intensities in the short chain range (avg. *n*-C_{15-29}/ Σ*n*-alk = 37%), and very low intensities in the long chain range (average *n*-C_{27-31}/Σ*n*-alk = 15%). Carbon preference indices lie between 1.0 and 1.1.

The Pr/Ph ratio for the VOL31 oil is 1.3 and ranges from 2.4 to 2.6 for the remaining oils, suggesting dysoxic conditions during deposition of the source rocks. The exceptional position of the VOL31 oil is also indicated by a relatively high sulphur content (1.74 wt%; Wieclaw et al., 2012). Pr/*n*-C_{17} and Ph/*n*-C_{18} ratios are moderately low and shown in Figure 24.

Aromatic hydrocarbon fractions contain methylated (C_1 to C_3) naphthalenes and methylated (C_1 to C_4) phenanthrenes. MPI-1 values have been calculated, and amount to an average of 0.78. Oleanane indices are very high and range from 16 to 29%.

5.4.2.2 Isotope Ratios

The data on $\delta^{13}C$ obtained from GC-IRMS are listed in Table 19. Figure 28 illustrates a graphical presentation of the GC-IRMS results.

Table 16. Carbon isotopic composition of individual *n*-alkanes of oil samples from the Carpathian Fold-and-Thrust belt.

Sample	*n*-C15	*n*-C16	*n*-C17	*n*-C18	*n*-C19	*n*-C20	*n*-C21	*n*-C22	*n*-C23	*n*-C24	*n*-C25	*n*-C26	*n*-C27	*n*-C28	*n*-C29
	δ13C (‰; PDB)														
PIV168			-26.6	-27.1	-26.9	-27.3	-27.5	-27.6	-27.3	-26.8	-27.0	-27.5	-27.6	-27.9	-28.1
VOL31			-27.8	-28.0	-28.0	-28.2	-28.6	-28.2	-27.8	-27.6	-28.1	-28.2	-28.0	-27.8	-28.1
NS25	-26.4	-26.6	-27.1	-27.1	-27.1	-27.2	-27.2	-27.2	-27.4	-27.2	-27.7	-28.0	-28.2	-28.1	-27.8
VM2		-26.5	-26.8	-27.2	-27.3	-27.5	-27.9	-27.4	-27.2	-27.0	-27.3	-27.8	-28.0	-27.9	
MVOS	-25.9	-26.2	-26.5	-26.7	-26.4	-26.4	-26.6	-26.6	-26.8	-26.9	-27.3	-27.7	-28.1	-28.3	-28.3

PDB = Peedee Belemnite (int. Standard)

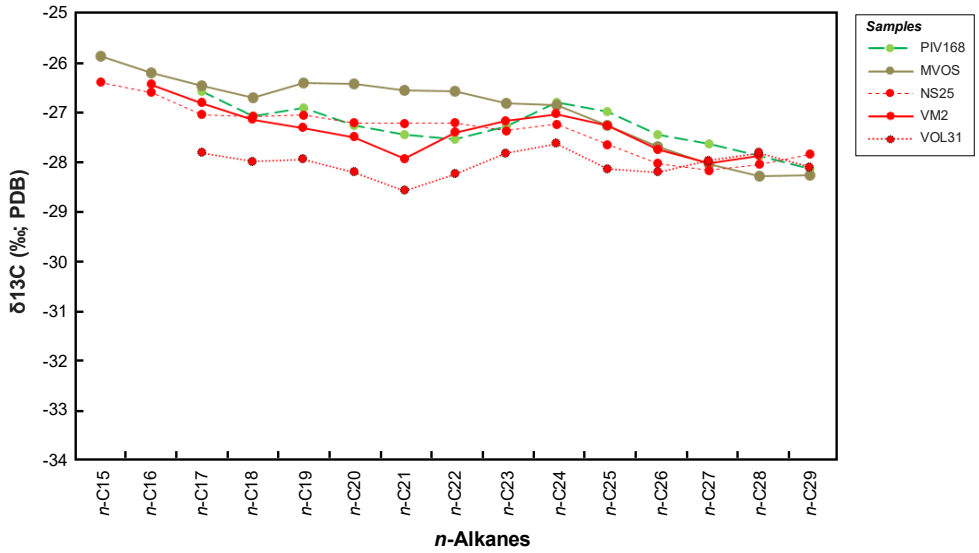

Figure 28. Carbon isotopic composition of individual *n*-alkanes of oil samples from the Carpathian Fold-and-Thrust belt.

The oils from the Carpathian Fold-and-Thrust belt are isotopically heavy with $\delta^{13}C$ (*n*-C_{17}) of -26.9‰. They have a flat curve and appear to show a wide variety of $\delta^{13}C$ values, ranging from $\delta^{13}C$ (*n*-C_{17}) of -27.8‰ in sample VOL31 to $\delta^{13}C$ (*n*-C_{17}) of -26.5‰ in sample MVOS. The slightly lower $\delta^{13}C$ values of sample VOL31 probably reflect a source rock facies with elevated sulphur content [Wieclaw et al., 2012]. The slightly higher $\delta^{13}C$ values of oil seep MVOS have probably been caused by biodegradation [Clayton, 1991]. The remaining samples show similar isotope values.

5.5 Carpathian Foredeep

5.5.1 Rocks

5.5.1.1 Biomarker Composition

The rock extracts of the Kokhanivka Formation from the basement of the Carpathian foredeep are characterized by relative proportions of hydrocarbon fractions between 18 and 36% and fractions of NSO compounds and asphaltenes between 64 and 82%. Saturated hydrocarbons and aromatic hydrocarbons concentrations are similar with an average 14% and 16% of the EOM.

Gas chromatograms (GC) of the saturated and aromatic hydrocarbon fractions of the Kokhanivka Formation are shown in Figure 29 (chromatograms of all rock samples from the Carpathian Foredeep are compiled in the Appendix). There are only minor differences in the molecular composition of the hydrocarbons between the samples, as reflected by organic geochemical facies and maturation parameters (Table 17).

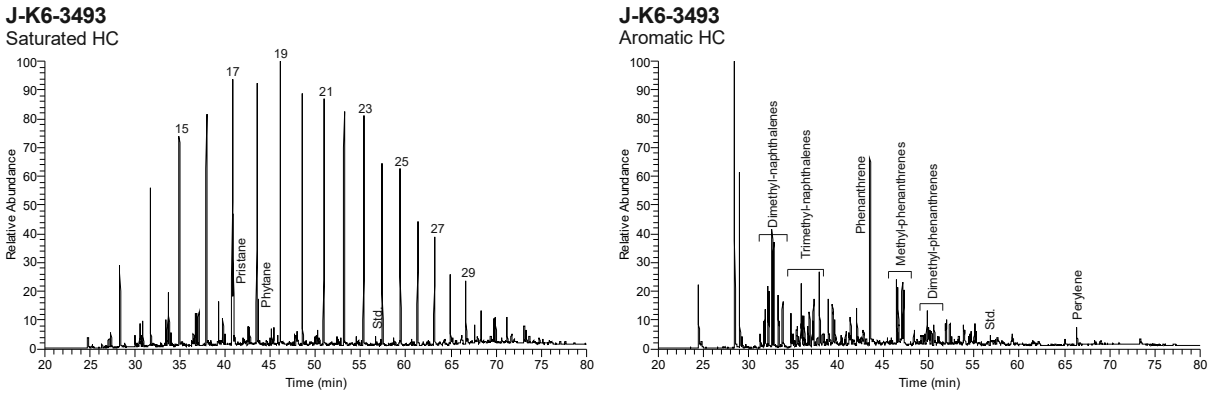

Figure 29. Chromatograms (Total Ion Current) of the saturated and aromatic hydrocarbon fractions of core sample J-K6-3493 from the Kokhanivka Formation (Carpathian Foredeep). *n*-Alkanes are labelled according to their carbon number. Std. = standard (1,1-binaphthyl).

Table 17. Bulk organic geochemical parameters, concentration and concentration ratios of core samples from the Kokhanivka Formation (Carpathian Foredeep).

Sample	TOC[A]	Tmax[A]	HI[A]	MPI*	Sat.HC (%)	Aro HC (%)	*n*-C15-19/ Σ*n*-alk.	*n*-C21-25/ Σ*n*-alk.	*n*-C27-31/ Σ*n*-alk.	CPI	Pr/ Ph	Pri/*n*-C17 [rel.prop]	Ph/*n*-C18 [rel.prop]	OI (%)
J-MS-2523	14.98	438	33	0.48	7	11	0.24	0.48	0.13	1.16	1.45	1.34	0.78	0
J-K6-3428	5.75	440	133	0.60	21	16	0.39	0.35	0.09	1.37	2.30	1.18	0.47	0
J-K6-3493	4.87	445	143	0.55	11	22	0.34	0.38	0.12	1.13	3.08	0.72	0.27	0
J-K6-3521	4.07	445	113	0.62	15	16	0.38	0.36	0.10	1.23	2.34	0.68	0.32	0

(TOC: total organic carbon in wt%; MPI*…MPI-1: methylphenanthrene index; Sat.HC: saturated hydrocarbons; Aro.HC: aromatic hydrocarbons; CPI: carbon preference index; Pr/Ph: pristane/phytane; OI: oleanane index)
[A]Data from J. Rauball [pers.comm. 2018]

The saturated hydrocarbons consist almost exclusively of *n*-alkanes.

n-alkanes - The *n*-alkane distribution in the Kokhanivka Formation shows maximum intensities in the short to mid chained *n*-alkanes. Longer chained *n*-alkanes are depleted. Higher maturity is likely the reason, as absence of higher land plants is ruled out due to the occurrence of perylene in the aromatic fraction. A weak odd-over-even predominance of long-chain *n*-alkanes, as indicated by carbon preference indices between 1.1 and 1.4, is consistent with high plant precursors.

Acyclic isoprenoids - Pr/Ph ratios range from 1.4 to 3.1 (mean Pr/Ph=2.3), indicating oxic conditions during early diagenesis [Didyk et al. 1978]. However, other factors contributing to the Pr/Ph ratios cannot be ruled out. Pr/*n*-C_{17} and Ph/*n*-C_{18} ratios are low and consistent with

(a) high plant sedimentary matter input [Tissot & Welte, 1984] (b) a higher degree of maturity (T_{max}: 438 – 445°C [pers.comm. J.Rauball, 2018]). Figure 30 shows a cross-plot of Pr/*n*-C_{17} versus Ph/*n*-C_{18}.

Aromatic hydrocarbons – Aromatic hydrocarbon fractions are dominated by naphthalene, methylated (C_1 to C_3) naphthalenes, phenanthrene and methylated (C_1 to C_2) phenanthrenes (Figure 29). MPI-1 values have been calculated for all samples, and amount to an average MPI-1 of 0.56. Higher plant biomarker perylene [Aizenshtat, 1973] occurs in all samples, and is consistent with a terrestrial influenced depositional environment.

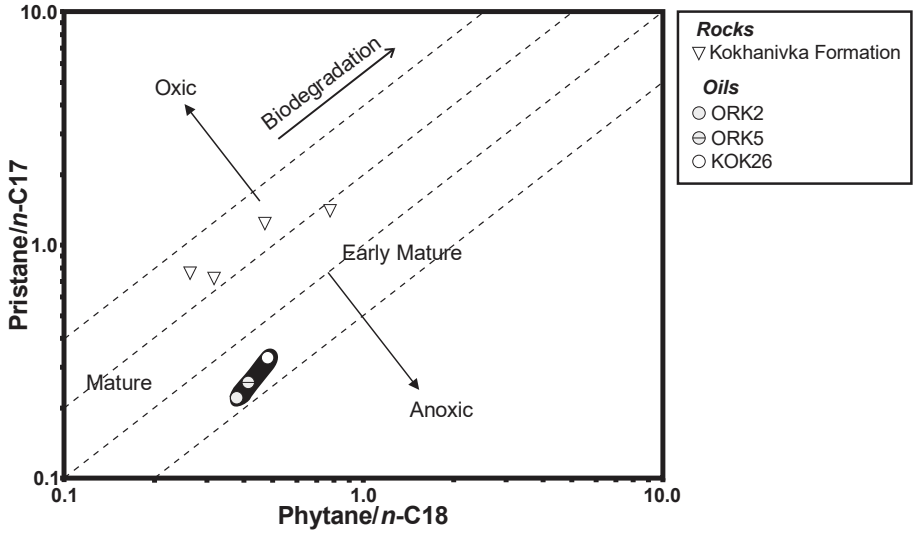

Figure 30. Correlation diagram of pristane/*n*-C17 ratios versus phytane/*n*-C18 ratios of rock and oil samples from the Carpathian Foredeep for the assessment of oil sources, as well as the effects of maturation and biodegradation (modified after Connan & Cassou [1980]).

5.5.1.2 Isotope Ratios

The data on $\delta^{13}C$ obtained from GC-IRMS are listed in Table 18. Figure 31 illustrates a graphical presentation of the GC-IRMS results.

The Khokanivka Formation is isotopically heavy with a mean $\delta^{13}C$ (*n*-C_{17}) of -27.2‰. It has a flat curve, and variation in $\delta^{13}C$ is small between all samples except for J-MS-2523, which is isotopically lighter.

Table 18. Carbon isotopic composition of individual *n*-alkanes of core samples from the Kokhanivka Formation (Carpathian Foredeep).

Sample	*n*-C15	*n*-C16	*n*-C17	*n*-C18	*n*-C19	*n*-C20	*n*-C21	*n*-C22	*n*-C23	*n*-C24	*n*-C25	*n*-C26	*n*-C27	*n*-C28	*n*-C29
	δ13C (‰; PDB)														
J-MS-2523		-27.3	-27.6	-28.0	-27.8	-28.0	-28.2	-28.3	-27.6	-27.7	-28.3	-27.8	-28.4	-28.6	
J-K6-3428	-26.2	-26.9	-27.2	-26.7	-26.7	-26.3	-26.5	-26.8	-27.0	-27.1	-26.9	-27.2	-27.3	-27.7	-28.1
J-K6-3493	-26.7	-26.8	-27.1	-26.9	-26.5	-26.2	-26.4	-26.5	-26.5	-26.8	-27.3	-27.4	-27.6	-27.4	-27.5
J-K6-3521	-26.4	-26.7	-27.0	-27.2	-26.8	-26.4	-26.6	-26.5	-26.9	-27.0	-26.9	-26.7	-27.3	-27.8	-27.4

PDB = Peedee Belemnite (int. Standard)

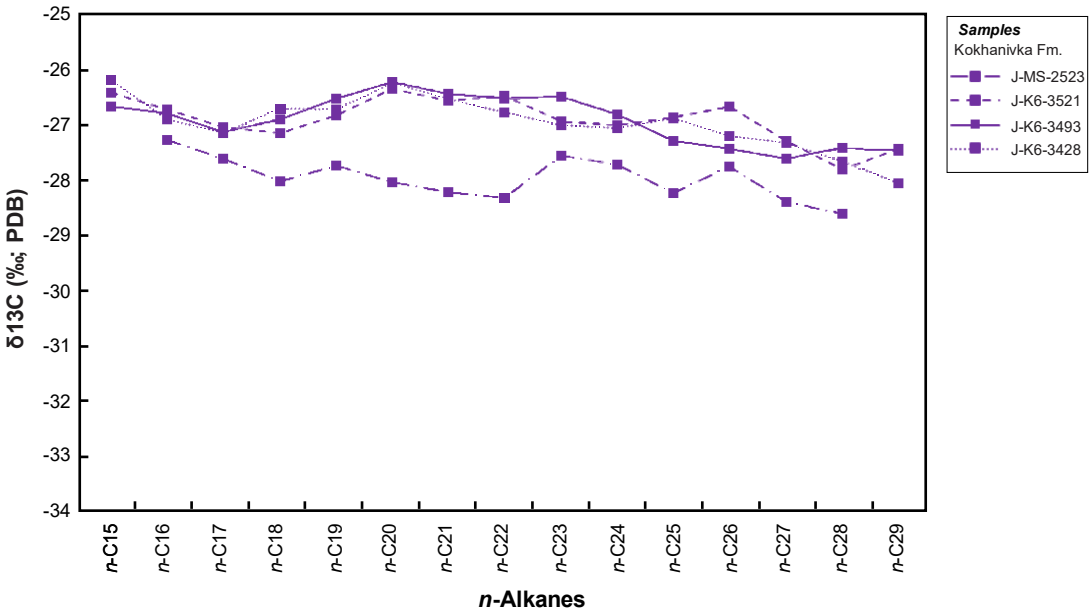

Figure 31. Carbon isotopic composition of individual *n*-alkanes of core samples from the Kokhanivka Formation (Carpathian Foredeep).

5.5.2 Oils

5.5.2.1 Biomarker Composition

Oils recovered from wells Kokhanivka-26 (sample KOK26), Orkhovychi-2 (ORK2), and Orkhovichy-5 (ORK5) occur within Upper Jurassic strata [pers.comm. Y.Koltun]. They are characterized by relative proportions of hydrocarbon fractions between 12 and 28% and fractions of NSO compounds and asphaltenes between 72 and 88%. API gravity data from Wieclaw et al. [2012] show values of 6.8°API and 13.4°API for samples KOK26 and ORK2, respectively. The values classify the oils as extra heavy and heavy oils [Tissot & Welte, 1984]. Wieclaw et al. [2012] also report high sulphur contents for the KOK26 (4.35 wt%) and ORK2 oils (6.5 wt%).

Gas chromatograms (GC) of the saturated and aromatic hydrocarbon fractions of oil sample ORK5 are shown in Figure 32 (chromatograms of all oil samples from the Carpathian Foredeep are compiled in the Appendix). There are only minor differences in the molecular composition of the hydrocarbons between the samples, as reflected by organic geochemical facies and maturation parameters (Table 19).

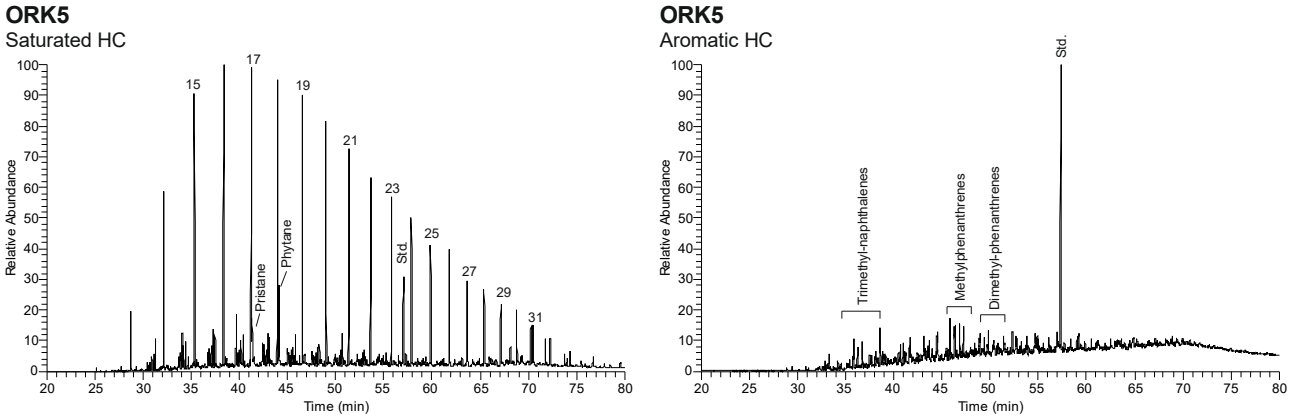

Figure 32. Chromatograms (Total Ion Current) of the saturated and aromatic hydrocarbon fractions of oil sample ORK5 from the Carpathian Foredeep. *n*-Alkanes are labelled according to their carbon number. Std. = standard (deuterated n-tetracosane).

Table 19. Organic geochemical parameters, concentration ratios of specific biomarkers of oil samples from the Carpathian Foredeep.

Sample	Grav. (API°)	Sat.HC (%)	Aro.HC (%)	N+A (%)	*n*-C15-19/ Σ*n*-alk.	*n*-C21-25/ Σ*n*-alk.	*n*-C27-31/ Σ*n*-alk.	CPI	Pr/Ph	Pri/*n*-C17 [rel.prop]	Ph/*n*-C18 [rel.prop]	MPI-1/ Rc	OI (%)
ORK2	n.a.	5	7	88	0.44	0.31	0.12	1.01	0.55	0.22	0.38	1.9/ 1.5	0
ORK5	n.a.	10	17	72	0.47	0.29	0.12	0.99	0.62	0.26	0.42	2.1/ 1.7	0
KOK26	[A]6.8	5	10	85	0.45	0.30	0.13	0.98	0.69	0.33	0.48	1.6/ 1.4	0

(Grav: gravity; API: american petroleum institute; Sat.HC: saturated hydrocarbons; Aro.HC: aromatic hydrocarbons; N+A: NSO compounds + asphaltenes; CPI: carbon preference index; Pr/Ph: pristane/phytane ratio; MPI-1: methylphenanthrene index; Rc: vitrinite reflectance, calculated; OI: oleanane index; n.a.: no data)
[A]Data from Kotarba et al. [2007]

The saturated hydrocarbons are dominated by *n*-alkanes. Steranes and hopanes are depleted. The *n*-alkane distribution shows maximum intensities in the short chain range (average *n*-C_{15-29}/Σ*n*-alk = 45%), and very low intensities in the long chain range (average *n*-C_{27-31}/Σ*n*-alk = 12%). Carbon preference indices lie between 0.98 and 1.01. Pr/Ph ratios are very low and range from 0.5 to 0.7 (average 0.6). Pr/*n*-C_{17} and Ph/*n*-C_{18} ratios are shown in Figure 30. They indicate a relatively high maturity of the oil samples. Aromatic hydrocarbon fractions contain methylated (C_2 to C_3) naphthalenes and methylated (C_1 to C_2) phenanthrenes. MPI-1 values are high and range from 1.6 to 2.1. This corresponds to calculated vitrinite reflectance values (R_c) of 1.4 to 1.7 (Table 19).

5.5.2.2 Isotope Ratios

The data on $\delta^{13}C$ obtained from GC-IRMS are listed in Table 20. Figure 33 Illustrates a graphical presentation of the GC-IRMS results.

Table 20. Carbon isotopic composition of individual *n*-alkanes of oil samples from the Carpathian Foredeep.

Sample	*n*-C15	*n*-C16	*n*-C17	*n*-C18	*n*-C19	*n*-C20	*n*-C21	*n*-C22	*n*-C23	*n*-C24	*n*-C25	*n*-C26	*n*-C27	*n*-C28	*n*-C29
	δ13C (‰; PDB)														
ORK2			-29.8	-30.2	-30.5	-30.7	-31.0	-30.8	-30.9	-31.1	-31.2	-31.5	-31.7		
ORK5		-30.5	-30.8	-30.9	-30.9	-31.3	-31.4	-31.7	-31.5	-31.6	-31.3	-31.9	-32.1	-31.9	
KOK26			-30.6	-30.9	-30.7	-31.2	-31.1	-31.4	-31.3	-31.7	-31.4	-31.8	-31.9	-32.0	

PDB = Peedee Belemnite (int. Standard)

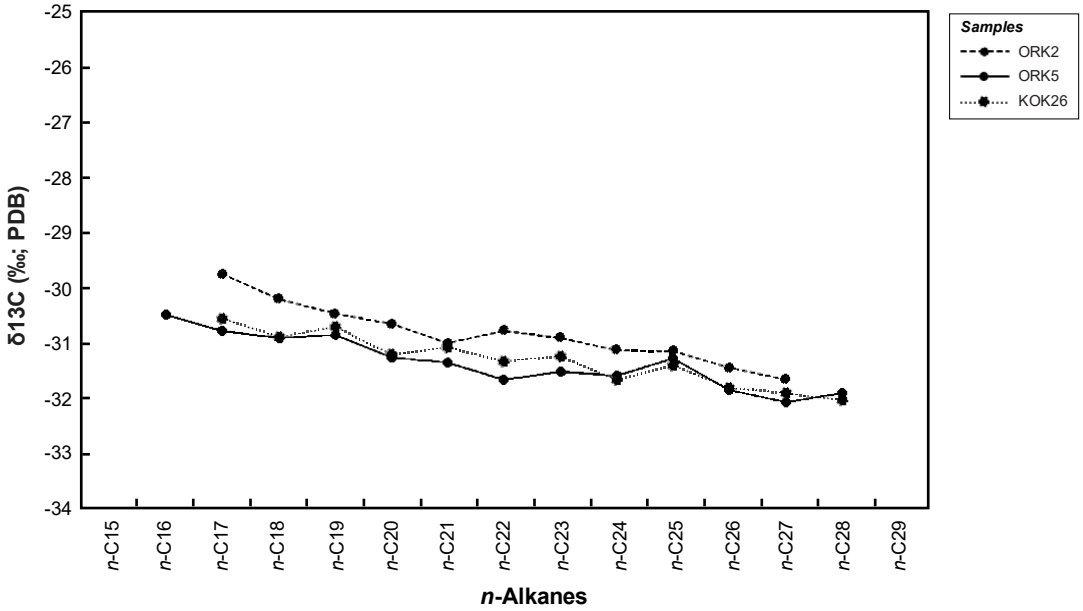

Figure 33. Carbon isotopic composition of individual *n*-alkanes of oil samples from the Carpathian Foredeep.

The oils are isotopically light with an average $\delta^{13}C$ (*n*-C_{17}) of -30.4‰. Variation between the samples is small, although the Kokhanivka oil (KOK26) is slightly heavier with a $\delta^{13}C$ (*n*-C_{17}) value of -30.6‰ than the Orkhovychi oils with an average $\delta^{13}C$ (*n*-C_{17}) of -30.3‰. The curve has a negative slope.

5.6 Western Black Sea

5.6.1 Source rocks

5.6.1.1 Biomarker Composition

The cuttings samples from the Western Black Sea are from two wells; Galata-1 (Gal- samples) and Varna Zapad-1 (VarZ1- samples). They have been previously described by Rupprecht [2014] and are characterized by relative proportions of hydrocarbon fractions between 15 and 42% and fractions of NSO compounds and asphaltenes between 58 and 85%. Saturated hydrocarbons predominate over aromatic hydrocarbons in samples from both wells.

Gas chromatograms (GC) of the saturated and aromatic hydrocarbons of samples from the Kaliakra Canyon Fill (VarZ1-733) and Ruslar Formation (VarZ1-892) from well Varna Zapad-1 are shown in Figure 34 and Figure 35 (chromatograms of all rock samples from the W. Black Sea are compiled in the Appendix). There are only minor differences in the molecular composition of the hydrocarbons between the samples, as reflected by organic geochemical facies and maturation parameters (Table 21.

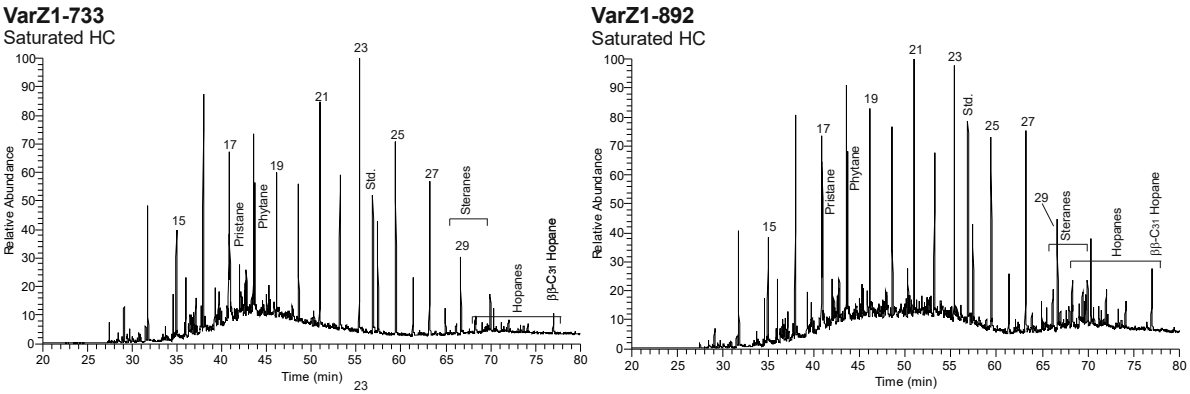

Figure 34. Chromatograms (Total Ion Current) of the saturated hydrocarbon fractions of cuttings samples VarZ1-733 (Kaliakra Cany. Fill) and VarZ1-892 (Ruslar-Fm.) from well Varna Zapad-1 offshore Bulgaria (W. Black Sea). *n*-Alkanes are labelled according to their carbon number. Std. = standard (1,1-binaphthyl).

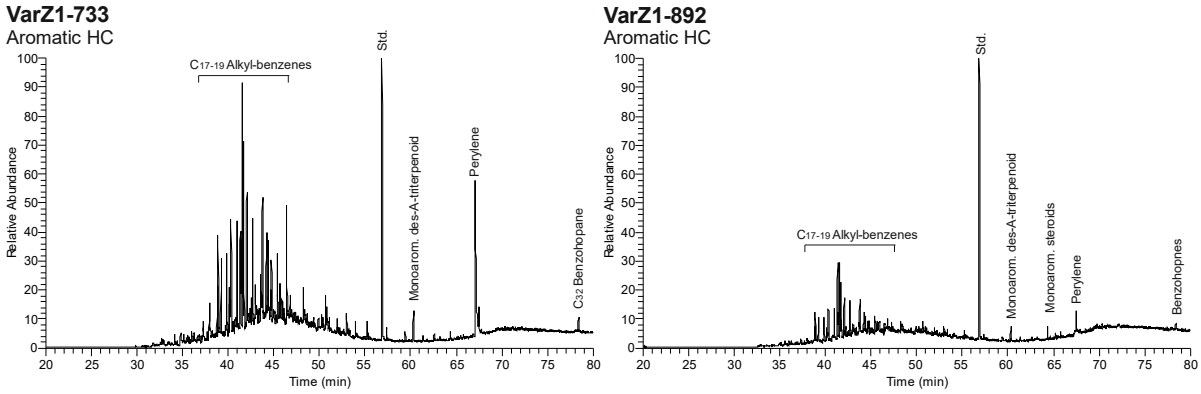

Figure 35. Chromatograms (Total Ion Current) of the aromatic hydrocarbon fractions of cuttings samples VarZ1-733 (Kaliakra Cany. Fill) and VarZ1-892 (Ruslar-Fm.) from well Varna Zapad-1 well offshore Bulgaria (W. Black Sea) Std. = standard (1,1-binaphthyl).

The saturated hydrocarbons are dominated by *n*-alkanes and hopanes, steranes are present in minor concentrations.

n-alkanes - The *n*-alkane distribution of the Kaliakra Canyon Fill shows maximum intensities in the mid chain range (average *n*-C_{21-25}/Σ*n*-alk = 44%), and lowest intensities in the long chain range (average *n*-C_{27-31}/Σ*n*-alk = 16%). The Ruslar Formation shows similar distributions, although compared to the Kaliakra Canoyon Fill it contains slightly less mid chain *n*-alkanes.

The Avren Formation (VarZ1-928) is dominated by long chain *n*-alkanes. Strong odd-over-even predominances of long-chain *n*-alkanes as indicated by high CPI values in the Kaliakra Canyon Fill (2.4 – 3.5), the Ruslar Formation (1.5 – 3.9), and the Avren Formation (5.0), indicate terrestrial organic matter input and are consistent with low maturity (T_{max}: avg. 431°C in Kaliakra C.F., avg. 421°C in Ruslar Fm. [Rupprecht, 2014], < 430°C in Avren Fm. [Mayer et al., 2018a]) .

Acyclic isoprenoids - Pr/Ph ratios range from 0.8 to 1.4 in the Kaliakra Canyon Fill, from 0.3 to 1.0 in the Ruslar Formation, and amount to 0.7 in the Avren Formation, indicating anoxic conditions during early diagenesis [Didyk et al. 1978]. Anoxic conditions for the Ruslar Formation have also been reported by Sachsenhofer et al. [2009], and are confirmed in the Kaliakra Canyon Fill by the presence of high concentrations of 28,30-bisnorhopane [Peters & Moldowan, 1993] in sample Gal-880. Pr/*n*-C_{17} and Ph/*n*-C_{18} ratios are low in all samples. A cross-plot of Pr/*n*-C_{17} versus Ph/*n*-C_{18} is shown in Figure 36.

Table 21. Bulk organic geochemical parameters, concentration and concentration ratios of specific biomarkers of cuttings samples of the Kaliakra Cany. Fill, Ruslar Fm. & Avren Fm. from wells Galata-1 and Varna Zapad-1 offshore Bulgaria (W. Black Sea).

Sample	Age	TOC[A]	HI[A]	Tmax[A] (%)	Sat.HC (%)	Aro HC (%)	N+A (%)	*n*-alk	*n*-C15-19/ Σ*n*-alk.	*n*-C21-25/ Σ*n*-alk.	*n*-C27-31/ Σ*n*-alk.	CPI
Kaliakra C.F.												
Gal-880	Miocene	2.21	399	429	16	10	74	851	0.35	0.41	0.15	2.5
Gal-910	Miocene	1.82	284	431	14	11	75	628	0.40	0.39	0.12	3.3
VarZ1-480	Miocene	1.73	245	430	28	8	63	637	0.39	0.52	0.08	n.a.
VarZ1-570	Miocene	2.61	360	432	12	3	85	573	0.22	0.51	0.18	2.6
VarZ1-600	Miocene	2.62	397	431	16	3	81	640	0.25	0.48	0.17	3.5
VarZ1-660	Miocene	2.56	270	435	12	5	83	370	0.28	0.54	0.10	3.0
VarZ1-753	Miocene	1.57	238	432	16	5	79	640	0.31	0.44	0.15	3.0
Ruslar Fm.												
VarZ1-817	Oligocene	2.29	337	424	14	3	83	795	0.17	0.49	0.23	3.9
VarZ1-883	Oligocene	1.89	309	420	32	10	58	702	0.30	0.35	0.20	1.5
VarZ1-892	Oligocene	2.05	350	426	18	7	75	556	0.30	0.38	0.20	2.3
Avren Fm.												
VarZ1-928	Eocene	3.62	201	n.a.	10	5	85	280	0.23	0.30	0.35	5.0

Sample	Pr/Ph [rel.prop]	Pri/*n*-C17 [rel.prop]	Ph/*n*-C18 [rel.prop]	Steranes (µg/g TOC)	Hopanes (µg/g TOC)	St / Hop	OI (%)	ααα R+S Steranes C27/ ΣC27-29St.	C28/ ΣC27-29St.	C29/ ΣC27-29St.
Kaliakra C.F.										
Gal-880	0.86	1.05	1.59	5.5	4.2	1.3	n.a.	0.44	0.23	0.32
Gal-910	0.94	1.56	1.43	1.8	5.0	0.4	52	0.39	0.27	0.34
VarZ1-480	1.38	1.15	0.72	n.a.	n.a.	n.a.	n.a.	n.a.	n.a.	n.a.
VarZ1-570	1.14	1.11	0.92	0.3	0.9	0.3	186	0.50	0.25	0.25
VarZ1-600	0.97	1.04	1.13	2.4	7.0	0.4	122	0.51	0.18	0.31
VarZ1-660	0.92	1.63	1.17	1.5	1.7	0.9	117	0.52	0.18	0.30
VarZ1-733	0.82	0.81	0.89	0.4	1.7	0.2	162	0.50	0.14	0.35
Ruslar Fm.										
VarZ1-817	0.25	0.90	4.36	1.9	4.6	0.4	74	0.51	0.22	0.27
VarZ1-883	0.90	1.02	0.94	1.8	3.9	0.5	156	0.39	0.28	0.33
VarZ1-892	1.00	1.18	1.02	1.7	5.2	0.3	138	0.39	0.27	0.35
Avren Fm.										
VarZ1-928	0.73	0.96	0.98	0.4	1.1	0.4	131	0.41	0.30	0.29

(TOC: total organic carbon in wt%; HI: hydrogen index in mg HC/g TOC; Sat.HC: saturated hydrocarbons; Aro.HC: aromatic hydrocarbons; N+A: NSO compounds + asphaltenes; n-alk: n-alkane concentration in µg/g TOC; CPI: carbon preference index; Pr/Ph: pristane/phytane ratio; OI: oleanane index; n.a.: no data)

[A]Data from Rupprecht [2014]

Steranes and hopanes - Steranes are present in small concentrations, ranging from 0.3 µg/g TOC to 5.5 µg/g. C_{27} steranes are dominating in all samples, although their concentrations are a little smaller in the lower parts of the Ruslar Formation (VarZ1-883, VarZ1-892).
Hopanes are present in concentrations from 0.9 µg/g TOC to 5.2 µg/g. Sterane/hopane ratios are very low for all samples except Gal-880, indicating terrestrial and/or microbially reworked organic matter [Tissot & Welte, 1984]. Bisnorhopane shows extremely high intensities in sample Gal-880.

Aromatic hydrocarbons – Aromatic hydrocarbon fractions are dominated by alkylated (C_{17} - C_{19}) benzenes (Figure 35). Additionally, land plant derived biomarkers simonellite, retene, perylene and monoaromatic des-A-triterpenoid occur in samples of the Varna Zapad-1 well, indicating terrestrial influence on the sedimentary source of the organic matter.

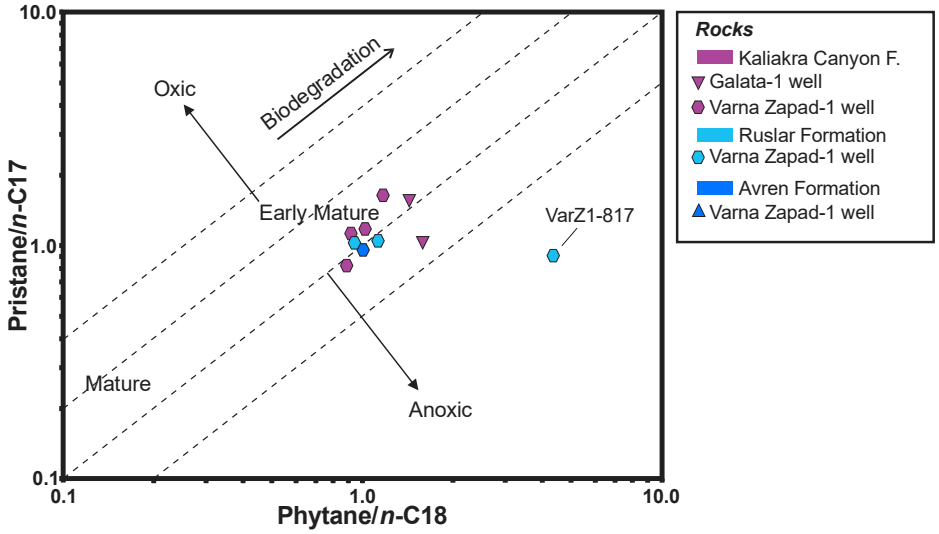

Figure 36. Correlation diagram of pristane/*n*-C17 ratios versus phytane/*n*-C18 ratios for the assessment of oil sources, as well as the effects of maturation and biodegradation of cuttings samples of the Kaliakra Cany. Fill, Ruslar Fm. & Avren Fm. from wells Galata-1 and Varna Zapad-1 offshore Bulgaria (W. Black Sea; modified after Connan & Cassou [1980]).

5.6.1.2 Isotope Ratios

The data on $\delta^{13}C$ obtained from GC-IRMS are listed in Table 22. Figure 37 illustrates a graphical presentation of the GC-IRMS results.

The samples of the Kaliakra Canyon Fill and the upper part of the Ruslar Formation (VarZ1-817) correlate well with each other. The deeper parts of the latter are are isotopically lighter. The Kaliakra Canyon Fill has an average $\delta^{13}C$ (*n*-C_{17}) value of -29.5‰, while the deeper parts of the Ruslar Formation have an average $\delta^{13}C$ (*n*-C_{17}) value of -29.7‰. The difference increases until the *n*-C_{21} alkane, where it amounts to approximately 1‰. Afterwards, the difference decreases, but still is very pronounced. The Avren Formation stands out in terms of shape, best visible in mid and long chain range. It has a $\delta^{13}C$ (*n*-C_{17}) value of -29.5‰ and $\delta^{13}C$ (*n*-C_{28}) value of -30.8‰ and is isotopically lighter in the higher chained *n*-alkanes, resulting in a negatively sloping curve.

Table 22. Average C isotopic composition of individual *n*-alkanes of cuttings samples from wells Galata-1 & Varna Zapad-1 offshore Bulgaria (W. Black Sea).

Sample	*n*-C15 δ13C (‰; PDB)	*n*-C16	*n*-C17	*n*-C18	*n*-C19	*n*-C20	*n*-C21	*n*-C22	*n*-C23	*n*-C24	*n*-C25	*n*-C26	*n*-C27	*n*-C28	*n*-C29
Kaliakra C.F.															
Gal-880	-29.0	-29.3	-29.6	-29.8	-29.5	-29.8	-30.2	-30.5	-30.2	-29.9	-29.7	-29.7	-29.5	-29.7	-29.4
Gal-910	-28.6	-29.2	-29.3	-29.8	-29.7	-30.0	-30.3	-30.6	-30.3	-29.8	-29.9	-30.0	-29.8	-29.5	-29.6
VarZ1-480	-29.0	-29.0	-29.7	-29.9	-29.7	-29.9	-30.0	-30.3	-30.0	-29.9	-29.6	-29.4	-29.4	-29.3	-29.0
VarZ1-570	-28.7	-28.9	-29.6	-29.5	-29.8	-29.7	-30.3	-30.4	-30.2	-29.8	-29.8	-29.6	-29.5	-29.3	-29.5
VarZ1-600	-28.6	-29.3	-29.6	-29.4	-29.7	-29.9	-30.1	-30.5	-29.9	-29.7	-29.4	-29.3	-29.2	-29.6	-29.1
VarZ1-660	-28.9	-29.1	-29.3	-29.2	-29.5	-30.0	-30.6	-30.4	-30.2	-29.8	-29.5	-29.8	-29.7	-29.2	-29.5
VarZ1-753	-28.7	-29.2	-29.2	-29.3	-29.4	-29.7	-30.4	-30.5	-30.4	-30.1	-29.8	-29.5	-29.5	-29.5	-29.6
Ruslar Fm.															
VarZ1-817	-28.9	-29.1	-29.2	-29.4	-29.6	-29.8	-30.5	-30.3	-29.9	-30.1	-29.9	-30.0	-29.8	-29.5	-29.4
VarZ1-883	-28.9	-29.3	-29.6	-29.9	-30.4	-30.5	-30.9	-30.6	-30.1	-30.3	-29.9	-30.1	-30.3	-29.8	-29.5
VarZ1-892		-29.1	-29.7	-30.0	-30.3	-30.6	-31.2	-30.8	-30.5	-30.3	-30.4	-30.3	-30.5	-30.2	
Avren Fm.															
VarZ1-928		-29.5	-29.8	-29.9	-30.2	-30.3	-30.6	-30.5	-30.8	-30.7	-30.9	-30.6	-31.0	-30.8	

PDB = Peedee Belemnite (int. Standard)

The Kaliakra Canyon Fill and Ruslar Formation show a similar V shape pattern as observed in the Schöneck Formation in the Molasse Basin, however, in the Kaliakra Canyon Fill the smallest $\delta^{13}C$ values are found alternating between *n*-C_{21} (VarZ1-660) and *n*-C_{22} (Gal-880, Gal-910, VarZ1-480, VarZ1-570, VarZ1-600, VarZ1-753) *n*-alkanes. Generally, $\delta^{13}C$ values decrease from a mean $\delta^{13}C$ (*n*-C_{15}) of -28.8‰ to a minimum mean $\delta^{13}C$ at *n*-C_{21} of -30.8‰ and a mean $\delta^{13}C$ at *n*-C_{22} of -30.5‰ respectively, and increase thereafter to a mean $\delta^{13}C$ (*n*-C_{28}) of -29.5‰.

The Avren Formation differs significantly and shows a constant decrease in $\delta^{13}C$ values with increasing chain length, resulting in a negatively sloping curve. The slightly lower $\delta^{13}C$ values of odd carbon numbered homologues in the *n*-C_{23} to *n*-C_{29} range in some samples is interpreted to reflect the contribution of leaf lipids of plants [Collister et al., 1994a].

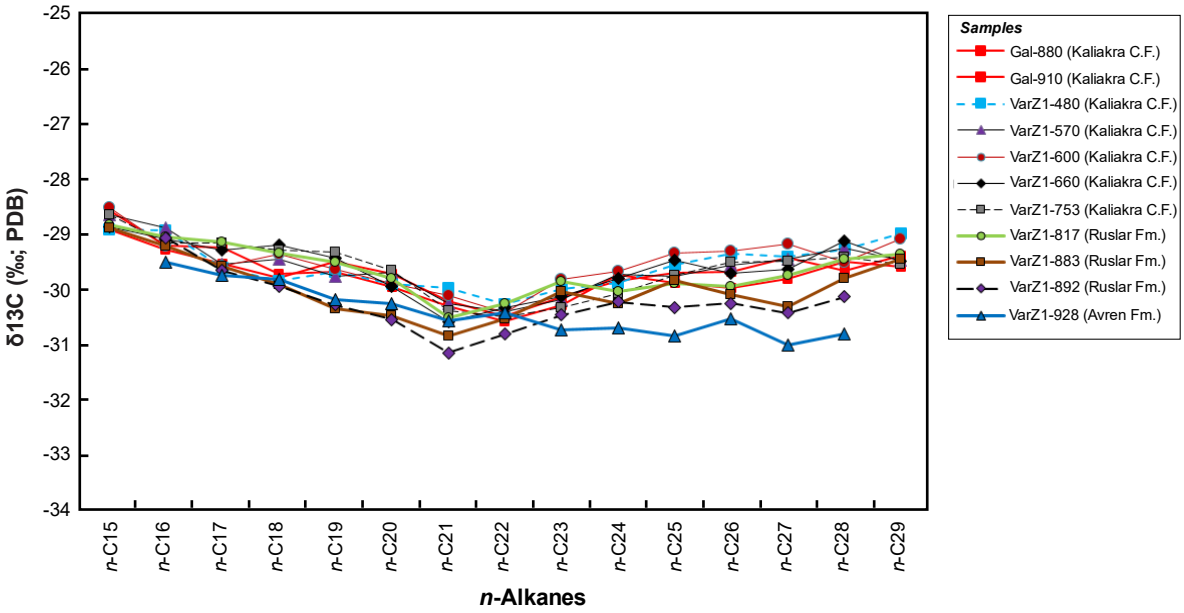

Figure 37. Carbon isotopic composition of individual *n*-alkanes of cuttings samples from wells Galata-1 & Varna Zapad-1 offshore Bulgaria (W. Black Sea).

5.6.2 Tjulenovo oil

5.6.2.1 Biomarker Composition

A gas chromatogram (GC) of the saturated and aromatic hydrocarbons of the Tjulenovo oil from the W. Black Sea is shown in Figure 38. Concentrations and concentration ratios in the hydrocarbon fractions are listed in Table 23. The Tjulenovo oil is depleted in *n*-alkanes; this is probably related to intense biodegradation.

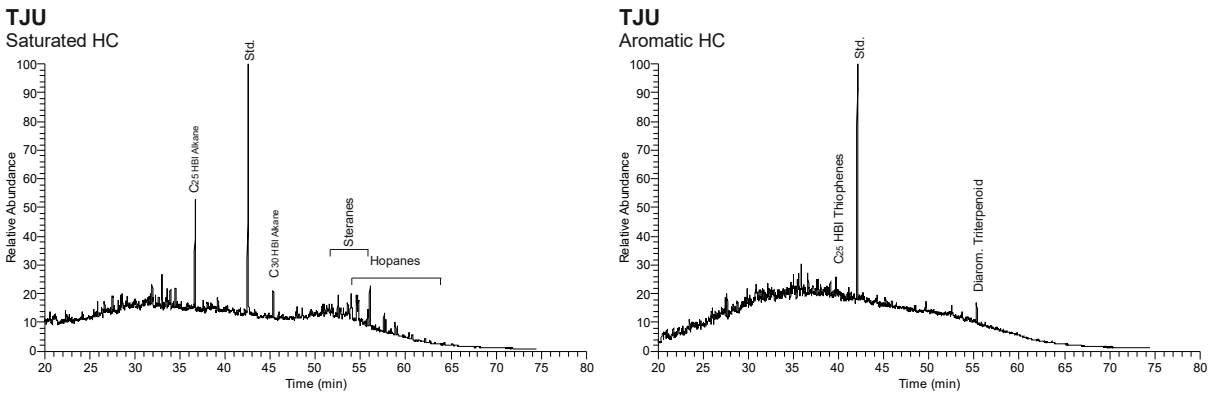

Figure 38. Chromatograms (Total Ion Current) of the saturated and aromatic hydrocarbon fractions of the Tjulenovo oil (W. Black Sea, Bulgaria). Std. = standard (deuterated n-tetracosane).

The saturated hydrocarbons are dominated by steranes and hopanes. Additionally, C_{25} and C_{30} HBI (highly branched isoprenoids) alkanes show high intensities. The low sterane/hopane ratio of 0.8 probably results of a special, bacteria-influenced facies [Mackenzie, 1984], as non-marine sources are unlikely due to the occurrence of diatom markers C_{25} HBI thiophenes [Volkman et al, 1994]. The aromatic hydrocarbon fraction is depleted.

Table 23. Organic geochemical parameters, concentration ratios of specific biomarkers of the Tjulenovo oil (sample TJU) from the W. Black Sea (Bulgaria).

Sample	Sat.HC (%)	Aro.HC (%)	N+A (%)	Steranes/ Hopanes	OI [A] (%)
TJU	0.41	0.25	0.32	0.80	36.5

(Sat.HC: saturated hydrocarbons; Aro.HC: aromatic hydrocarbons; N+A: NSO compounds + asphaltenes; OI: oleanane index)
[A]Data from Mayer et al. [2018b]

5.6.2 Isotope Ratios

The data on $\delta^{13}C$ obtained from GC-IRMS are listed in Table 24. Figure 39 illustrates a graphical presentation of the GC-IRMS results.

The Tjulenovo oil is lighter than the rock extracts of the Ruslar and Avren Formation (5.6.1.2), as can be expected from expelled hydrocarbons [Peters et al., 1981, Liao et al., 2004]. It has a pronounced V shape pattern; showing a decrease in $\delta^{13}C$ values from *n*-C_{17} (-29.9‰) to a minimum $\delta^{13}C$ (*n*-C_{21}) of -31.8‰ and an increase thereafter to $\delta^{13}C$ (*n*-C_{28}) -29.2‰.

Table 24. Carbon composition of individual *n*-alkanes of the Tjulenovo oil (sample TJU) from the W. Black Sea (Bulgaria).

Sample	*n*-C15	*n*-C16	*n*-C17	*n*-C18	*n*-C19	*n*-C20	*n*-C21	*n*-C22	*n*-C23	*n*-C24	*n*-C25	*n*-C26	*n*-C27	*n*-C28	*n*-C29
	δ13C (‰; PDB)														
TJU			-29.9	-30.4	-30.7	-31.4	-31.8	-31.3	-30.7	-30.5	-30.3	-29.8	-29.7	-29.5	-29.2

PDB = Peedee Belemnite (int. Standard)

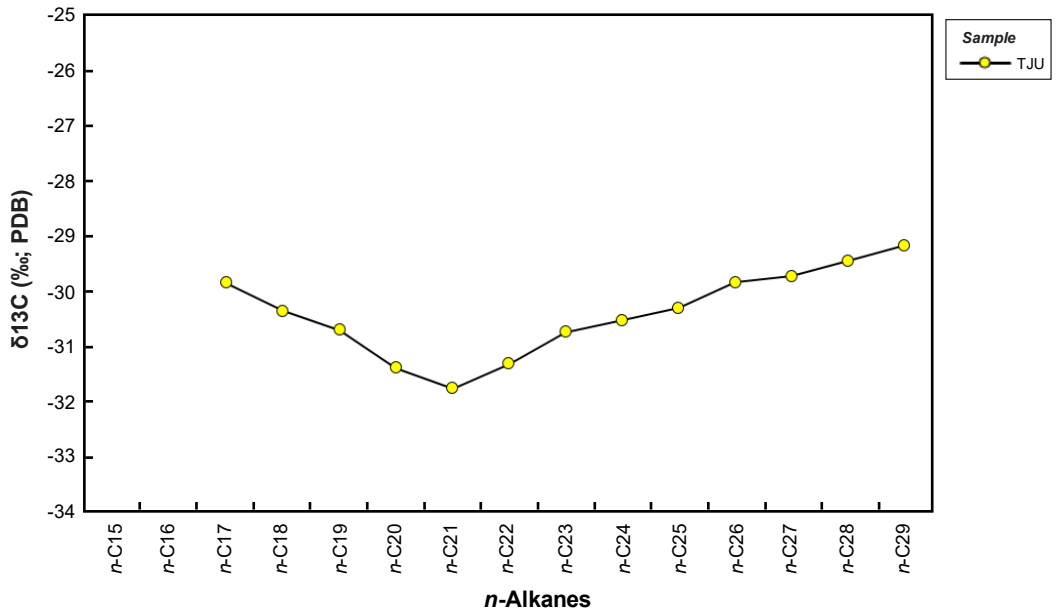

Figure 39. Carbon isotopic composition of individual *n*-alkanes of the Tjulenovo oil (sample TJU) from the W. Black Sea (Bulgaria).

5.7 Rioni Basin

5.7.1 Source rocks

5.7.1.1 Biomarker composition

Extracts of Maikopian sediments from the Rioni Basin (Martvili section; [Pupp et al., 2018b]) are characterized by relative proportions of hydrocarbon fractions between 16 and 21% and fractions of NSO compounds and asphaltenes between 79 and 84%. Saturated hydrocarbons are predominant over aromatic hydrocarbons.

Kuma Formation rock samples from the same section show similar relative proportions of (saturated + aromatic) hydrocarbons and NSO + asphaltene fractions, however, their aromatic hydrocarbon fraction is on average more abundant than their saturated fractions.

Gas chromatograms (GC) of the saturated and aromatic hydrocarbons of the Maikopian sediments and of samples from the Kuma Formation are shown in Figure 40 and Figure 41 (chromatograms of all rock samples from the Rioni Basin are compiled in the Appendix). There are significant differences in the molecular composition of the hydrocarbons between Maikop and Kuma samples, as reflected by organic geochemical facies and maturation parameters (Table 25).

The saturated hydrocarbons are dominated by *n*-alkanes, steranes, and hopanes.

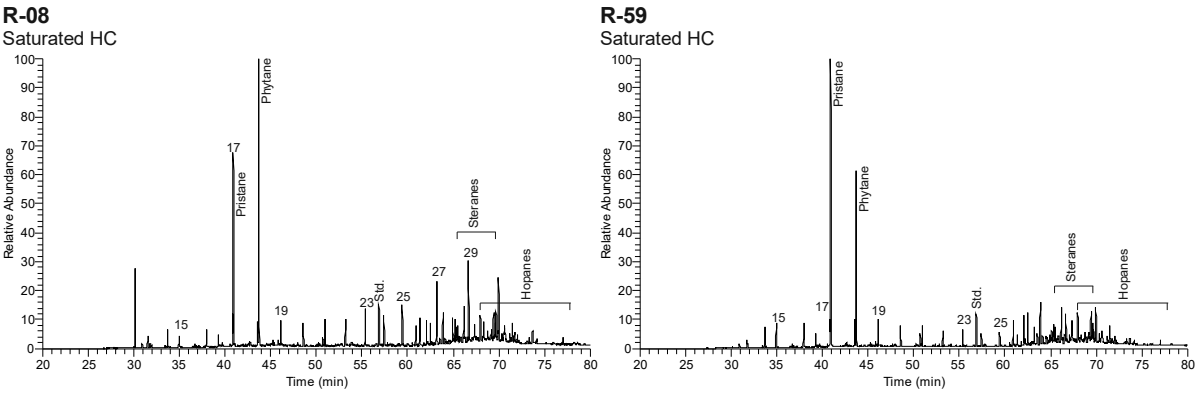

Figure 40. Chromatograms (Total Ion Current) of the saturated hydrocarbon fractions of rock extracts of the Maikopian sed. (sample R-08) and Kuma Fm. (sample R-59) from the Rioni Basin (Georgia). *n*-Alkanes are labelled according to their carbon number. Std. = standard (1,1-binaphthyl).

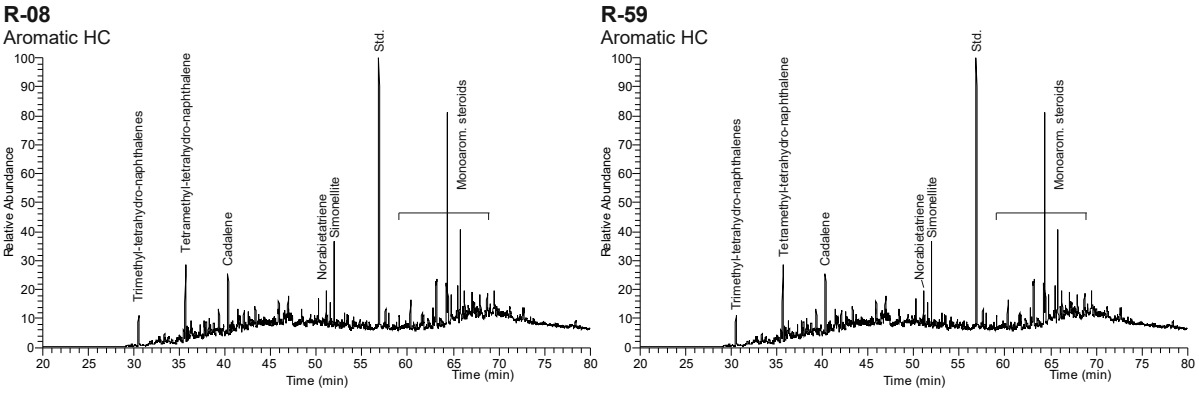

Figure 41. Chromatograms (Total Ion Current) of the aromatic hydrocarbon fractions of rock extracts of the Maikopian sed. (sample R-08) and Kuma Fm. (sample R-59) from the Rioni Basin (Georgia). Std. = standard (1,1-binaphthyl).

n-alkanes - The *n*-alkane distribution shows maximum intensities in the long chain range (avg. *n*-C_{27-31}/Σ*n*-alk = 48%) in the Maikopian sediments, which is consistent with higher plant

contribution, as also indicated by the occurrence of angiosperm and conifer biomarkers. The relatively high concentration of long chain *n*-alkanes for the fully marine Kuma formation [Pupp et al., 2018b] is likely due to immaturity (T_{max}: 413 – 414°C [Pupp et al., 2018b]). Carbon preference indices between 2.2 and 2.5 and the bimodial distribution of the *n*-alkanes in the GC traces are consistent with low maturity for both formations [Peters & Moldowan, 1993; Tissot & Welte, 1984].

Table 25. Bulk organic geochemical parameters, concentration and concentration ratios of specific biomarkers of rock extracts from the Rioni Basin (Georgia).

Sample	TOC[A]	HI[A]	Tmax[A] (°C)	EOM	Sat.HC (%)	Aro HC (%)	N+A (%)	*n*-alk (µg/g TOC)	*n*-C15-19/ Σ*n*-alk.	*n*-C21-25/ Σ*n*-alk.	*n*-C27-31/ Σ*n*-alk.	CPI
Maikopian sed.												
R-102	2.97	252	407	16	11	5	84	239	0.17	0.26	0.48	2.2
R-94	2.64	230	408	29	12	6	82	298	0.23	0.22	0.46	2.5
R-08	2.16	227	426	26	14	7	79	506	0.14	0.28	0.49	2.4
Kuma Fm.												
R-59	2.96	522	414	23	8	12	80	205	0.32	0.23	0.36	2.4
R-31	7.18	471	413	24	7	8	85	181	0.43	0.21	0.26	2.4

Sample	Pr/Ph [rel.prop]	Pri/*n*-C17 [rel.prop]	Ph/*n*-C18 [rel.prop]	Steranes (µg/g TOC)	Hopanes (µg/g TOC)	St / Hop	OI (%)	αααR+S Steranes C27/ ΣC27-29St.	C28/ ΣC27-29St.	C29/ ΣC27-29St.
Maikopian sed.										
R-102	0.33	10.67	32.75	92	98	0.94	76	0.40	0.32	0.28
R-94	0.37	8.67	23.57	127	112	1.13	99	0.32	0.39	0.28
R-08	0.73	6.29	11.28	134	159	0.84	116	0.39	0.34	0.28
Kuma Fm.										
R-59	1.61	11.67	7.26	81	78	1.03	109	0.32	0.39	0.29
R-31	1.90	8.93	4.71	51	58	0.88	82	0.37	0.31	0.32

(TOC: total organic carbon in wt%; HI: hydrogen index in mg HC/g TOC; EOM: extractable organic matter in mg/g TOC; Sat.HC: saturated hydrocarbon; Aro.HC: aromatic hydrocarbons; N+A: NSO compounds + asphaltenes, CPI: carbon preference index; Pr/Ph: pristane/phytane ratio; OI: oleanane index)
[A]Data from Rupprecht [2014]

Acyclic isoprenoids - In the Maikopian sediments Pr/Ph ratios range from 0.3 to 0.7, indicating anoxic conditions during early diagenesis [Didyk et al. 1978]. In the Kuma Formation Pr/Ph ratios (1.6 – 1.9) are higher, indicating dysoxic conditions, which are confirmed by the occurrence of trimethyl- and tetramethyl-tetrahydro-naphthalenes (oxidation products of β-carotene [Sommerburg et al., 2013], and therefore markers for oxic environments). Extremely high Pr/*n*-C_{17} and Ph/*n*-C_{18} ratios are likely related to immaturity. A cross plot of Pr/*n*-C_{17} versus Ph/*n*-C_{18} is shown in Figure 42 (*note*: the scale has been adjusted to illustrate the high values).

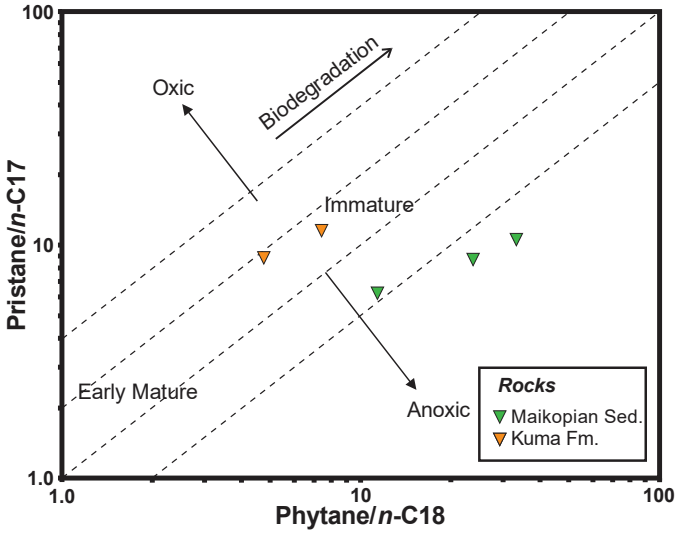

Figure 42. Correlation diagram of pristane/*n*-C17 ratios versus phytane/*n*-C18 ratios of rock extracts of Maikopian sed. & Kuma Fm. from the Rioni Basin (Georgia), for the assessment of oil sources, as well as the effects of maturation and biodegradation (modified after Connan & Cassou [1980]) (note: the scale has been adjusted to illustrate the high values)

Steranes and hopanes - Steranes show similar proportions (Figure 43, Table 25). A depositional environment with both marine and terrestrial influence is suggested. Hopanes are slightly more abundant in the Maikopian sediments than in the Kuma Formation.

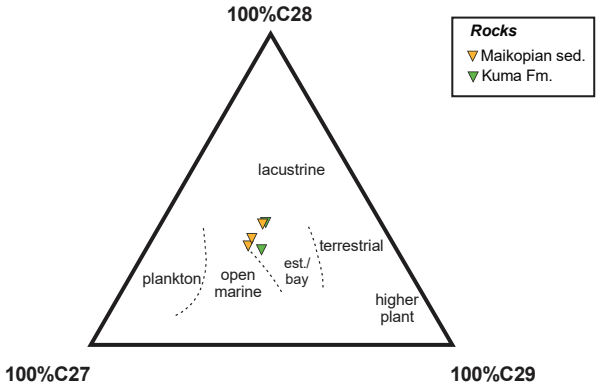

Figure 43. Ternary plot of relative proportions of C27, C28 and C29 steranes in samples of Maikopian sed. & Kuma Fm. from the Rioni Basin, Georgia (modified after Huang & Meinschein, [1979]).

Aromatic hydrocarbons – Aromatic hydrocarbon fractions in both the Kuma Formation and the Maikopian sediments show high intensities of monoaromatic steroids. A variety of higher plant biomarkers are present in high concentrations; trimethyl- and tetramethyl-tetrahydro-naphthalenes, all indirect biomarkers of angiosperms, occur in Maikopian samples R-08 & R-94 and Kuma Formation sample R-59, whereas conifer markers cadalene, norabietatriene and simonellite occur in all samples except R-31 (Kuma Fm). Diatom marker C_{25} HBI thiophenes present in Maikopian sample R-102 suggests the presence of diatom biomass.

5.7.1.2 Isotope Ratios

Isotope data from the samples from the Rioni Basin have been studied within the frame of the present thesis, but have already been published in the paper of Mayer et al. [2018b]. The data on $\delta^{13}C$ obtained from GC-IRMS are listed in Table 26. Figure 44 illustrates a graphical presentation of the GC-IRMS results.

Table 26. Carbon isotopic composition of individual *n*-alkanes of rock extracts of the Maikopian sed. & Kuma Fm. from the Rioni Basin (Georgia).

Sample	*n*-C16	*n*-C17	*n*-C18	*n*-C19	*n*-C20	*n*-C21	*n*-C22	*n*-C23	*n*-C24	*n*-C25	*n*-C26	*n*-C27	*n*-C28	*n*-C29
	δ13C (‰; PDB)													
Maikopian sed.														
R-102	-27.7	-27.8	-28.2	-28.4	-28.7	-28.9	-28.9	-29.0	-28.5	-28.3	-28.5	-28.3	-28.6	-29.1
R-94	-28.1	-28.5	-28.4	-28.8	-29.0	-29.4	-28.9	-29.0	-28.4	-28.4	-28.7	-28.9	-28.8	-29.2
R-08	-27.6	-27.9	-28.1	-28.3	-28.6	-29.1	-29.0	-28.7	-28.5	-28.8	-29.0	-28.6	-28.8	-29.3
Kuma Fm.														
R-59	-29.5	-29.7	-29.6	-29.4	-29.6	-29.2	-28.8	-28.8	-28.5	-28.4	-28.8	-28.8	-28.7	
R-31	-29.3	-29.5	-29.6	-29.5	-29.4	-29.1	-28.5	-28.6	-28.7	-28.6	-28.7	-28.7	-28.4	

PDB = Peedee Belemnite (int. Standard)

A V shape pattern is suggested for the Maikopian sediments. However, it is not as pronounced as in the Schöneck Formation, due to the irregular slope in the *n*-C_{25} to *n*-C_{29} region. The slightly lower $\delta^{13}C$ values of odd carbon numbered homologues in the *n*-C_{25} to *n*-C_{29} range observed in the Maikopian sediments is interpreted to reflect the contribution of leaf lipids of plants [Collister et al., 1994a]. The Kuma Formation has a positively sloping curve up to *n*-C_{24} and a relatively even curve for *n*-alkanes with longer chain lengths.

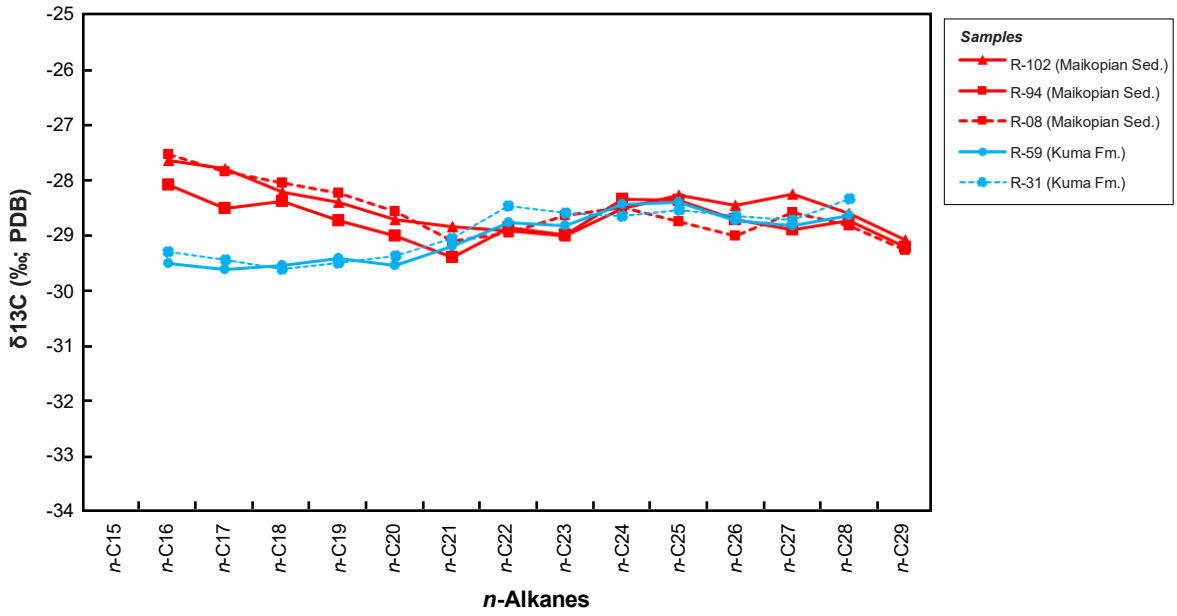

Figure 44. Carbon isotopic composition of individual *n*-alkanes of rock extracts of Maikopian sed. & Kuma Fm. from the Rioni Basin (Georgia).

5.7.2 Shromisubani oil

5.7.2.1 Biomarker Composition

Gas chromatograms of the saturated and aromatic hydrocarbon fractions of the Shromisubani oil (sample PG) from the Rioni Basin are shown in Figure 45. Concentrations and concentration ratios in the hydrocarbon fractions are listed in Table 27.

Table 27. Organic geochemical parameters, concentration ratios of specific biomarkers of the Shromisubani oil (sample PG) from the Rioni Basin (Georgia).

Sample	Sat.HC (%)	Aro.HC (%)	*n*-C15-19/ Σ*n*-alk.	*n*-C21-25/ Σ*n*-alk.	*n*-C27-31/ Σ*n*-alk.	CPI	Pr/ Ph	Pr/*n*-C17 [rel.prop]	Ph/*n*-C18 [rel.prop]	S*	H*	S*/ H*	OI (%)	MPI-1/Rc[A]
PG	32	20	0.33	0.34	0.19	1.6	1.6	3.43	2.33	7	11	0.59	18	0.4/ 0.6

(Sat.HC: saturated hydrocarbons; Aro.HC: aromatic hydrocarbons; CPI: carbon preference index; Pr/Ph: pristane/phytane ratio; S*: sterane concentrations in µg/g TOC; H*: hopane concentrations in µg/g TOC; S/H: steranes/hopanes ratio; OI: oleanane index; MPI-1: methylphenanthrene index; Rc: vitrinite reflectance, calculated [Radke et al., 1984])
[A]Data from Mayer et al. [2018b]

The Shromisubani oil is characterized by a relative proportion of the hydrocarbon fractions of 52% and of fractions of NSO compounds + asphaltenes of 48%.

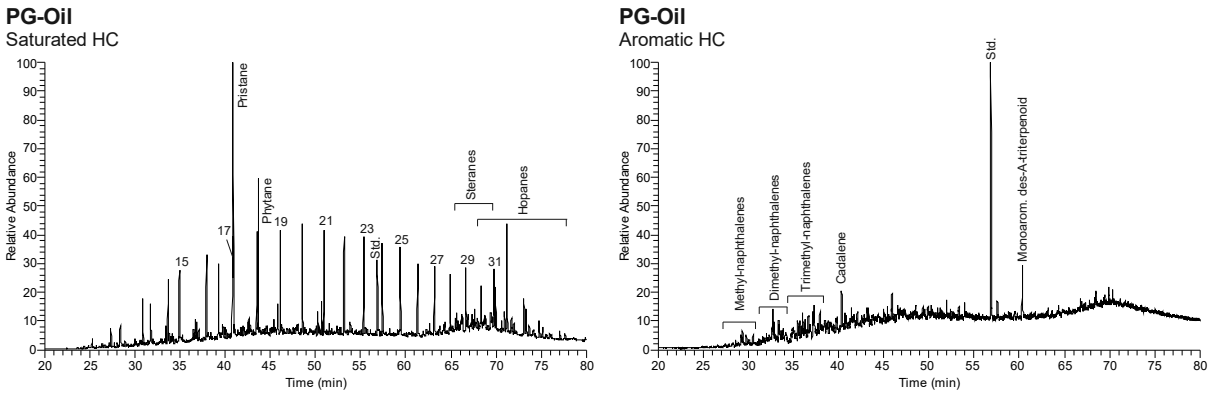

Figure 45. Chromatograms (Total Ion Current) of the saturated and aromatic hydrocarbon fractions of the Shromisubani oil from the Rioni Basin (Georgia). Std. = standard (1,1-binaphthyl).

The saturated hydrocarbons are dominated by *n*-alkanes, steranes and hopanes are present in small concentrations. The *n*-alkane distribution shows equal intensities in the short and mid

chain length and low intensities in the long chain range. This is probably related to relatively low maturity of the oil (R_c: 0.64; beginning of oil window), as the absence of higher plants is unlikely due to (a) a low Sterane/Hopane ratio of 0.6 [Mackenzie, 1984] (b) high plant markers cadalene and monoaromatic des-A-triterpenoid occurring in the aromatic hydrocarbon fraction [Tissot & Welte, 1984]. A moderate odd-over-even predominance of long chain *n*-alkanes as indicated by a carbon preference index of 1.6 is consistent with lower maturity. Pr/Ph ratio (1.6) Pr/*n*-C_{17} and Ph/*n*-C_{18} ratios are quite high.

5.7.2.2 Isotope Ratios

The data on $\delta^{13}C$ obtained from GC-IRMS have been published by Mayer et al. [2018b] and are listed in Table 28. Figure 46 illustrates a graphical presentation of the GC-IRMS results.

Table 28. Carbon isotopic composition of individual *n*-alkanes of the Shromisubani oil (sample PG) from the the Rion Basin (Georgia).

Sample	*n*-C15	*n*-C16	*n*-C17	*n*-C18	*n*-C19	*n*-C20	*n*-C21	*n*-C22	*n*-C23	*n*-C24	*n*-C25	*n*-C26	*n*-C27	*n*-C28	*n*-C29
	δ13C (‰; PDB)														
PG	-28.7	-29.0	-29.1	-29.1	-29.2	-29.2	-28.9	-28.7	-28.5	-28.4	-28.8	-28.6	-29.1	-28.7	-28.9

PDB = Peedee Belemnite (int. Standard)

The Shromisubani oil is characterized by a narrow range of $\delta^{13}C$ values. Hence no clear dependency of $\delta^{13}C$ values from chain length can be observed. Odd carbon numbered homologues in the *n*-C_{23} to *n*-C_{29} range show lower $\delta^{13}C$ values. This is interpreted to reflect land plant input to the organic matter of the source rock [Collister et al., 1994a].

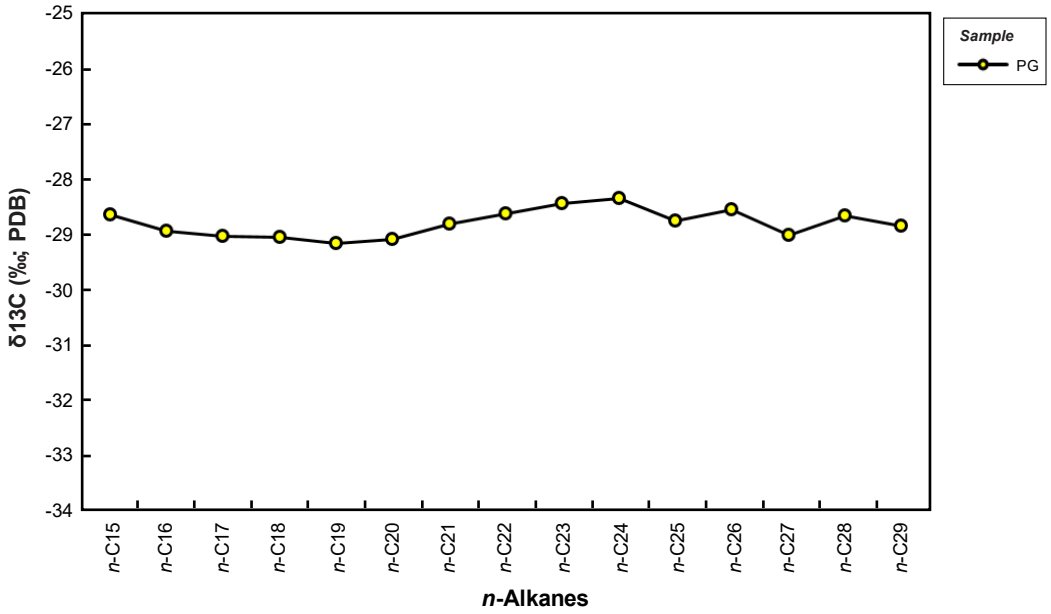

Figure 46. Carbon isotopic composition of individual *n*-alkanes of the Shromisubani oil (sample PG) from the Rioni Basin (Georgia).

6. Discussion

6.1 Oil-Source correlations

Source rock depositional setting is considered to be the primary control on the shape of the *n*-alkane isotope signature [e.g. Murray et al., 1994]. Because CSI patterns are not changed during hydrocarbon generation, with the exception, that oils usually are isotopically lighter than source rock extracts [e.g. Liao et al., 2004], CSI patterns of oils should look similar to those of the relevant source rock. However, biodegradation can affect the oils and increase $\delta^{13}C$ values of individual compounds [e.g. Pedentchouk & Turich, 2017].

In many Paratethyan provinces oil source rocks are clear and well defined [e.g. Gratzer et al., 2011; Sachsenhofer et al., 2017; Boote et al., 2018]. However, they have in most cases not been confirmed by CSIA-A. For this purpose, oil-source correlations with focus on CSIA-A are conducted within this chapter. Average carbon isotopic compositions of *n*-alkanes from oils and source rocks have been calculated from GC-IRMS data presented in Chapter 5.

6.1.1 Molasse Basin

The studied oils are isotopically lighter than the postulated Lower Oligocene source rocks. This is common for oils, i.e. expelled hydrocarbons, as petroleum generation and maturation involves C-C bond cleavage, with kinetic fractionation effects resulting in the preferential breaking of ^{12}C - ^{12}C bonds relative to ^{13}C - ^{12}C bonds [Peters et al., 1981, Liao et al., 2004]. The lower $\delta^{13}C$ values of saturated hydrocarbons from the oils in the eastern part of the Molasse Basin (Oberschauersberg) have been explained by a higher relative contribution of unit c of the Schöneck Formation to hydrocarbon expulsion [Gratzer et al., 2011].

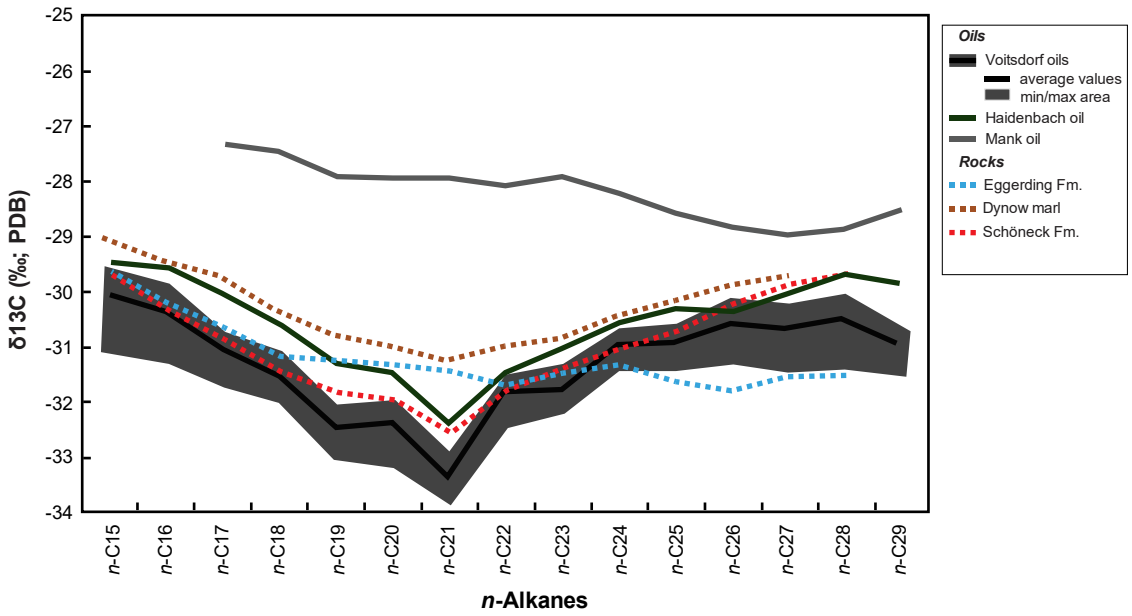

Figure 47. Average carbon isotopic compositions of individual *n*-alkanes of oils and source rocks from the Molasse Basin, calculated from results of GC-IRMS data.

Good oil-source correlations are obtained for the Voitsdorf and Haidenbach oils and the Schöneck Formation by (1) the characteristic V shape pattern observed in oil and rock samples (Figure 47) and by (2) matching relative sterane proportions (Figure 48). This is in accordance with previous concepts of Gratzer et al. [2011] and Bechtel et al. [2013]. The Dynow marl, although it also has a V shape pattern, and the Eggerding Formation, which has excellent

source rock quality, do not have generated the studied oils, as shown by differences in relative sterane proportions.

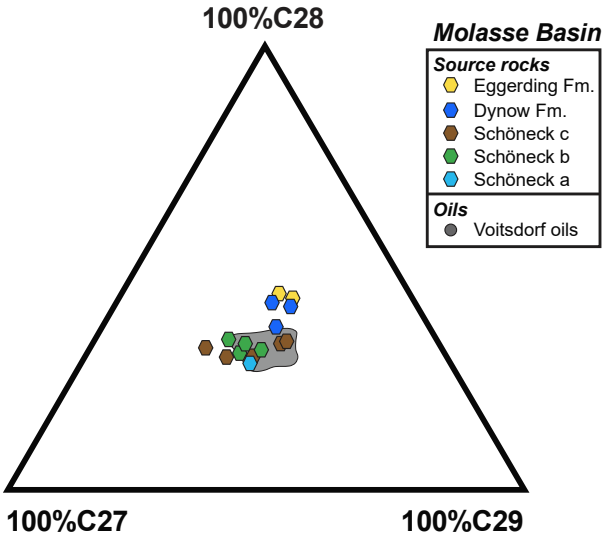

Figure 48. Ternary diagram of relative proportions of C27, C28 and C29 steranes in samples from the Molasse Basin for the assessment of oil sources (data of Voitsdorf oils taken from Gratzer et al. [2011]).

The oil stains in borehole Mank, clearly have a different source. Based on CSI patterns (and considering biodegradation), the Oligocene Eggerding Formation might be a potential source. However, the absence of oleanane suggests a pre-Upper Cretaceous source rock. $\delta^{13}C$ values of the Mank and Urmannsau oils are similar, and a common source, for example Mesozoic rocks in the Alpine nappe stack, is possible.

6.1.2 Carpathian Fold-and-Thrust belt

Good oil-source correlations are obtained based on CSI patterns of the oils from the Carpathian Fold-and-Thrust belt (PIV168, NS25, VM2) and the Menilite Formation (Figure 49). The Shypot Formation is ruled out as a significant source rock for these oils due to its different CSI pattern. The slightly lighter isotopy of the VOL31 sample may indicate mixture with a second source. Wieclaw et al. [2012] discussed mixing with hydrocarbons generated from

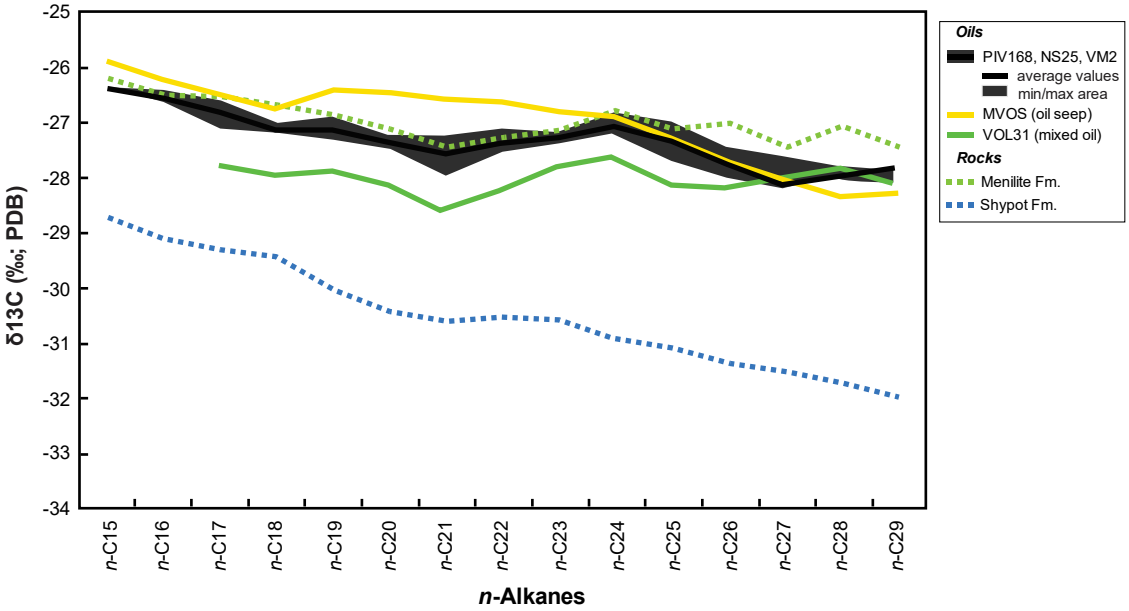

Figure 49. Average carbon isotopic compositions of individual *n*-alkanes of oils and source rocks of the Carpathian Fold-and-Thrust belt, calculated from results of GC-IRMS data.

Jurassic rocks in the basement of the Carpathian Foredeep or mixing with hydrocarbons generated from Menilite shales with high sulphur contents. Indeed, this type of organic matter (type-IIS) was detected in the Polish Carpathians [Curtis et al., 2004; Kotarba et al., 2007].

The Shypot Formation in the Carpathian Fold-and-Thrust belt shows similar CSI patterns than oils from Mesozoic reservoirs in the basement of the Carpathian Foredeep (ORK2, ORK5, KOK26). However, based on geological evidence and the absence of oleanane in these oils, the Shypot Formation can be ruled out as the source rock for these oils.

6.1.3 Carpathian Foredeep

Wieclaw et al. [2012] studied the oils from the Carpathian Foredeep (ORK2, KOK26) and suggested that they were generated from high sulphur Type-IIS kerogen deposited in a carbonate environment. They suggested Jurassic strata for probable source rocks. It is unlikely however, that the Kokhanivka Formation (Middle Jurassic) is the source rock. The oils have much lower Pr/Ph ratios (< 1.0 in oils versus >2.0 of the Kokhanivka Fm.) and are nearly 5‰ lighter isotopically (Figure 50). Only intense biodegradation of the Kokhanivka Formation, during which the hydrocarbon fraction would become enriched in ^{13}C, would justify it to be the source rock of the oils; this is, however, ruled out based on biomarker parameters and gas chromatograms (Chapter 5.5.1.1). The Shypot Formation, as mentioned before (6.1.2), is ineligible as a source rock due to its oleanane showings. Other potential sources of the region have not been part of this study. The real source of the Carpathian Foredeep, therefore, remains unclear.

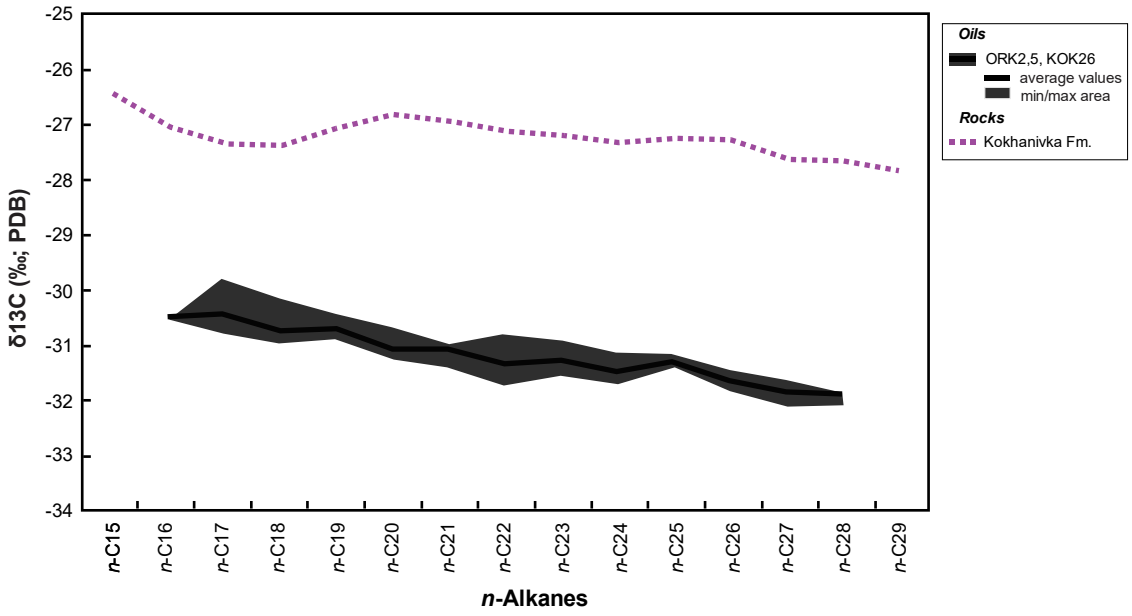

Figure 50. Average carbon isotopic compositions of individual *n*-alkanes of oils and source rocks of the Carpathian Foredeep, calculated from results of GC-IRMS data.

6.1.4 Western Black Sea and Rioni Basin

Oil-source correlations in the W. Black Sea and Rioni Basin after Mayer et al. [2018b] are given below:

W. Black Sea

There is convincing evidence for an Oligocene or Early Miocene age for the source rock (Figure 52). This includes (i) the high oleanane index, which is exclusively found in Upper Cretaceous and Cenozoic source rocks; (ii) very high NCR and NDR ratios and the position of the Tjulenovo sample in a cross-plot of both parameters; and (iii) similarities in compound-specific

isotope patterns between the Tyulenovo oil and Oligocene and Lower Miocene source rocks in the region (Figure 51). Although the fit between the observed isotope pattern in the Tjulenovo oil and the Lower Oligocene part of the source succession is closest, a contribution by Lower Miocene rock cannot be excluded [Mayer et al., 2018b].

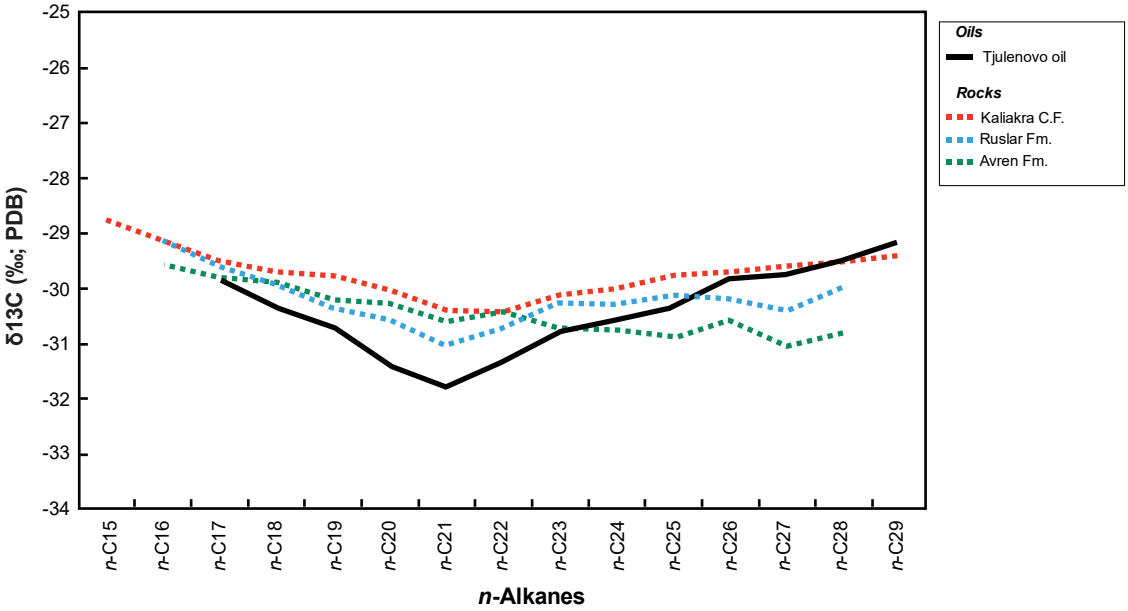

Figure 51. Average carbon isotopic compositions of individual *n*-alkanes of oils and source rocks of the W. Black Sea, calculated from results of GC-IRMS data.

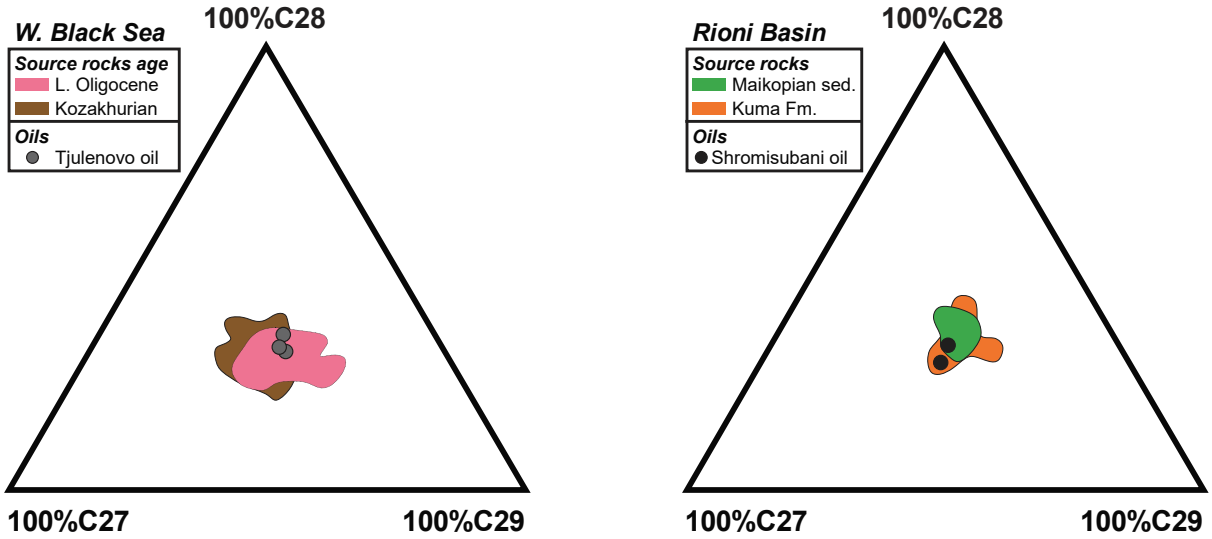

Figure 52. Ternary diagram of relative proportions of C27, C28 and C29 steranes in samples from the W. Black Sea & Rioni Basin for the assessment of oil sources (slightly modified after Mayer et al. [2018b]).

Rioni Basin

A moderately high oleanane index (average 0.14) suggests an Upper Cretaceous or Cenozoic source rock. Based on the steranes triangle (Figure 52), both the Middle Eocene Kuma Formation and the Oligocene Maikop Group are potential source rocks for the Shromisubani oil. Although the carbon isotope ratios of short-chain *n*-alkanes in the oil are slightly higher than those in source rocks from the Kuma Formation, a major contribution by the Middle Eocene unit to the oil is likely (Figure 53). Most probably, the difference is due to the presence of a significant admixture of oil generated by the Oligocene part of the Maikop Group [Mayer et al., 2018b].

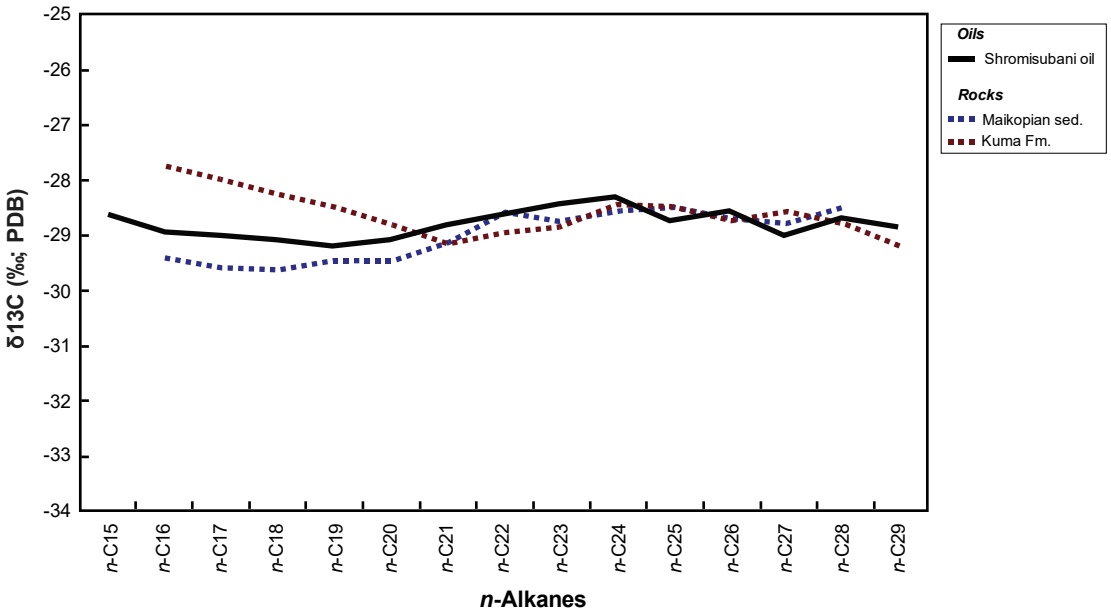

Figure 53. Average carbon isotopic compositions of individual *n*-alkanes of oils and source rocks of the Rioni Basin, calculated from results of GC-IRMS data.

6.2 Stratigraphic control on carbon isotopy of *n*-alkanes

In general, isotopic compositions of *n*-alkanes may be influenced by factors such as organic matter source, isotope ratios of CO_2 in the air and the water column which may change significantly through time [e.g. Jahren et al., 2001; Gröcke, 2002; Köhler & Fischer, 2006; Smith et al., 2007; Tipple et al., 2010; Hare et al., 2018], maturity, and biodegradation. These factors (some of which have been quantified by different biomarker parameters in Chapter 5) are tied to stratigraphy, which changes with depth.

In the following chapter, the stratigraphic control on the carbon isotopy of individual *n*-alkanes is investigated. For this purpose, $\delta^{13}C$ values of individual *n*-alkanes have been correlated with depth. Only in three sample locations, the sample number allowed this approach (Oberschauersberg well in the Molasse Basin; Varna Zapad-1 well in the W. Black Sea; Martvili section in the Rioni Basin). One representative numbered *n*-alkane has been chosen for each chain length range; *n*-C_{16} (short chain), *n*-C_{21} (mid chain), *n*-C_{26} (long chain).

6.2.1 Oberschauersberg Well

The data on $\delta^{13}C$ obtained from GC-IRMS are listed in Chapter 5.1.1.2, Table 4. Sample depths are listed in Table 29. CSI vs depth profile is illustrated in Figure 54.

Table 29. Oberschauersberg well - sample depths

Sample	Formation	Depth [A] (m)
Osch-5	Eggerding Fm.	1369
Osch-6	Eggerding Fm.	1371
Osch-8d	Dynow Fm.	1375
Osch-7d	Dynow Fm.	1377
Osch-2	Schöneck c	1381
Osch-3	Schöneck c	1383
Osch-1	Schöneck b	1385
Osch-4	Schöneck a	1389

[A]Data from Schulz [2003]

$\delta^{13}C$ values of short, mid, and long cain *n*-alkanes show significant variations with depth (stratigraphy). The following observations can be made:

(1) Short and long chain *n*-alkanes of the Schöneck Formation and Dynow marl show similar $\delta^{13}C$ values. Both, short and long chain *n*-alkanes get lighter in the Eggerding Formation,

(2) mid chain *n*-alkanes are significantly lighter than short and long chain *n*-alkanes in the Schöneck Formation and get heavier in the Dynow marl and the Eggerding Formation, which show similar $\delta^{13}C$ values,

(3) n-alkanes from Dynow marl extracts are generally heavy,

(4) in the Schöneck Formation there is no big variation of $\delta^{13}C$ values between subunits a, b and c.

The different behavior of mid- and long-chain *n*-alkanes may indicate that the isotopy of the CO_2 pool avaialable for land plants (represented by long-chain *n*-alkanes) and aquatic organisms (represented by mid-chain *n*-alkanes) did not change simultaneously. Something similar has been observed by Smith et al. [2007]; they found a 1 - 2‰ difference in $\delta^{13}C$ between leaf-wax *n*-alkanes (sourced from higher land plants, which absorb CO_2 from the air) and marine carbonate records in the Bighorn Basin, Wyoming (Paleocene-Eocene). They

explained it as due to a rapid transition of mixed angiosperm/conifer flora to a purely angiosperm flora. Mechanisms that would enable this, have been reviewed previously by Tipple et al. [2010]; Carbon fluxes into and out of ocean-atmosphere reservoirs can vary overtime [e.g. Berner, 1998; Kump & Arthur, 1999], and alter the $\delta^{13}C$ values of individual carbon reservoirs [e.g. Katz et al., 2005] and the partial pressure of atmospheric carbon dioxide [e.g. Pagani et al., 2005].

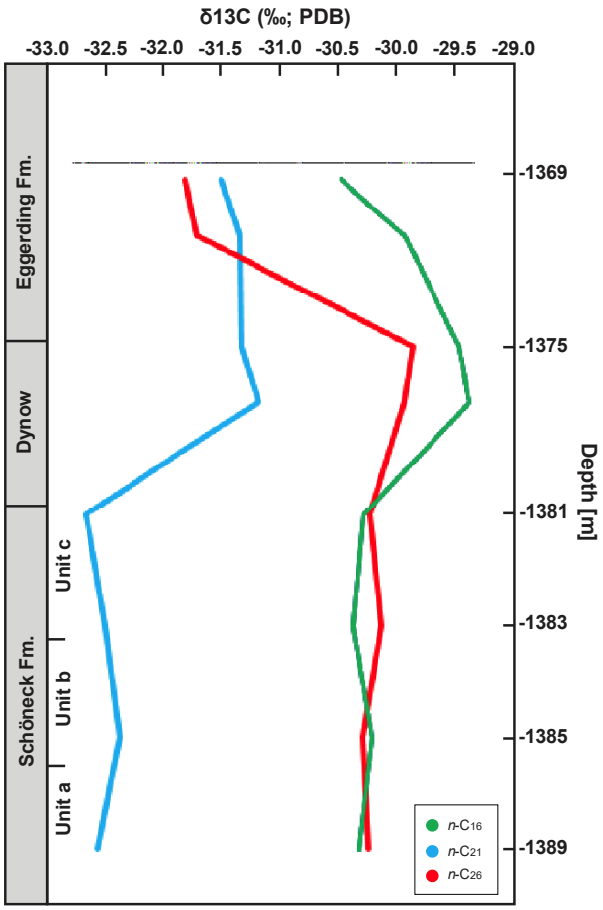

Figure 54. $\delta^{13}C$ values of individual *n*-alkanes versus depth of the Oberschauersberg well (Molasse Basin) for the assessment of stratigraphic control on carbon isotopy of individual *n*-alkanes.

6.2.2 Varna Zapad-1 Well

The data on $\delta^{13}C$ obtained from GC-IRMS are listed in Chapter 5.6.1.2, Table 22. Sample depths are listed in Table 30. CSI vs depth profile is illustrated in Figure 55.

Table 30. Varna Zapad-1 well - sample depths

Sample	Formation	Depth (m)
VarZ1-480	Kaliakra Cany. Fill	480
VarZ1-570	Kaliakra Cany. Fill	570
VarZ1-600	Kaliakra Cany. Fill	600
VarZ1-660	Kaliakra Cany. Fill	660
VarZ1-753	Kaliakra Cany. Fill	753
VarZ1-817	Ruslar Fm.	817
VarZ1-883	Ruslar Fm. (NP23)	883
VarZ1-892	Ruslar Fm.	892
VarZ1-928	Avren Fm.	928

Although there are variations within the Kaliakra Canyon Fill (sample VarZ-1 660), the $\delta^{13}C$ values of mid and long chain *n*-alkanes decrease continuously with depth (age) throughout the Kaliakra Canyon Fill and Ruslar Formation. The decrease becomes stronger in the Ruslar

Formation. Short chain *n*-alkanes do not decrease with depth. The Avren Formation differs strongly from the overlying formations.

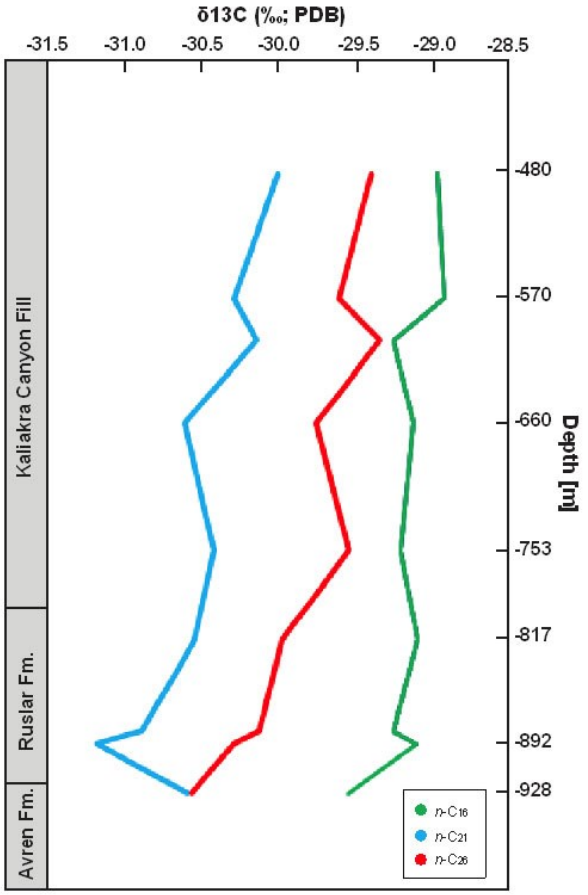

Figure 55. $\delta^{13}C$ values of individual *n*-alkanes versus depth of the Varna Zapad-1 well (W. Black Sea) for the assessment of stratigraphic control on carbon isotopy of individual *n*-alkanes.

6.3.1 Martvili Section

The data on $\delta^{13}C$ obtained from GC-IRMS are listed in Chapter 5.7.1.2, Table 26. Sample heights ("depths") in the outcrop section are listed in Table 31. CSI vs depth profile is illustrated in Figure 56.

Table 31. Martvili section - sample depth locations

Sample	Formation	Depth [A] (m)
R-102	Maikopian sed.	270
R-94	Maikopian sed.	287
R-08	Maikopian sed.	485
R-59	Kuma Fm.	545
R-31	Kuma Fm.	581

[A]Data from Pupp et al. [2018b]

$\delta^{13}C$ values of mid and long chain *n*-alkanes do not show high variation with depth and between the formations. However, there is a strong contrast between short chain *n*-alkanes of the Maikopian sediments, which are isotopically heavy, and the Kuma Formation. This may indicate that the isotopy of the CO_2 pool available for aquatic algae, plankton and photosynthetic bacteria (represented by short-chain n-alkanes) and land plants and aquatic organisms (represented by mid-chain n-alkanes) did not change simultaneously.

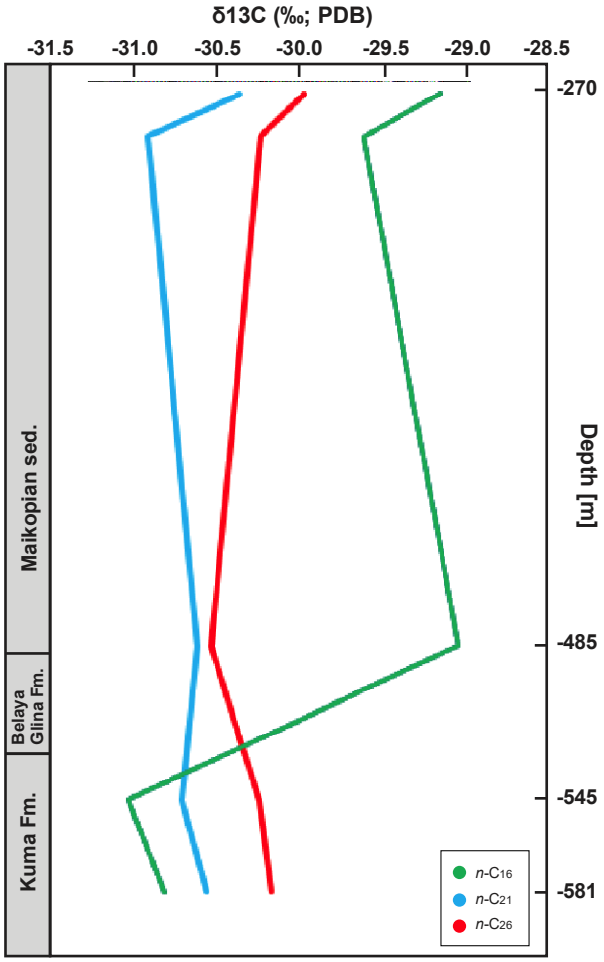

Figure 56. $\delta^{13}C$ values of individual *n*-alkanes versus depth of the Martvili section (Rioni Basin) for the assessment of stratigraphic control on carbon isotopy of individual *n*-alkanes.

6.2 Regional distribution of CSI patterns of the Paratethys

In the following chapter, the regional distribution of CSI patterns of the Paratethys is investigated. For this purpose, averaged $\delta^{13}C$ values of individual *n*-alkanes of the source rocks are illustrated next to the approximate location of deposition on three paleogeographic maps; (1) Lower Oligocene (Pshekian – Solenovian Event), (2) "Middle" Oligocene (Late Solenovian) to Early Miocene, (3) Mesozoic (Cenomanian). Calculations of average $\delta^{13}C$ values are based on GC-IRMS results (Chapters 5.1.1.2, 5.2.1.2, 5.3.2, 5.4.1.2, 5.5.1.2, 5.6.1.2, 5.7.1.2).

Map 1: Early Oligocene (Pshekian – Solenovian Event / Early Kiscellian)

Average $\delta^{13}C$ values are listed in Table 32. Regional distribution of CSI patterns of Pshekian – Solenovian source rocks is illustrated in Figure 57. The paleogeographic map was modified after Rögl [1999].

The Schöneck Formation and Dynow marl of the Molasse Basin all show a characteristic V shape pattern. It occurs as well, although less pronounced, in the Ruslar Formation of the Western Black Sea. As source rock depositional setting and with it source organic material seem to be the primary control of carbon isotopic composition of individual *n*-alkanes, it is suggested, that similar conditions and organic matter contributions occurred in the Molasse Basin and the W. Black Sea. The Lower Oligocene Menilite Formation (Carpathian Fold-and-Thrust belt) and Maikopian sediments in the Rioni Basin have a flat curve. The Menilite Formation is the isotopically heaviest unit presented in this time and has a very pronounced zigzag shape in the long chain range which reflects the contribution of leaf lipids of plants [Collister et al., 1994a].

Table 32. Average carbon isotopic compositions of individual *n*-alkanes calculated from GC-IRMS data of Lower Oligocene source rocks from the Paratethyan realm.

Map-label	*n*-C15	*n*-C16	*n*-C17	*n*-C18	*n*-C19	*n*-C20	*n*-C21	*n*-C22	*n*-C23	*n*-C24	*n*-C25	*n*-C26	*n*-C27	*n*-C28	*n*-C29
Molasse Basin (W: West Bavaria; E: East Bavaria; O: Oberschauersberg; S: Schöneck Fm.; D: Dynow Fm.)															
W-S,D	Samples: B-21, B-32, B-40, B-47														
	-29	-29	-30	-30	-30	-31	-31	-31	-31	-31	-30	-30	-29	-29	-29
E-S	Samples: A-01, A-09, A-14														
	-28	-28	-29	-29	-30	-30	-31	-31	-30	-30	-29	-29	-29	-28	-28
O-S,D	Samples: Osch-8d; Osch-7d, Osch-2, Osch-3, Osch-1, Osch-4,														
		-30	-30	-31	-31	-32	-32	-31	-31	-31	-30	-30	-30		
Carpathian Fold-and-Thrust belt (MEN: Menilite Fm.)															
MEN	Samples: U-B-22, U-66														
	-26	-26	-27	-27	-27	-27	-27	-27	-27	-27	-27	-27	-28	-27	-27
Western Black Sea (RUS: Ruslar Fm.)															
RUS	Samples: VarZ1-883, VarZ1-892														
		-29	-30	-30	-30	-31	-31	-31	-30	-30	-30	-30	-30	-30	
Rioni Basin (MAI: Maikopian sed.)															
MAI	Samples: R-08														
		-28	-28	-28	-28	-29	-29	-29	-29	-29	-29	-29	-29	-29	-29

ocene times (S: Schöne
d/Thrust belt; MO: Moes

Map 2: Late Oligocene – Early Miocene (L.Pshekian – Karadhalganian / M.Kiscellian – L.Egerian)

Average $\delta^{13}C$ values are listed in Table 33. Regional distribution of CSI patterns of Upper Solenovian to Early Miocene source rocks are illustrated in Figure 58. The paleogeographic map was modified after Rögl [1999].

The Upper Solenovian to Early Miocene source rocks of the Molasse Basin, Waschberg Zone, Carpathian Fold-and-Thrust belt, W. Black Sea, and Rioni Basin, all show different patterns and carbon isotopic weights. Different depositional settings and source organic matter contributions to the source rocks are suggested. The Menilite Formation (MEN, Carpathian Fold-and-Thrust belt) and the Kaliakra Canyon Fill (KCF, W. Black Sea) show a similar carbon isotopic composition as their Pshekian to Solenovian Event equivalents (Map 1), suggesting constant depositional settings and source organic material contributions throughout these times. The younger Maikopian sediments have slightly different $\delta^{13}C$ values in mid and long chain range, reflecting a weak change in depositional setting during the Oligocene.

Table 33. Average carbon isotopic compositions of individual *n*-alkanes calculated from GC-IRMS data of "Middle" Oligocene to Early Miocene source rocks from the Paratethyan realm.

Map-label	*n*-C15	*n*-C16	*n*-C17	*n*-C18	*n*-C19	*n*-C20	*n*-C21	*n*-C22	*n*-C23	*n*-C24	*n*-C25	*n*-C26	*n*-C27	*n*-C28	*n*-C29
Molasse Basin (EGG: Eggerding Fm.)															
EGG	Samples:			Osch-5, Osch-6											
		-30	-31	-31	-31	-31	-31	-32	-31	-31	-32	-32	-32		
Waschberg Zone (THO: Thomasl Fm.)															
THO	Samples:			THO-1650, THO-1720, THO-1760											
	-28	-28	-28	-28	-29	-29	-29	-29	-29	-29	-29	-29	-29	-30	
Carpathian Fold-and-Thrust belt (MEN: Menilite Fm.)															
MEN	Samples:			U-C-63, U-C-4											
	-26	-26	-27	-27	-27	-27	-27	-27	-27	-27	-27	-27	-27	-27	-28
Western Black Sea (KCF: Kaliakra Canyon Fill)															
KCF	Samples:			VarZ1-480, VarZ1-570, VarZ1-600, VarZ1-753											
	-29	-29	-29	-29	-30	-30	-30	-30	-30	-30	-30	-30	-29	-29	-29
Rioni Basin (MAI: Maikopian sed.)															
MAI	Samples:			R-102, R-94											
		-28	-28	-28	-29	-29	-29	-29	-29	-28	-28	-29	-29	-29	-29

ocene to E. Miocene ti
ans; CF: Carp. Fold/Th

Map 3: Mesozoic (Middle Cretaceous)

Average $\delta^{13}C$ values are listed in Table 34. Regional distribution of CSI patterns of Mesozoic source rocks are illustrated in Figure 59. The paleogeographic map was modified after Csiki-Sava et al. [2015]. Paleogeographical locations of Allgäu Formation and Shypot Formation follow interpretations of Neumeister et al. [2015] and Slaczska et al. [2014] respectively.

The source rocks from the Mesozoic basement of the Paratethyan provinces (Calcareous Alps, Carpathian Foredeep) all show different patterns and carbon isotopic weights. Different depositional settings and source organic matter contributions to the source rocks are suggested.

The Bächental bituminous marls are extremely light. The origin of the generally light $\delta^{13}C$ values in is not yet clear, and several mechanisms have been postulated by Neumeister et al. [2015]: (1) ^{13}C-depleted organic matter produced by means of carbon recycling processes mediated by chemoautotrophic and methanotrophic microbes within an anoxic, stratified water column [e.g., Küspert, 1982, 1983; Hollander and Smith, 2001]. Biogenic methane oxidation at the oxic/anoxic interface during periods of highest nutrient concentrations in the water column may have reinforced this signal; hence, the level of eutrophication controls the biogeochemical processes that influence $\delta^{13}C$ compositions [Hollander & Smith, 2001]. (2) Varying contributions of organic matter from eukaryotic algae, anaerobic chemoautotrophs, and other microbial plankton [e.g., Luo et al., 2014]. In that study, chemoautotrophic bacteria were suggested to be the source of strongly ^{13}C-depleted organic matter in deepwater environments. (3) Expandable smectite possibly derived from alteration of volcanic ash is abundant in all samples; hence a contribution of isotopically light CO_2 from volcanic emissions is possible [Neumeister et al., 2015].

Compared with other rocks presented in this study, only the Eggerding Formation (Molasse Basin) comes close to the light molecular weight of the Bächental bituminous marls. Because *n*-alkane $\delta^{13}C$ values between -31‰ and -39‰ are reported to be associated to plants that use the Calvin-Benson cycle (C3) [Schefub et al., 2003], such organic matter sources are suggested. However, as isotope ratios of CO_2 in air and water vary over time, other contributing factors cannot be excluded.

Table 34. Average carbon isotopic compositions of individual *n*-alkanes calculated from GC-IRMS data of the rock samples of the Mesozoic basement of Paratethyan provinces.

Map-label	*n*-C15	*n*-C16	*n*-C17	*n*-C18	*n*-C19	*n*-C20	*n*-C21	*n*-C22	*n*-C23	*n*-C24	*n*-C25	*n*-C26	*n*-C27	*n*-C28	*n*-C29
Calcareous Alps (ALL: Allgäu Fm.)															
ALL Samples: BT-35, BT-26, BT-25															
			-32	-32	-32	-32	-32	-32	-31	-31	-31	-30	-30		
Carpathian Foredeep (KOK: Kokhanivka Fm.)															
KOK Samples: J-MS-2523, J-K6-3428, J-K6-3493, J-K6-3521															
		-27	-27	-27	-27	-27	-27	-27	-27	-27	-27	-27	-28	-28	
Carpathian Fold-and-Thrust belt (SHY: Shypot Fm.)															
SHY Samples: J-05, J-39, J-77															
	-29	-29	-29	-29	-30	-30	-31	-31	-31	-31	-31	-31	-31	-32	-32

ic times (ALL: Allgäu F
P: Silesian&Audia-, Du

7 Summary and Conclusion

Compound specific carbone isotope analysis of *n*-alkanes combined with biomarker analysis were carried out on rock and oil samples from Paratethyan oil provinces in order to (1) conduct oil-source correlations, (2) investigate the stratigraphic control on carbon isotopic composition of individual *n*-alkanes, (3) observe the regional distribution of CSI patterns during Oligo-Miocene and Mesozoic times. Based on the analyses, the following conclusions can be drawn:

1. Oil-Source Correlations

- The Voitsdorf oils and Haidenbach oil have been generated from the Schöneck Formation.
- The Mank oil was probably generated by a Mesozoic source rock given absence of oleanane. This source rock may have also generated the oil recovered from borehole Urmannsau-1 in the Northern Calcareous Alps.
- Oils from the Carpathian Fold-and-Thrust belt have been generated by the Menilite Formation.
- The Kokhanivka Formation is not a probable source rock for heavy oils in Jurassic reservoirs (ORK2, ORK5, KOK26) from the Mesozoic basement of the Carpathian Foredeep.
- The Tjulenovo oil has been generated by either the Ruslar Formation, or the Kaliakra Canyon Fill, or both. The Avren Formation is ruled out as a source rock.
- The Shromisubani oil in the Rioni Basin probably represents a mixed oil, partially derived from Maikopian sediments and the Kuma Formation.

2. Stratigraphic control on carbon isotopy of individual *n*-alkanes

Molasse Basin

- The carbon isotopic composition of individual *n*-alkanes in different subunits of the Schöneck Formation is similar, but a significant difference exists between the Schöneck Formation and the overlying units. This is best visible for mid (*n*-C_{21}) and short chain *n*-alkanes (*n*-C_{16}).
- In contrast, long chain n-alkanes (e.g. *n*-C_{26}) remain constant at the Schöneck/Dynow boundary and change only at the Dynow/Eggerding boundary.
- Mid chain *n*-alkanes of Eggerding Formation and Dynow marl show similar $\delta^{13}C$ values.
- The Dynow marl contains isotopically heavier *n*-alkanes than other Molasse Basin units.
- The different behavior of mid- and long-chain *n*-alkanes may indicate that the isotopy of the CO_2 pool avaialable for land plants (represented by long-chain *n*-alkanes) and aquatic organisms (represented by mid-chain *n*-alkanes) did not change simultaneously.

Western Black Sea

- In the Kaliakra Canyon Fill and the Ruslar Formation from the Varna Zapad-1 well offshore Bulgaria $\delta^{13}C$ values of mid and long chain *n*-alkanes get lighter with depth (increasing age). Short chain *n*-alkanes do not follow this trend. The isotope – depth relationship ends at the top of the Eocene Avren Formation.

Rioni Basin

- $\delta^{13}C$ values of mid and long chain *n*-alkanes do not show high variation with depth and between the Maikopian Sediments and Kuma Formation. Short chain *n*-alkanes on the other hand are significantly lighter in the Kuma Formation than in the Maikop Group.

3. Regional distribution of CSI patterns during Oligo-/Miocene and Mesozoic time

Pshekian – Solenovian Event

- The Molasse Basin source rocks are the isotopically lightest, and the Menilite Formation the isotopically heaviest Pshekian – Solenovian Event samples.
- The Schöneck Formation and Dynow marl have a characteristic V shape pattern.
- The Ruslar Formation has a V shape pattern, although it is less pronounced as in the Molasse Basin source rocks.
- The Lower Oligocene Menilite Formation and Maikopian Sediments have a flat curve.

Late Solenovian – Early Miocene

- The Eggerding and Thomasl Formations are the isotopically lightest, and the Menilite Formation is the isotopically heaviest Late Solenovian – Early Miocene units.
- The Eggerding Formation has a flat curve.
- The Menilite Formation has a flat curve with a pronounced zigzag shape in the long chain range which reflects the contribution of leaf lipids of plants.
- The Kaliakra Canyon Fill has a V shape pattern with minimum at *n*-C_{22}.
- The Menilite Formation and the Kaliakra Canyon Fill show a similar carbon isotopic composition as their Pshekian to Solenovian equivalents, suggesting constant environments throughout times of deposition.
- The Maikopian sediments have slightly different $\delta^{13}C$ values in mid and long chain range compared to their Pshekian – Solenovian Event equivalent; possibly resulting from weak environmental changes during deposition.
- $\delta^{13}C$ values of short chain *n*-alkanes up to *n*-C_{21} differ between Maikopian and Kuma sediments. This difference does not exist for longer chain *n*-alkanes.

Mesozoic (Middle Cretaceous)

- The Allgäu Formation is the isotopically lightest, and the Kokhanivka Formation is the isotopically heaviest of the studied Mesozoic rock samples.
- The Allgäu Formation has a V shape pattern with minimum $\delta^{13}C$ values at *n*-C_{18}.
- The Kokhanivka Formation has a flat curve.
- The Shypot Formation has a pronounced negatively sloping curve.

Regarding the method it can be said, that CSIA-A provides a powerful tool for oil source correlations and as an environmental indicator, with the full potential of the latter not yet fully recognized. With the better understanding of stratigraphic control on carbon isotopy of individual *n*-alkanes, the potential will be revealed and possibly new investigation methods will be created. This would allow to re-evaluate existing geological models or reservoirs, provide new opportunities, and potentially open new exploration targets. However, further research is needed.

List of References

AIZENSHTAT Z. (1973): Perylene and its geochemical significance. In: Geochimica et Cosmochimica Acta 37, pp 559–67

ADAMIA S., ALANIA V., CHABUKIANI A., CHICHUA G., ENUKIDZE O., SADRADZE N. (2010): Evolution of the Late Cenozoic basins of Georgia (SW Caucasus): a review. In: Sedimentary Basin Tectonics from the Black Sea and Caucasus to the Arabian Platform (Geol. Soc. Lond., Spec. Publ., 340), pp 239–259

BANKS C.J. & ROBINSON A.G. (1997): Mesozoic strike-slip back-arc basins of the Western Black Sea region. In: Regional and Petroleum Geology of the Black Sea and Surrounding Region (ed. Robinson A.G.), AAPG Memoirs 68, pp 53–62

BARWISE A.J.G. (1990): Role of Nickel and Vanadium in petroleum classification. In: Energy & Fuels 4 (6), pp 647-652

BECHTEL A., JIA J., STROBL S.A.I., SACHSENHOFER R.F., LIU Z., GRATZER R., PÜTTMANN W. (2012): Palaeoenvironmental conditions during deposition of the Upper Cretaceous oil shale sequences in the Songliao Basin (NE China): Implications from geochemical analysis. In: Organic Geochemistry 46, pp 76-95

BECHTEL A., GRATZER R., LINZER H.-G., SACHSENHOFER R.F. (2013): Influence of migration distance, maturity and facies on the stable isotopic composition of alkanes and on carbazole distributions in oils and source rocks of the Alpine Foreland Basin of Austria. In: Organic Geochemistry 62, pp 74–85

BERNER R.A. (1998): The carbon cycle and carbon dioxide over Phanerozoic time: the role of land plants. In: Philosophical Transactions of the Royal Society B 353 (1365), pp 75-82

BJORØY M., HALL K., GILLYON P., JUMEAU J. (1991): Carbon isotope variations in *n*-alkanes and isoprenoids of whole oils. In: Chemical Geology 93, pp 13-20

BJORØY M., HALL P.B., HUSTAD E., WILLIAMS J.A. (1992): Variation in stable carbon isotope ratios of individual hydrocarbons as a function of artificial maturity. In: Organic Geochemistry 19, pp 89-105

BJORØY M., HALL P.B., MOE R.P. (1994): Stable carbon isotope variation of *n*-alkanes in central graben oils. In: Organic Geochemistry 22, pp 355–381

BOOTE D.R.D, SACHSENHOFER R. F., TARI, G., ARBOUILLE, D. (2018): Petroleum provinces of the Paratethyan region. In: Journal of Petroleum Geology 41(3), pp 247-298

BOREHAM C.G., SUMMONS R.E., ROKSANDIC Z.R., DOWLING L.M., HUTTON A.C. (1994): Chemical, molecular and isotopic differentiation of organic facies in the tertiary lacustrine Duaringa oil shale deposit, Queensland, Australia. In: Organic Geochemistry 21, pp 685-712

BRAY E.E. & EVANS E.D. (1961): Distribution of *n*-paraffins as a clue to recognition of source beds. In: Geochimica et Cosmochimica Acta 22, pp 2–15

BRINCAT D., YAMADA K., ISHIWATARI R., UEMURA H. NARAOKA H. (1999): Molecular-isotopic stratigraphy of long-chain *n*-alkanes in Lake Baikal Holocene and glacial age sediments.In: Organic Geochemistry 31, pp 287-294

BRUNET M.F., KOROTAEV M.V., ERSHOV A.V., NIKISHIN A.M. (2002): The South Caspian Basin: a review of its evolution from subsidence modeling. In: Sedimentary Geology 156, pp 119-148

CHENG P., XIAO X.M., GAI H.F., LI T.F., ZHANG Y.Z., HUANG B.J., WILKINS R.W.T. (2015): Characteristics and origin of carbon isotopes of *n*-alkanes in crude oils from the western Pearl River Mouth Basin, South China sea. In: Marine and Petroleum Geology 67, pp 217-229

CHUNG H. M., CLAYPOOL G. E., ROONEY M. A., SQUIRES R. M. (1994): Source characteristics of marine oils as indicated by carbon isotopic ratios of volatile hydrocarbons. In: AAPG Bulletin 78, pp 396–408

CLAYTON C.J. (1991): Effect of maturity on carbon isotope ratios of oils and condensates. In: Organic Geochemistry 17, pp 887-899

CLAYTON C. J. & BJORØY M. (1994): Effect of maturity on $^{13}C/^{12}C$ ratios of individual compounds in North-Sea oils. In: Organic Geochemistry 21, pp 737–750

COLLISTER J.W., RIELEY G., STERN B., EGLINTON G., FRY B. (1994a): Compound-specific $\delta^{13}C$ analysis of leaf lipids from plants with differing carbon dioxide metabolism. In: Organic Geochemistry 21, pp 619–627

COLLISTER J.W., LICHTFOUSE E., HIESHIMA G., HAYES J.M. (1994b): Partial resolution of sources of *n*-alkanes in the saline portion of the Parachute Creek Member, Green River Formation (Piceance Creek Basin, Colorado). In: Organic Geochemistry 21, pp 645-659

CONNAN J. & CASSOU A.M. (1980): Properties of gases and petroleum lipids derived from terrestrial kerogen at various maturation levels. In: Geochimica et Cosmochimica Acta 44, pp 1-23

CURRY D.J., EMMETT J.K., HUNT J.W.(1994): Geochemistry of aliphatic-rich coals in the Cooper Basin, Australia and Taranaki Basin, New Zealand: implications for the occurrence of potentially oil-generative coals. In: Coal and Coal-bearing Strata as Oil-prone Source Rocks (ed. Fleet A.J.), Geological Society of London, pp 149–82

CURTIS, J.B., KOTARBA, M.J., LEWAN, M.D., Wieclaw, D., 2004. Oil/source rock correlations in the Polish Flysch Carpathians and Mesozoic basement and organic facies of the Oligocene Menilite Shales: insights from hydrous pyrolysis experiments. Organic Geochemistry, 35, 1573-1596.

CSIKI-SAVA Z., BUFFETAUT E., ÖSI A., PEREDA-SUBERBIOLA X., BRUSATTE SL. (2015): Island life in the Cretaceous - faunal composition, biogeography, evolution, and extinction of land-living vertebrates on the Late Cretaceous European archipelago. In: ZooKeys 469, pp 1-161

DE LEEUW J.W., FREWIN N.L., VAN BERGEN P.F., SINNINGHE DAMSTÉ J.S, COLLINSON M.E. (1995): Organic carbon as a palaeoenvironmental indicator in the marine realm. In: BOSENCE, D.W.J. & ALLISON, P.A. (eds) Marine Palaeoenvironmental Analysis from Fossils. Geological Society, London, Special Publications, 83, 43–71, https://doi.org/10.1144/GSL.SP.1995.083.01.04

DIDYK B.M., SIMONEIT B.R.T., BRASSELL S.C., EGLINTON G. (1978): Organic geochemical indicators of paleoenvironmental conditions of sedimentation. In: Nature, 272, pp 216-222

EGLINTON G. & HAMILTON R.J. (1967): Leaf epicuticular waxes. In: Science 156, pp 1322-1335

GEORGIEV G. (2000): Structure and evolution of the Western Black Sea region and Kamchiya Foredeep. In: Geophysical Journal 22, pp 91

GRICE K., DE MESMAY R., GLUCINA A., WANG S. (2008): An improved and rapid 5A molecular sieve method for gas chromatography isotope ratio mass spectrometry of *n*-alkanes (C8–C30+). In: Organic Geochemistry 39, pp 284–288

GRATZER R., BECHTEL A., SACHSENHOFER R.F., LINZER H.G., REISCHENBACHER D., SCHULZ H.M. (2011): Oil-oil and oil-source rock correlations in the Alpine Foreland Basin of Austria: Insights from biomarker and stable carbon isotope studies. In: Marine and Petroleum Geology 28, pp 1171-1186

GRATZER R., BECHTEL A., SACHSENHOFER R.F., GAWLICK H.J. (2015): Geogenic versus Anthropogenic: Hydrocarbons in the Spoil from the Falkenstein and Spering Tunnels (A9 Pyhrn Autobahn, Austria). In: Geomechanics and Tunneling 9 (4), pp 356-363

GRÖCKE D.R. (2002): The carbon isotope composition of ancient CO2 based on higher-plant organic matter. In: Philosophical Transactions of the Royal Society A 360

GROSS, D., SACHSENHOFER, R.F., BECHTEL, A., GRATZER, R., GRUNDTNER, M.-L., LINZER, H.-G., MISCH, D., PYTLAK, L., SCHEUCHER, L. (2018): Petroleum systems in the Austrian sector of the North Alpine Foreland Basin: An overview. In: Journal of Petroleum Geology 41, pp 299-318

HARE V.J., LOFTUS E., JEFFREY A., RAMSEY C.B. (2018): Atmospheric CO2 effect on stable carbon isotope composition of terrestrial fossil archives. In: Nature Communications 9

HARRIS S. A., WHITICAR M. J., FOWLER M. G. (2003): Classification of Duvernay sourced oils from central and southern Alberta using compound specific isotope correlation (CSIC). In: Bulletin of Canadian Petroleum Geology 51, pp 99–125

HAYES J.M., FREEMAN K.H., POPP B.N., HOHAM C.H. (1990): Compound-specific isotopic analyses: a novel tool for reconstruction of ancient biochemical processes. In: Organic Geochemistry 16, pp 1115–1128

HE M., MOLDOWAN M., NEMCHENKO-ROVENSKAYA A., PETERS K.E. (2012): Oil families and their inferred source rocks in the Barents Sea and northern Timan-Pechora Basin, Russia. In: AAPG Bulletin 96 (6), pp 1121–1146

HOCKUN K., MOLLENHAUER G., HO S.L., HEFTER J., OHLENDORF C., ZOLITSCHKA B., MAYR C., LÜCKE A., SCHEFUß E. (2016): Using distributions and stable isotopes of *n*-alkanes to disentangle organic matter contributions to sediments of Laguna Potrok Aike, Argentina. In: Organic Geochemistry 102, pp 110–119

HOLLANDER D.J. & SMITH M.A. (2001): Microbially mediated carbon cycling as a control on the d13C of sedimentary carbon in eutrophic Lake Mendota (USA): new models for interpreting isotopic excursions in the sedimentary record. In: Geochimica et Cosmochim Acta 65, pp 4321–4337

HUANG W.-Y. & MEINSCHEIN W.G. (1979): Sterols as ecological indicators. In: Geochemica et Cosmochemica Acta 43, pp 739–745

HUSSAIN S.Z., MAQBOOL K. (2014): GC-MS: Principle, Technique and its application in Food Science. In: International Journal of Current Science (13), pp 116-126

JAHREN A.H., ARENS N.C., SARMIENTO G., GUERRERO J., AMUNDSON R. (2001): Terrestrial record of methane hydrate dissociation in the Early Cretaceous. In: Geology 29, pp 159-162

JIA W., WANG Q., PENG P., XIAO Z., LI B. (2013): Isotopic compositions and biomarkers in crude oils from the Tarim Basin: Oil maturity and oil mixing. In: Organic Geochemistry 57, pp 95-106

KATZ M.E., WRIGHT J.D., MILLER K.G., CRAMER B.S., FENNEL K., FALKOWSKI P.G. (2005): Biological overprint of the geological carbon cycle. In: Marine Geology 217, pp 323-338

KÖHLER P. & FISCHER H. (2006): Simulating low frequency changes in atmospheric CO_2 during the last 740 000 years. In: Climate of the Past 2, pp 57–78

KOLTUN Y.V. (1992): Organic matter in Oligocene Menilite formation rocks of the Ukrainian Carpathians: palaeoenvironment and geochemical evolution. In: Organic Geochemistry 18 (4), pp 423-430

KOLTUN Y.V., ESPITALIE J., KOTARBA M., ROURE F., ELLOUZ N., KOSAKOWSKI P. (1998): Petroleum generation in the Ukrainian external Carpathians and the adjacent foreland. In: Journal of Petroleum Geology 21(3), pp 265–288

KOSAKOWSKI P., WIECLAW D., KOWALSKI A., KOLTUN Y.V. (2012): Assessment of hydrocarbon potential of Jurassic and Cretaceous source rocks in the Tarnogród—Stryi area (SE Poland and W Ukraine). In: Geologica Carpathica 63 (4), pp 319-333

KOTARBA M.J. & KOLTUN Y.V. (2006): The origin and habitat of hydrocarbons of the Polish and Ukrainian parts of the Carpathian Province. In: The Carpathians and their foreland: geology and hydrocarbon resources (ed. Golonka J. & Picha F.J.), AAPG Memoir 84, pp 321-368

KOTARBA M.J., WIĘCŁAW D., KOLTUN Y.V., MARYNOWSKI L., KUŚMIEREK J., DUDOK I.V. (2007): Organic geochemical study and genetic correlation of natural gas, oil and Menilite source rocks in the area between San and Stryi rivers (Polish and Ukrainian Carpathians). In: Organic Geochemistry 38 (8), pp 1431-1456

KUMP L.R. & ARTHUR M.A. (1998): Interpreting carbon-isotope excursions: carbonates and organic matter. In: Chemical Geology 161, pp 181-198

KÜSPERT W. (1982): Environmental changes during oil shale deposition as deduced from stable isotope ratios. In: Cyclic and Event Stratification (ed. Einsele G., Seilacher A.), Springer, Berlin, pp 482-501

KÜSPERT W. (1983): Faziestypen des Posidonienschiefers (Toarcium, Süddeutschland): Eine isotopegeologische, organisch-chemische und petrographische Studie. Dissertation, Tübingen University

LI S.M., GUO D. (2010): Characteristics and application of compound specific isotope in oil-source identification for oils in Dongying Depression, Bohai Bay Basin. In: Geoscience 24, pp 252-258

LI Y. & XIONG Y. (2009): Identification and quantification of mixed sources of oil spills based on distributions and isotope profiles of long-chain *n*-alkanes. In: Marine Pollution Bulletin 58, pp 1868–1873

LIAO Y., GENG A., XIONG Y., LIU D., LU J., LIU J., ZHANG H., GENG X. (2004): The influence of hydrocarbon expulsion on carbon isotopic compositions of individual *n*-alkanes in pyrolysates of selected terrestrial kerogens. In: Organic Geochemistry 35, pp 1479-1488

LICHTFOUSE E., DERENNE S., MARIOTTI A., LARGEAU C. (1994): Possible algal origin of long chain odd *n*-alkanes in immature sediments as revealed by distribution and carbon isotope ratios. In: Organic Geochemistry 22, pp 1023-1027

LIU Z., MOLDOWAN M., NEMCHENKO-ROVENSKAYA A., PETERS K.E. (2016): Oil families and mixed oil of the North–Central West Siberian basin, Russia. In: AAPG Bulletin 100 (3), pp 319–343

LUO G.M., ALGEO T.J., ZHOU W.F., WANG Y.B., YANG H., HUANG J.H., RICHOZ S., XIE S.C. (2014): Vertical $\delta^{13}C_{org}$ gradients record changes in planktonic microbial community composition during the end-Permian mass extinction. In Palaeogeography Palaeoclimatology Palaeoecology 396, pp 119–131

MACKENZIE A.S., HOFFMANN C.F., MAXWELL J.R. (1981): Molecular parameters of maturation in the Toarcian shales, Paris Basin, France, III. Changes in aromatic steroid hydrocarbons. In: Geochimica et Cosmochimica Acta 45, pp 1345–1355

MAGOON L.B., BEAUMONT E.A. (1999): Exploring for Oil and Gas Traps. In: Handbook of Petroleum Geology (ed. Beaumont E.A. & Foster N.H.)

MAIOLI O.L.G., DE OLIVEIRA C.R., DAL SASSO M.A., DOS SANTOS MADUREIRA L.A., DE ALMEIDA AZEVEDO D., DE AQUINO NETO F.R. (2012): Evaluation of the organic matter sources using the $\delta^{13}C$ composition of individual *n*-alkanes in sediments from Brazilian estuarine systems by GC/C/IRMS. In: Estuarine, Coastal and Shelf Science 114, pp 140-147

MANTOVANI E., VITI M., BABBUCCI D., TAMBURELLI C., ALBARELLO D. (2006): Geodynamic connection between the indentation of Arabia and the Neogene tectonics of the central–eastern Mediterranean region. In: GSA Special Papers 409, pp 15-41

MAYER J., RUPPRECHT B.J., SACHSENHOFER R.F., TARI G., BECHTEL A., CORIC S., SIEDL W., KOSI W., FLOODPAGE J. (2018a): Source potential and depositional environment of Oligocene and Miocene rocks offshore Bulgaria. In: Geological Society London Special Publications 464, pp 307-328

MAYER J., SACHSENHOFER R.F., UNGUREANU, C., BECHTEL A., GRATZER R., SWEDA M., TARI G. (2018b): Petroleum charge and migration in the Black Sea: Insights from oil and source rock geochemistry. In: Journal of Petroleum Geology 41, pp 337-350

MISCH D., LEU W., SACHSENHOFER R.F., GRATZER R., RUPPRECHT B., BECHTEL A. (2017): Shallow hydrocarbon indications along the Alpine Foreland Basin: Distribution and implications for petroleum exploration. In: Journal of Petroleum Geology 40, pp 341-362

MOLDOWAN J.M., SEIFERT W.K., GALLEGOS E.J.(1985): Relationship between petroleum composition and depositional environment of petroleum source rocks. In: AAPG Bulletin 69, pp 1255–68

MURRAY A. P., SUMMONS R. E., BOREHAM C. J., DOWLING L. M. (1994): Biomarker and *n*-alkane isotope profiles for Tertiary oils - relationship to source-rock depositional setting. In: Organic Geochemistry 22, pp 521–542

NEUMEISTER S., GRATZER R., ALGEO T.J., BECHTEL A., GAWLICK H.-J., NEWTON R.J., SACHSENHOFER R.F. (2015): Oceanic response to Pliensbachian and Toarcian magmatic events: Implications from an organic-rich basinal succession in the NW Tethys. In: Global and Planetary Change 126, pp 62-83

NEUMEISTER S., ALGEO T.J., BECHTEL A., GAWLICK H.-J., GRATZER R., SACHSENHOFER R.F. (2016): Redox conditions and depositional environment of the Lower Jurassic Bächental bituminous marls (Tyrol, Austria). In: Austrian Journal of Earth Sciences 109/2, pp 142-159

NIKISHIN A.M., ZIEGLER P.A., ET AL. (2001): Mesozoic and Cainozoic evolution of the Scythian Platform–Black Sea–Caucasus domain. In: Peri-Tethys Memoir 6: Peri-Tethyan Rift/Wrench Basins and Passive Margins (Memoires du Museum National d`Histoire Naturelle 186), pp 295–346

NIKISHIN A.M., KOROTAEV M., ERSHOV A., BRUNET M. (2003): The Black Sea basin: tectonic history and Neogene–Quaternary rapid subsidence modelling. In: Sedimentary Geology 156, pp 149–168

NOBLE R.A., KNOW J., ALEXANDER R., KAGI R.I. (1985): Identification of tetracyclic diterpane hydrocarbons in Australian crude oils and sediments. In: Journal of Chemical Society (Chemical Communications, 32–3)

ODDEN W., BARTH T., TALBOT M.R. (2002): Compound-specific carbon isotope analysis of natural and artificially generated hydrocarbons in source rocks and petroleum fluids from offshore Mid-Norway. In: Organic Geochemistry 33, pp 47-65

OHM S.E., KARLSEN D.A., PHAN N.T., STRAND T., IVERSEN G. (2012): Present Jurassic petroleum charge facing Paleozoic biodegraded oil: Geochemical challenges and potential upsides, Embla field, North Sea. In: AAPG Bulletin 96 (8), pp 1523–1552

OSZCZYPKO N. (2006): Late Jurassic-Miocene evolution of the Outer Carpathian fold-and-thrust belt and its foredeep basin (Western Carpathians, Poland). In: Geological Quarterly 50 (1), pp 169-194

OURISSON G., ALBRECHT P., ROHMER M. (1979): The hopanoids: palaeo-chemistry and biochemistry of a group of natural products. In: Pure Applied Chemistry 51, pp 709-729

PAGANI M., FREEMAN K.H., ARTHUR A. (1999): Isotope analyses of molecular and total organic carbon from Miocene sediments. In: Geochimica et Cosmochimica Acta 64 (1), pp 37–49

PAGANI M., ZACHOS J.C., FREEMAN K.H., TIPPLE B., BOHATY S. (2005): Marked Decline in Atmospheric Carbon Dioxide Concentrations During the Paleogene. In: Science 309, pp 600-603

PEDENTCHOUK N. & TURICH C. (2017): Carbon and hydrogen isotopic compositions of *n*-alkanes as a tool in petroleum exploration. In: Hydrocarbon Systems, Geological Society, London, Special Publications 468

PETERS K.E., ROHRBACK B.G., KAPLAN I.R. (1981): Carbon and hydrogen stable isotope variations in kerogen during laboratory-simulated thermal maturation. In: AAPG Bulletin 65, pp 501–508

PETERS K.E. & MOLDOWAN J.M. (1993): The Biomarker Guide—Interpreting Molecular fossils in Petroleum and Ancient Sediments, Englewood Cliffs, New Jersey, Prentice-Hall, 363pp

PERYT T.M. & PERYT D. (2016): Carpathian Foredeep Basin (Miocene, Poland and Ukraine): Significance of Evaporite Deposition. In: Poster Presentation given at AAPG Annual Convention and Exhibition, Calgary, Alberta, Canada, June 19-22 2016

POPOV S.V., RÖGL F., ROZANOV A.Y., STEININGER F.F., SHCHERBA I.G., KOVAC M. (2004): Lithological– Paleogeographic Maps of Paratethys: 10 Maps Late Eocene to Pliocene. In: Courier Forschungsinstitut Senckenberg, Frankfurt

POPADYUK I., VUL M., LADYZHENSKY G., SHPAK P. (2006): Petroleum Geology of the Boryslav–Pokuttya Zone, the Ukrainian Carpathians. In: The Carpathians and Their Foreland: Geology and Hydrocarbon Resources, AAPG Memoir 84

PUPP M., BECHTEL A., GRATZER R., HEINRICH M., KOZAK S., LIPIARSKI P., SACHSENHOFER R.F. (2018a): Depositional environment and petroleum potential of Oligocene rocks in the Waschberg Zone (Austria). In: Geologica Carpathica 69, pp 410-436

PUPP M., BECHTEL A., CORIC S., GRATZER R., RUSTAMOV J., SACHSENHOFER R.F. (2018b): Eocene and Oligo-Miocene Source Rocks in the Rioni and Kura basins of Georgia: depositional environment and petroleum potential. In: Journal of Petroleum Geology 41(3), pp 367-392

PUPP M. (2018): Hydrocarbon potential of Eocene and Oligocene-Miocene source rocks of the Paratethys. Dissertation, Montanuniversitaet Leoben, Chair of Petroleum Geology

RADKE M., WILLSCH H., WELTE D.H. (1980): Preparative hydrocarbon group type determination by automated medium pressure liquid chromatography. In: Analytical Chemistry 52, pp 406–411

RADKE M., LEYTHAEUSER D., TEICHMÜLLER M. (1984): Relationship between rank and composition of aromatic hydrocarbons for coal of different origins. In: Organic Geochemistry 6, pp 423-430

RATSCHBACHER L., DINGELDEY C., MILLER C., HACKER B.R., MCWILLIAMS M.O. (2004): Formation, subduction, and exhumation of Penninic oceanic crust in the Eastern Alps: time constraints from 40Ar/39Ar geochronology. In: Tectonophysics 394, pp 155–170

RAUBALL J. & SACHSENHOFER R.F. (2017): Hydrocarbon potential of the Menilite Formation in western Ukraine. In: AAPG/SEG International Conference and Exhibition, London, England, October 15-18

RIELEY G., COLLIER R.J., JONES D.M., EGLINTON G., EAKIN P.A., FALLICK A.E. (1991): Sources of sedimentary lipids deduced from stable carbon isotope analyses of individual compounds. In: Nature 352, pp 425-427

ROBINSON A., SPADINI G., CLOETINGH S., RUDAT J. (1995): Stratigraphic evolution of the Black Sea: inferences from basin modelling. In: Marine and Petroleum Geology 12, pp 821–835

RÖGL F. (1998): Palaeogeographic considerations for Mediterranean and Paratethys seaways (Oligocene to Miocene). In: Annalen des Naturhistorischen Museums in Wien 99, pp 279–310

RÖGL F. & NAGYMAROSY A. (2004): Biostratigraphy and correlation of the Lower Miocene Michelstetten and Ernstbrunn sections in the Waschberg Unit, Austria (Upper Egerian to Eggenburgian, Central Paratethys). In: Courier Forschungsinstitut Senckenberg 246, pp 129–151

ROONEY M. A., VULETICH A. K., GRIFFITH C. E. (1998): Compoundspecific isotope analysis as a tool for characterizing mixed oils: An example from the west of Shetlands area. In: Organic Geochemistry 29, pp 241–254

RUBLE T.E., BAKEL A.J., PHILP R.P. (1994): Compound specific isotopic variability in Uinta Basin native bitumens: paleoenvironmental implications. In: Organic Geochemistry 21, pp 661-671

RUPPRECHT B. (2014): Source rocks in the western Black Sea offshore Bulgaria: distribution, potential and maturity of Mesozoic and Cenozoic units. Master Thesis, Montanuniversitaet Leoben, Chair of Petroleum Geology

SACHSENHOFER R.F. & KOLTUN Y.V. (2012): Black shales in Ukraine - A review. In: Marine and Petroleum Geology 31, pp 125-136

SACHSENHOFER R.F. & SCHULZ H.-M. (2006): Architecture of Lower Oligocene source rocks in the Alpine Foreland Basin: a model for syn- and post-depositional sourcerock features in the Paratethyan realm. In: Petroleum Geoscience 12, pp 363–377

SACHSENHOFER R.F., STUMMER B.C., GEORGIEV G., DELLMOUR R., BECHTEL A., GRATZER R., CORIC S. (2009): Depositional environment and hydrocarbon source potential of the Oligocene Ruslar Formation (Kamchia Depression; Western Black Sea). In: Marine and Petroleum Geology 26, pp 57–84

SACHSENHOFER R.F., LEITNER B., ET AL. (2010): Deposition, erosion and hydrocarbon source potential of the Oligocene Eggerding Formation (Molasse Basin, Austria). In: Austrian Journal Earth Sciences 103, pp 76–99

SACHSENHOFER R.F., POPOV S.V., BECHTEL A., CORIC S., FRANCU J., GRATZER R., GRUNERT P., KOTARBA M., MAYER J., PUPP M., RUPPRECHT B.J., VINCENT S.J. (2017): Oligocene and Lower Miocene source rocks in the Paratethys: palaeogeographical and stratigraphic controls. In: Geological Society London Special Publications 464

SACHSENHOFER R.F., POPOV S.V., CORIC S., MAYER J., MISCH D., MORTON M.T., PUPP M., RAUBALL J., TARI G. (2018): Paratethyan Petroleum Source Rocks: An Overview. In: Journal of Petroleum Geology 41 (3), pp 219-246

SCHEFUB E., RATMEYER V., STUUT J.B., JANSEN J.H.F., SINNINGHE DAMSTÈ J.S. (2003): Carbon isotope analyses of n-alkanes in dust from the lower atmosphere over the central eastern Atlantic. In: Geochimica et Cosmochimica Acta 67, pp 1757-1767

SCHOELL M.(1984): Recent advances in petroleum isotope geochemistry. In: Organic Geochemistry 6, pp 645–663

SCHULZ H.-M., SACHSENHOFER R.F., BECHTEL A., POLESNY H., WAGNER L. (2002): The origin of hydrocarbon source rocks in the Austrian Molasse Basin (Eocene–Oligocene transition). In: Marine and Petroleum Geology 19, pp 683-709

SCHULZ H.-M. (2003): Die westliche Zentral-Paratethys an der Wende Eozän/Oligozän – Ozeanographie eines Randmeeres und Bildung von Erdölmuttergesteinen. Habilitationsschrift, Technische Universität Clausthal

SCHULZ H.-M., BECHTEL A., RAINER T., SACHSENHOFER R.F., STRUCK U. (2004): Paleoceanography of the western Central Paratethys during nannoplankton zone NP 23: The Dynow Marlstone in the Austrian Molasse Basin. In: Geologica Carpathica 55, pp 311–323

SENKOVSKY Y., CHEPIL P., GRIGORCHUK K., GNIDETS V., KOLTUN Y. (2010): Tethyan anoxic events. Carpathian-Black Sea segment. In: AAPG European Region Annual Conference, October 17-19, 2010, Kiev, Ukraine

SINNINGHE D.J.S., KENIG F., KOOPMANS M. P., KOSTER J., SCHOUTEN S., HAYES J.M., DE LEEUW J.W. (1995): Evidence for gammacerane as an indicator of water-column stratification. In: Geochimica et Cosmochimica Acta 59, pp 1895-1900

SLACZKA A., GOLONKA J., OSZCZYPKO N., CIESZKOWSKI M., SLOMKA T., MATYASIK I. (2014): Occurrence of Upper Jurassic – Lower Cretaceous black organic-rich politic sediments as targets for unconventional hydrocarbon exploration in the Outer Carpathians and adjacent part of the Alps. In: AAPG Bulletin 98, pp 1967-1994

SMITH F.A., WING S.L., FREEMAN K.H. (2007): Magnitude of the carbon isotope excursion at the Paleocene-Eocene thermal maximum: The role of plant community change. In: Earth and Planetary Science Letters 262, pp 50-65

SOMMERBURG O., SIEMS W., KRAEMER K. (2013): Carotenoids and Vitamin A in Translational Medicine. In: CRC Press

SOFER Z. (1984): Stable carbon isotope compositions of crude oils: application to source depositional environments and petroleum alteration. In: AAPG Bulletin 68, pp 31-49

STAHL W. (1977): Carbon and nitrogen isotopes in hydrocarbon research and exploration. In: Chemical Geology 20, pp 121–149

STASHENKO E., MARTÍNEZ R. (2014): Gas Chromatography-Mass Spectrometry. In: Advances in Gas Chromatography (ed. Guo X.)

STUMMER B.C. (2006): The Oligocene Ruslar Formation (Kamchia Trough, offshore Bulgaria): Source Rock characteristics and log-response. Master Thesis, Montanuniversitaet Leoben, Chair of Petroleum Geology

TISSOT B. P., WELTE D. H. (1984): Petroleum Formation and Occurrence. Springer Verlag Berlin

TIPPLE B.J., MEYERS S.R., PAGANI M. (2010): Carbon isotope ratio of Cenozoic CO2: A comparative evaluation of available geochemical proxies. In: Paleoceanography 25

TOLLMANN, A., (1976): Analyse des klassischen nordalpinen Mesozoikums. Stratigraphie, Fauna und Fazies der Nördlichen Kalkalpen. Deuticke Wien

VAN AARSSEN B.G.K., ALEXANDER R., KAGI R.I. (2000): Higher plant biomarkers reflect palaeovegetation changes during Jurassic times. In: Geochimica et Cosmochimica Acta 64, pp 1417–24

VOLKMAN J.K. & MAXWELL J.R. (1986): Acyclic isoprenoids as biological markers. In: Biological Markers in the Sedimentary Record (ed. Johns R.B.), Elsevier Amsterdam, pp 1-42

VOLKMAN J.IK, BARNETT S.M., DUNSTAN G.A., JEFFREY S.W. (1994): C25 and C30 highly branched isoprenoid alkenes in laboratory cultures of two marine diatoms. In: Organic Geochemistry 21, pp 407–13

WAGNER L.R. (1996): Stratigraphy and hydrocarbons in the Upper Austrian Molasse Foredeep (active margin). In: Oil and gas in Alpidic Thrustbelts and Basins of Central and Eastern Europe (ed. Wessely G. & Liebl W.), EAGE Special Publication 5, pp 217-235

WEHNER H. & KUCKELKORN K. (1995): Zur Herkunft der Erdöle im nördlichen Alpen-/Karpatenvorland. In: Erdöl, Erdgas, Kohle 111, pp 508-514

WESSELY G. (2006): Geologie der Österreichischen Bundesländer. In: Geologische Bundesanstalt Wien

WIECLAW D., KOTARBA M., KOWALSKI A., KOLTUN Y. (2012): Origin and maturity of oils in the Ukrainian Carpathians and their Mesozoic basement. In: Geological Quarterly 56 (1), pp 158–168

WHITICAR M. J. & SNOWDON L. R. (1999): Geochemical characterization of selected western Canada oils by C5-C8 compound specific isotope correlation (CSIC). In: Organic Geochemistry 30, pp 1127–1161

XIONG Y.Q., GENG A.S. (2000): Carbon isotopic composition of individual *n*-alkanes in asphaltene pyrolysates of biodegraded crude oils from the Liaohe Basin, China. In: Organic Geochemistry 31, pp 1441-1449

XIONG Y.Q., GENG A.S., SHEN G.Y., FU J.M. (2001): Characteristics of carbon isotopic composition of *n*-alkanes during hydrocarbon generation and expulsion and its significance. In: Acta Sedimentology Sinica 19, pp 469-473

ZIEGLER P.A. (1987): Late Cretaceous and Cenozoic intraplate compressional deformations in the Alpine foreland. In: Tectonophysics 137, pp 389–420

ZIMMER W. & WESSELY G. (1996): Exploration results in thrust and subthrust complexes in the Alps and below the Vienna Basin in Austria. In: Oil and gas in Alpidic Thrustbelts and Basins of Central and Eastern Europe (ed. Wessely G. & Liebl W.), EAGE Special Publication 5, pp 81-107

List of Figures

Figure 1. Paleogeography of the Paratethyan realm during early Oligocene time. (W & C Par.: Western and Central Paratethys) [Sachsenhofer et al., 2018]. 10

Figure 2. Stratigraphic chart of the investigated sections [Sachsenhofer et al., 2018]. 16

Figure 3. Approximate sample locations. (W.Bav*: Western Bavaria; E.Bav*: Eastern Bavaria; Osch*: Oberschauersberg; V*: Voitsdorf; FST*: Falkenstein tunnel; HNB*: Haidenbach; BOPR*: Boryslav oil producing region; DOPR*: Dolyna oil producing region). 22

Figure 4. Schematic diagram of GC-MS system [Hussain & Maqbool, 2014]. 25

Figure 5. A simplied schmeatic of a GC-IRMS system for δ13C measurements [Pedentchouk & Turich, [2017]. 26

Figure 6. Chromatograms (Total Ion Current) of the saturated hydrocarbon fractions of core samples B-32 (Schöneck b), A-14 (Schöneck b), Osch-1 (Schöneck b) and Osch-8d (Dynow) from the Molasse Basin. *n*-Alkanes are labelled according to their carbon number. Std. = standard (1,1-binaphthyl). 28

Figure 7. Chromatograms (Total Ion Current) of the aromatic hydrocarbon fractions of core samples B-32 (Schöneck b), A-14 (Schöneck b), Osch-1 (Schöneck b) and Osch-8d (Dynow) from the Molasse Basin. Std. = standard (1,1- binaphthyl). 28

Figure 8. Correlation diagram of pristane/*n*-C17 ratios versus phytane/*n*-C18 ratios of rock and oil samples from the Molasse Basin for the assessment of oil sources, as well as the effects of maturation and biodegradation (modified after Connan & Cassou [1980]). 30

Figure 9. Ternary diagram of relative proportions of C27, C28 and C29 steranes in samples from Molasse Basin source rocks (modified after Huang & Meinschein [1979]). 30

Figure 10. Carbon isotopic composition of individual *n*-alkanes of source rocks from the Molasse Basin. 32

Figure 11. Chromatograms (Total Ion Current) of the saturated hydrocarbon fractions of Molasse oil samples V-8, V-23, HNB-1 & Mank-157. *n*-Alkanes are labelled according to their carbon number. Std. = standard (deuterated n-tetracosane: V- samples; 1,1-binaphthyl: HNB-1 and Mank-157 samples). 33

Figure 12. Chromatograms (Total Ion Current) of the aromatic hydrocarbon fractions of Molasse oil samples V-8, V-23, HNB-1 & Mank-157. Std. = standard (deuterated n-tetracosane: V- samples; 1,1-binaphthyl: HNB-1 and Mank-157 samples). 33

Figure 13. Carbon isotopic composition of individual n-alkanes of oils from the Molasse Basin. 35

Figure 14. Chromatograms (Total Ion Current) of the saturated and aromatic hydrocarbon fractions of rock sample BT-25 from the Bächental bituminous marls (Calc. Alps). *n*-Alkanes are labelled according to their carbon number. Std. = standard (deuterated n-tetracosane). 36

Figure 15. Carbon isotopic composition of individual *n*-alkanes of the Bächental bituminous marls from the Calcareous Alps. 37

Figure 16. Chromatograms (Total Ion Current) of the saturated hydrocarbon fractions of oil stain samples from the Falkenstein tunnel (KB-07) and Urmannsau borehole (Urman-152) (both Calc. Alps). *n*-Alkanes are labelled according to their carbon number. Std. = standard (deuterated n-tetracosane: KB- samples; 1,1-binaphthyl: Urman- samples). 38

Figure 17. Chromatograms (Total Ion Current) of the aromatic hydrocarbon fractions of oil stain samples from the Falkenstein tunnel (KB-07) and Urmannsau borehole (Urman-152 (both Calc. Alps). Std. = standard (deuterated n-tetracosane: KB- samples; 1,1-binaphthyl: Urman-samples). 38

Figure 18. Carbon isotopic composition of individual *n*-alkanes of oil stain samples from the Falkenstein tunnel and Urmannsau borehole (Calc. Alps). 39

Figure 19. Chromatograms (Total Ion Current) of the saturated and aromatic hydrocarbon fractions of cuttings sample THO-1650 from the Thomasl Fm. (Waschberg Zone). *n*-Alkanes are labelled according to their carbon number. Std. = standard (1,1-binaphthyl). 41

Figure 20. Ternary plot of relative proportions of C27, C28 and C29 steranes in cuttings samples from the Thomasl Fm. (Waschberg Zone; modified after Huang & Meinschein [1979]). 42

Figure 21. Carbon isotopic composition of individual *n*-alkanes of cuttings samples from the Thomasl Fm. (Waschberg Zone). 42

Figure 22. Chromatograms (Total Ion Current) of the saturated hydrocarbon fractions of samples of the Menilite Fm. (U-C-4) and Shypot Fm. (J-39) from the Carpathian Fold-and-Thrust belt. *n*-Alkanes are labelled according to their carbon number. Std. = standard (deuterated n-tetracosane). 44

Figure 23. Chromatograms (Total Ion Current) of the aromatic hydrocarbon fractions of samples of the Menilite Fm. (U-C-4) and Shypot Fm. (J-39) from the Carpathian Fold-and-Thrust belt. Std. = standard (deuterated n-tetracosane). 45

Figure 24. Correlation diagram of Pr/*n*-C17 ratios versus Ph/*n*-C18 ratios of rock and oil samples from the Carpathian Fold-and-Thrust belt for the assessment of oil sources, as well as the effects of maturation and biodegradation (modified after Connan & Cassou [1980]).. 46

Figure 25. Ternary plot of relative proportions of C27, C28 and C29 steranes in samples of the Menilite Fm. from the Carpathian Fold-and-Thrust belt (modified after Huang & Meinschein [1979]). 46

Figure 26. Carbon isotopic composition of individual *n*-alkanes of samples from the Menilite Fm. and Shypot Fm. (Carpathian Fold-and-Thrust belt). 47

Figure 27. Chromatograms (Total Ion Current) of the saturated and aromatic hydrocarbon fractions of oil sample NS25 from the Carpathian Fold-and-Thrust belt. *n*-Alkanes are labelled according to their carbon number. Std. = standard (deuterated n-tetracosane). 48

Figure 28. Carbon isotopic composition of individual *n*-alkanes of oil samples from the Carpathian Fold-and-Thrust belt. 49

Figure 29. Chromatograms (Total Ion Current) of the saturated and aromatic hydrocarbon fractions of core sample J-K6-3493 from the Kokhanivka Formation (Carpathian Foredeep). *n*-Alkanes are labelled according to their carbon number. Std. = standard (1,1-binaphthyl). ... 50

Figure 30. Correlation diagram of pristane/*n*-C17 ratios versus phytane/*n*-C18 ratios of rock and oil samples from the Carpathian Foredeep for the assessment of oil sources, as well as the effects of maturation and biodegradation (modified after Connan & Cassou [1980]). 51

Figure 31. Carbon isotopic composition of individual *n*-alkanes of core samples from the Kokhanivka Formation (Carpathian Foredeep)..... 52

Figure 32. Chromatograms (Total Ion Current) of the saturated and aromatic hydrocarbon fractions of oil sample ORK5 from the Carpathian Foredeep. *n*-Alkanes are labelled according to their carbon number. Std. = standard (deuterated n-tetracosane). 52

Figure 33. Carbon isotopic composition of individual *n*-alkanes of oil samples from the Carpathian Foredeep. 53

Figure 34. Chromatograms (Total Ion Current) of the saturated hydrocarbon fractions of cuttings samples VarZ1-733 (Kaliakra Cany. Fill) and VarZ1-892 (Ruslar-Fm.) from well Varna Zapad-1 offshore Bulgaria (W. Black Sea). *n*-Alkanes are labelled according to their carbon number. Std. = standard (1,1-binaphthyl). 54

Figure 35. Chromatograms (Total Ion Current) of the aromatic hydrocarbon fractions of cuttings samples VarZ1-733 (Kaliakra Cany. Fill) and VarZ1-892 (Ruslar-Fm.) from well Varna Zapad-1 well offshore Bulgaria (W. Black Sea) Std. = standard (1,1-binaphthyl)..... 54

Figure 36. Correlation diagram of pristane/*n*-C17 ratios versus phytane/*n*-C18 ratios for the assessment of oil sources, as well as the effects of maturation and biodegradation of cuttings samples of the Kaliakra Cany. Fill, Ruslar Fm. & Avren Fm. from wells Galata-1 and Varna Zapad-1 offshore Bulgaria (W. Black Sea; modified after Connan & Cassou [1980]). 56

Figure 37. Carbon isotopic composition of individual *n*-alkanes of cuttings samples from wells Galata-1 & Varna Zapad-1 offshore Bulgaria (W. Black Sea)..... 57

Figure 38. Chromatograms (Total Ion Current) of the saturated and aromatic hydrocarbon fractions of the Tjulenovo oil (W. Black Sea, Bulgaria). Std. = standard (deuterated n-tetracosane)..... 57

Figure 39. Carbon isotopic composition of individual *n*-alkanes of the Tjulenovo oil (sample TJU) from the W. Black Sea (Bulgaria). 58

Figure 40. Chromatograms (Total Ion Current) of the saturated hydrocarbon fractions of rock extracts of the Maikopian sed. (sample R-08) and Kuma Fm. (sample R-59) from the Rioni Basin (Georgia). *n*-Alkanes are labelled according to their carbon number. Std. = standard (1,1-binaphthyl)..... 59

Figure 41. Chromatograms (Total Ion Current) of the aromatic hydrocarbon fractions of rock extracts of the Maikopian sed. (sample R-08) and Kuma Fm. (sample R-59) from the Rioni Basin (Georgia). Std. = standard (1,1-binaphthyl). 59

Figure 42. Correlation diagram of pristane/*n*-C17 ratios versus phytane/*n*-C18 ratios of rock extracts of Maikopian sed. & Kuma Fm. from the Rioni Basin (Georgia), for the assessment of oil sources, as well as the effects of maturation and biodegradation (modified after Connan & Cassou [1980]) (note: the scale has been adjusted to illustrate the high values)..... 60

Figure 43. Ternary plot of relative proportions of C27, C28 and C29 steranes in samples of Maikopian sed. & Kuma Fm. from the Rioni Basin, Georgia (modified after Huang & Meinschein, [1979]). 61

Figure 44. Carbon isotopic composition of individual *n*-alkanes of rock extracts of Maikopian sed. & Kuma Fm. from the Rioni Basin (Georgia). 62

Figure 45. Chromatograms (Total Ion Current) of the saturated and aromatic hydrocarbon fractions of the Shromisubani oil from the Rioni Basin (Georgia). Std. = standard (1,1-binaphthyl). 62

Figure 46. Carbon isotopic composition of individual *n*-alkanes of the Shromisubani oil (sample PG) from the Rioni Basin (Georgia). 63

Figure 47. Average carbon isotopic compositions of individual *n*-alkanes of oils and source rocks from the Molasse Basin, calculated from results of GC-IRMS data. 64

Figure 48. Ternary diagram of relative proportions of C27, C28 and C29 steranes in samples from the Molasse Basin for the assessment of oil sources (data of Voitsdorf oils taken from Gratzer et al. [2011]). 65

Figure 49. Average carbon isotopic compositions of individual *n*-alkanes of oils and source rocks of the Carpathian Fold-and-Thrust belt, calculated from results of GC-IRMS data. 65

Figure 50. Average carbon isotopic compositions of individual *n*-alkanes of oils and source rocks of the Carpathian Foredeep, calculated from results of GC-IRMS data. 66

Figure 51. Average carbon isotopic compositions of individual *n*-alkanes of oils and source rocks of the W. Black Sea, calculated from results of GC-IRMS data. 67

Figure 52. Ternary diagram of relative proportions of C27, C28 and C29 steranes in samples from the W. Black Sea & Rioni Basin for the assessment of oil sources (slightly modified after Mayer et al. [2018b]). 67

Figure 53. Average carbon isotopic compositions of individual *n*-alkanes of oils and source rocks of the Rioni Basin, calculated from results of GC-IRMS data. 68

Figure 54. $\delta^{13}C$ values of individual *n*-alkanes versus depth of the Oberschauersberg well (Molasse Basin) for the assessment of stratigraphic control on carbon isotopy of individual *n*-alkanes. 70

Figure 55. $\delta^{13}C$ values of individual *n*-alkanes versus depth of the Varna Zapad-1 well (W. Black Sea) for the assessment of stratigraphic control on carbon isotopy of individual *n*-alkanes. 71

Figure 56. $\delta^{13}C$ values of individual *n*-alkanes versus depth of the Martvili section (Rioni Basin) for the assessment of stratigraphic control on carbon isotopy of individual *n*-alkanes. 72

Figure 57. Regional distribution of CSI patterns ($\delta^{13}C$ -25‰ to -34‰) during Early Oligocene times (S: Schöneck Fm.; S,D: Schöneck Fm. & Dynow Fm.; MEN: Menilite Fm.; RUS: Ruslar Fm.; MAI: Maikopian sed.; MB: Molasse Basin; A: Alps; C: Carpathians; CF: Carp. Fold/Thrust belt; MO: Moesian platf.; WBS: W. Black Sea; RB: Rioni Basin) (map background modified after Rögl [1999]). 74

Figure 58. Regional distribution of CSI patterns ($\delta^{13}C$ -25‰ to -34‰) during L. Oligocene to E. Miocene times (EGG: Eggerding Fm.; THO: Thomasl Fm.; MEN: Menilite Fm.; KCF: Kaliakra Canyon Fill; MAI: Maikopian sed.; MB: Molasse Basin; A: Alps; C: Carpathians; CF: Carp. Fold/Thrust belt; MO: Moesian platf.; WBS: W. Black Sea; RB: Rioni Basin) (map background modified after Rögl [1999]). 76

Figure 59. Regional distribution of CSI patterns ($\delta^{13}C$ -25‰ to -34‰) during Mesozoic times (ALL: Allgäu Fm.; KOK: Kokhanivka Fm.; SHY: Shypot Fm.; AMC: Arm.-Fr. Cent. Mass.; LBH: London-Brabant High; BM: Bohemian Mass.; AA: Austroalpine dom.; SA-D-P: Silesian&Audia-, Dukla-, Porkulec Basins; MO: Moesian platf.; UM: Ukrainian Mass.) (map background modified after Csiki-Sava et al. [2015]). 78

List of Tables

Table 1. Summary of source rocks in key sections with bulk geochemical parameters (see text for references). 11

Table 2. List of rock and oil samples together with province, location, stratigraphy, formation and sample type. 23

Table 3. Bulk organic geochemical parameters, concentration and concentration ratios of specific biomarkers of source rocks from the Molasse Basin. 29

Table 4. Carbon isotopic composition of individual *n*-alkanes of source rocks from the Molasse Basin. 32

Table 5. Organic geochemical parameters, concentration and concentration ratios of specific biomarkers of oils from the Molasse Basin. 34

Table 6. Carbon isotopic composition of individual *n*-alkanes of oils from the Molasse Basin. 35

Table 7. Bulk organic geochemical parameters, concentration and concentration ratios of samples of the Bächental bituminous marls from the Calcareous Alps. 36

Table 8. Carbon isotopic composition of individual *n*-alkanes of samples of the Bächental bituminous marls from the Calcareous Alps. 37

Table 9. Organic geochemical parameters, concentration ratios of specific biomarkers of oil stain samples from the Falkenstein tunnel and Urmannsau borehole (Calc. Alps). 39

Table 10. Carbon isotopic composition of individual *n*-alkanes of oil stain samples from the Falkenstein tunnel and Urmannsau borehole (Calc. Alps). 39

Table 11. Bulk organic geochemical parameters, concentration and concentration ratios of specific biomarkers of cuttings samples the Thomasl Fm. from the Waschberg zone. 41

Table 12. Carbon isotopic composition of individual *n*-alkanes of cuttings samples from the Thomasl Fm. (Waschberg Zone). 42

Table 13. Bulk organic geochemical parameters, concentration and concentration ratios of specific biomarkers of samples of the Menilite Fm. and Shypot Fm. from the Carpathian Fold-and-Thrust belt. 45

Table 14. Carbon isotopic composition of individual *n*-alkanes of samples from the Menilite Fm. and Shypot Fm. (Carpathian Fold-and-Thrust belt). 47

Table 15. Organic geochemical parameters, concentration ratios of specific biomarkers of oils from Carpathian Fold-and-Thrust belt. 48

Table 16. Carbon isotopic composition of individual *n*-alkanes of oil samples from the Carpathian Fold-and-Thrust belt. 49

Table 17. Bulk organic geochemical parameters, concentration and concentration ratios of core samples from the Kokhanivka Formation (Carpathian Foredeep). 50

Table 18. Carbon isotopic composition of individual *n*-alkanes of core samples from the Kokhanivka Formation (Carpathian Foredeep). 51

Table 19. Organic geochemical parameters, concentration ratios of specific biomarkers of oil samples from the Carpathian Foredeep. 53

Table 20. Carbon isotopic composition of individual *n*-alkanes of oil samples from the Carpathian Foredeep. 53

Table 21. Bulk organic geochemical parameters, concentration and concentration ratios of specific biomarkers of cuttings samples of the Kaliakra Cany. Fill, Ruslar Fm. & Avren Fm. from wells Galata-1 and Varna Zapad-1 offshore Bulgaria (W. Black Sea). 55

Table 22. Average C isotopic composition of individual *n*-alkanes of cuttings samples from wells Galata-1 & Varna Zapad-1 offshore Bulgaria (W. Black Sea). 56

Table 23. Organic geochemical parameters, concentration ratios of specific biomarkers of the Tjulenovo oil (sample TJU) from the W. Black Sea (Bulgaria). 58

Table 24. Carbon composition of individual *n*-alkanes of the Tjulenovo oil (sample TJU) from the W. Black Sea (Bulgaria). 58

Table 25. Bulk organic geochemical parameters, concentration and concentration ratios of specific biomarkers of rock extracts from the Rioni Basin (Georgia). 60

Table 26. Carbon isotopic composition of individual *n*-alkanes of rock extracts of the Maikopian sed. & Kuma Fm. from the Rioni Basin (Georgia). 61

Table 27. Organic geochemical parameters, concentration ratios of specific biomarkers of the Shromisubani oil (sample PG) from the Rioni Basin (Georgia). 62

Table 28. Carbon isotopic composition of individual *n*-alkanes of the Shromisubani oil (sample PG) from the the Rion Basin (Georgia). 63

Table 29. Oberschauersberg well - sample depths 69

Table 30. Varna Zapad-1 well - sample depths 70

Table 31. Martvili section - sample depth locations 71

Table 32. Average carbon isotopic compositions of individual *n*-alkanes calculated from GC-IRMS data of Lower Oligocene source rocks from the Paratethyan realm. 73

Table 33. Average carbon isotopic compositions of individual *n*-alkanes calculated from GC-IRMS data of “Middle” Oligocene to Early Miocene source rocks from the Paratethyan realm. 75

Table 34. Average carbon isotopic compositions of individual *n*-alkanes calculated from GC-IRMS data of the rock samples of the Mesozoic basement of Paratethyan provinces. 77

Appendix: Biomarkers: GC-MS (Chromatograms for saturated and aromatic fractions)

B-21
Saturated HC

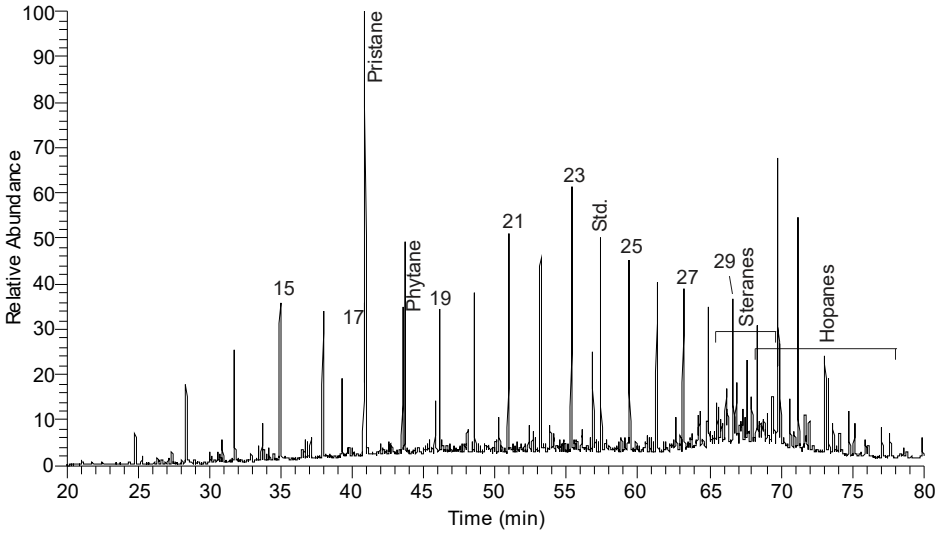

B-21
Aromatic HC

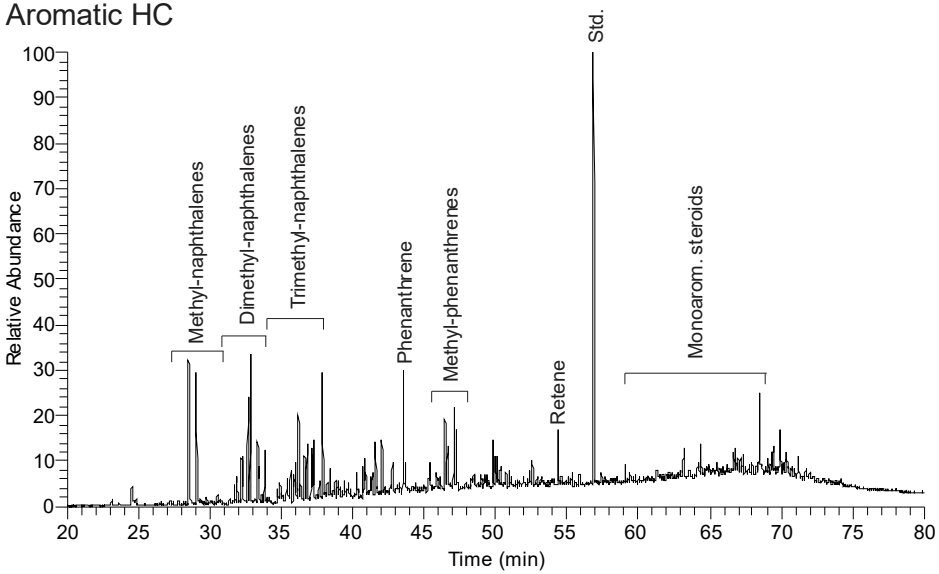

B-40
Saturated HC

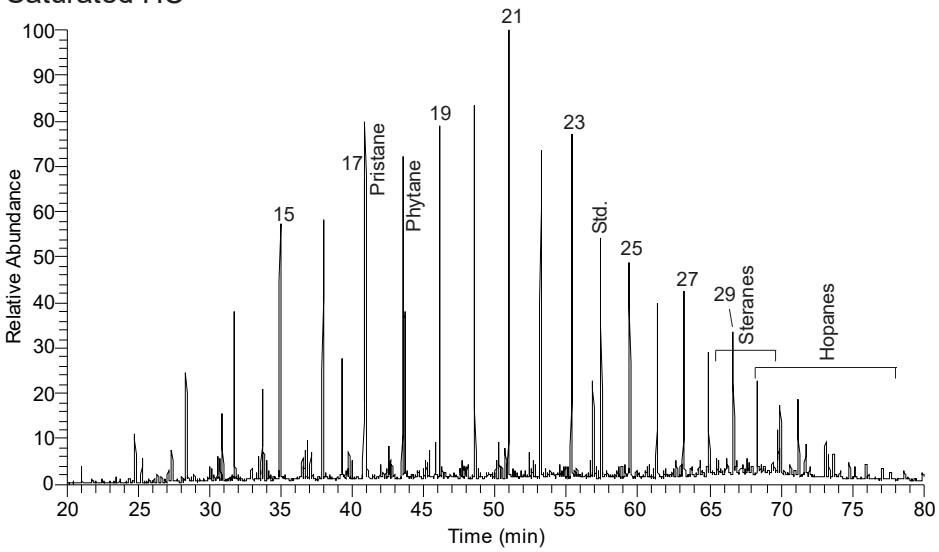

B-40
Aromatic HC

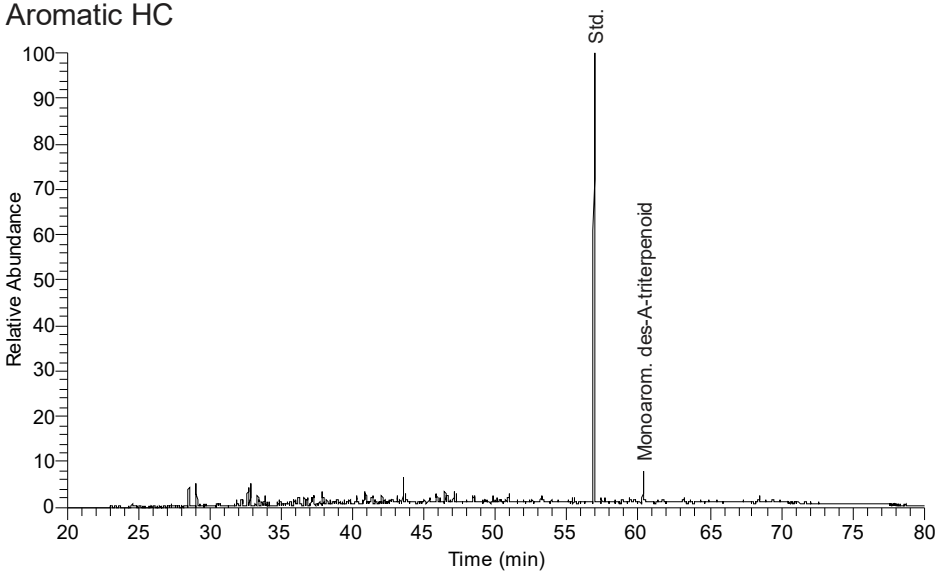

B-47

Saturated HC

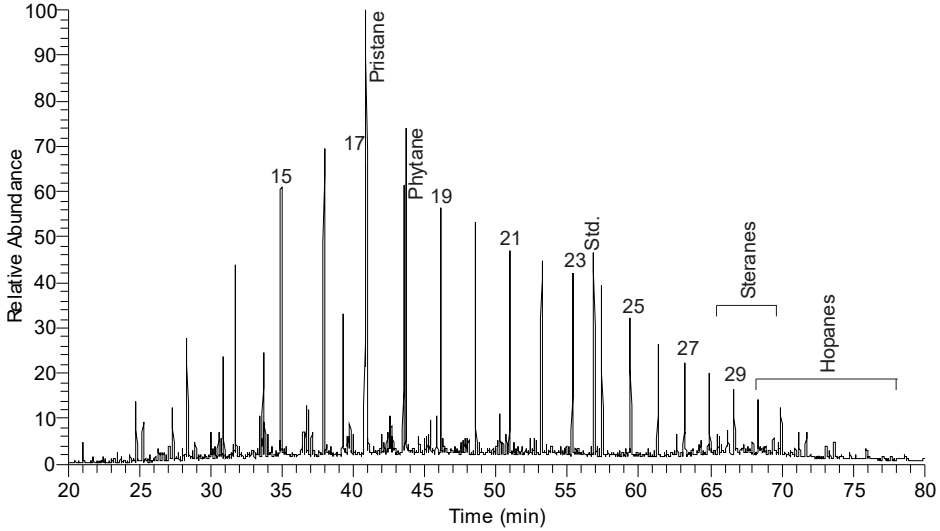

B-47

Aromatic HC

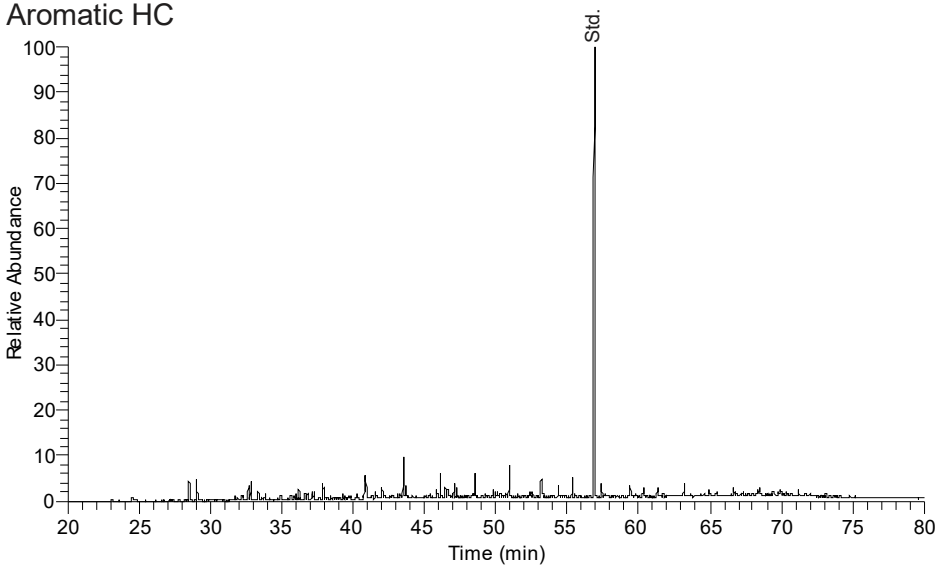

A-01

Saturated HC

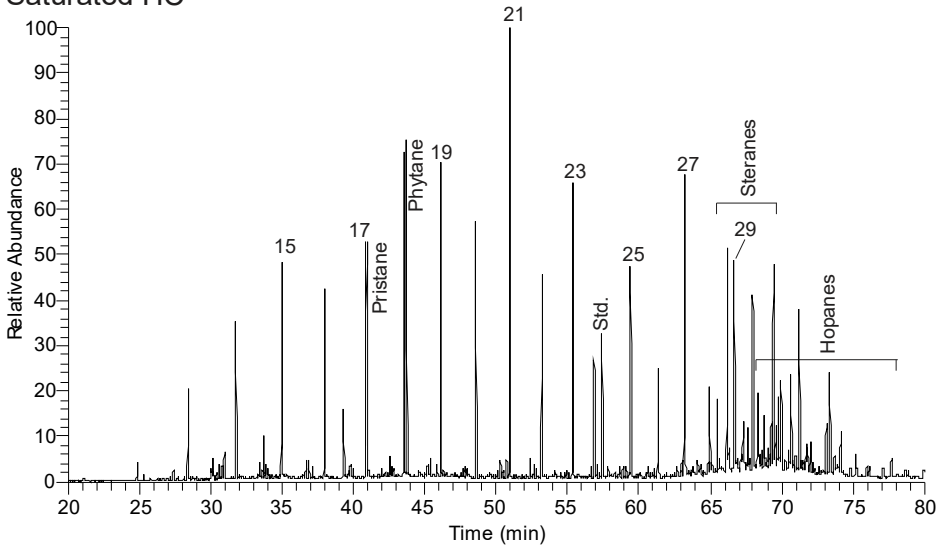

A-01

Aromatic HC

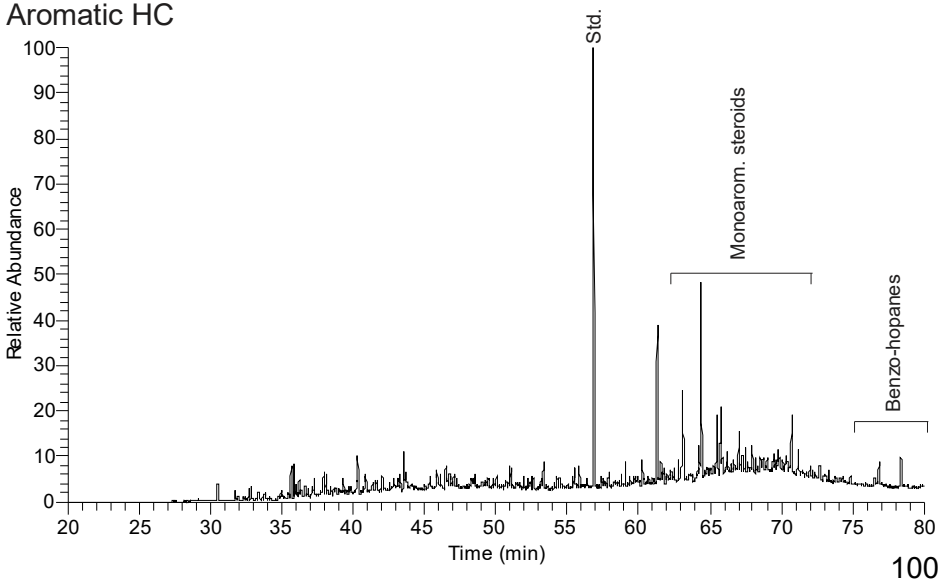

A-09
Saturated HC

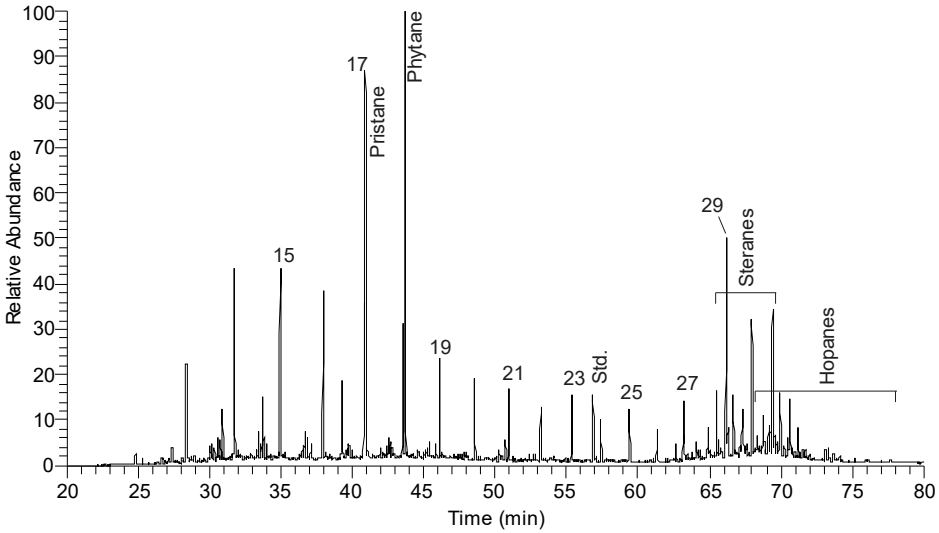

A-09
Aromatic HC

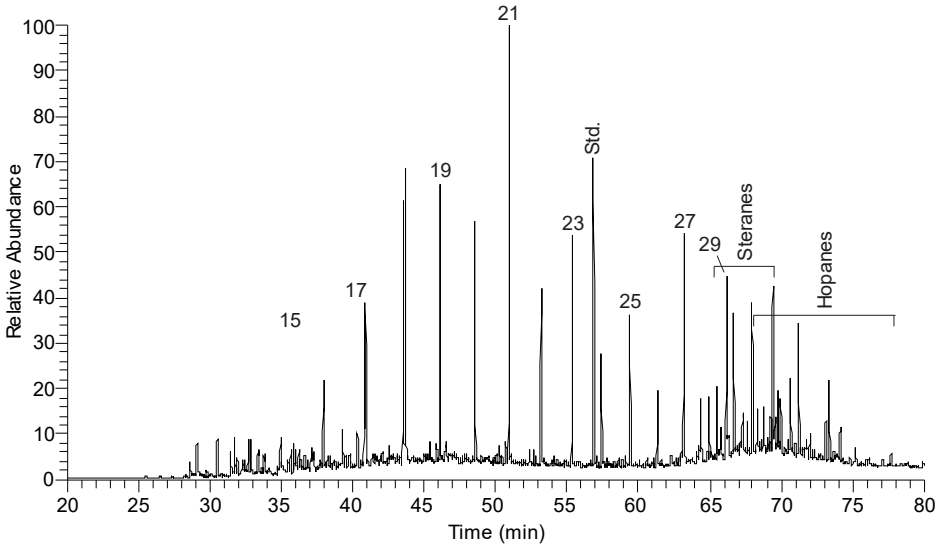

Osch-5
Saturated HC

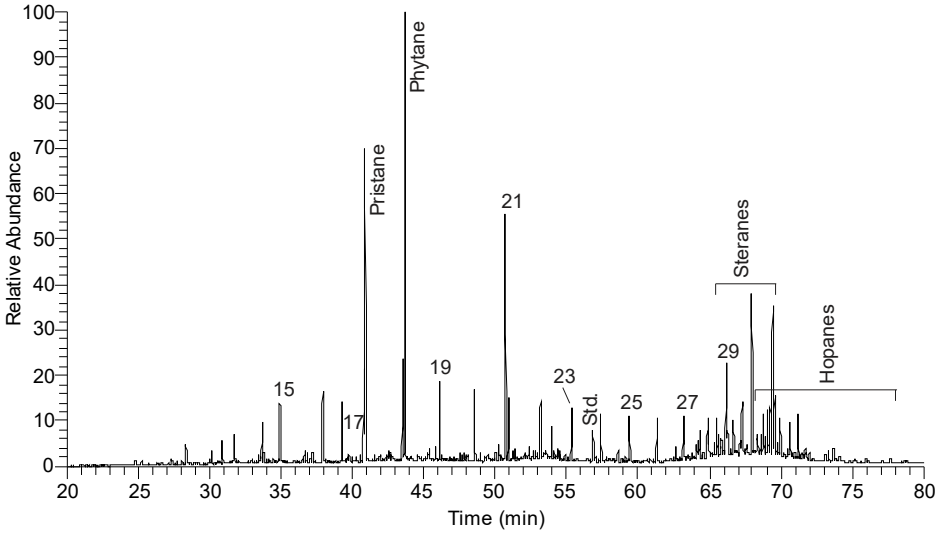

Osch-5
Aromatic HC

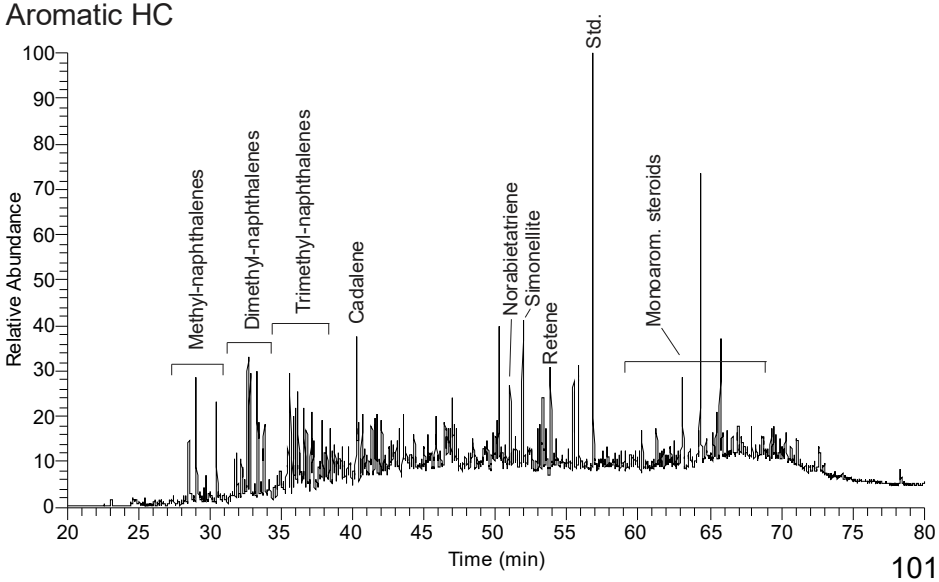

Osch-6
Saturated HC

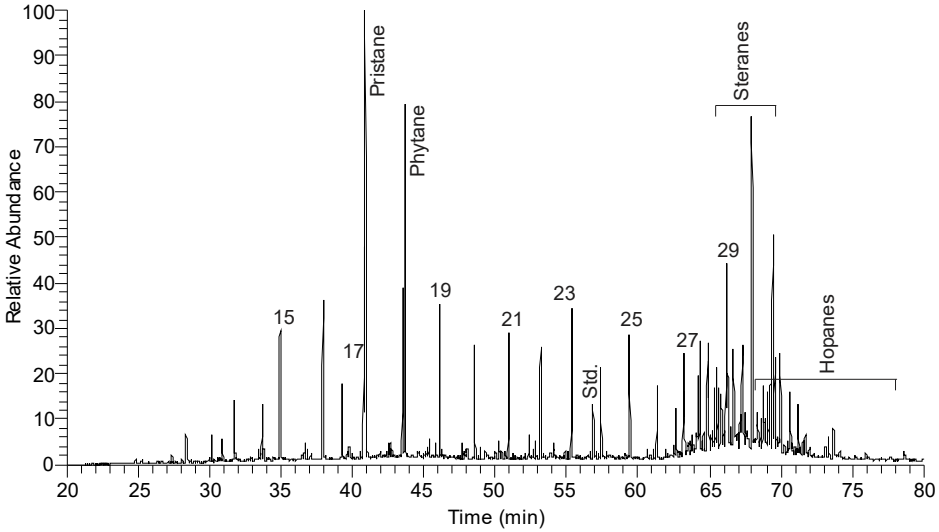

Osch-6
Aromatic HC

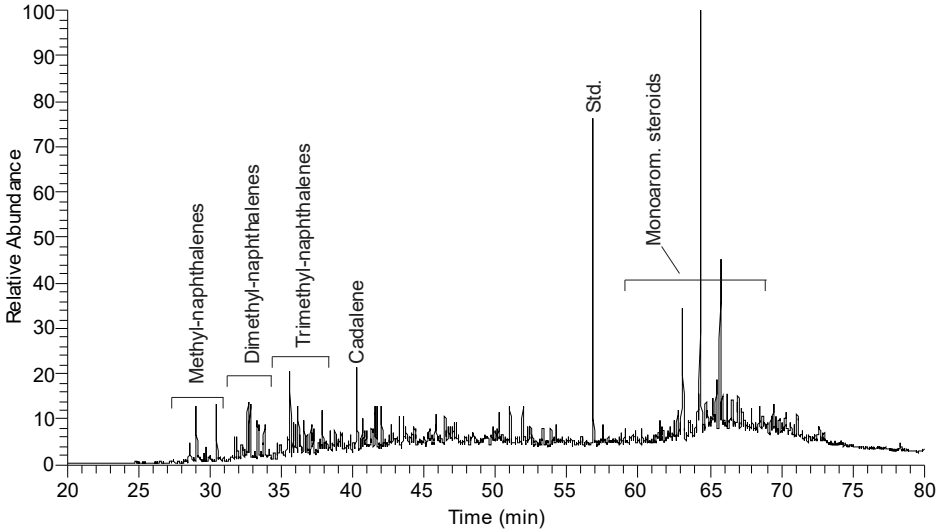

Osch-7d
Saturated HC

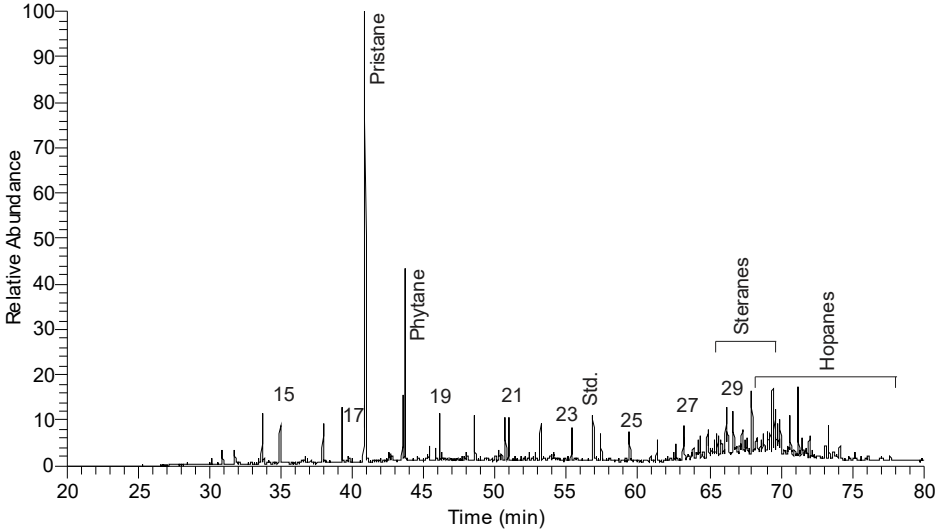

Osch-7d
Aromatic HC

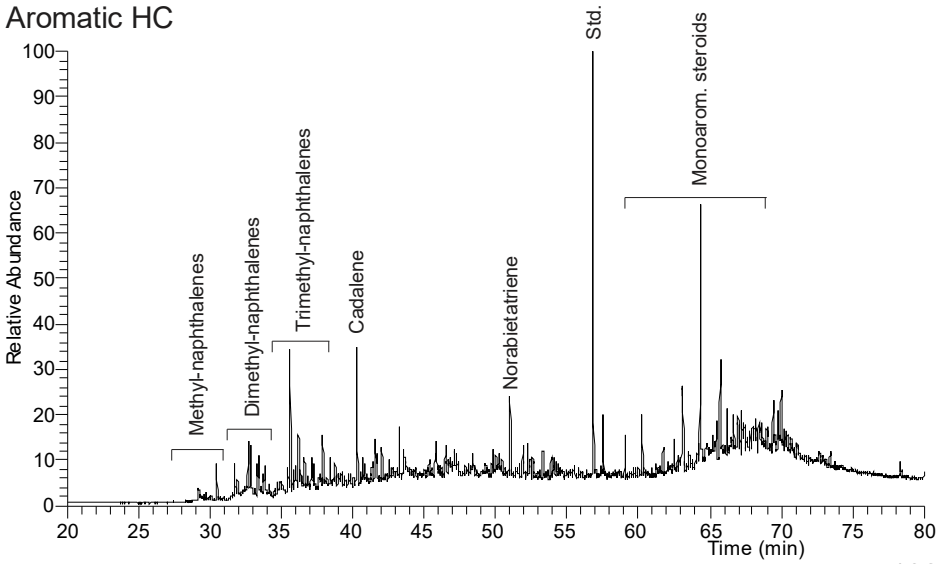

Osch-2
Saturated HC

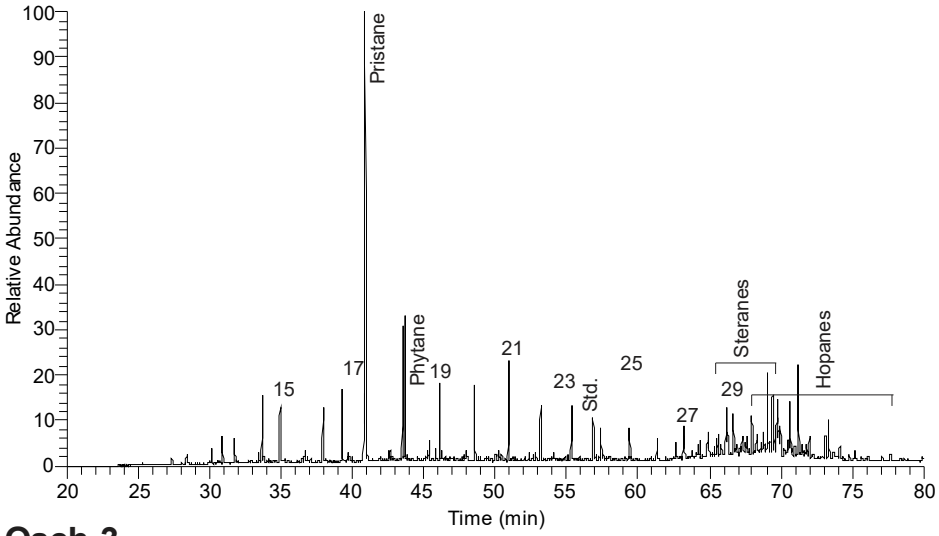

Osch-2
Aromatic HC

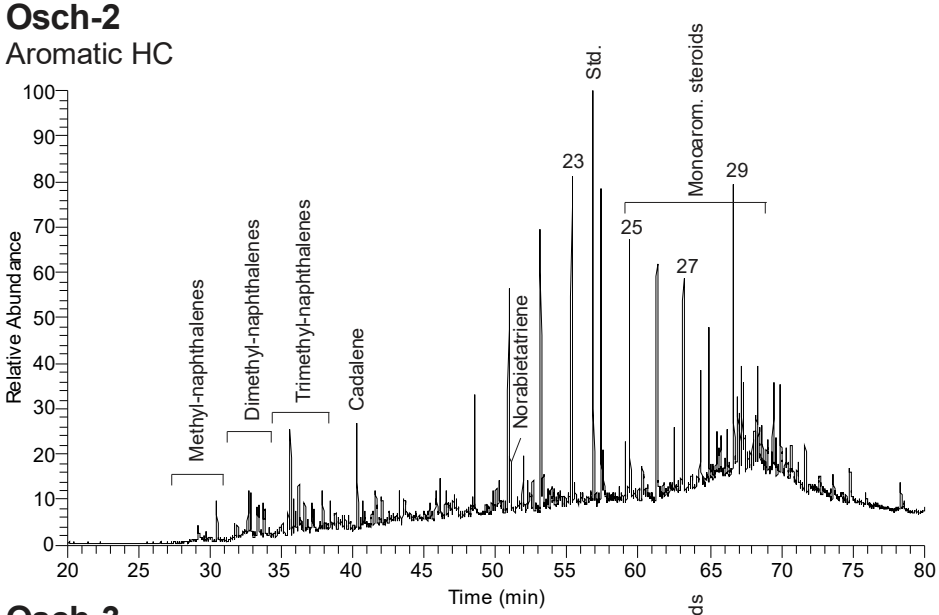

Osch-3
Saturated HC

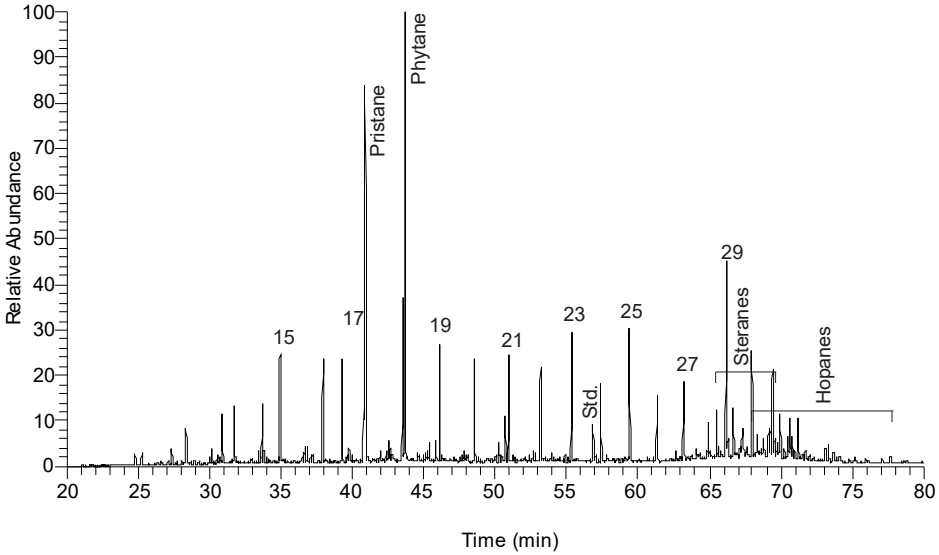

Osch-3
Aromatic HC

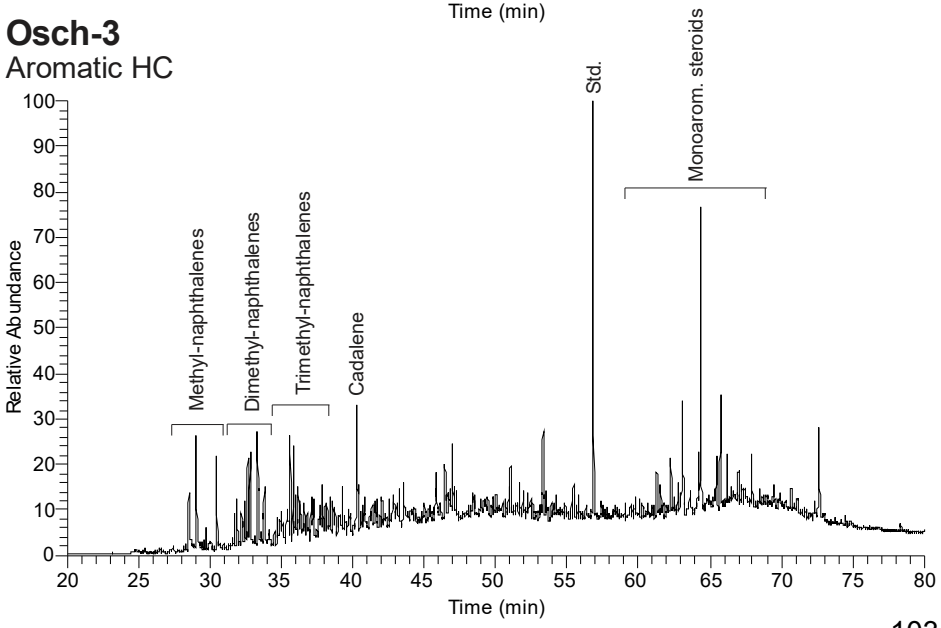

Osch-1
Saturated HC

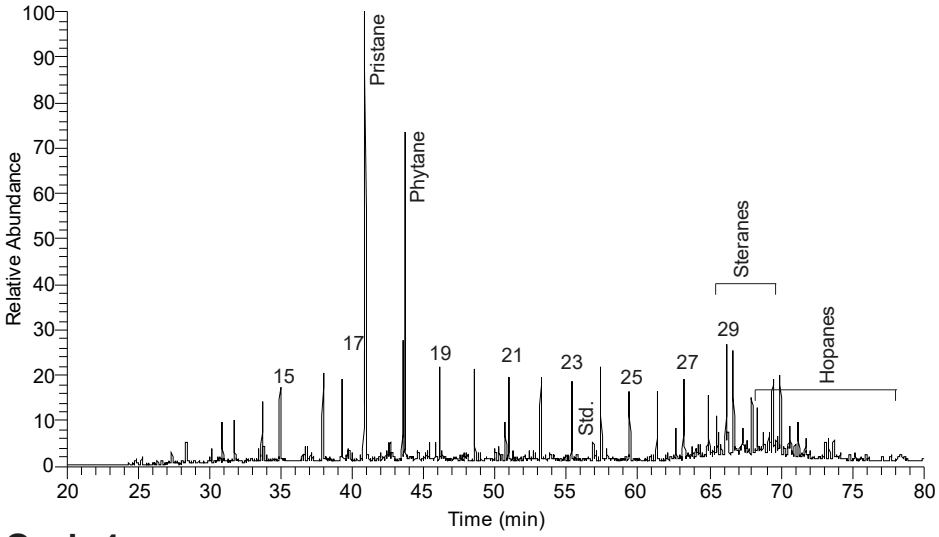

Osch-1
Aromatic HC

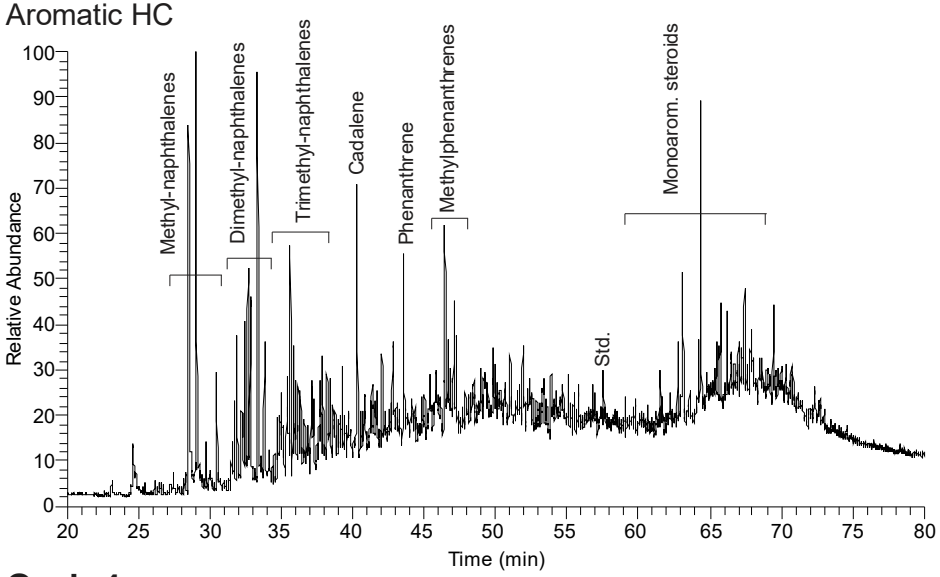

Osch-4
Saturated HC

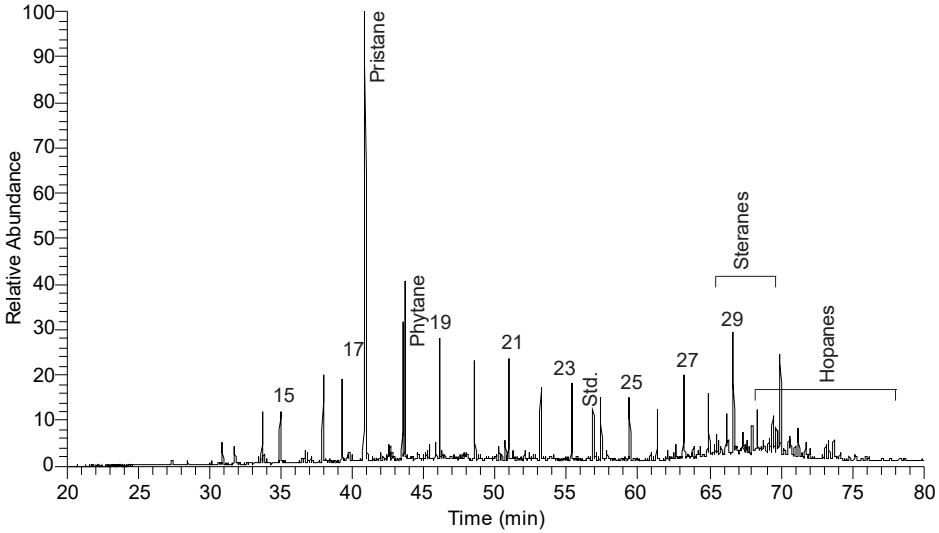

Osch-4
Aromatic HC

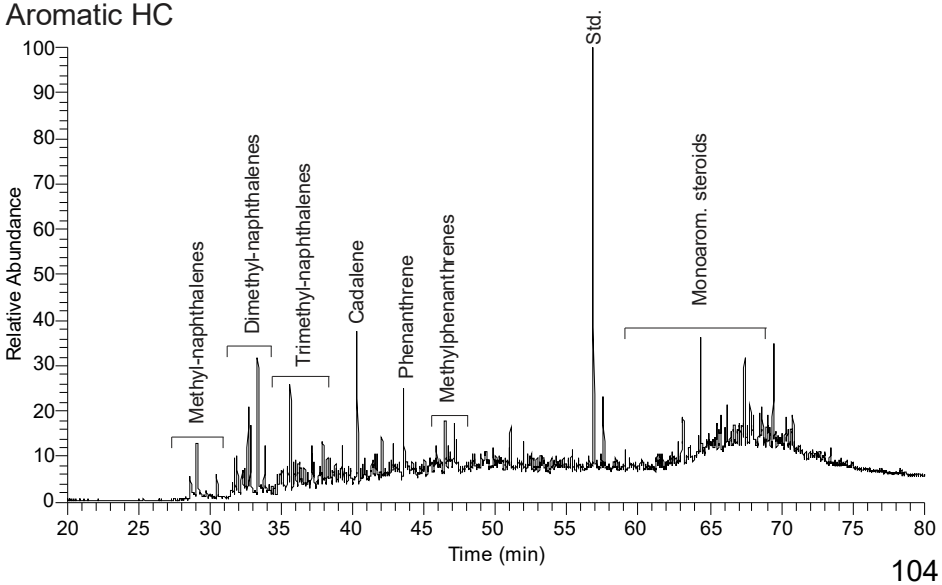

BT-35
Saturated HC

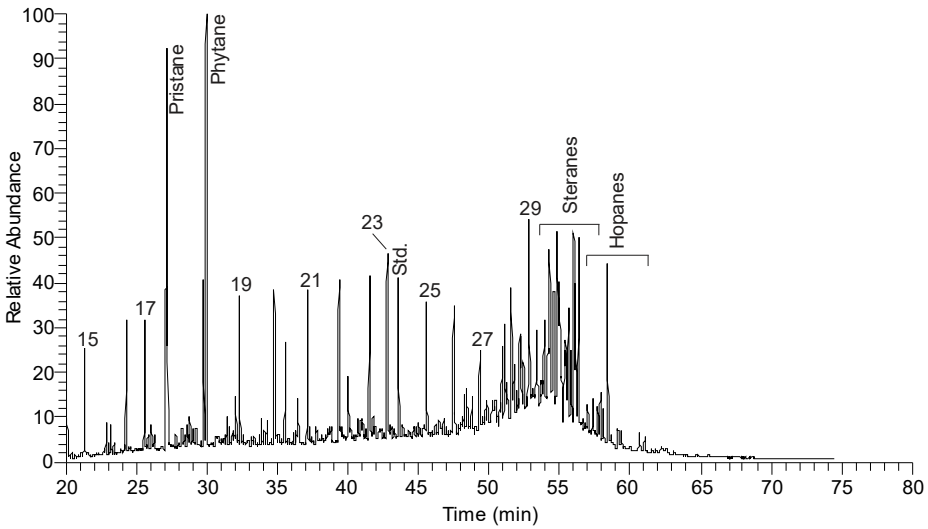

BT-35
Aromatic HC

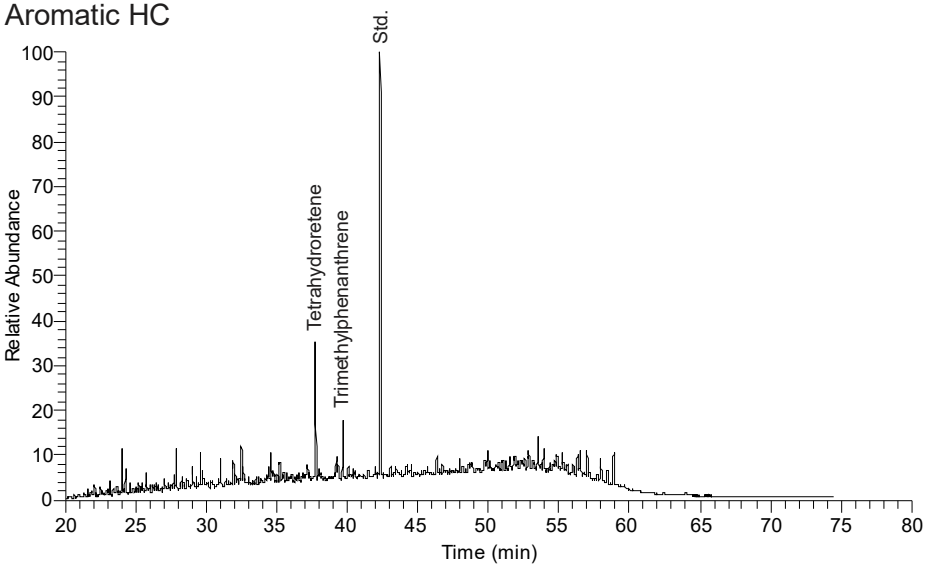

BT-26
Saturated HC

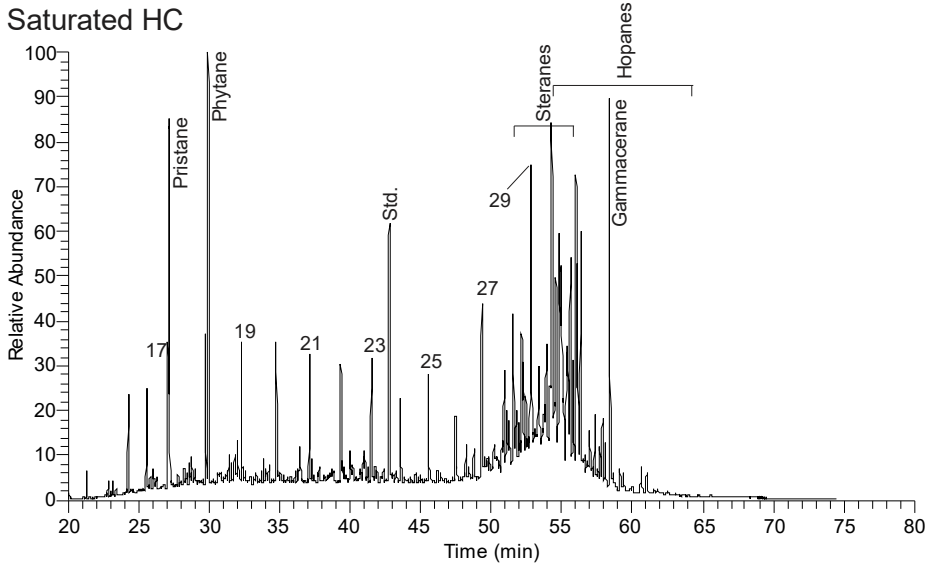

BT-26
Aromatic HC

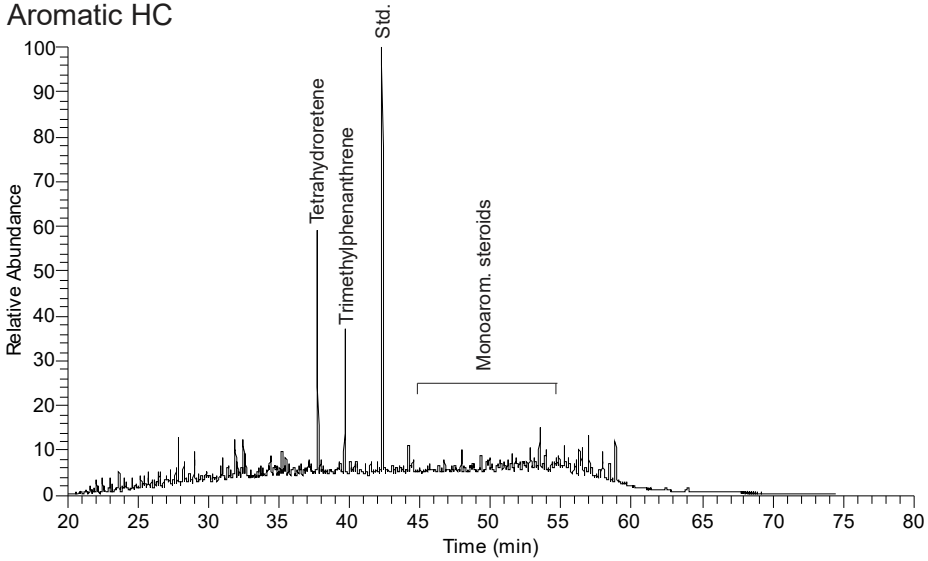

Tho-1720
Saturated HC

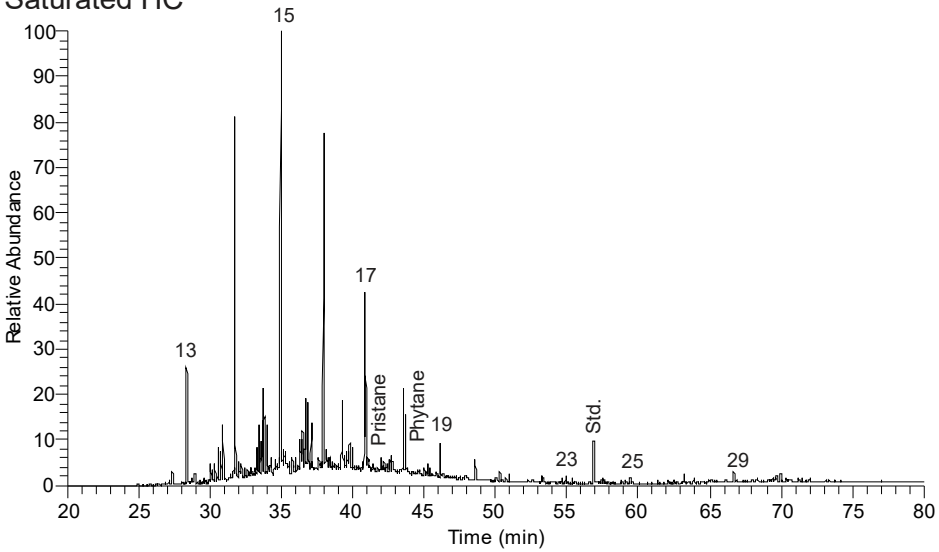

Tho-1720
Aromatic HC

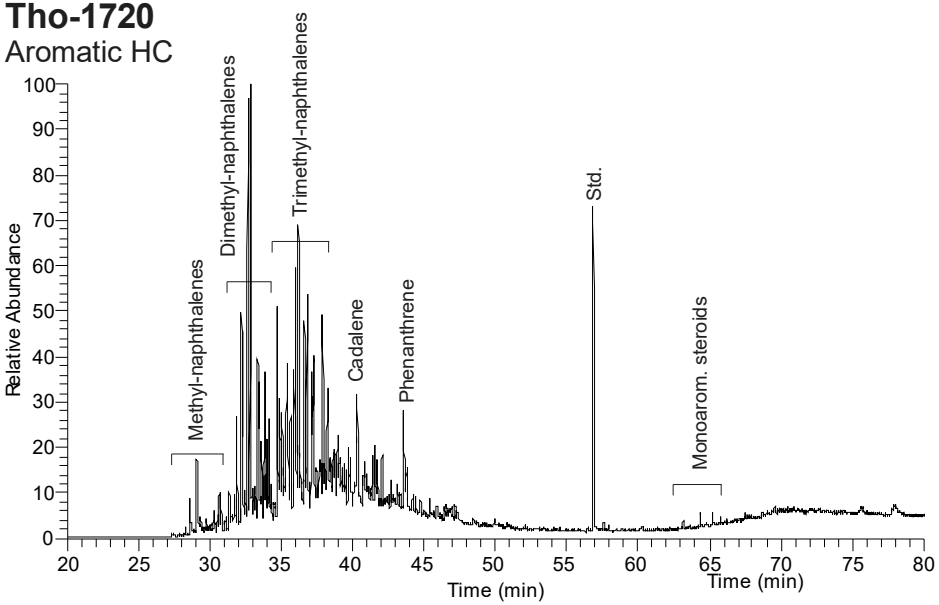

Tho-1760
Saturated HC

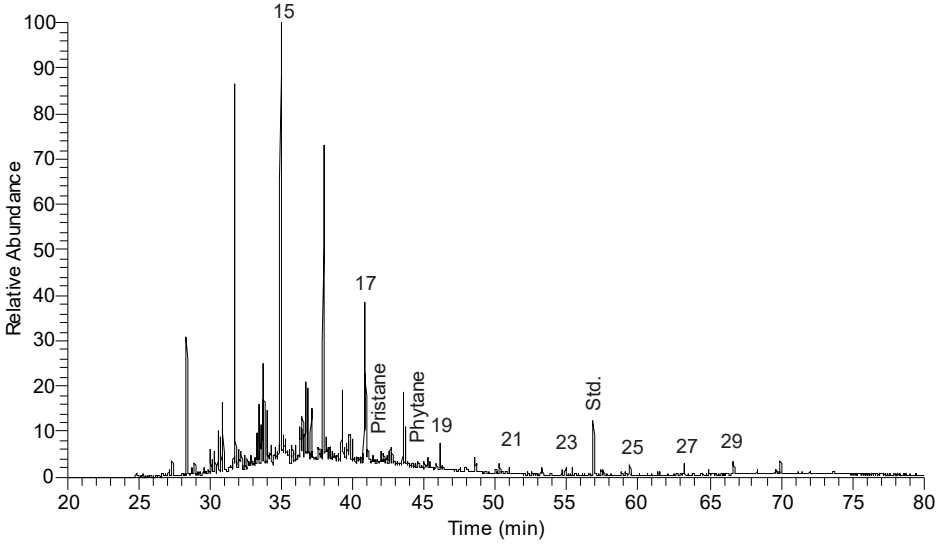

Tho-1760
Aromatic HC

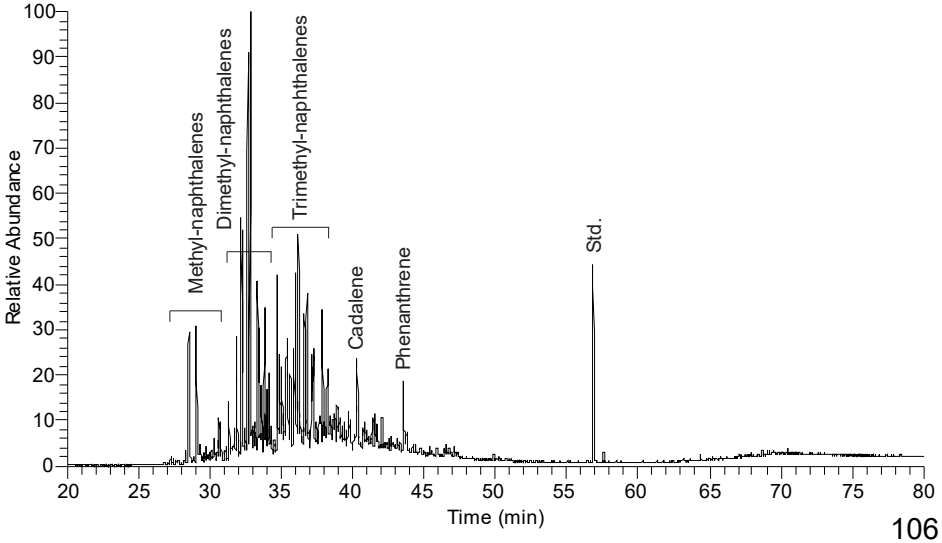

U-C63
Saturated HC

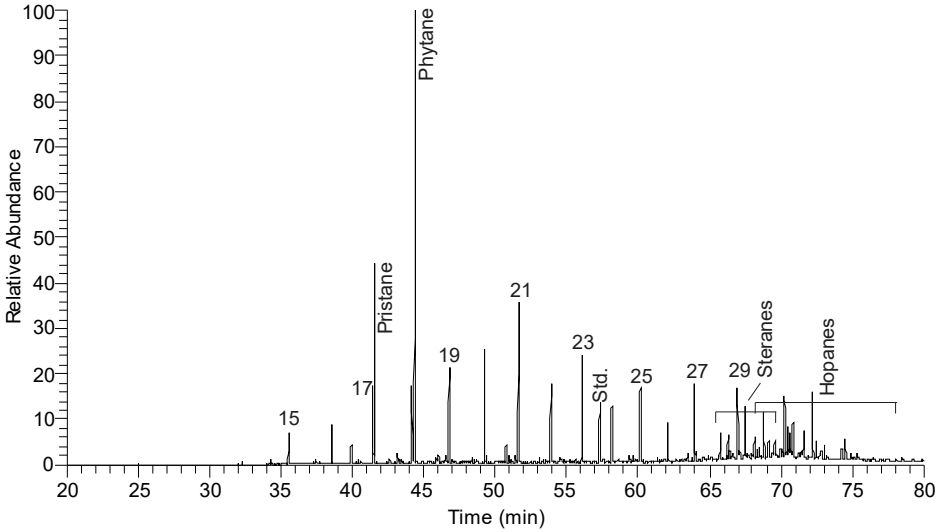

U-C63
Aromatic HC

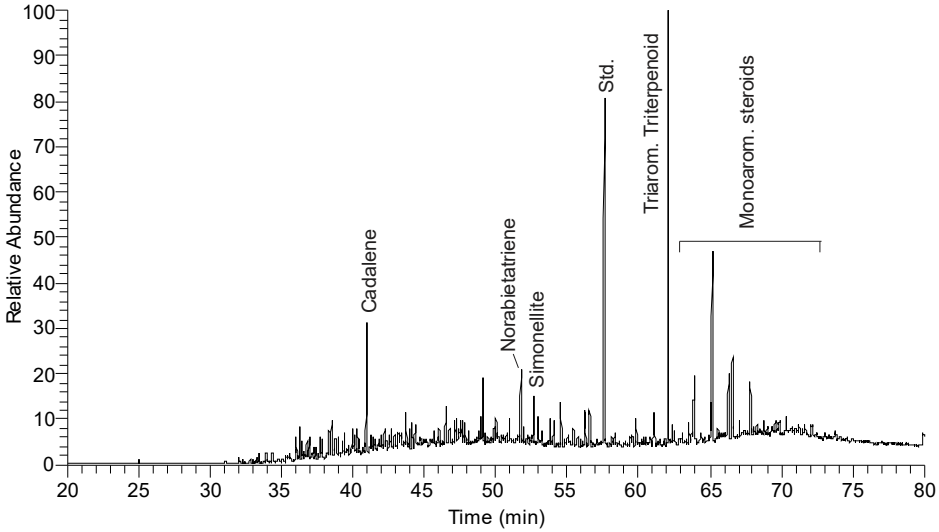

U-B-22
Saturated HC

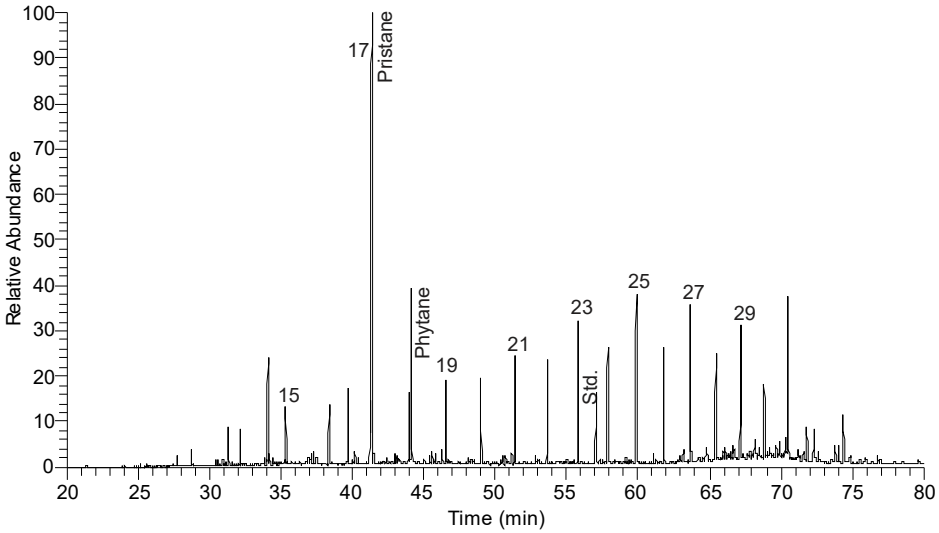

U-B-22
Aromatic HC

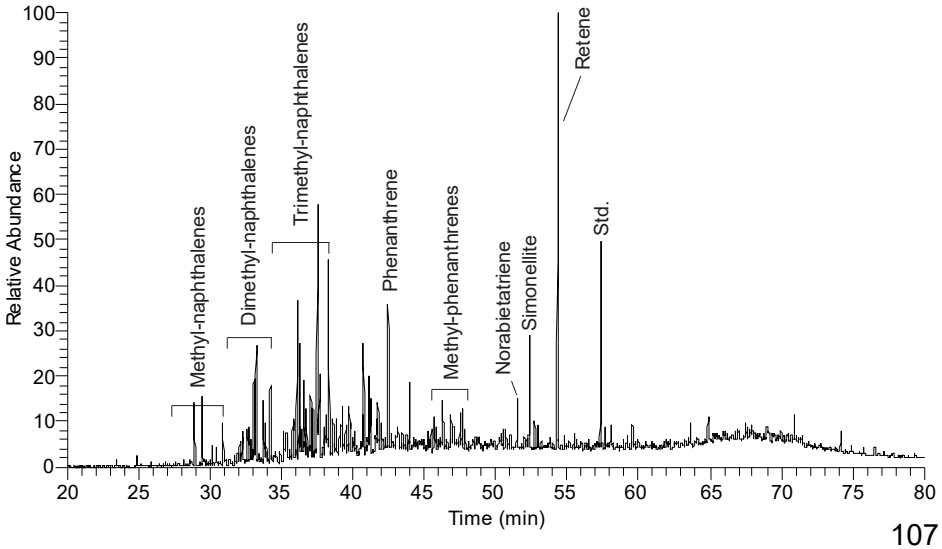

U-66
Saturated HC

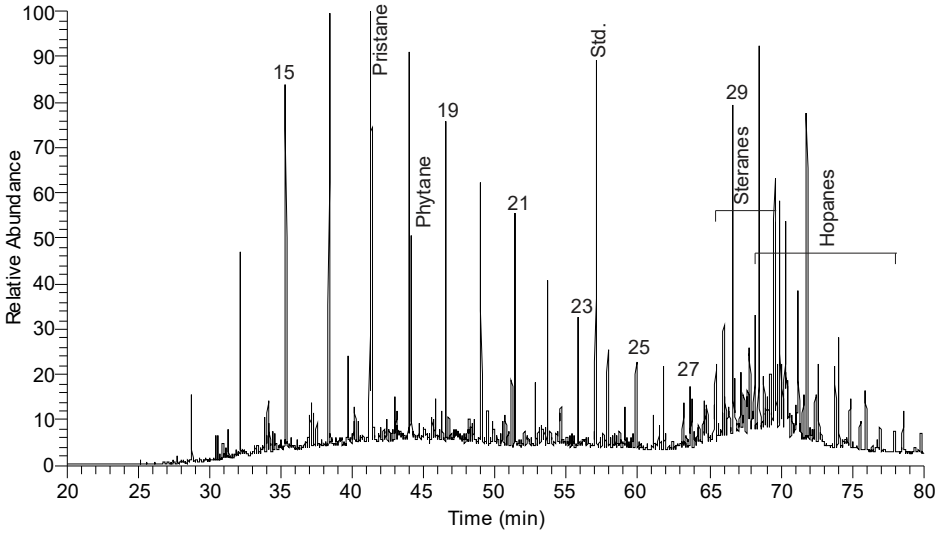

U-66
Aromatic HC

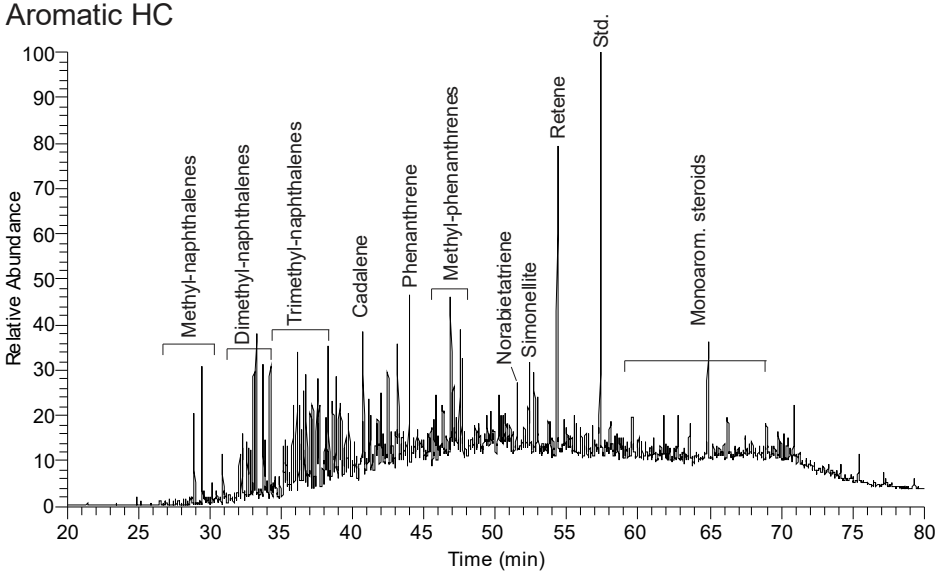

J-5
Saturated HC

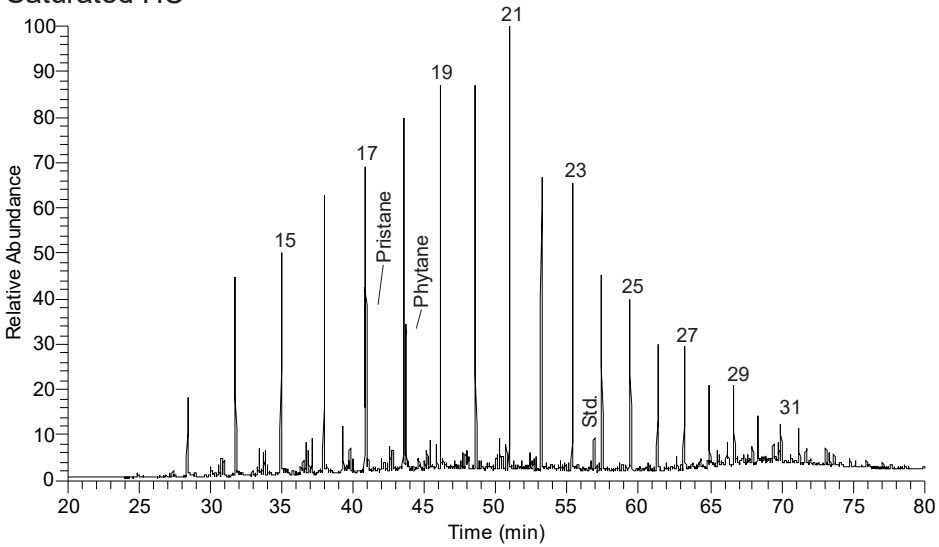

J-5
Aromatic HC

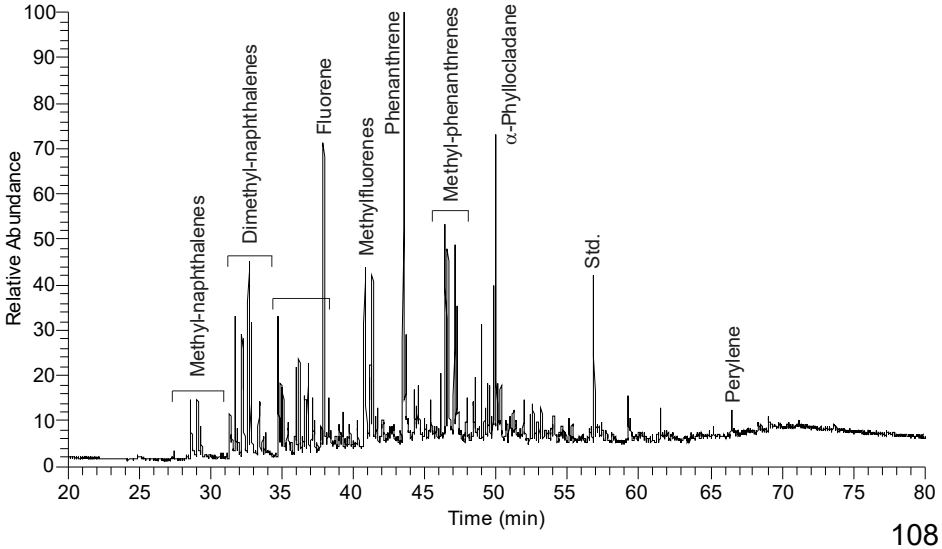

J-77
Saturated HC

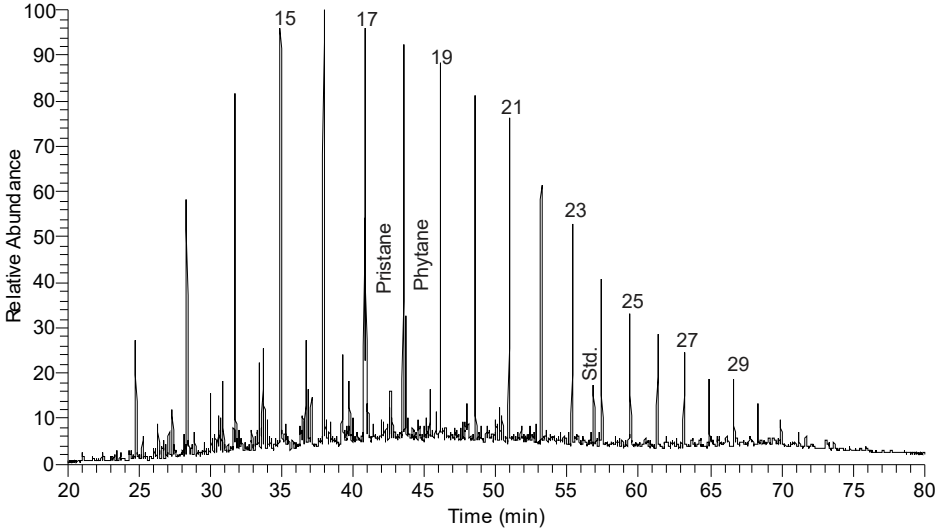

J-77
Aromatic HC

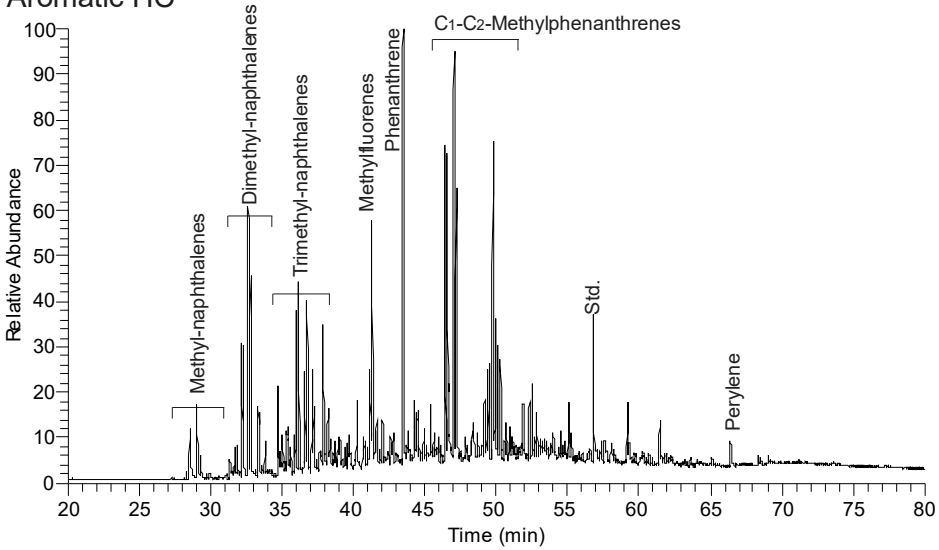

J-MS-2523
Saturated HC

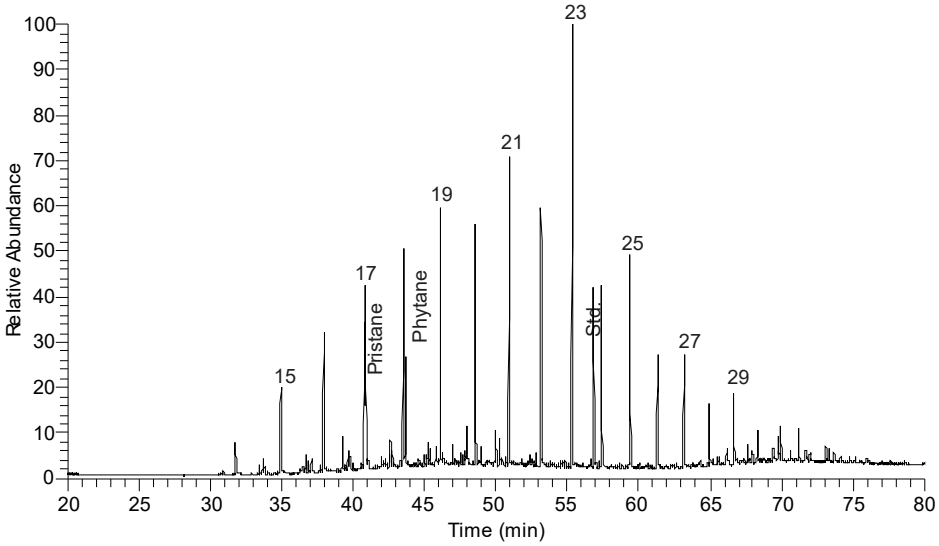

J-MS-2523
Aromatic HC

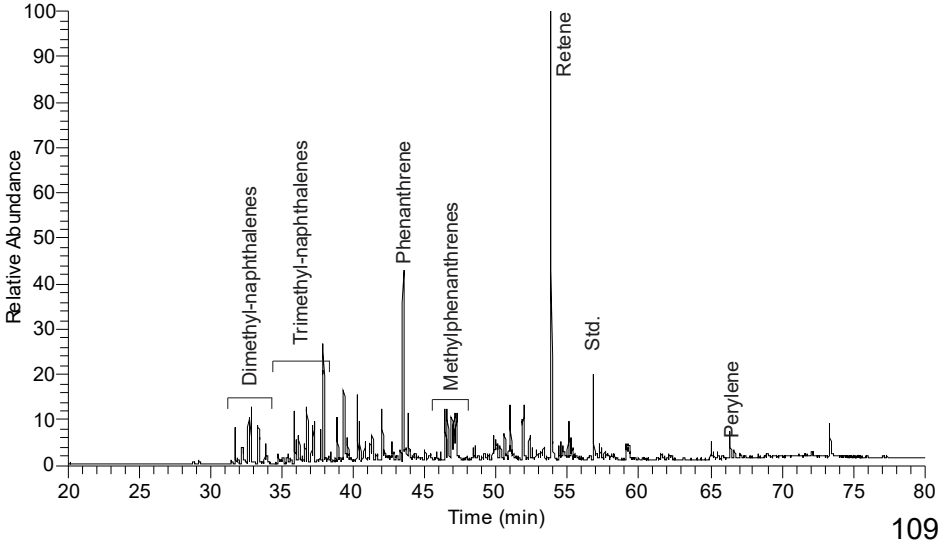

J-K6-3428
Saturated HC

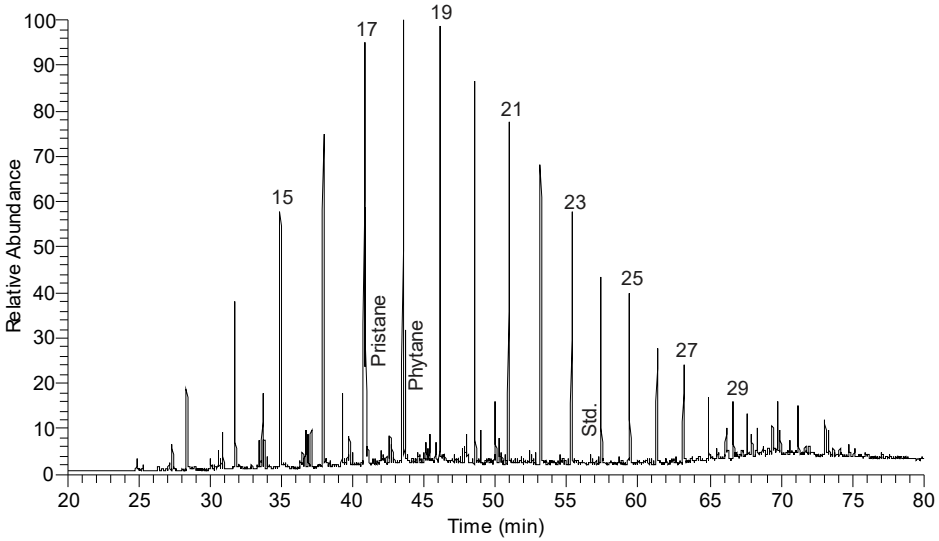

J-K6-3428
Aromatic HC

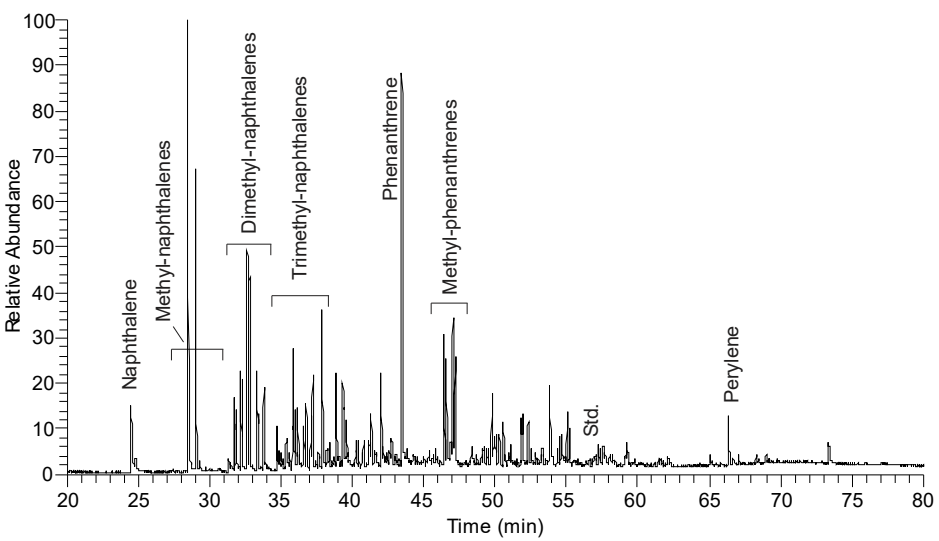

J-K6-3521
Saturated HC

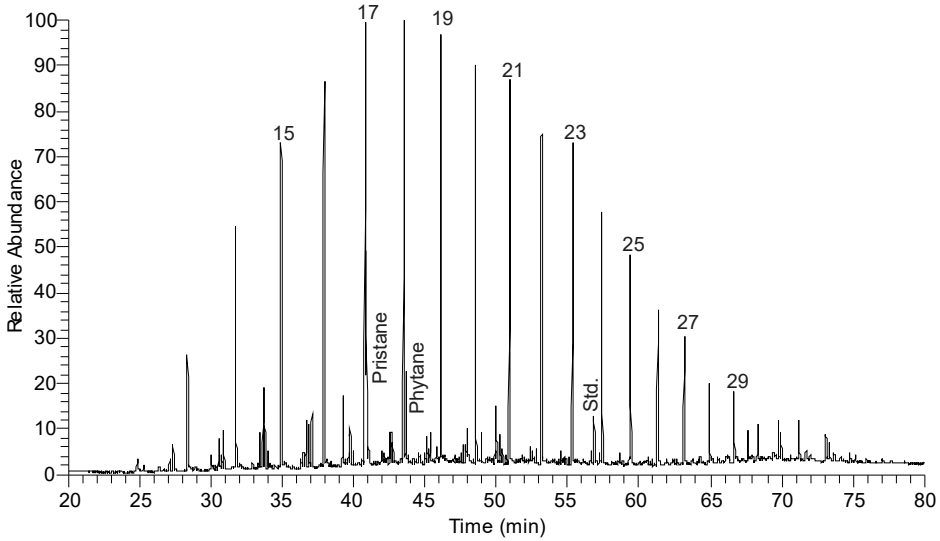

J-K6-3521
Aromatic HC

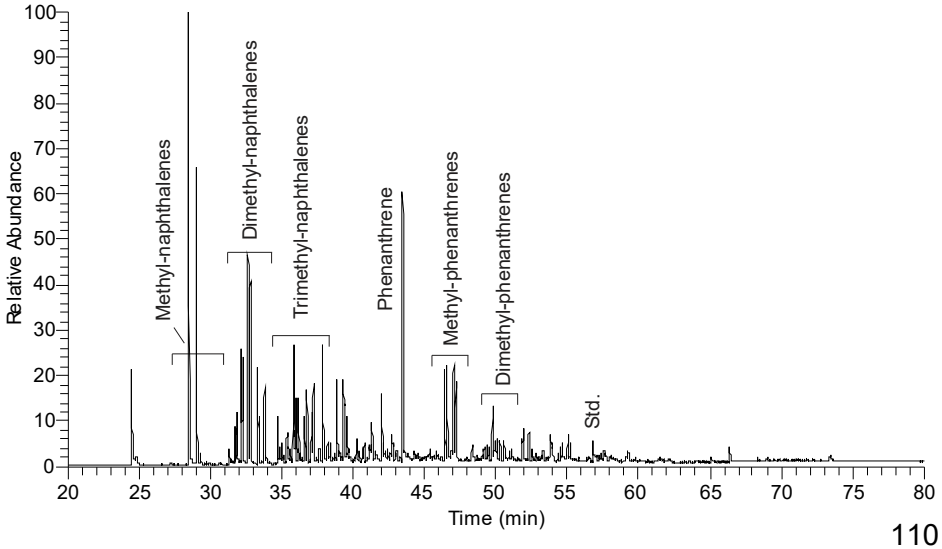

Gal-880
Saturated HC

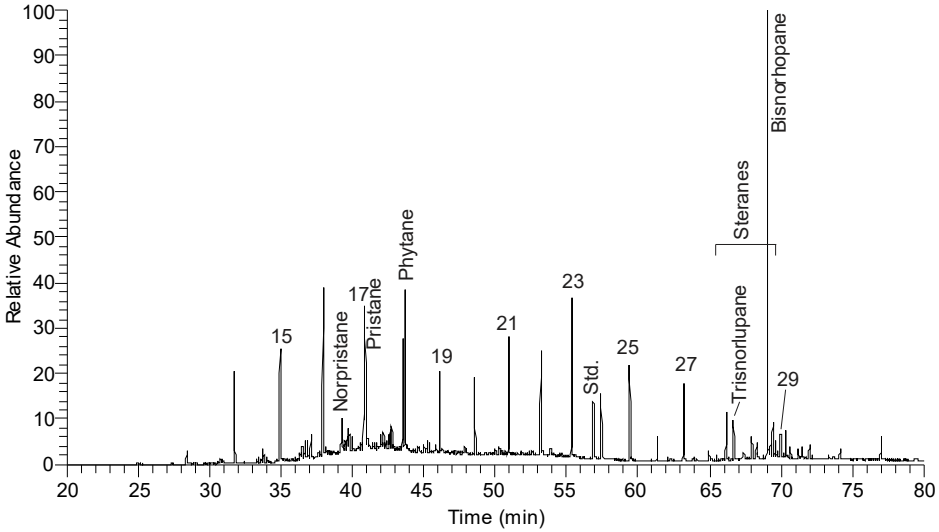

Gal-880
Aromatic HC

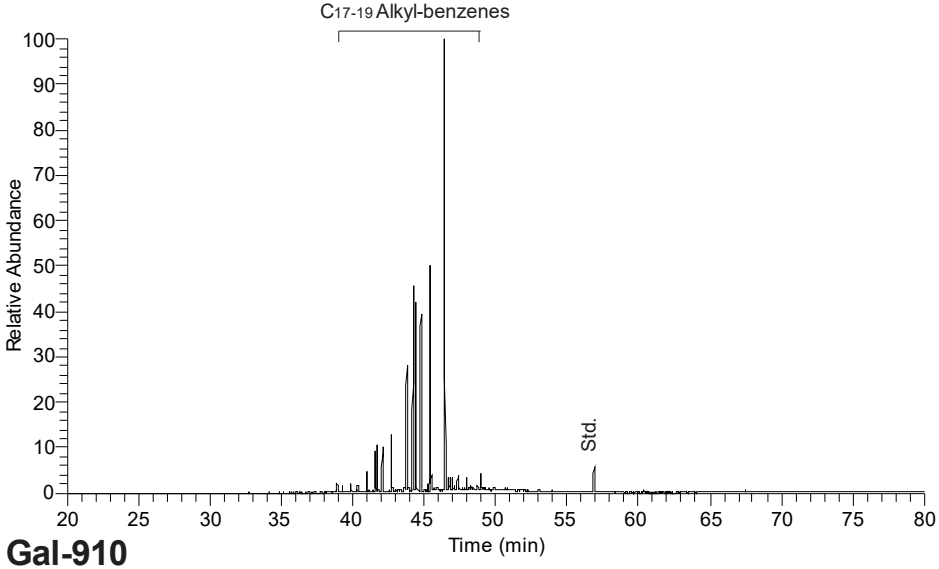

Gal-910
Saturated HC

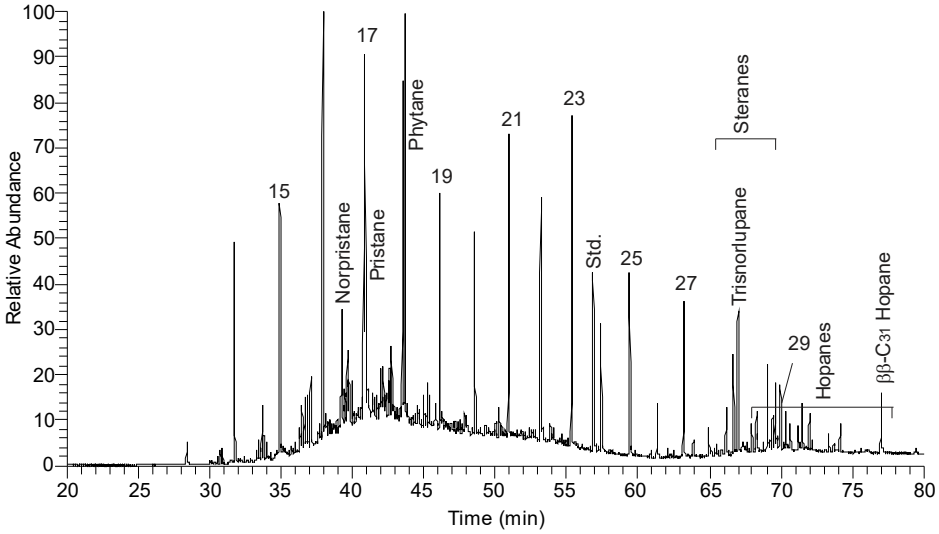

Gal-910
Aromatic HC

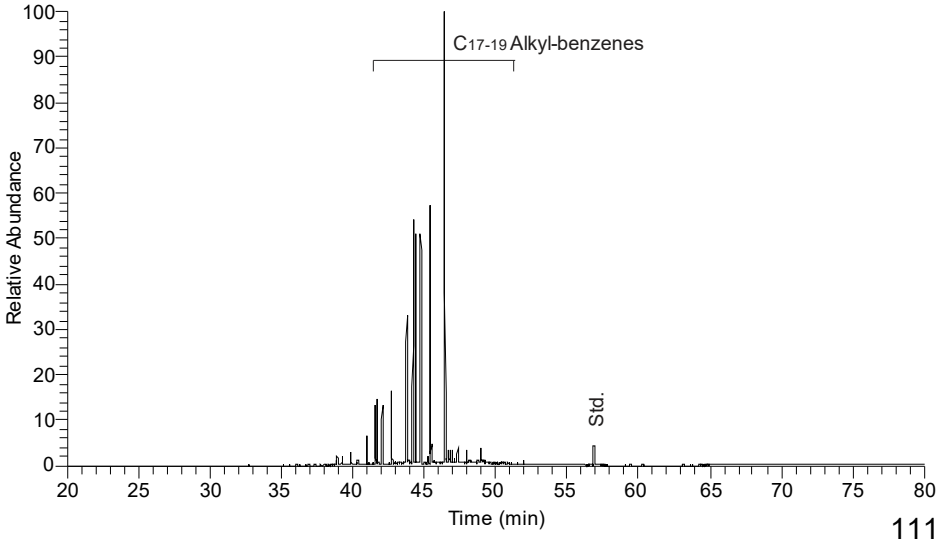

VarZ1-480
Saturated HC

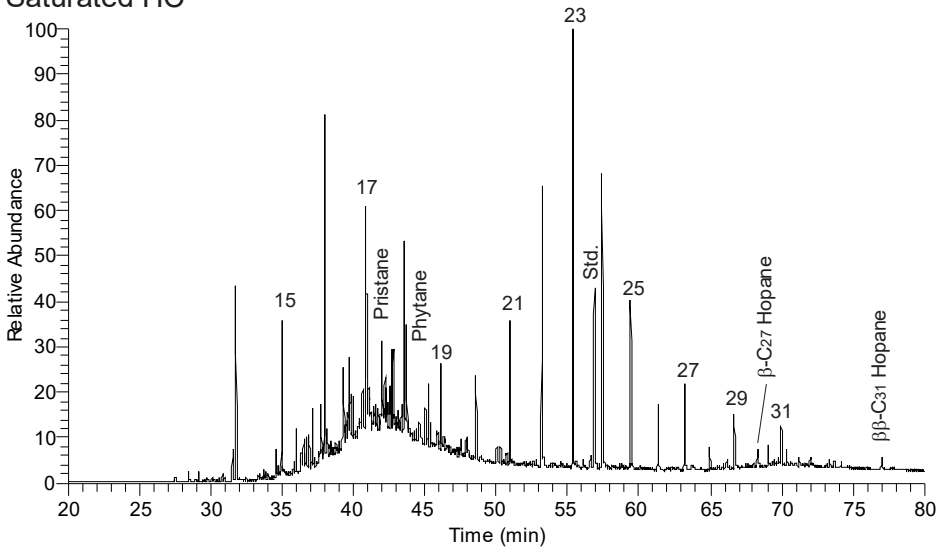

VarZ1-480
Aromatic HC

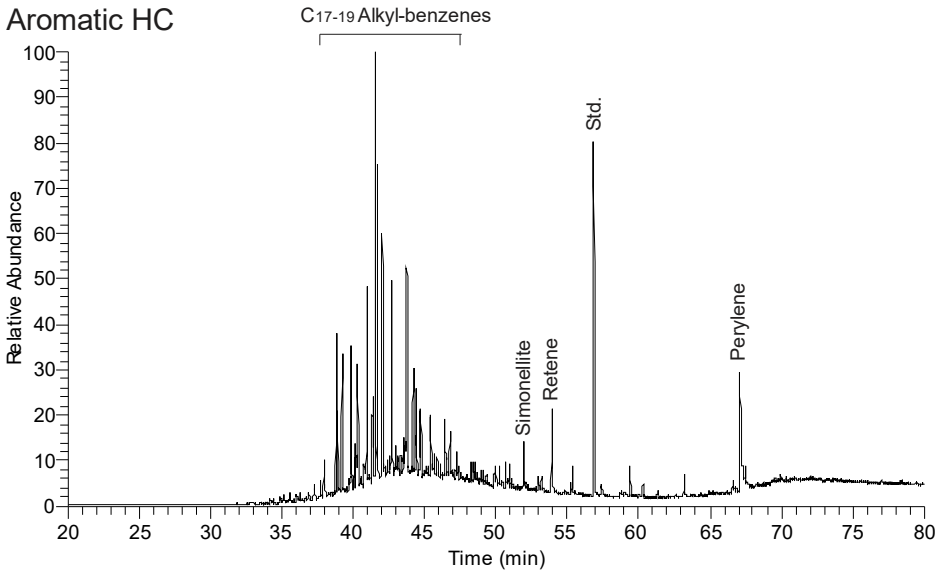

VarZ1-570
Saturated HC

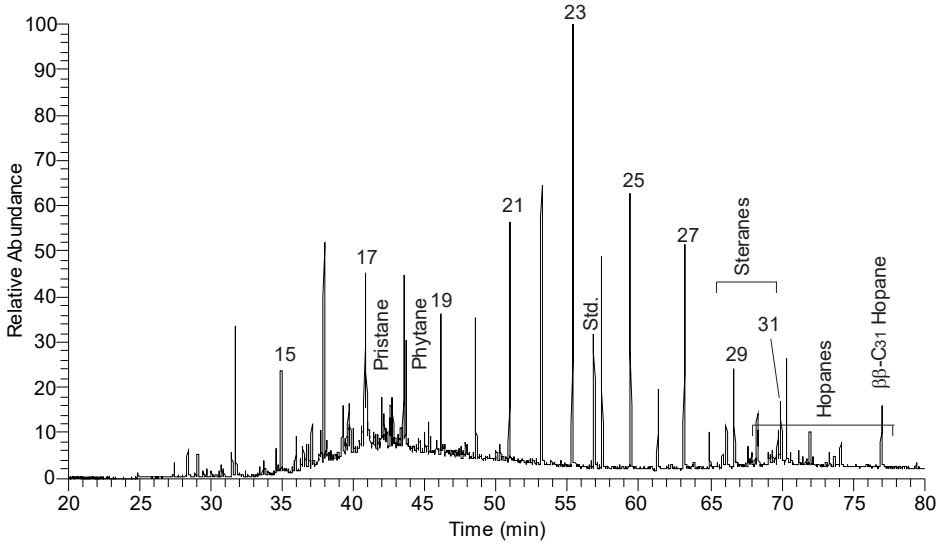

VarZ1-570
Aromatic HC

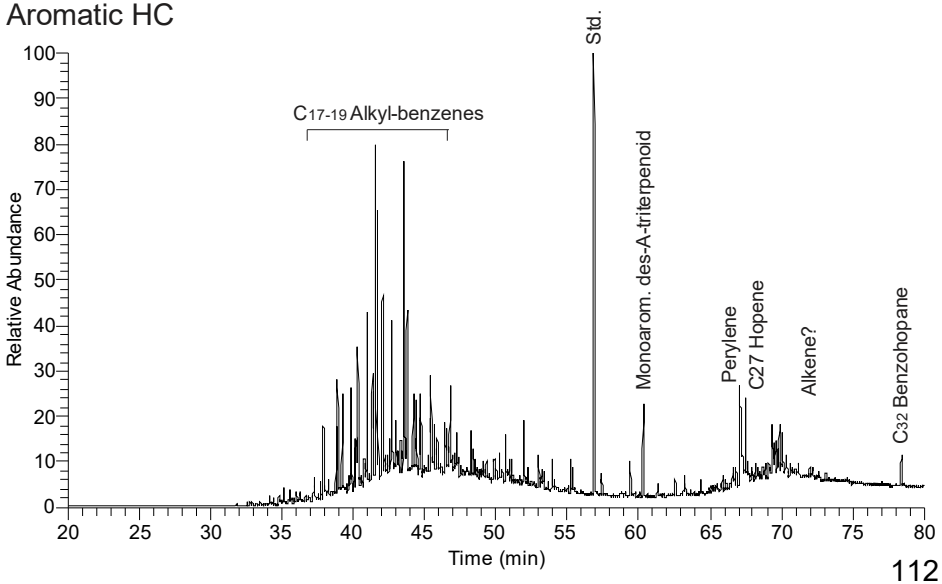

VarZ1-600
Saturated HC

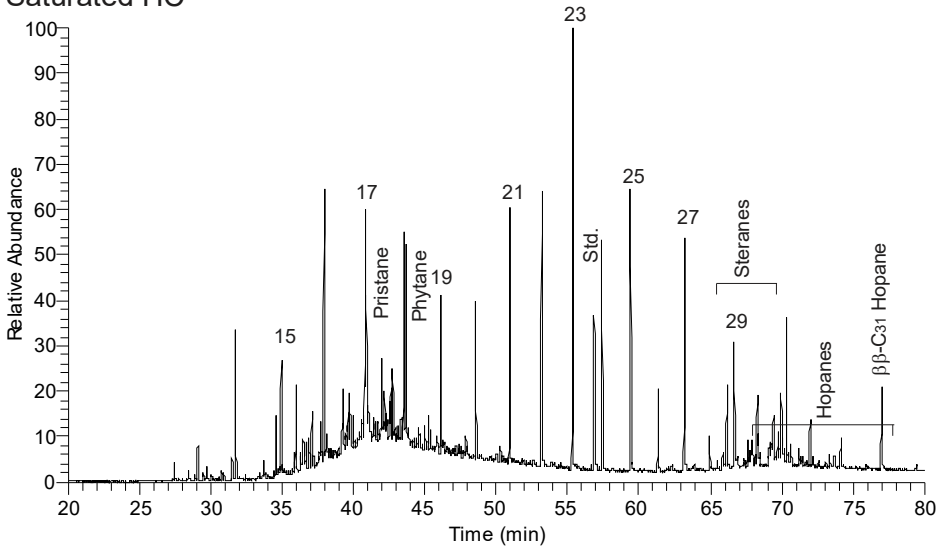

VarZ1-600
Aromatic HC

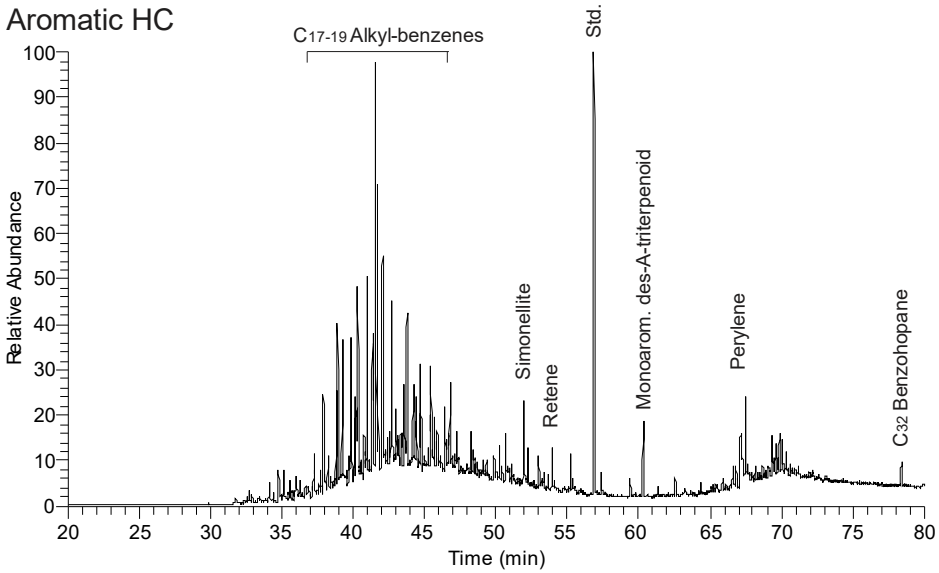

VarZ1-660
Saturated HC

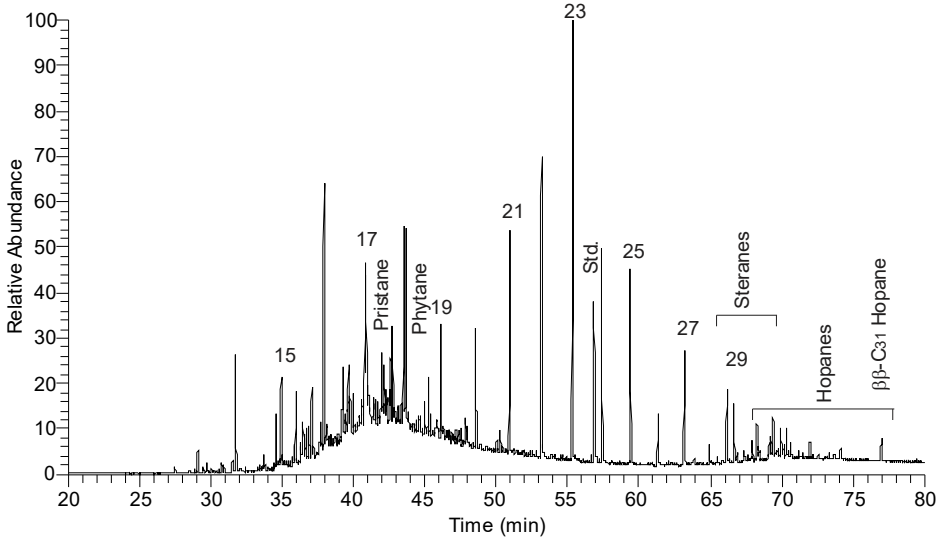

VarZ1-660
Aromatic HC

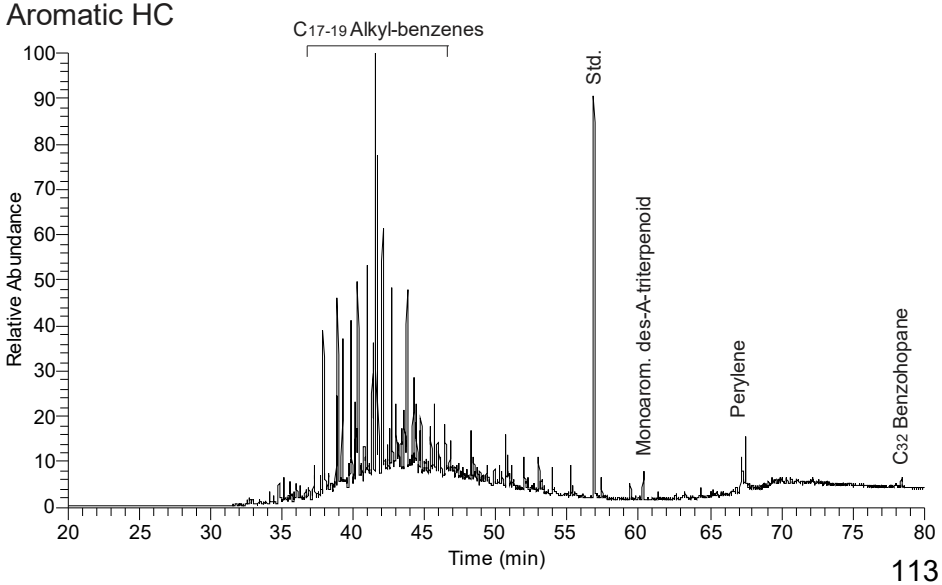

VarZ1-817
Saturated HC

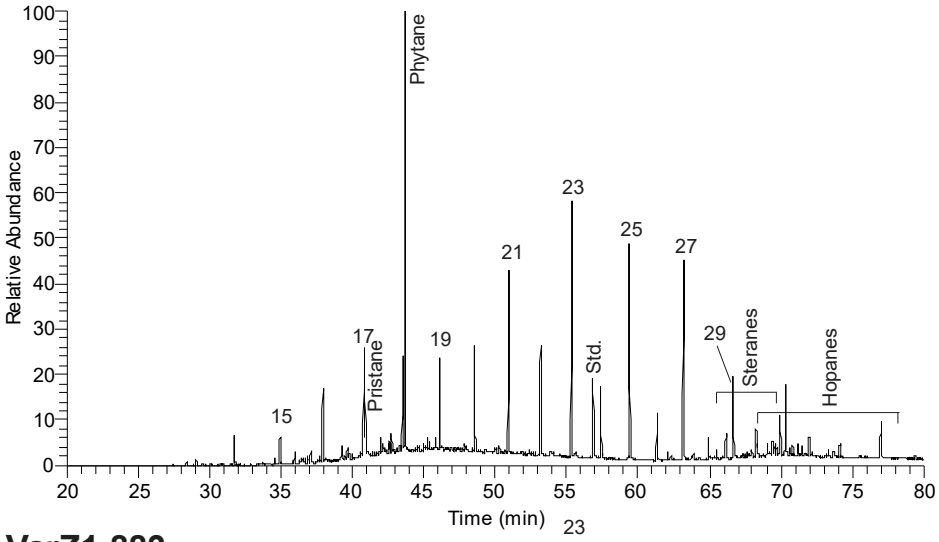

VarZ1-817
Aromatic HC

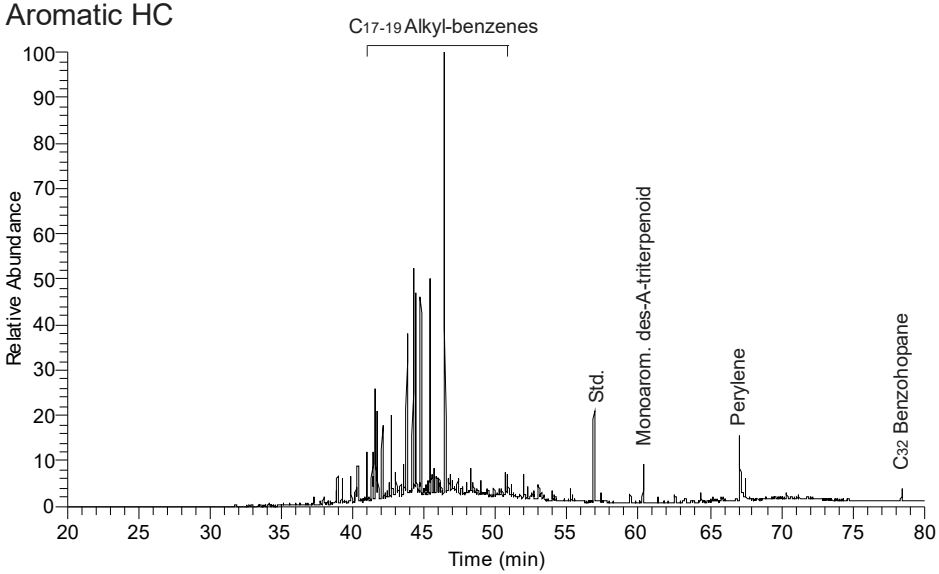

VarZ1-883
Saturated HC

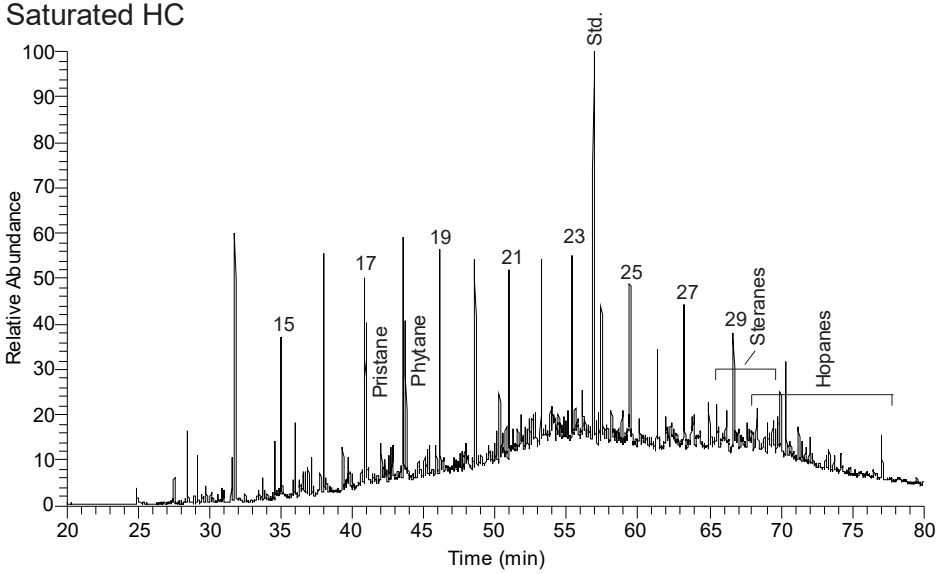

VarZ1-883
Aromatic HC

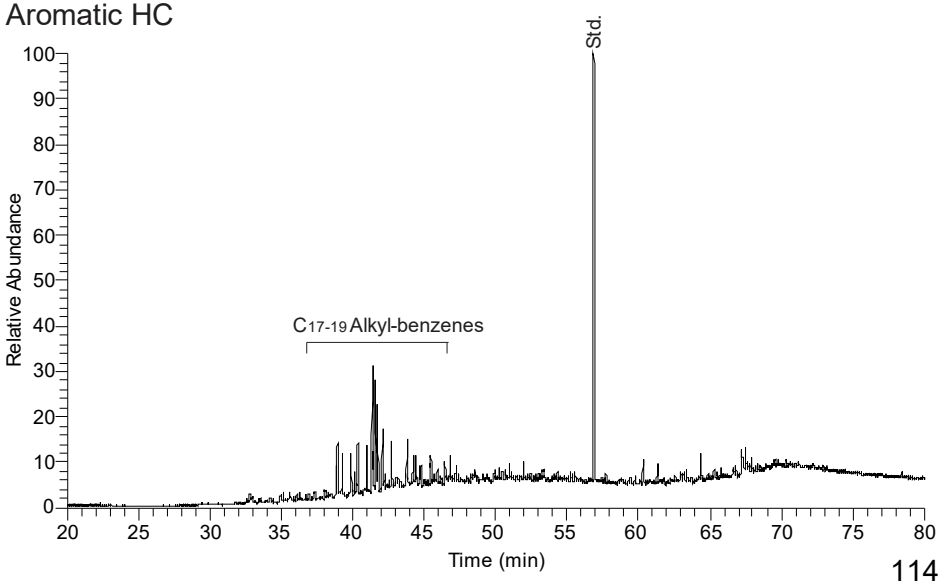

VarZ1-928
Saturated HC

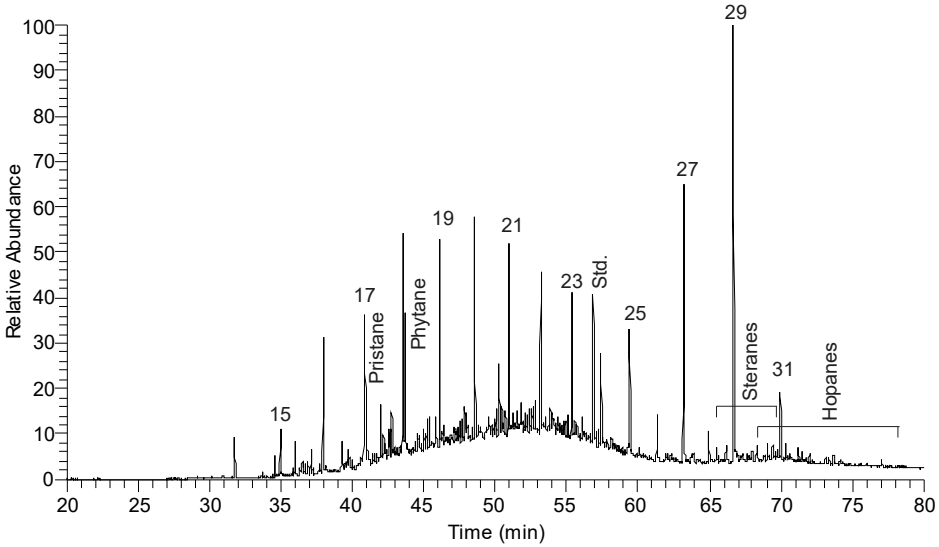

VarZ1-928
Aromatic HC

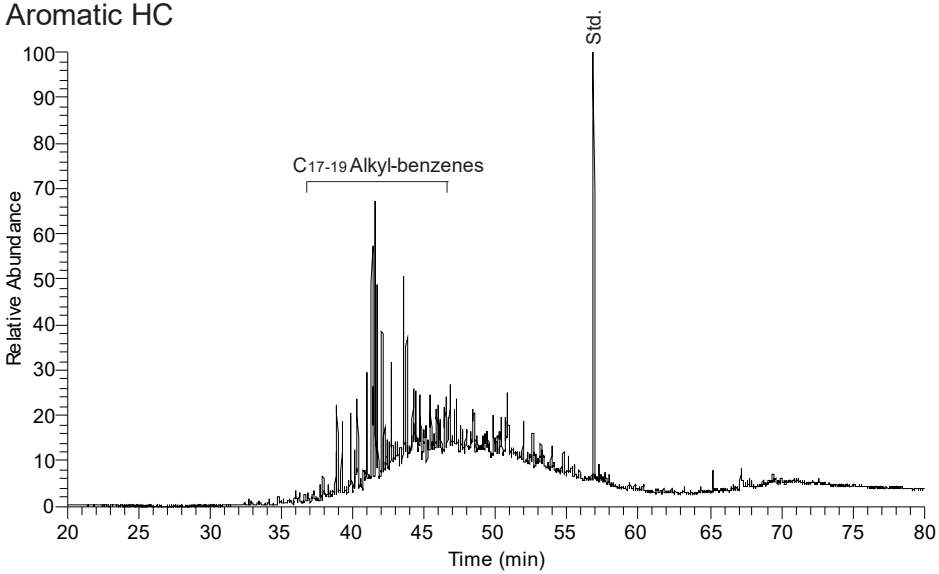

R-102
Saturated HC

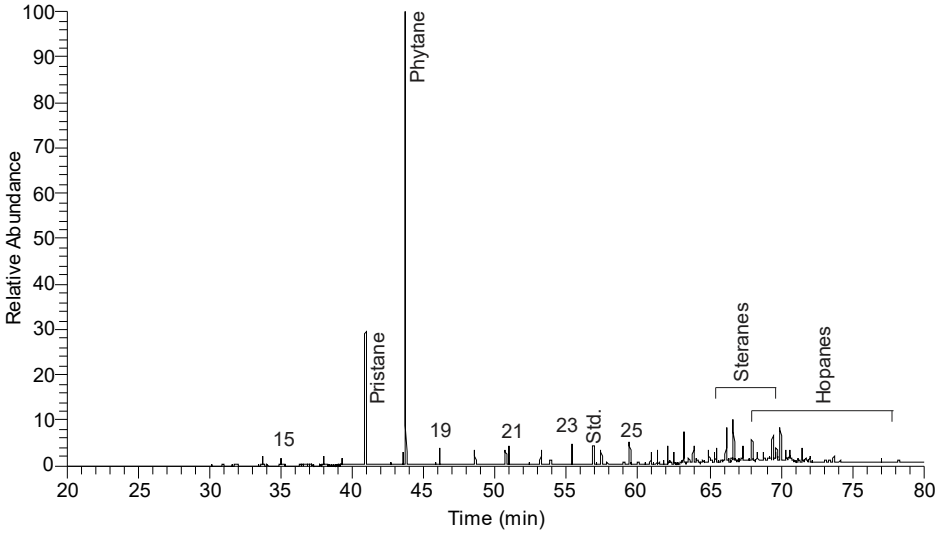

R-102
Aromatic HC

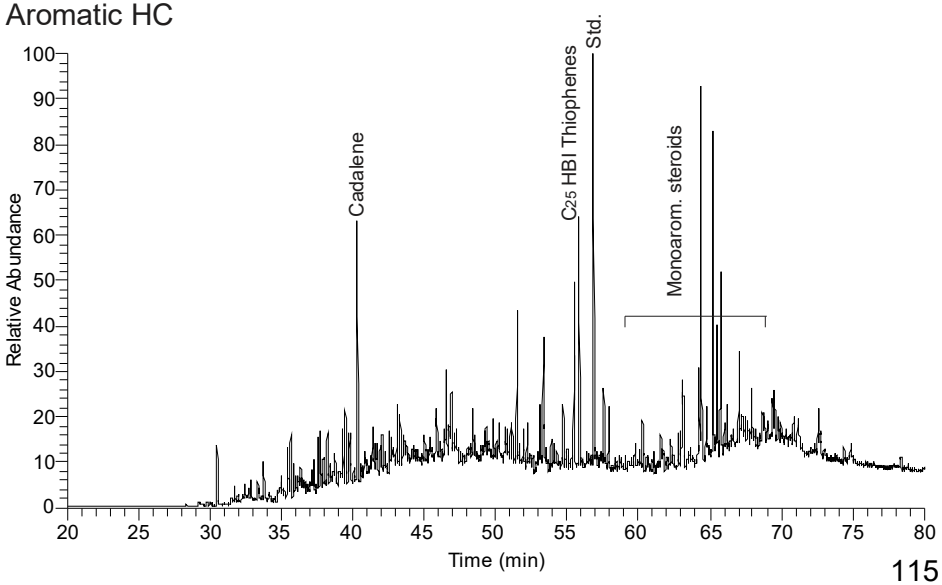

R-94
Saturated HC

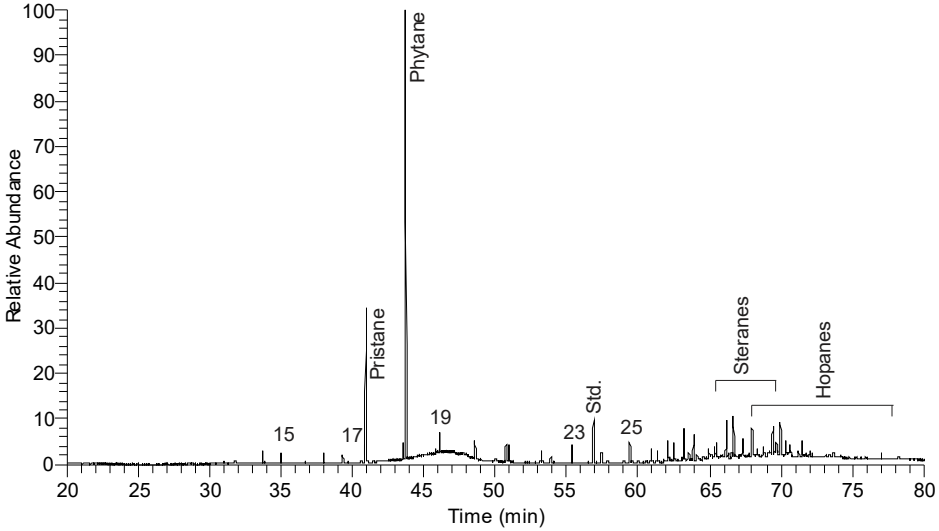

R-94
Aromatic HC

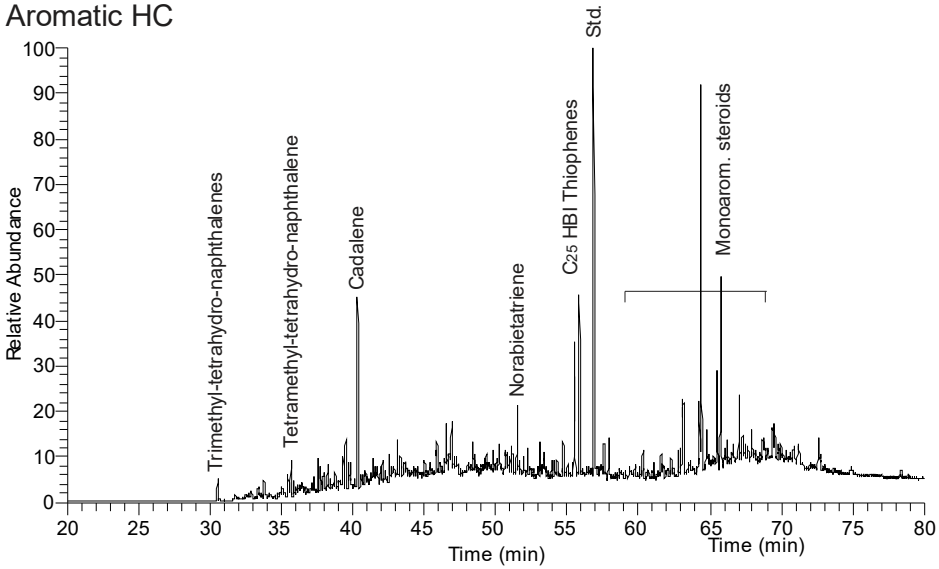

R-31
Saturated HC

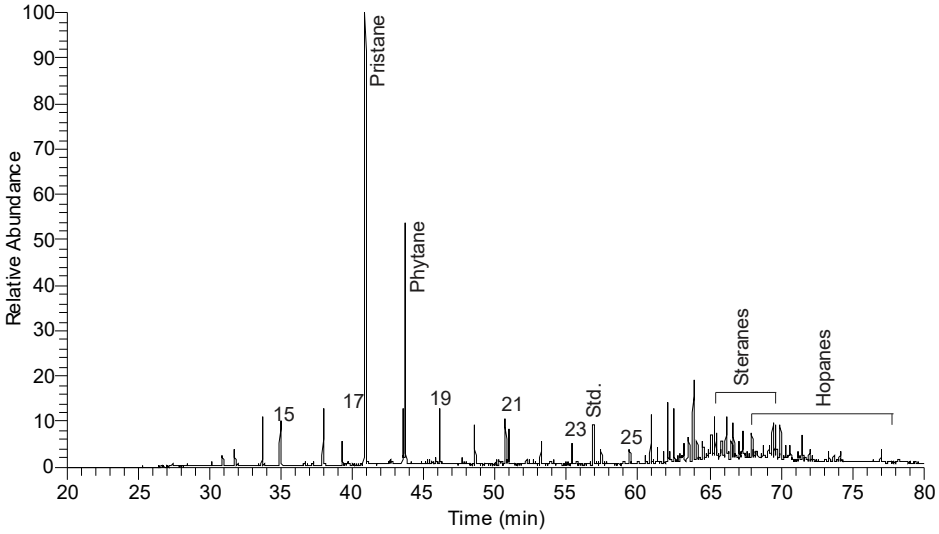

R-31
Aromatic HC

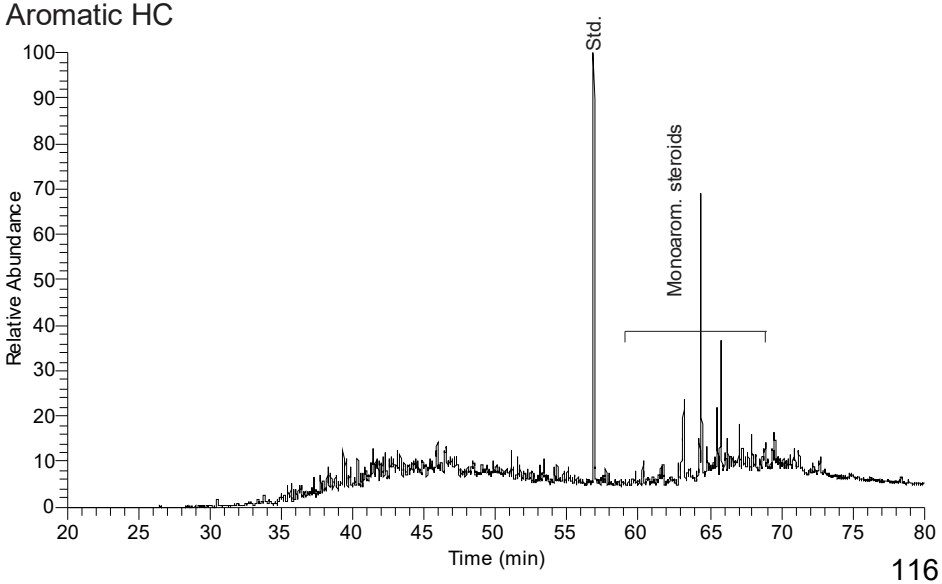

V-1
Saturated HC

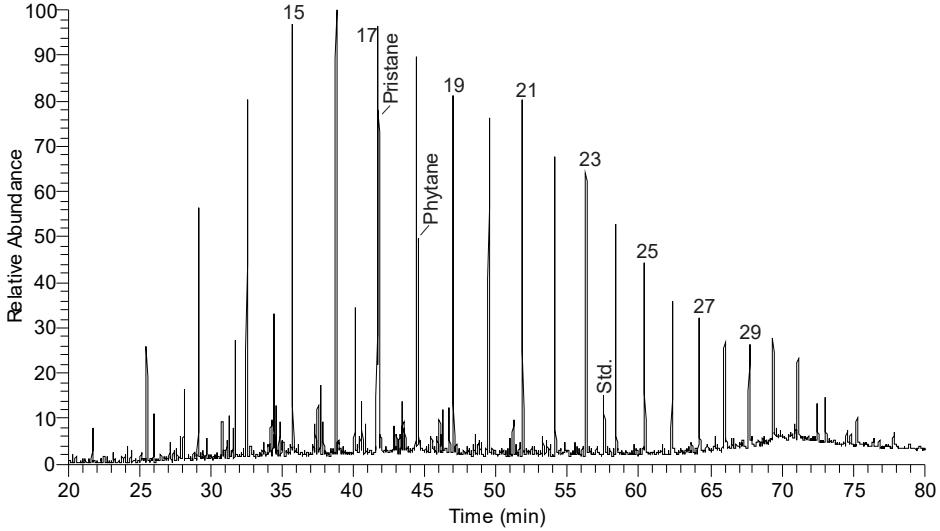

V-1
Aromatic HC

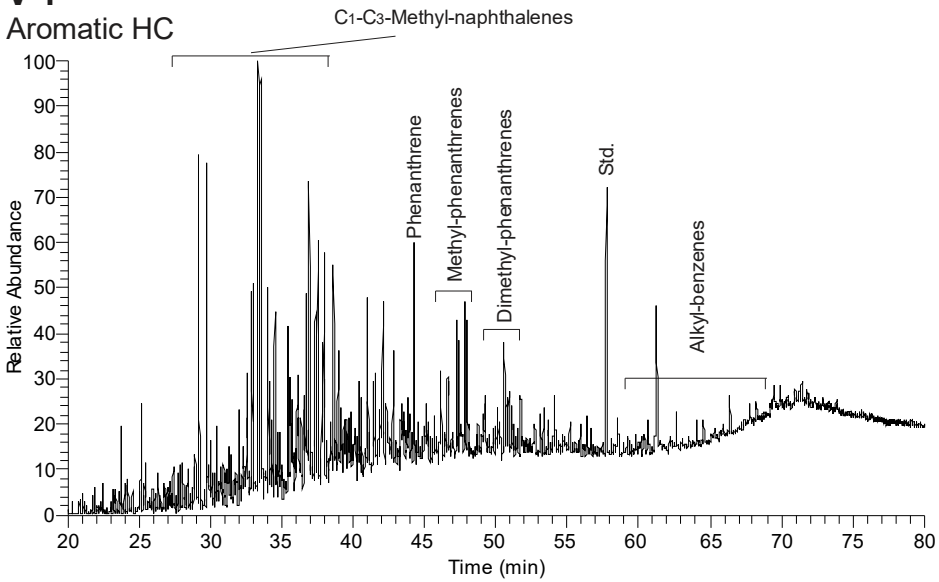

V-2
Saturated HC

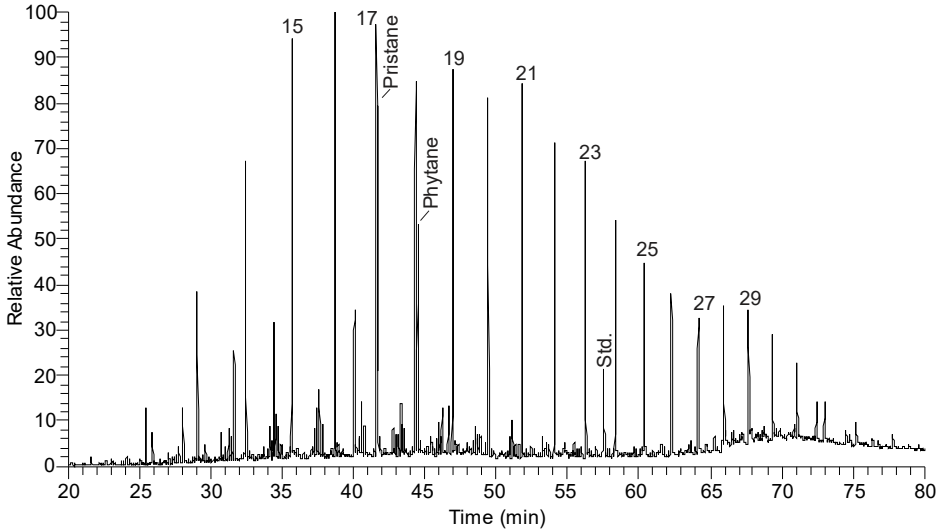

V-2
Aromatic HC

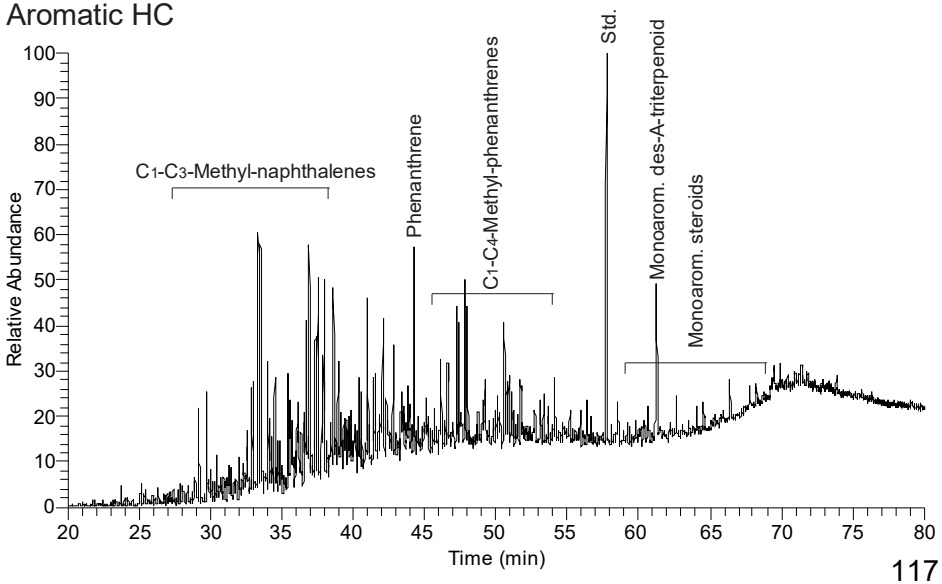

V-11
Saturated HC

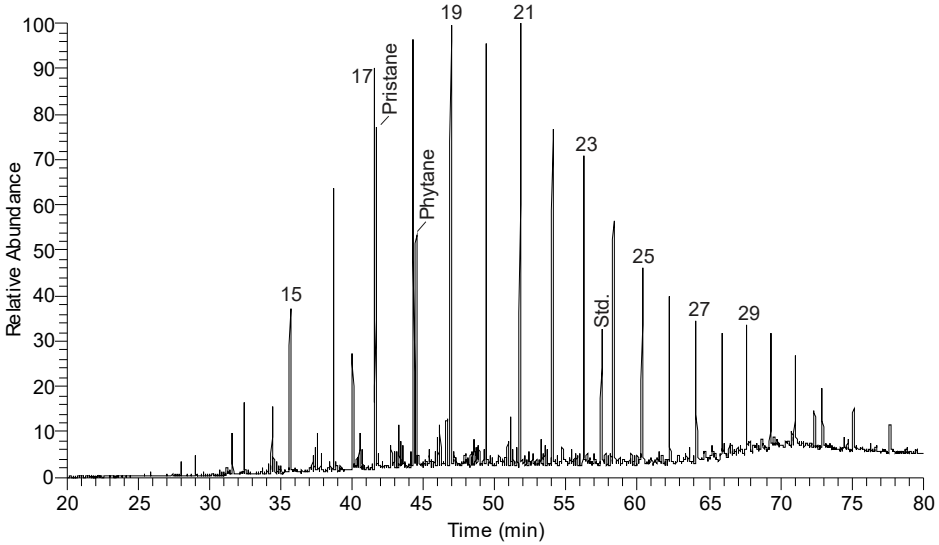

V-11
Aromatic HC

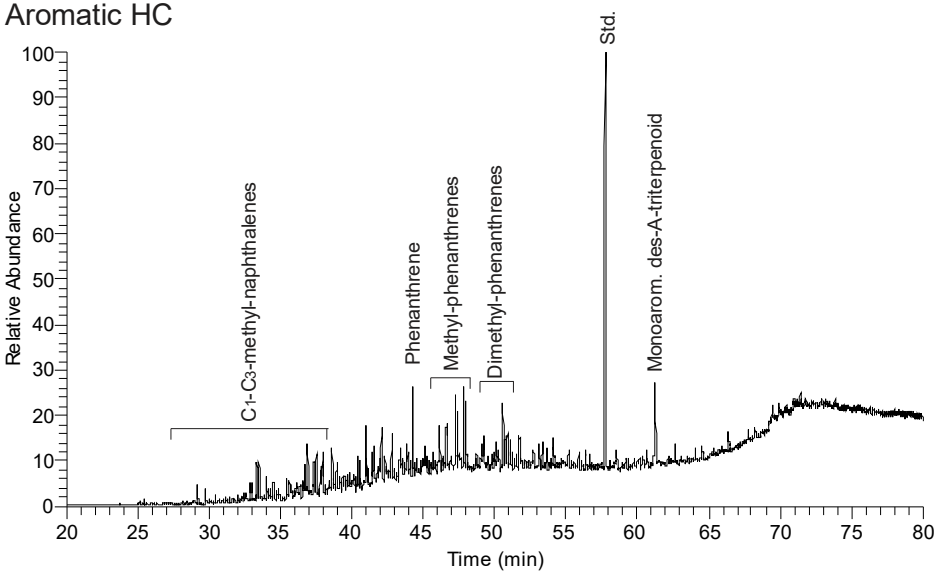

V-13
Saturated HC

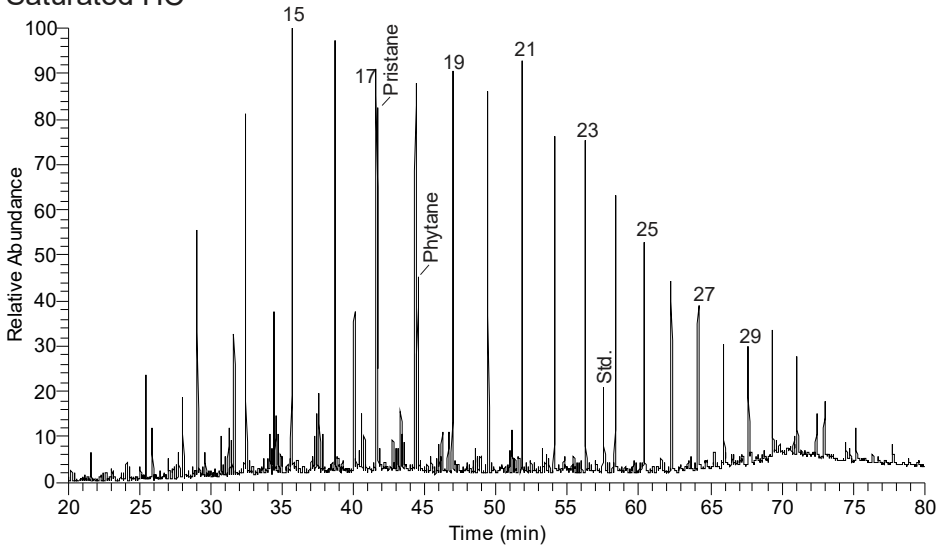

V-13
Aromatic HC

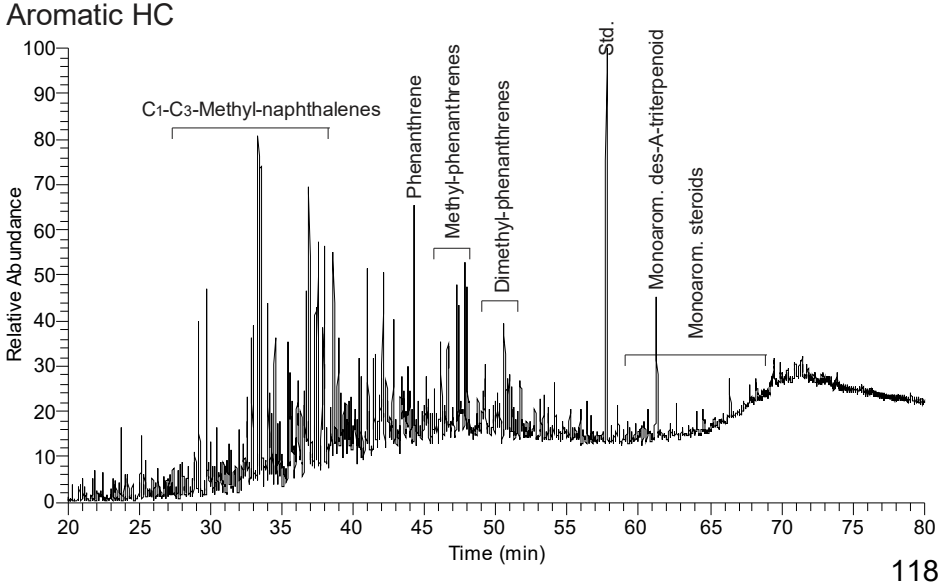

V-15
Saturated HC

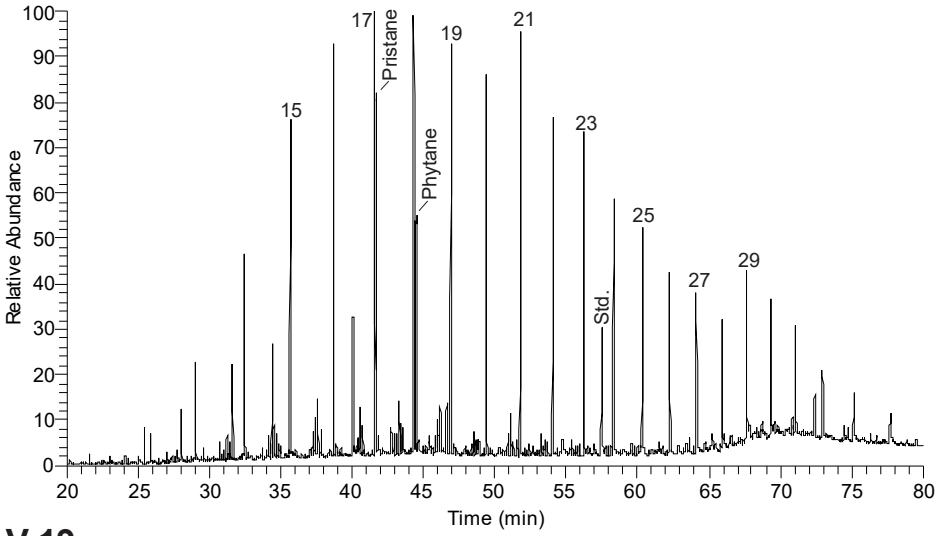

V-15
Aromatic HC

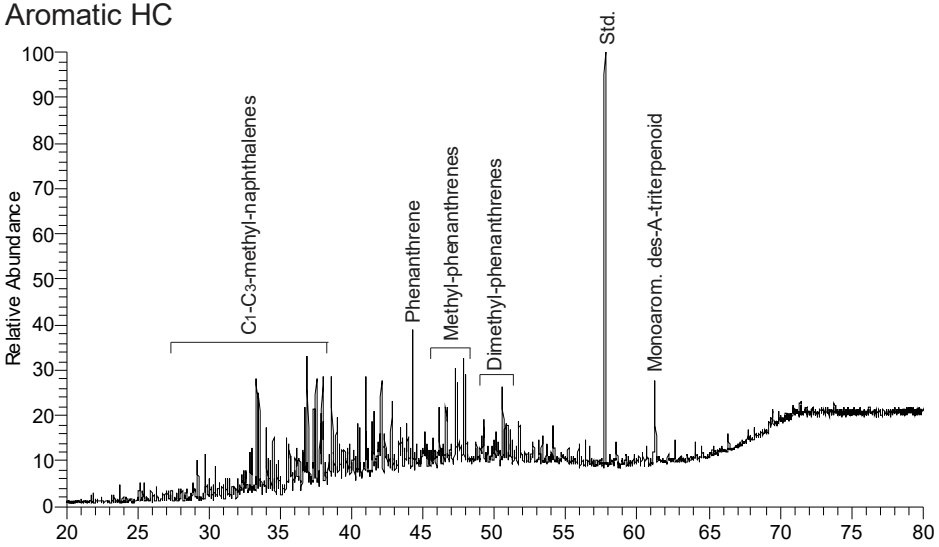

V-19
Saturated HC

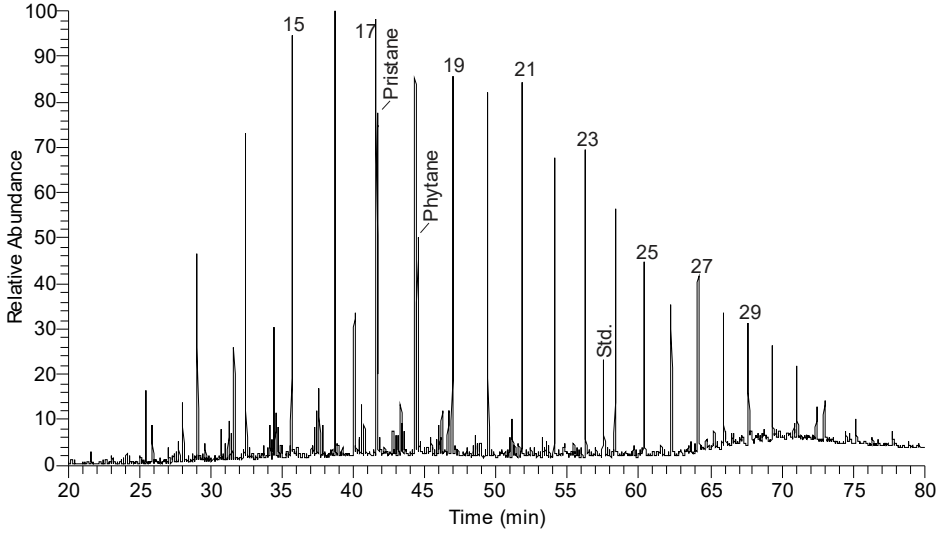

V-19
Aromatic HC

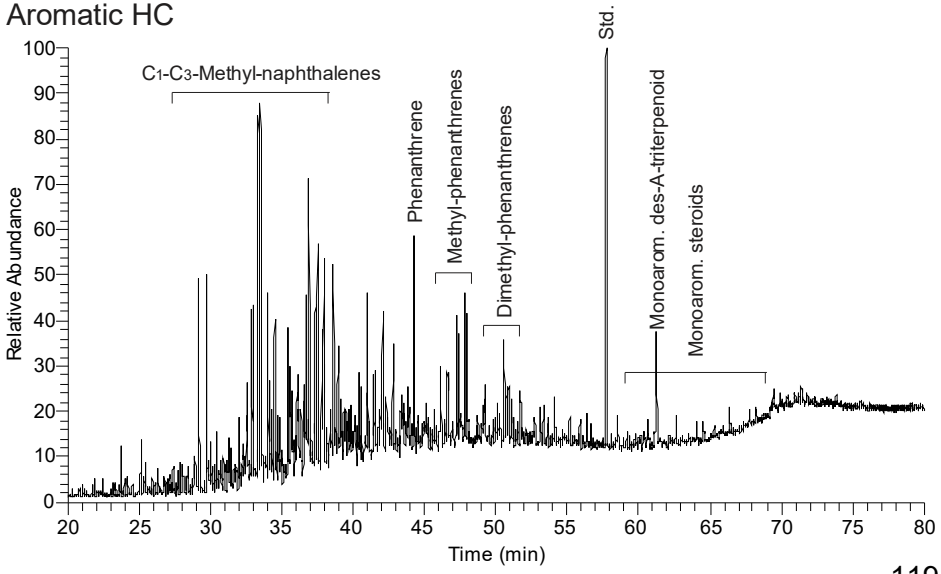

V-21
Saturated HC

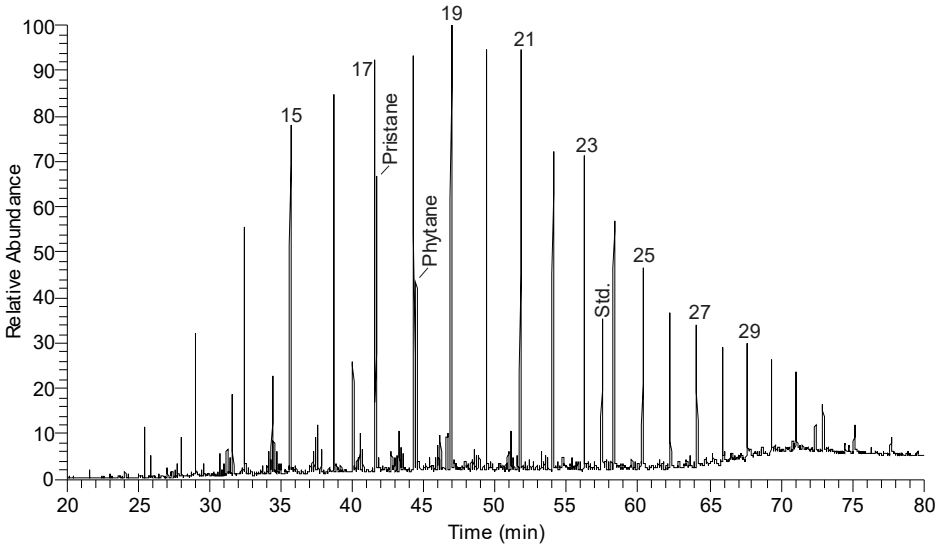

V-21
Aromatic HC

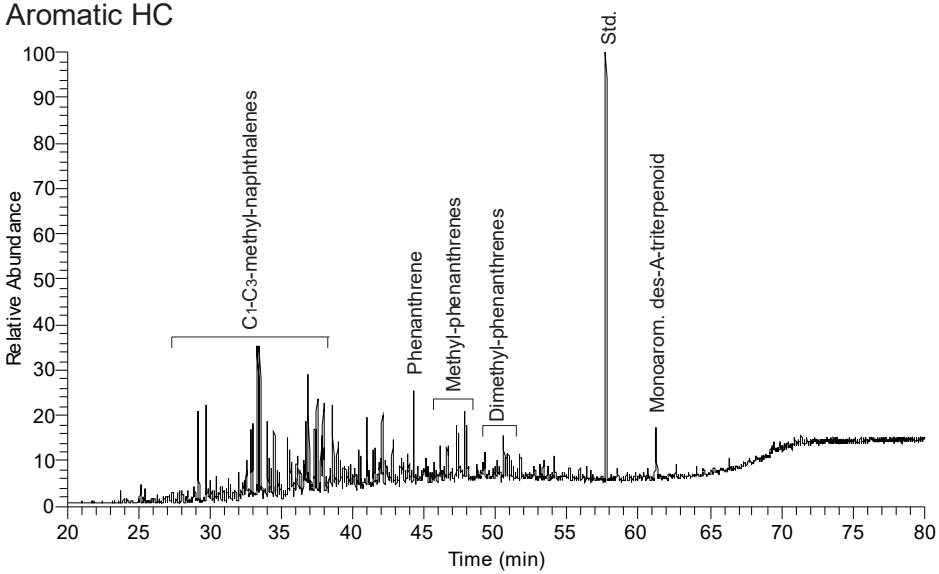

V-33
Saturated HC

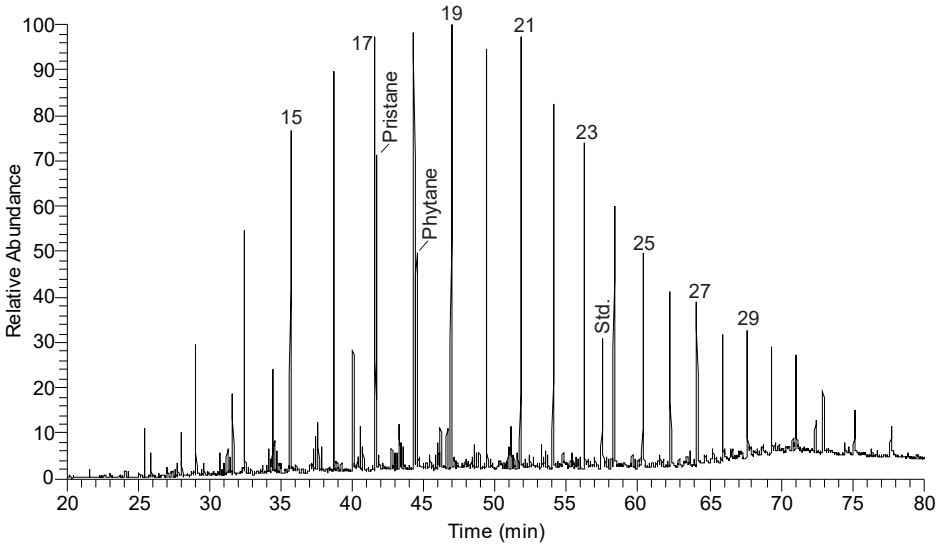

V-33
Aromatic HC

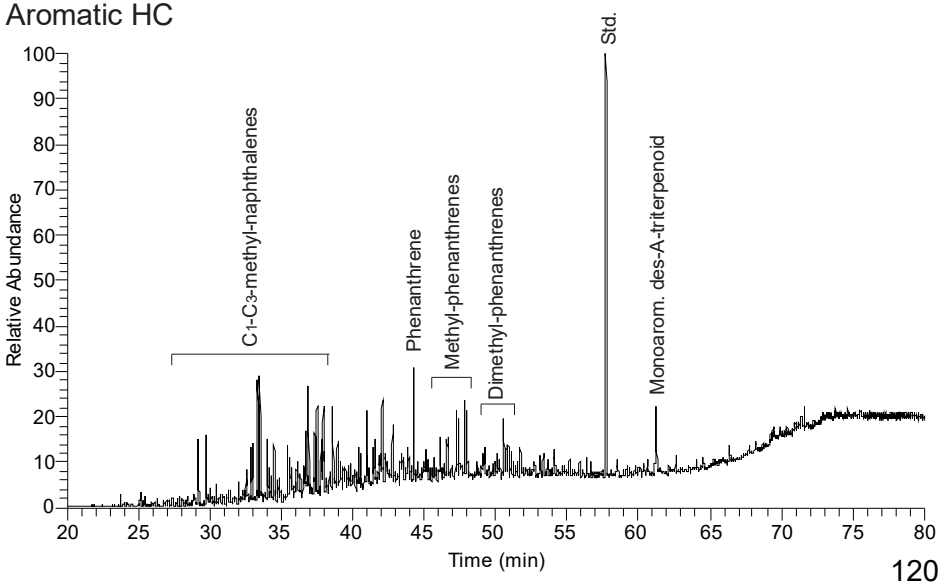

V-39
Saturated HC

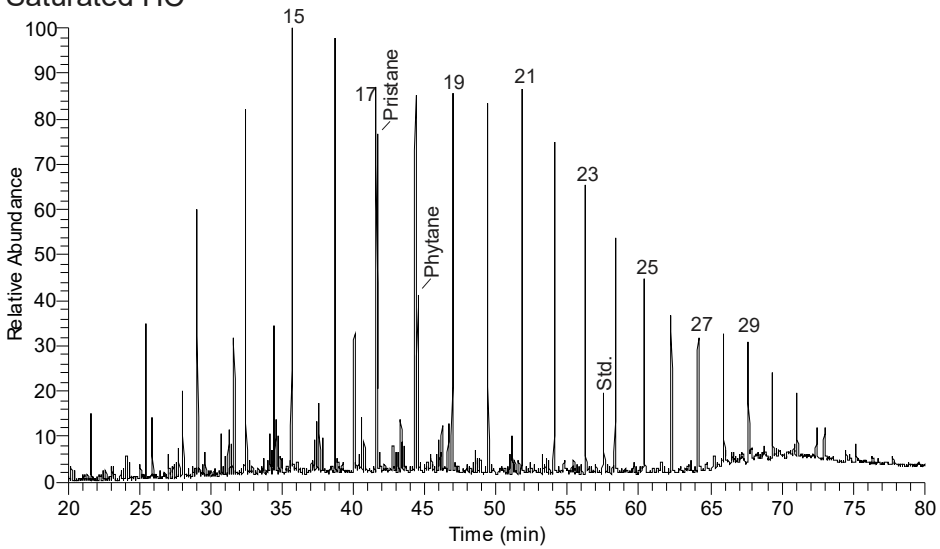

V-39
Aromatic HC

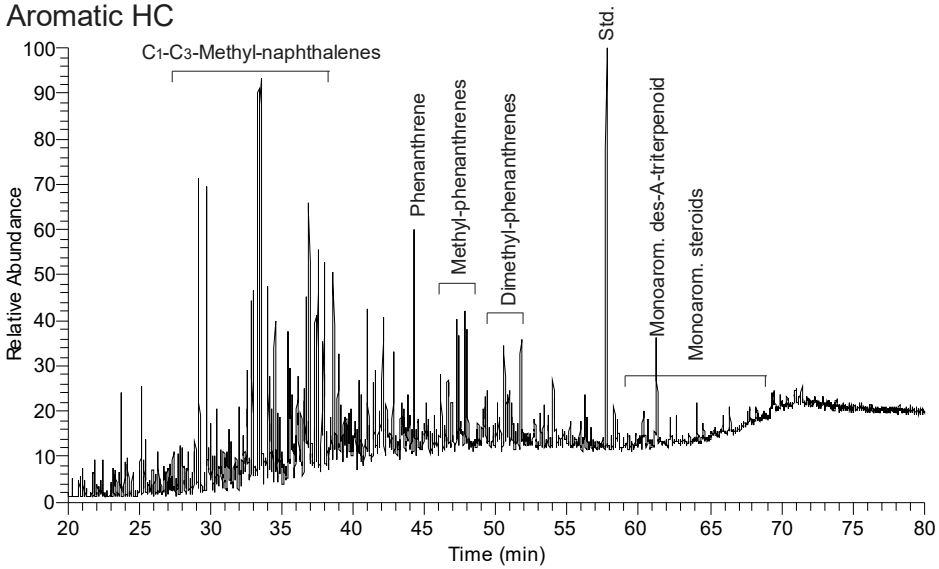

V-41
Saturated HC

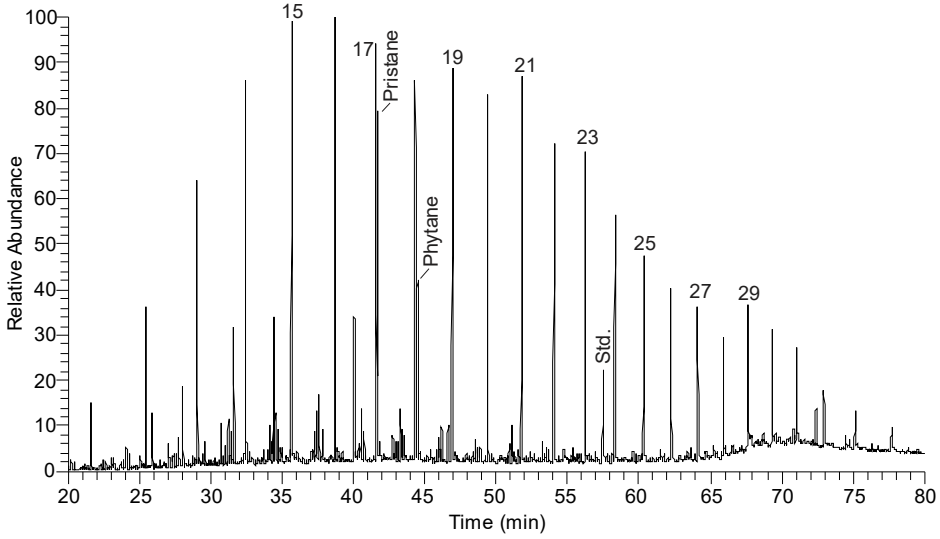

V-41
Aromatic HC

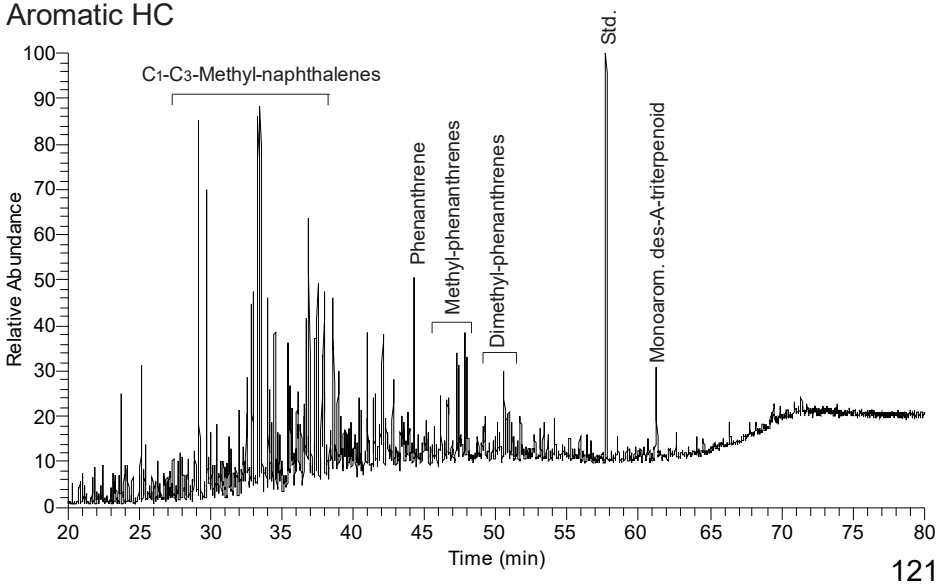

KB-04

Saturated HC

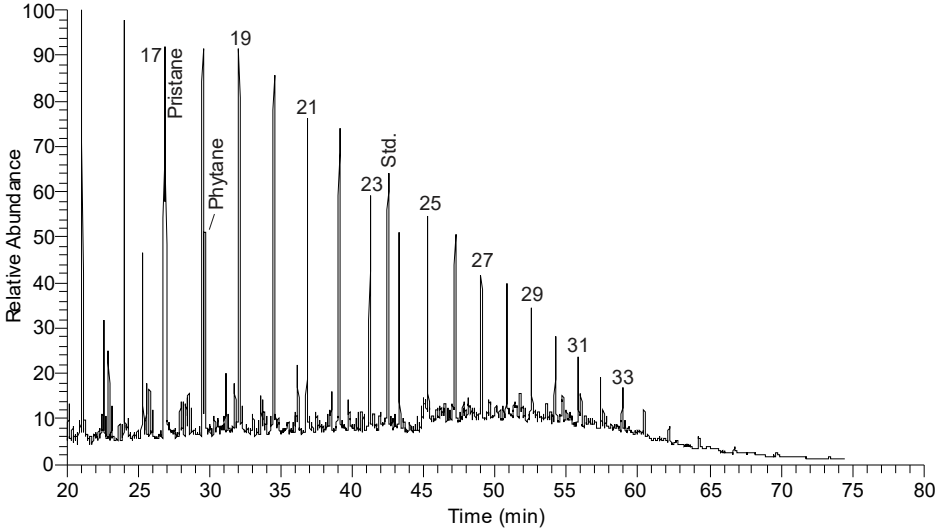

KB-04

Aromatic HC

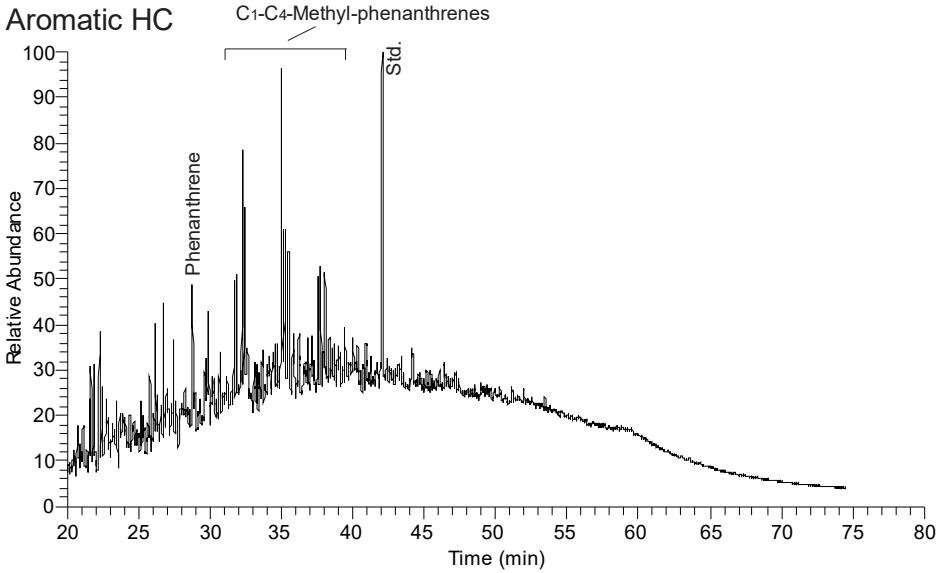

KB-05

Saturated HC

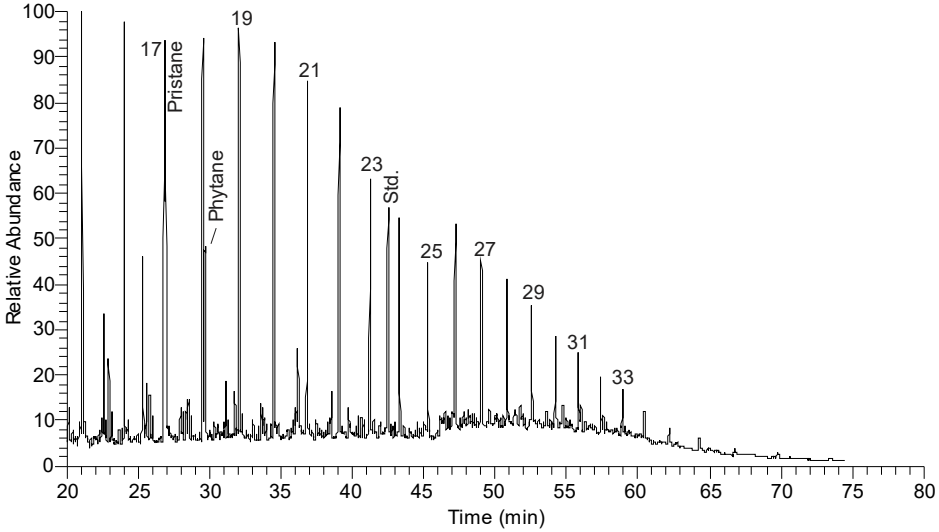

KB-05

Aromatic HC

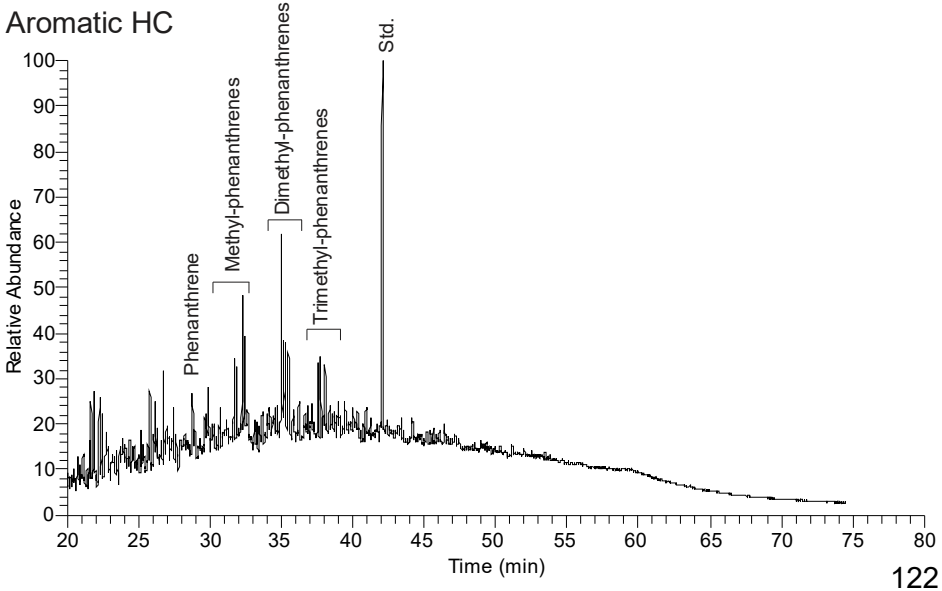

Urman-758
Saturated HC

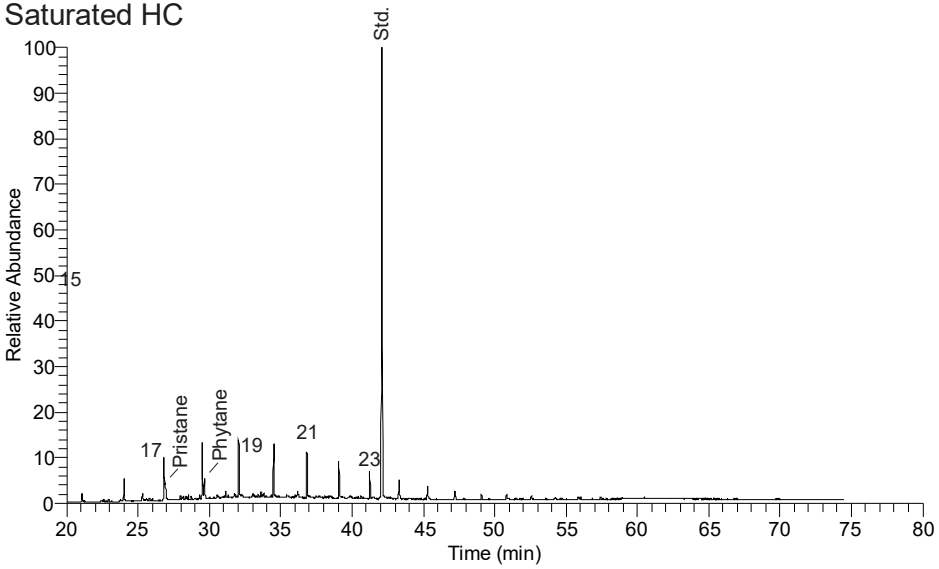

Urman-758
Aromatic HC

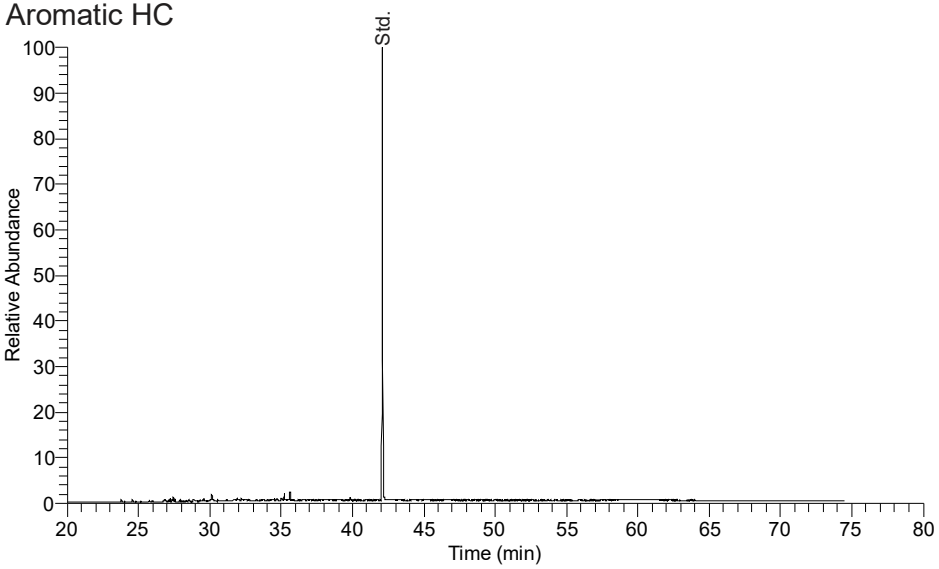

PIV168
Saturated HC

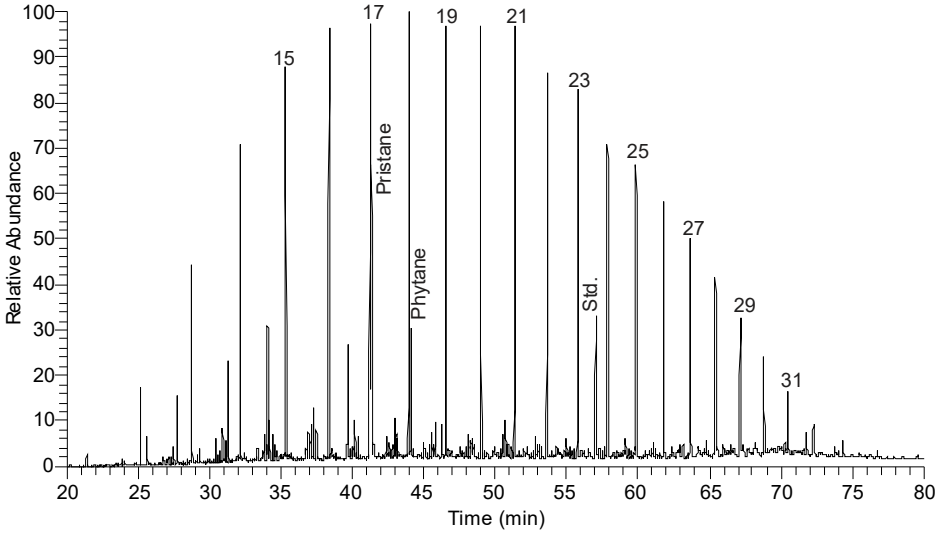

PIV168
Aromatic HC

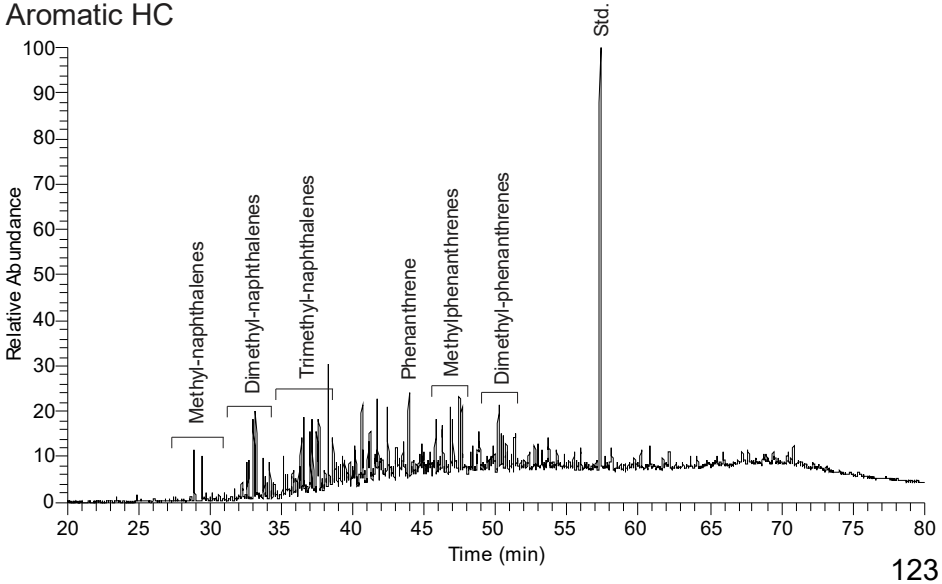

VOL31

Saturated HC

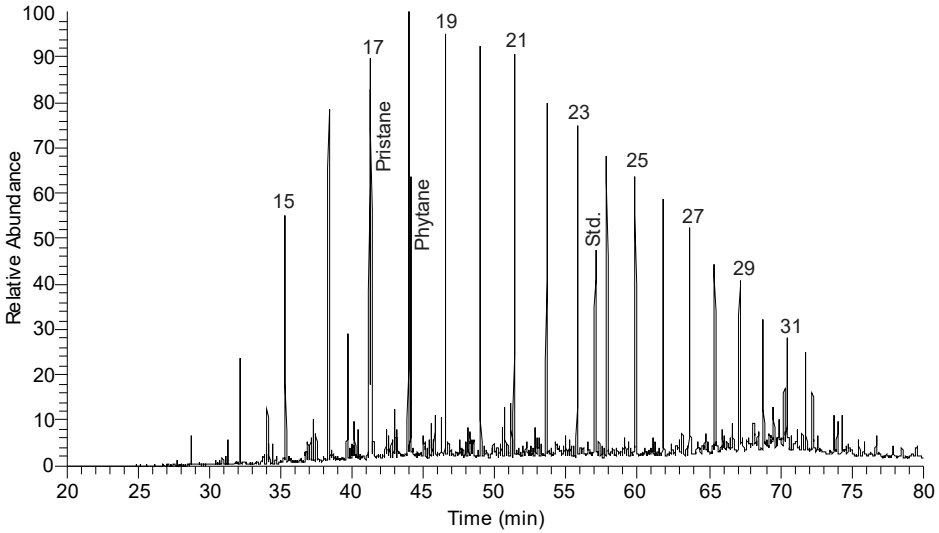

VOL31

Aromatic HC

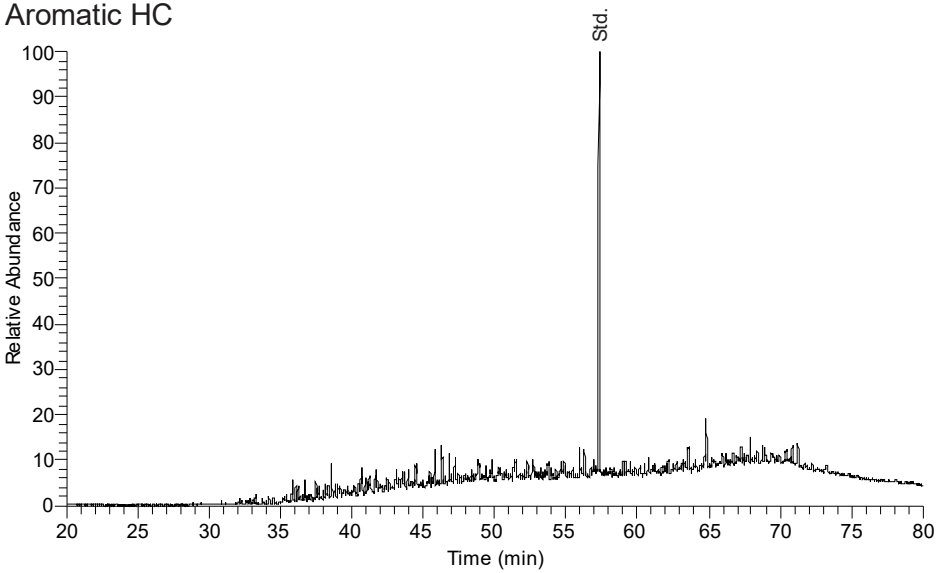

VM2

Saturated HC

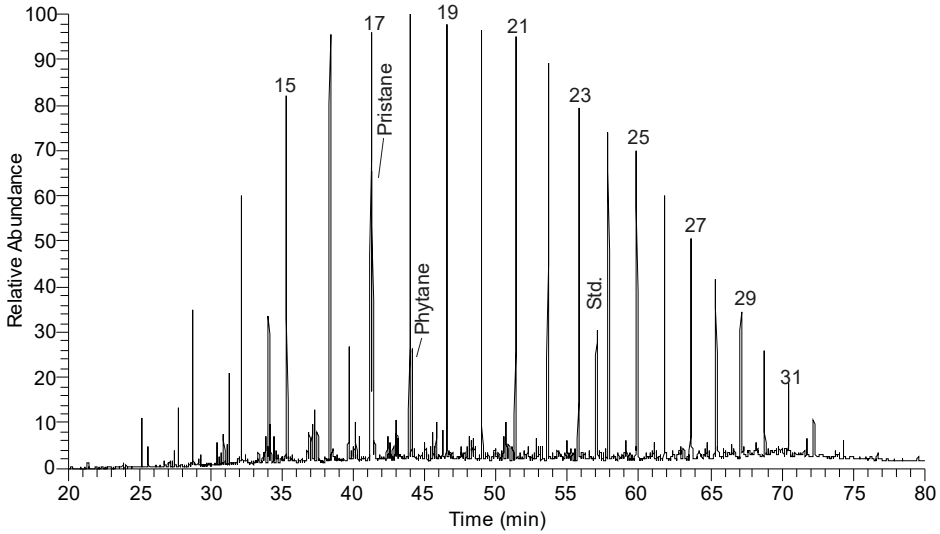

VM2

Aromatic HC

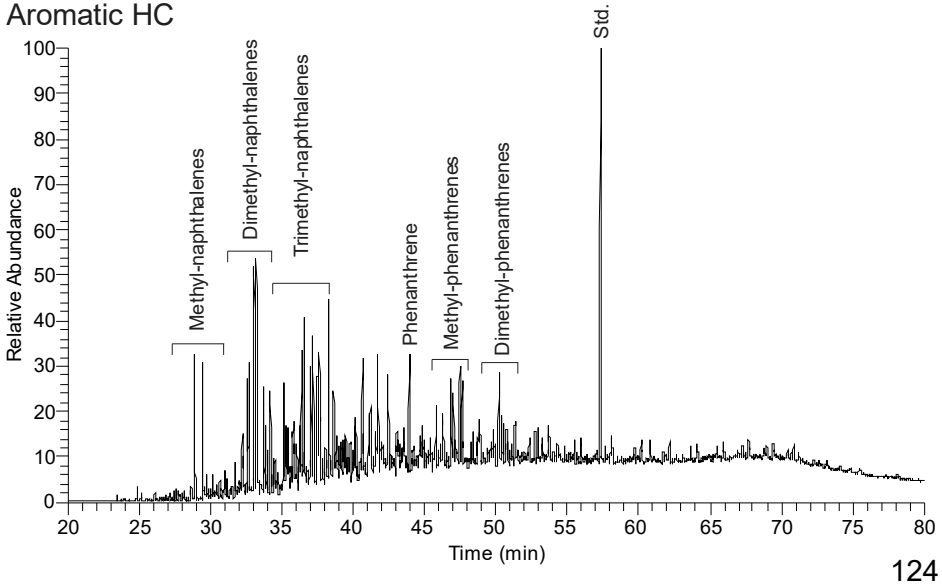

MVOS

Saturated HC

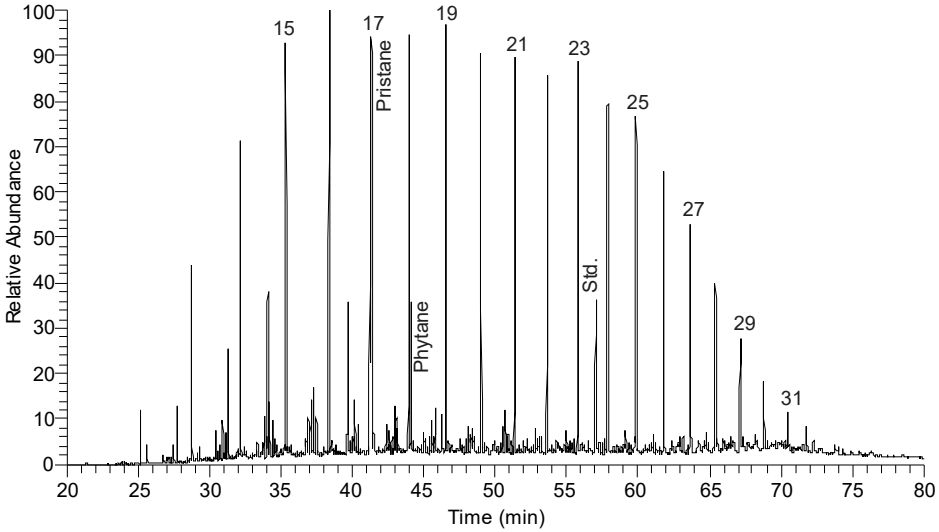

MVOS

Aromatic HC

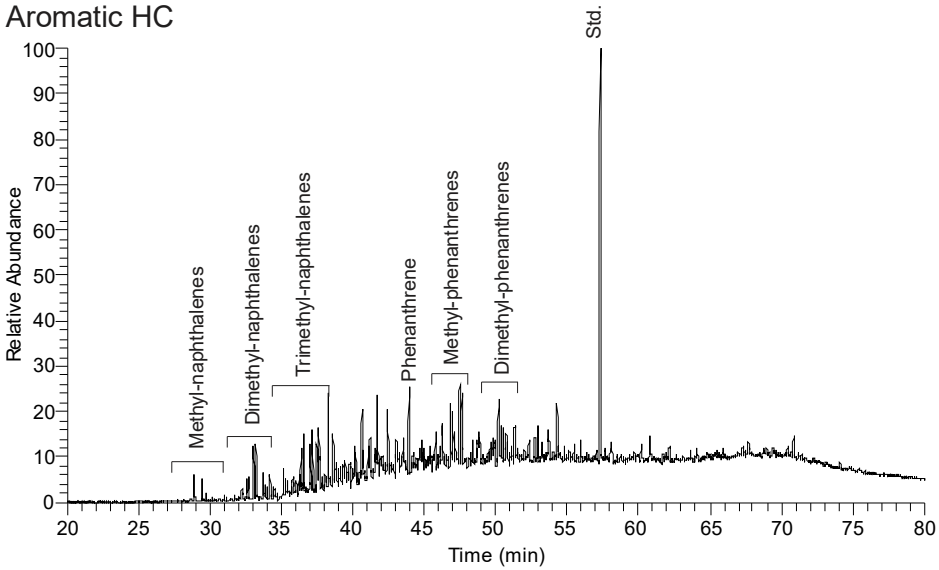

ORK2

Saturated HC

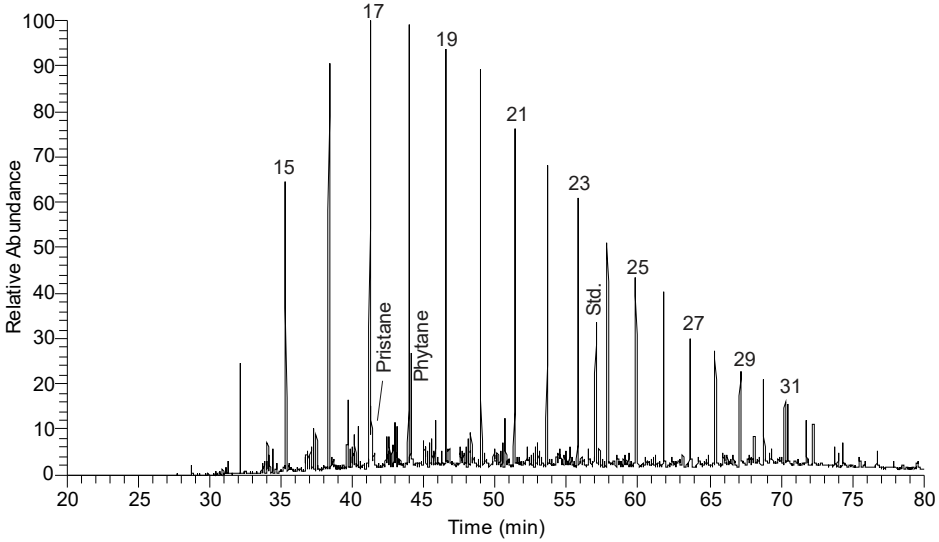

ORK2

Aromatic HC

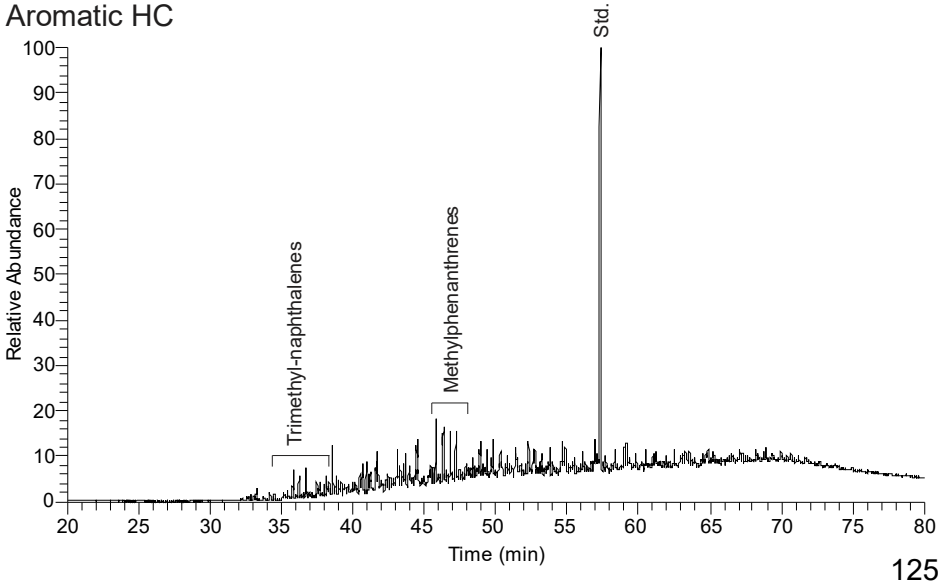

KOK26

Saturated HC

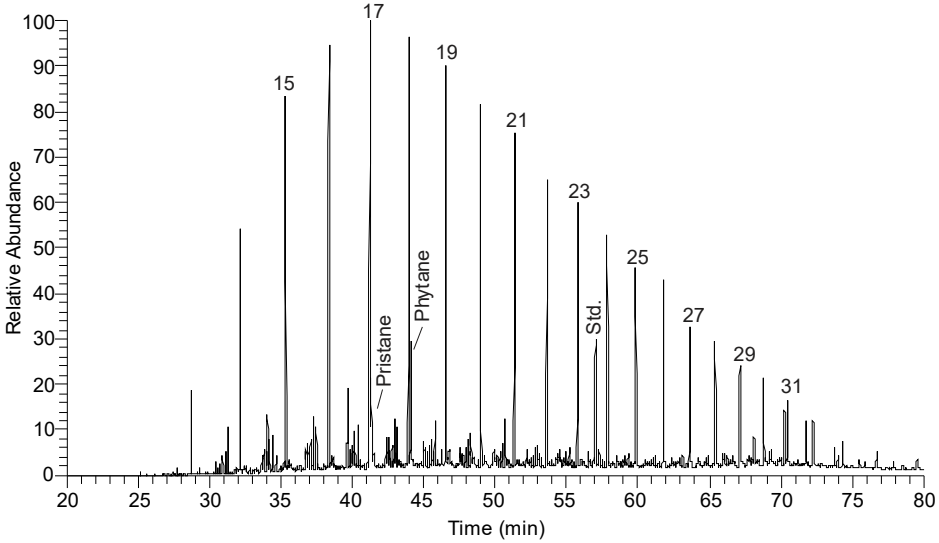

KOK26

Aromatic HC